Universidad de Concepción
Dirección de Postgrado
Facultad de Ciencias Físicas y Matemáticas
Programa de Doctorado en Ciencias Aplicadas
con Mención en Ingeniería Matemática

LEYES DE CONSERVACIÓN CON FLUJO DISCONTINUO MODELANDO COLUMNAS DE FLOTACIÓN

CONSERVATION LAWS WITH DISCONTINUOUS FLUX MODELING FLOTATION COLUMNS

Tesis para optar al grado de Doctor en Ciencias Aplicadas
con mención en Ingeniería Matemática

Yolanda María Vásquez Bernal

CONCEPCIÓN-CHILE
2022

Profesor Guía: Dr. Raimund Bürger
CI^{2}MA y Departamento de Ingeniería Matemática
Universidad de Concepción, Chile

Cotutor: Dr. Stefan Diehl
Centre for Mathematical Sciences
Lund University, Sweden

Cotutor: Dr. María del Carmen Martí
Departament de Matemàtiques
Universitat de València, España

Conservation laws with discontinuous flux modeling flotation columns

Yolanda María Vásquez Bernal

Directores de Tesis: Raimund Bürger, Universidad de Concepción, Chile.
María del Carmen Martí, Universitat de València, España.
Stefan Diehl, Lund University, Sweden.

Director de Programa: Raimund Bürger, Universidad de Concepción, Chile.

Comisión evaluadora

Prof.

Prof.

Prof.

Prof.

Comisión examinadora

Firma: _____
Prof.

Firma: _____
Prof.

Firma: _____
Prof.

Firma: _____
Prof.

Calificación: _____

Concepción, 16 de Diciembre de 2019

Abstract

In this thesis, a newly developed dynamic one-dimensional model formulated in terms of PDEs is used to predict the process of simultaneous flotation of bubbles and sedimentation of particles that are not attached to bubbles. The governing model is a triangular system of conservation laws for the primary phase (aggregates, bubbles with particles attached) and secondary phase (solids) volume fractions as functions of height and time. The thesis has the following objectives.

The first objective of this thesis is to demonstrate that the model and numerical scheme provide a tool for the simulation of the operation of a flotation column in the case of a common feed inlet of the three phases and when no aggregation occurs in the column. In particular, responses of the unit to changes in operating conditions such as changes in the rates and composition of feed flows as well as transitions between operating conditions are illustrated.

The second objective of this thesis is to show applications of the model and numerical scheme to the wastewater treatment industry and identify desired steady states for the dissolved air flotation application analyzing the non-linear ingredients of the governing equations.

The third objective of this thesis is to generalize the triangular system of conservation laws and show that the numerical scheme is monotone and satisfies an invariant-region property, i.e., the volume fractions of the three phases stay between zero and one.

The fourth objective of this thesis is to demonstrate that the numerical scheme for the primary and secondary phases converge to a solution under certain simplifying assumptions.

The fifth goal of this thesis is to extend the one-dimensional hyperbolic model of the hydrodynamics of a flotation column into one that include capillarity, which means that the governing PDE is of parabolic type in the froth region, whereas it is hyperbolic in regions without froth.

Resumen

En esta tesis, se utiliza un modelo unidimensional dinámico desarrollado recientemente, formulado en términos de EDPs para predecir el proceso simultáneo de flotación de burbujas y sedimentación de partículas que no están adheridas a las burbujas. El modelo governante es un sistema triangular de dos leyes de conservación para las fracciones de volumen de la fase primaria (agregados, burbujas cargadas de partículas) y la fase secundaria (sólidos) en función de la altura y el tiempo. La tesis tiene los siguientes objetivos.

El primer objetivo de esta tesis es demostrar que el modelo y el esquema numérico proporcionan una herramienta para la simulación del funcionamiento de una columna de flotación en el caso de una entrada de alimentación común de las tres fases y cuando no se produce agregación en la columna. En particular, se ilustran las respuestas de la unidad a los cambios en las condiciones de operación, como los cambios en las tasas y la composición de los flujos de alimentación, así como las transiciones entre las condiciones de funcionamiento.

El segundo objetivo de esta tesis es mostrar aplicaciones del modelo y del esquema numérico a la industria de tratamiento de aguas servidas e identificar los estados estacionarios deseados para la aplicación de flotación por aire disuelto analizando los ingredientes no lineales de las ecuaciones gobernantes.

El tercer objetivo de esta tesis es generalizar el sistema triangular de leyes de conservación y demostrar que el esquema numérico es monótono y satisface la propiedad de región invariante, es decir, las fracciones de volumen de las tres fases permanecen entre cero y uno.

El cuarto objetivo de esta tesis es demostrar que los esquemas numéricos para las fases primaria y secundaria, bajos ciertas suposiciones, convergen a una solución.

El quinto objetivo de esta tesis es extender el modelo hiperbólico unidimensional de la hidrodinámica de una columna de flotación a uno que incluya capilaridad, lo que significa que la EDP gobernante es del tipo parabólica en la región con espuma, mientras que es hiperbólica en regiones sin espuma.

Agradecimientos

En primer lugar agradezco a Dios por permitirme llegar a este momento tan importante y por nunca soltarme la mano en los momentos difíciles. A mis padres Yolanda Bernal y Marcelino Vásquez, que hicieron todo en la vida para que yo pudiera lograr todas mis metas; por ser los pilares más importante de mi vida, y demostrarme siempre su cariño y apoyo incondicional.

Quiero agradecer a mi director de tesis, profesor Raimund Bürger, primero como director del programa por llegar a Panamá y mostrarnos todo sobre el doctorado, y por las gestiones necesarias para que yo pudiera viajar a Chile. Por sus enseñanzas como profesor, y por su guía y paciencia durante el desarrollo de esta tesis.

A mi co-tutor, Stefan Diehl por permitirme trabajar con él y por su apoyo en este trabajo, por su amabilidad al recibirme en Suecia durante mi pasantía y por su disposición a resolver todas las dudas que surgían.

A mi co-tutora María del Carmen Martí por su gran paciencia, por tomar este reto como su primera estudiante de doctorado, gracias por el tiempo dedicado durante las diferentes horas del día, por las conversaciones sobre el trabajo y sobre la vida, por su cordialidad durante mi pasantía y permitirme pasar tiempo con su familia, por los ricos postres durante su estancia en el CI^{2}MA, por siempre estar pendiente de todos mis avances.

A la Universidad de Concepción y todos los profesores del programa de doctorado los cuales me ayudaron en mi formación académica y personal. Al Centro de Investigación en Ingeniería Matemática (CI^{2}MA) de la Universidad de Concepción y a sus respectivos directores durante este tiempo, por brindarme el espacio para poder trabajar cómodamente durante mis estudios. A todo el personal administrativo en especial a la Sra. Lorena y la Sra. Paola por su disposición de ayudar siempre y por su alegría contagiosa.

A mis compañeros del doctorado que desde el día uno me dieron la bienvenida y con los cuales he compartido gratos momentos: Cristian, Joaquín, Daniel, Paulo, Camilo, Rafael, Bryan, Paul, William, Iván, Ramiro, Mario, Juan Paulo, Romel e Isaac; en especial a mis compañeros de generación Adrián, Nestor y Yissedt gracias por su apoyo durante todos estos años y por convertirse en buenos amigos para mí. Ha sido muy grato compartir este camino con ustedes.

Agradezco también a todas aquellas personas que pasaron por mi vida a darme un respiro de

mis "problemas" y hacer de mis días en Chile una gran experiencia: Abi, Nancy, Edu, Enzo, los salseros de la Escalera, Angie, Fer y en especial a Francisco, los llevo a todos y todas conmigo. A Viviana que se convirtió en mi familia durante estos 5 años en Chile, gracias por los consejos, los abrazos de ánimo, las aventuras y sobre todo por darme un espacio en tu hogar.

A mis hermanos (Rony, Chano y Edward) por brindarme siempre su apoyo incondicional, a mis abuelos que con su sabiduría influyeron en mi crecimiento, a mis tíos, tías, primos, primas, y amigos en Panamá (Mayrlen, Lupe, Juan) que siempre estuvieron brindándome todo su apoyo; a mi primo Cristhian por las incontables horas de videollamdas y por siempre estar ahí desde que tengo uso de razón. A mi bella comunidad de El Bongo por su constante apoyo y preocupación por mí en la distancia. Y de manera muy especial dedico esta tesis a mis sobrinos que me inspiran cada día.

Agradecer además a todas las instituciones que permitieron realizar este trabajo: al programa de becas IFARHU-SENACYT (Panamá) a través del "Subprograma de becas doctorales y post-doctorales"; ANID (Chile) a través de su proyecto Anillo ANID/PIA/ACT210030; al Centro de Modelamiento Matemático (proyectos BASAL ACE210010 and FB210005); proyecto Fondecyt 1210610 y al Centro de Recursos Hídrico para la Agricultura y Minería (CRHIAM). Al Consejo Sueco de Investigación (Vetenskapsrådet, 2019-04601); a la subvención MTM2017-83942 financiada por MINECO España y la subvención PID2020-117211GB-I00 financiada por MCIN/AEI/10.13039/501100011033.

Yolanda María Vásquez Bernal

Contents

List of Tables

List of Figures

Introduction

Motivation

Froth flotation is commonly used in mineral processing for the recovery of valuable minerals, such as copper and lead-bearing minerals, from low-grade ores; and in industrial wastewater treatment to remove contaminants that are otherwise difficult to separate such as floating solids, residual chemicals, and droplets of oil and fat. This process selectively separates hydrophobic materials (repelled by water) from hydrophilic (attracted to water), where both are suspended in a viscous fluid. It is well known that this physico-chemical separation process functions roughly as follows: gas is introduced close to the bottom of a column, and the bubbles generated rise upwards throughout the pulp that contains the solid particles, which can be divided into two main groups. The hydrophobic particles (minerals or ores that should be recovered) attach to the bubbles that float to the top of the column, forming foam or froth carrying the valuable material that is removed usually through a launder. On the other hand, the hydrophilic particles (slimes or gangue) do not attach to bubbles, but settle to the bottom of the vessel, unless they are trapped in the bulk upflow. Close to the top, additional wash water can be injected to assist with the rejection of entrained impurities [111] and to increase the froth stability and improve recovery [53, 91]. Mathematical models are required for the design, simulation, and eventually control of flotation columns.

Motivated by [38, 54, 106], Bürger et al. [17] presented a one-dimensional two-phase model describing only the movement of gas bubbles and fluid. The flotation column modeled in that work has a separate gas inlet near the bottom, which is commonly used in mineral processing so that a collection zone is created in which the hydrophobic particles attach to the gas bubbles inside the column. Other devices have a common feed inlet for both slurry and gas bubbles, so that the aggregation process (the attachment of hydrophobic particles to bubbles) mostly occurs in the inlet pipe. (These variants are illustrated e.g. in Figure 1 of [18].) Here, we model such a column (see Figure 1) and assume that the bubbles are fully loaded with hydrophobic particles as the mixture enters the column, so that the aggregation process is concluded when particles and bubbles enter the column.

The governing equation of the two-phase model studied by [17] is a scalar, quasilinear first-order partial differential equation (PDE) (known as conservation law; see, e.g., [60] or [77] for the

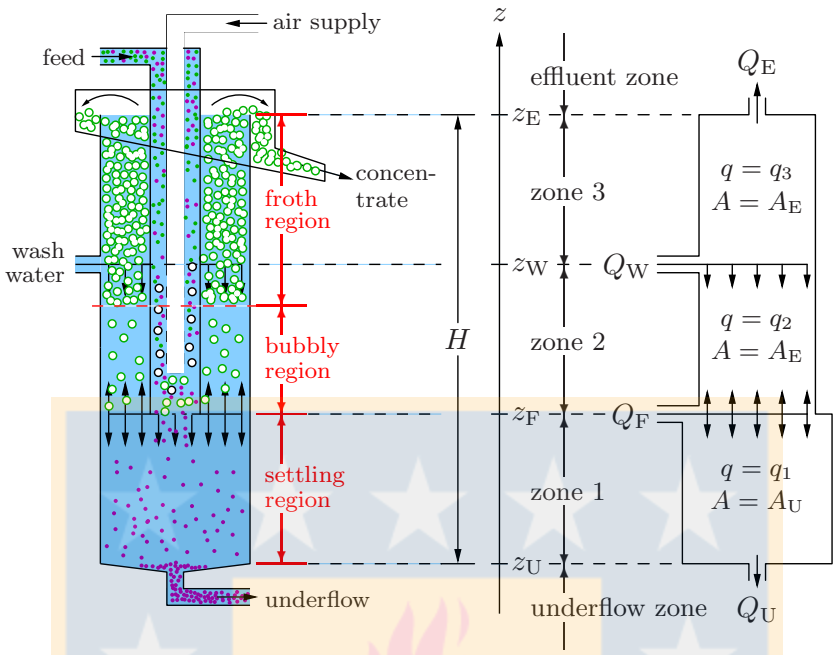

Figure 1: Left: Schematic of a flotation column with non-constant cross-sectional area $A(z)$ (A_U below and A_E above the feed level) utilized for numerical simulations in this thesis (**Chapters 1–4**). Right: corresponding one-dimensional conceptual model. The unit is fed with wash water at level $z = z_W$ and a mixture of aggregates and feed slurry at $z = z_F$, where $z_U < z_F < z_W < z_E$ divide the real line into the zones inside the column and the underflow and effluent zones. The volumetric flows correspond to the injection of wash water ($Q_W \geq 0$) and feed slurry ($Q_F > 0$). These quantities and the volumetric underflow rate $Q_U \geq 0$ are assumed to be chosen such that the effluent volumetric overflow $Q_E = Q_W + Q_F - Q_U$ is nonnegative, $Q_E \geq 0$.

background). A non-standard ingredient of that model is a flux function that is discontinuous at several spatial positions due to the feed sources of gas, slurry, and wash water, and the lower and upper outlets of tailings and concentrate. That formulation was recently extended in [18] to a three-phase model that also includes the settling of solid particles within the flotation column. The three-phase flow of solids, gas (bubbles or aggregates) and fluid is modelled in one space dimension. We herein utilize that same model of [18] and present new numerical results relevant to applications.

To state the governing PDEs of our approach, we assume that the independent variables are time $t \geq 0$ and height z, i.e., z is a scalar spatial coordinate that increases in the upward direction, and that the unknowns are the volume fraction of aggregates $\phi = \phi(z,t)$ and the volume fraction of solids in the solid-liquid suspension $\varphi = \varphi(z,t)$, where

$$\varphi = \frac{\psi}{1-\phi}, \tag{1}$$

with $\psi = \psi(z,t)$ is the volume fraction of (hydrophilic) solids and $1-\phi = 1-\phi(z,t)$ is the volume

fraction of the suspension outside the aggregates. (Equation 1 means that if a small volume V is given, then φ is the local ratio of the volume occupied by the solids ψV and the volume occupied by the suspension $(1-\phi)V$.) Moreover, we assume that the rise of bubbles and settling of solids is described by given flux functions $J(\phi, z, t)$ and $F(\varphi, \phi, z, t)$, respectively, that involve nonlinear constitutive functions of ϕ and φ and whose precise definition will be made explicit later. The fluxes J and F are discontinuous in z at several positions (namely at $z = z_{\mathrm{U}}$, z_{F}, z_{W} and z_{E}) associated with singular feed sources, the underflow and the effluent, and in general depend on t through the control of in- and -outflows; see Figure 1. The level z_{F} is associated with a singular feed source with nonnegative feed volume fractions of the aggregates ϕ_{F} and solids ψ_{F}. Finally, we consider that the (possibly variable) cross-sectional area at height z is given by $A(z)$. Then the governing PDEs can be written as the system

$$A(z)\frac{\partial \phi}{\partial t} + \frac{\partial}{\partial z}\big(A(z)J(\phi, z, t)\big) = Q_{\mathrm{F}}(t)\phi_{\mathrm{F}}(t)\delta(z - z_{\mathrm{F}}), \tag{2a}$$

$$A(z)\frac{\partial}{\partial t}\big((1-\phi)\varphi\big) - \frac{\partial}{\partial z}\big(A(z)F(\varphi, \phi, z, t)\big) = Q_{\mathrm{F}}(t)\psi_{\mathrm{F}}(t)\delta(z - z_{\mathrm{F}}), \tag{2b}$$

where the right-hand sides of the equations contain the Dirac function. The model is complete with initial conditions $\phi(z, 0) = \phi_0(z)$ and $\psi(z, 0) = \psi_0(z)$ for all $z \in \mathbb{R}$. No boundary conditions are required: the bounds of the vessel at $z = z_{\mathrm{U}}$ and $z = z_{\mathrm{E}}$ are captured by discontinuities of $J(\phi, z, t)$ and $F(\varphi, \phi, z, t)$. Equations (2) have been specified in such a way that away from the feed level, $J(\phi, z, t) > 0$ ($J(\phi, z, t) < 0$) means that at position z and time t, bubbles move upward (downward), while $F(\varphi, \phi, z, t) > 0$ ($F(\varphi, \phi, z, t) < 0$) means that at position z and time t, solid particles move downward (upward).

Related Work

Modelling flotation and developing strategies to control this process are research areas that have generated many contributions. Cruz [36] advanced a dynamic model of flotation with many ingredients, which is also based on the division of the tank into three regions: a collection region, a stabilized froth, and a draining froth. Those models incorporate numerous additional equations for subprocesses that require calibration of further parameters. See also the review by Quintanilla [95] and references therein. The development of control strategies requires dynamic models along with a categorization of steady-state (stationary) solutions of such models. Since the volume fractions depend on both time and space, the resulting governing equations are PDEs. With the aim of developing controllers, the authors of [109, 110] and [4, 5] use hyperbolic systems of PDEs for the froth or pulp regions coupled to ODEs for the lower part of the column. They include the attachment and detachment processes; however, the phases seem to have constant velocities, which is not in agreement with the established drift-flux theory by Wallis [113], see, e.g., [13, 36, 38, 47, 54, 55, 62, 75, 99, 106, 111, 115]. The theory considers the relationships between the nonlinear flux of bubbles relative to the fluid (denoted here the batch drift flux) and the applied bulk flows that arise due to the inlets and outlets of the column that

theory has mostly been used for steady-state investigations of flotation columns [38, 54, 55, 106, 111]. Models of and numerical schemes for column froth flotation with the drift-flux assumption and possibly simultaneous sedimentation have been presented by Bürger et al. [17, 18, 20, 28].

The analogy of the drift-flux theory for sedimentation is the established solids-flux theory [41, 44, 49, 50, 73, 74]. With an additional constitutive assumption on sediment compressibility, the model becomes a second-order degenerate parabolic PDE [29]. Sedimentation in a clarifier-thickener unit is mathematically similar to the column-flotation case. A full PDE model of such a vessel necessarily contains source terms and spatial discontinuities at both inlets and outlets. Steady-state analyses, numerical schemes, dynamic simulations and control of such models can be found in [16, 22, 24–26] and [39–43]. The model of flotation proposed herein is based on this experience. Because of the discontinuous coefficients and degenerate diffusion term of the PDE, so-called entropy conditions are needed to guarantee a unique physically relevant solution [26, 45, 52]. Those results will be utilized in this thesis.

The one-dimensional formulation chosen here has the advantage that only equations for the gas and solids concentrations need to be solved, while two- or three-dimensional formulations invariably require solving additional equations for the flow of the mixture. However, the one-dimensional setting requires to describe the feed mechanism and diverging bulk flows by discontinuities with respect to z in the definitions of F and J. These abrupt changes, in combination with the nonlinearities of these constitutive functions arising from the drift- and solid-flux theories, cause the principal mathematical difficulty for the construction of connections of ϕ, φ and ψ (or ϕ_s) values across jumps in the definitions of F and J. An in-depth discussion of these mathematical issues along with a comprehensive analysis and detailed descriptions on how to obtain and categorize the steady states are given by Bürger et al. [18].

Phenomenological models for two-phase systems with bubbles rising (or, analogously, particles settling) in a liquid, are derived from physical laws of conservation of mass and momentum [6, 13, 29, 30]. Under certain simplifying assumptions on the stress tensor and partial pressure of the bubbles/solids, one can obtain first- or second-order PDEs involving one or two constitutive (material specific) functions, respectively. Tian et al. [109] advance a hyperbolic system that includes the attachment process; however, they assume that the flux functions are linear. In particular, their approach does not constitute an extension of the drift- or solids-flux theories, in contrast to the one presented in this work. While the vast majority of references to flotation processes are related to mineral processing, we mention that flotation processes are also used for removing other small particles, oil droplets, printing ink and organic matter in diverse processes such as wastewater treatment, Rubio et al. [100].

For oil–water separation in wastewater treatment, there exist several induced and dissolved air flotation (DAF) technologies [102]; see also handbook entries [48, 61, 81, 114]. DAF has been used for many years for the thickening of waste activated sludge (WAS) [31, 33, 58]. One of many advantages is that DAF can thicken sludge to concentrations at least a factor two higher than gravity settling [96, 114].

The systems presented in this thesis model the evolution of the primary unknown ϕ independently of the secondary unknown ψ. Various applications of such triangular systems can be found in the literature. Two-component chromatography, which describes the evolution of the concentration of two solutes, can be written as a triangular system; see e.g. Andreianov et al. [1]. Polymer flooding in oil recovery is modelled by a 2×2 system (e.g. [63]), which can be converted to a triangular system in Lagrange coordinates [103]. In [37, 83, 101], the authors study the delta shock wave formation in solutions of triangular system of conservation laws from the so-called generalized pressureless gas dynamics model. Bressan et al. [14] established the existence and uniqueness of vanishing viscosity solutions for scalar conservation laws for a Cauchy problem and their results can be applied to a triangular system under suitable assumptions. The results of Karlsen et al. [64, 67] for general triangular systems can be applied to models of three-phase flows in porous media, for example, in oil-recovery processes.

Numerical simulations were performed with a staggered-grid scheme that utilizes the triangular structure of (2). Such a semi-Godunov scheme for general triangular hyperbolic systems is one of the two suggested schemes by Karlsen et al. [64, 67], who proved convergence of the numerical solutions under certain assumptions on the flux functions. We here propose a simpler numerical scheme (on a single grid) that is easier to implement and analyze. The analysis (of the scheme proposed under simplifying assumptions) relies on the aligned version of the scheme introduced in [67] and in particular on the convergence analysis of an Engquist-Osher scheme for multi-dimensional triangular system of conservation laws by Coclite et al. [34]. These analyses, and the present treatment, rely on compactness techniques that use discrete entropy inequalities and the compensated compactness framework.

A well-known alternative approach to modeling froth flotation is provided by Neethling and Cilliers [89], see also [86–88]. This approach is fundamentally based on microscopical structural properties of the foam as consisting of thin films (lamellae) separating bubbles from each other. Three of these films meet to form so-called Plateau borders that form a branched network of channels through the froth. Without going into detail, the cited works provide an accurate description of the behaviour of froths including coalescence of bubbles, liquid drainage, and motion of attached and non-attached particles through the froth (see [87, 88] for details). Capillarity in the foam effect have been studied intensively by Neethling and Cilliers [89, 90] and Neethling and Brito-Parada [85]; see more references in [95].

Organization of this thesis

The present thesis is organized as follows:

In **Chapter 1**, we present a spatially one-dimensional model for the hydrodynamics of a flotation column based on one continuous phase, the fluid, and two disperse phases: the aggregates, that is, bubbles with attached hydrophobic valuable particles, and the solid particles that form the gangue. A common feed inlet for slurry mixture and gas is considered and the bubbles

are assumed to be fully aggregated with hydrophobic particles as they enter the column. The conservation law of the three phases yields a model expressed as a system of partial differential equations where the nonlinear constitutive flux functions come from the drift-flux and solids-flux theories. In addition, the total flux functions are discontinuous in the spatial (height) coordinate because of two inlets (slurry and wash water) and outlets at the top and bottom. The desired stationary solutions of this model can be characterized by operating charts. A novel numerical method is used for simulations of the hydrodynamics under variable operating conditions such as control actions that drive the process to desired states of operation. The numerical simulations illustrate applications in mineral processing.

The contents of Chapter 1 correspond to the article [20]:

- R. Bürger, S. Diehl, M. C. Martí, Y. Vásquez, Flotation with sedimentation: Steady states and numerical simulation of transient operation, *Min. Eng.* 157 (2020), p.106419.

In **Chapter 2**, we show applications of flotation processes that include dissolved air flotation (DAF) in industrial wastewater treatment and column froth flotation (CFF) in wastewater treatment and mineral processing as we mentioned in Chapter 1. The one-dimensional model is the same mentioned in the previous chapter and an analysis of nonlinear ingredients of the governing equations helps to identify desired steady-state operating conditions, this is detailed for the DAF thickening process. Dynamic simulations are obtained with the previously developed numerical method. Responses to control action are demostrated with scenarios in CFF and DAF.

The contents of Chapter 2 correspond to the article [28]:

- R. Bürger, S. Diehl, M. C. Martí, Y. Vásquez, Simulation and control of dissolved air flotation and column froth flotation with simultaneous sedimentation, *Water Sci. Tech.* 81 (2020), 1723–1732.

In **Chapter 3**, we present a generalization of the model discussed in Chapters 1 and 2 made up of a triangular system of conservation laws with discontinuous flow that arises in the aforementioned applications and explore the mathematical properties of the numerical method. A monotone numerical scheme to approximate solutions to this model is formulated and it is proven that it satisfies an invariant-region property, i.e., the approximate volume fractions of the three phases stay between zero and one. Some numerical examples, along with error and convergence-order estimations, are presented for counter-current and co-current flows of the two disperse phases.

The contents of Chapter 3 correspond to part of the following manuscript [21]:

- R. Bürger, S. Diehl, M. C. Martí, Y. Vásquez, A difference scheme for a triangular system of conservation laws with discontinuous flux modelling three-phase flows, *in preparation*.

In **Chapter 4**, under the assumption of flow in a column with constant cross-sectional area it is shown that the scheme for the primary phase converges to an entropy solution. Under the additional assumption of absence of flux discontinuities it is further demonstrated, by invoking arguments of compensated compactness, that the scheme for the secondary disperse phase converges to a weak solution of the corresponding conservation law.

The contents of Chapter 4 correspond to part of the following manuscript (see **Chapter 3**) [21]:

- R. Bürger, S. Diehl, M. C. Martí, Y. Vásquez, A difference scheme for a triangular system of conservation laws with discontinuous flux modelling three-phase flows, *in preparation*.

In **Chapter 5**, we study the drainage of liquid in the flotation process due to capillarity, which is essential for the formation of a stable froth layer. This effect is included into previously formulated hyperbolic system of partial differential equations used in Chapter 3 that models the volume fractions of floating aggregates and settling hydrophilic solids [18]. The construction of desired steady-state solutions with a froth layer is detailed and feasibility conditions on the feed volume fractions and the volumetric flows of feed, underflow and wash water are visualized in so-called operating charts. A monotone numerical scheme is derived and employed to simulate the dynamic behaviour of a flotation column. It is also proven that, under a suitable Courant-Friedrichs-Lewy (CFL) condition, the approximate volume fractions are bounded between zero and one when the initial data are.

The contents of Chapter 5 correspond to the following submitted manuscript [19]:

- R. Bürger, S. Diehl, M. C. Martí, Y. Vásquez, A degenerating convection-diffusion system modelling froth flotation with drainage *Centro de Investigación en Ingeniería Matemática (CI^{2}MA)*, Preprint 2022, Universidad de Concepción, Chile 2022.

Introducción

Motivación

La flotación por espuma se usa comúnmente en el procesamiento de minerales para la recuperación de minerales valiosos, como cobre y minerales que contienen plomo, a partir de minerales de baja ley; y en el tratamiento de aguas residuales industriales para eliminar contaminantes que de otro modo serían difíciles de separar como sólidos flotantes, productos químicos residuales y gotitas de aceite y grasa. Este proceso separa selectivamente los materiales hidrofóbicos (que son repelidos por el agua) de los hidrofílicos (que serían atraídos por el agua), donde ambos quedan suspendidos en un fluido viscoso. Es bien sabido que este proceso de separación físico-químico funciona más o menos de la siguiente manera: el gas se introduce cerca del fondo de una columna y las burbujas generadas ascienden hacia arriba por toda la pulpa que contiene las partículas sólidas, que se pueden dividir en dos grupos principales. Las partćulas hidrofóbicas (minerales o menas que deben recuperarse) se adhieren a las burbujas que flotan a la parte superior de la columna, formando una capa espuma que transporta el material valioso que generalmente se remueve a través de un lavado. Por otro lado, las partículas hidrofílicas (limos o ganga) no se adhieren a las burbujas, sino que sedimentan en el fondo del recipiente, a menos que queden atrapadas en el flujo ascendente a granel. Cerca de la parte superior, se puede inyectar agua de lavado adicional para ayudar con el rechazo de las impurezas arrastradas [111] y para aumentar la estabilidad de la espuma y mejorar la recuperación [53,91]. Por lo tanto, modelos matemáticos son necesarios para el diseño, simulación y eventual control de columnas de flotación.

Motivado por [38,54,106], Bürger y compañía [17] presentaron un modelo uni-dimensional de dos fases donde se describe solo el movimiento de las burbujas de gas y el fluido. La columna de flotación modelada en ese trabajo tiene una entrada de gas separada cerca del fondo, la cual es comúnmente usada en el procesamiento de minerales de modo que se crea una zona de colección en la cual las partículas hidrofóbicas se adhieren a las burbujas de gas dentro de la columna. Otros dispositivos tienen una entrada de alimentación común tanto para lodos como para las burbujas de gas, de modo que el proceso de agregación (la unión de partículas hidrofóbicas a las burbujas) ocurre principalmente en la tubería de entrada. (Estas variantes se ilustran, por ejemplo, en la Figura 1 de [18]). Aquí, modelamos una columna de este tipo (ver Figura 1) y

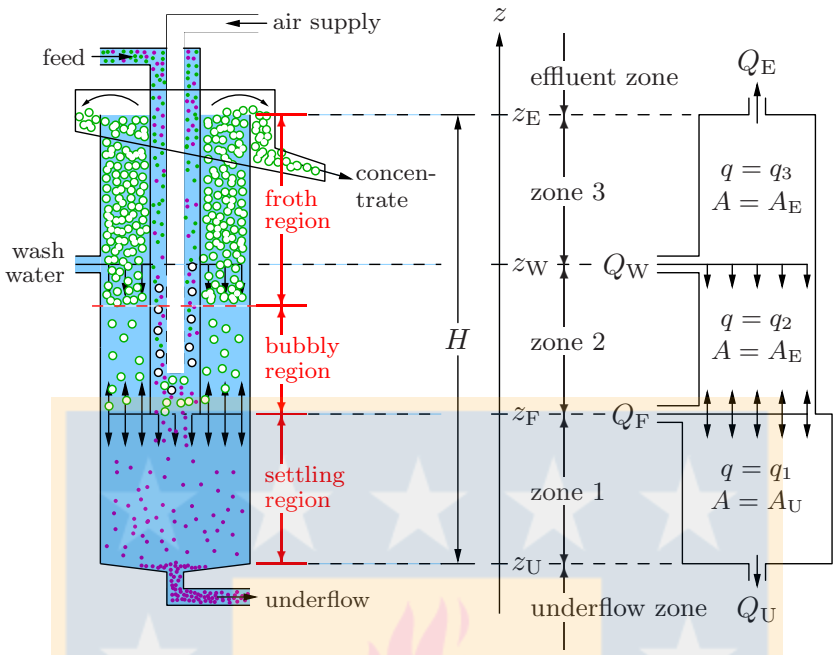

Figure 1: Izquierda: Esquema de una columna de flotación con área de sección transversal no constante $A(z)$ (A_U por debajo y A_E por encima del nivel de alimentación) utilizada para simulaciones numéricas en esta tesis (**Capítulos 1–4**). Derecha: modelo conceptual unidimensional correspondiente. La unidad se alimenta con agua de lavado en el nivel $z = z_W$ y una mezcla de agregados y lodos de alimentación en $z = z_F$, donde $z_U < z_F < z_W < z_E$ divide la línea real en las zonas dentro de la columna y las zonas de subdesbordamiento y efluentes. Los flujos volumétricos corresponden a la inyección de agua de lavado ($Q_W \geq 0$) y lodo de alimentación ($Q_F > 0$). Se supone que estas cantidades y la tasa de subdesbordamiento volumétrico $Q_U \geq 0$ se eligen de tal manera que el desbordamiento volumétrico del efluente $Q_E = Q_W + Q_F - Q_U$ es no negativo, $Q_E \geq 0$.

asumimos que las burbujas están completamente cargadas con partículas hidrofóbicas cuando la mezcla ingresa a la columna, de modo que el proceso de agregación concluye cuando las partículas y las burbujas ingresan a la columna.

La ecuación gobernante del modelo de dos fases estudiado por [17] es una ecuación diferencial parcial (EDP) de primer orden escalar, cuasi-lineal (conocida como ley de conservación; véase, por ejemplo, [60] o [77] para el antecedente). Un ingrediente no estándar de ese modelo es una función de flujo que es discontinua en varias posiciones espaciales debido a las fuentes de alimentación de gas, lodo y agua de lavado, y las salidas inferior y superior de relaves y concentrado. Esa formulación se amplió recientemente en [18] a un modelo de tres fases que también incluye la sedimentación de partículas sólidas dentro de la columna de flotación. El flujo trifásico de sólidos, gas (burbujas o agregados) y fluido se modela en una dimensión espacial. Aquí utilizamos el mismo modelo de [18] y presentamos nuevos resultados numéricos

relevantes para las aplicaciones.

Para enunciar las EDPs gobernantes de nuestro enfoque, suponemos que las variables independientes son el tiempo $t \geq 0$ y la altura z, es decir, z es una coordenada espacial escalar que aumenta en dirección ascendente, y que las incógnitas son la fracción de volumen de los agregados $\phi = \phi(z,t)$ y la fracción de volumen de los sólidos en la suspensión sólido-líquido $\varphi = \varphi(z,t)$, donde

$$\varphi = \frac{\psi}{1-\phi}, \tag{1}$$

donde $\psi = \psi(z,t)$ es la fracción de volumen de sólidos (hidrofílicos) y $1-\phi = 1-\phi(z,t)$ es la fracción de volumen de la suspensión fuera de los agregados. (La ecuación 1 significa que si se da un volumen pequeño V, entonces φ es la relación local del volumen ocupado por los sólidos ψV y el volumen ocupado por la suspensión $(1-\phi)V$.) Además, asumimos que el ascenso de las burbujas y el asentamiento de los sólidos se describe mediante funciones de flujo dadas $J(\phi,z,t)$ y $F(\varphi,\phi,z,t)$, respectivamente, que involucran funciones constitutivas no lineales de ϕ y φ y cuya definición precisa se explicitará más adelante. Los flujos J y F son discontinuos en z en varias posiciones (es decir, en $z = z_{\mathrm{U}}$, z_{F}, z_{W} y z_{E}) asociados con fuentes de alimentación singulares, el flujo inferior y el efluente, y en general dependen de t a través del control de flujos de entrada y salida ; ver Figura 1. El nivel z_{F} está asociado con una fuente de alimentación única con fracciones de volumen de alimentación no negativas de los agregados ϕ_{F} y sólidos ψ_{F}. Finalmente, consideramos que el área de sección transversal (posiblemente variable) en la altura z viene dada por $A(z)$. Entonces las EDPs gobernantes se pueden escribir como el sistema

$$A(z)\frac{\partial \phi}{\partial t} + \frac{\partial}{\partial z}\big(A(z)J(\phi,z,t)\big) = Q_{\mathrm{F}}(t)\phi_{\mathrm{F}}(t)\delta(z-z_{\mathrm{F}}), \tag{2a}$$

$$A(z)\frac{\partial}{\partial t}\big((1-\phi)\varphi\big) - \frac{\partial}{\partial z}\big(A(z)F(\varphi,\phi,z,t)\big) = Q_{\mathrm{F}}(t)\psi_{\mathrm{F}}(t)\delta(z-z_{\mathrm{F}}), \tag{2b}$$

donde los lados derechos de las ecuaciones contienen la función de Dirac. El modelo se completa con las condiciones iniciales $\phi(z,0) = \phi_0(z)$ y $\psi(z,0) = \psi_0(z)$ para todo $z \in \mathbb{R}$. No se requieren condiciones de contorno: los límites del recipiente en $z = z_{\mathrm{U}}$ y $z = z_{\mathrm{E}}$ son capturados por discontinuidades de $J(\phi,z,t)$ y $F(\varphi,\phi,z,t)$. Las ecuaciones (2) se han especificado de tal manera que fuera del nivel de alimentación, $J(\phi,z,t) > 0$ ($J(\phi,z,t) < 0$) significa que en la posición z y en el tiempo t, las burbujas se mueven hacia arriba (hacia abajo), mientras que $F(\varphi,\phi,z,t) > 0$ ($F(\varphi,\phi,z,t) < 0$) significa que en la posición z y en el tiempo t, las partículas sólidas se mueven hacia abajo (hacia arriba).

Trabajo relacionado

Modelar la flotación y desarrollar estrategias para controlar este proceso son áreas de investigación que han generado muchas contribuciones; Cruz [36] propuso un modelo de flotación

con muchos ingredientes, que también se basa en dividir el tanque en tres regiones: una región de recolección, una de espuma estabilizada y una espuma de drenaje. Esos modelos incorporan numerosas ecuaciones adicionales para subprocesos que requieren calibración de otros parámetros. Véase la recopilación hecha por Quintanilla en [95] y las referencias que contiene. El desarrollo de estrategias de control requiere modelos dinámicos junto con una categorización de soluciones de estado estacionario de tales modelos. Dado que las fracciones de volumen dependen tanto del tiempo como del espacio, las ecuaciones gobernantes resultantes son EDPs. Con el objetivo de desarrollar controladores, los autores de [109, 110] y [4, 5] utilizan sistemas hiperbólicos de EDPs para las regiones de espuma o pulpa acopladas a ecuaciones diferenciales ordinarias para la parte inferior de la columna. Incluyen los procesos de adhesión y no adhesión a las burbujas; sin embargo, las fases parecen tener velocidades constantes, lo que no está en acuerdo con la teoría del flujo de deriva establecida por Wallis [113], véase, por ejemplo, [13, 36, 38, 47, 54, 55, 62, 75, 99, 106, 111, 115]. La teoría considera las relaciones entre el flujo no lineal de burbujas relativo al fluido (denotado aquí el flujo de deriva del lote) y los flujos a granel aplicados que surgen debido a las entradas y salidas de la columna; esta teoría se ha utilizado principalmente para investigaciones de estado estacionario en columnas de flotación [38, 54, 55, 106, 111]. Bürger y compañía [17, 18, 20, 28] han presentado modelos y esquemas numéricos para la flotación por espuma de columnas con el supuesto de flujo de deriva y posiblemente sedimentación simultánea.

La analogía de la teoría del flujo de deriva para la sedimentación establece la teoría del flujo de sólidos [41, 44, 49, 50, 73, 74]. Con una suposición constitutiva adicional sobre la compresibilidad de los sedimentos, el modelo se convierte en una EDP parabólica degenerada de segundo orden [29]. La sedimentación en una unidad clarificador-espesador es matemáticamente similar al caso de flotación en una columna. Un modelo EDP completo de tal recipiente necesariamente contiene términos fuente y discontinuidades espaciales tanto en las entradas como en las salidas. Los análisis de estado estacionario, los esquemas numéricos, las simulaciones dinámicas y el control de tales modelos se pueden encontrar en [16, 22, 24–26] y [39–43]. El modelo de flotación que aquí se propone se basa en esta experiencia. Debido a los coeficientes discontinuos y al término de difusión degenerado de la EDP, se necesitan las llamadas condiciones de entropía para garantizar una solución única físicamente relevante [26, 45, 52]. Esos resultados serán utilizados en esta tesis.

La formulación unidimensional escogida aquí tiene la ventaja de que solo es necesario resolver ecuaciones para las concentraciones de gas y sólidos, mientras que las formulaciones bidimensionales o tridimensionales invariablemente requieren resolver ecuaciones adicionales para el flujo de la mezcla. Sin embargo, la configuración unidimensional requiere describir el mecanismo de alimentación y los flujos a granel divergentes, por discontinuidades con respecto a z en las definiciones de F y J. Estos cambios abruptos, en combinación con las no linealidades de estas funciones constitutivas que surgen de las teorías de flujo de deriva y flujo de sólidos, causan la principal dificultad matemática para la construcción de conexiones de los valores ϕ, φ y ϕ_s a través de saltos en las definiciones de F y J. El análisis y las descripciones detalladas sobre

cómo obtener y categorizar los estados estacionarios se dan por Bürger y compañía en [18].

Los modelos fenomenológicos para sistemas de dos fases con burbujas que ascienden (o, de manera análoga, partículas que sedimentan) en un líquido, se derivan de las leyes físicas de conservación de la masa y el momento [6, 13, 29, 30]. Bajo ciertas suposiciones simplificadoras sobre el tensor de tensión y la presión parcial de las burbujas/sólidos, se pueden obtener EDPs de primer o segundo orden que involucran una o dos funciones constitutivas (específicas del material), respectivamente. Tian et al. [109] anticipa un sistema hiperbólico que incluye el proceso de adhesión; sin embargo, asume que las funciones de flujo son lineales. En particular, su enfoque no constituye una extensión de las teorías del flujo de deriva o del flujo de sólidos, en contraste con el nuestro. Si bien la gran mayoría de las referencias a los procesos de flotación están relacionadas con el procesamiento de minerales, mencionamos que los procesos de flotación también se utilizan para eliminar otras partículas pequeñas, gotas de aceite, tinta de impresión y materia orgánica en diversos procesos, como el tratamiento de aguas servidas, Rubio y compañía [100].

Para la separación de agua y aceite en el tratamiento de aguas residuales, existen varias tecnologías de flotación por aire disuelto (DAF, por sus siglas en inglés) e inducido [102]; véanse también [48, 61, 81, 114]. La flotación por aire disuelto se ha utilizado durante muchos años para el espesamiento de lodos residuales activados (WAS) [31, 33, 58]. Una de las muchas ventajas es que la flotación por aire disuelto (DAF) puede espesar el lodo a concentraciones de al menos un factor dos veces más alto que la sedimentación por gravedad [96, 114].

Los sistemas presentados en esta tesis modelan la evolución de la incógnita primaria ϕ independientemente de la incógnita secundaria ψ. Varias aplicaciones de tales sistemas triangulares se pueden encontrar en la literatura. La cromatografía de dos componentes, que describe la evolución de la concentración de dos solutos, se puede escribir como un sistema triangular; ver por ejemplo Andreianov y compañía [1]. El crecimiento de polímeros en la recuperación de petróleo se modela mediante un sistema 2×2 (por ejemplo, [63]), que se puede convertir en un sistema triangular en coordenadas de Lagrange [103]. En [37, 83, 101], los autores estudian la formación de "delta shock wave" en soluciones de un sistema triangular de leyes de conservación del llamado modelo de dinámica de gas sin presión generalizada. Bressan y compañía [14] estableció la existencia y unicidad de soluciones de viscosidad nula para leyes de conservación escalares para un problema de Cauchy y sus resultados se pueden aplicar a un sistema triangular bajo suposiciones adecuadas. Los resultados de Karlsen y colaboradores [64, 67] para sistemas triangulares generales se pueden aplicar a modelos de flujos trifásicos en medios porosos, por ejemplo, en procesos de recuperación de petróleo.

Las simulaciones numéricas se realizaron con un esquema de malla escalonada que utiliza la estructura triangular de (2). Tal esquema semi-Godunov para sistemas hiperbólicos triangulares generales es uno de los dos esquemas sugeridos por Karlsen y colaboradores [64, 67], quienes demostraron la convergencia de las soluciones numéricas bajo ciertas suposiciones sobre las funciones de flujo. Aquí proponemos un esquema numérico más simple (en una sola

malla) que es más fácil de implementar y analizar. El análisis (del esquema propuesto bajo supuestos simplificadores) se basa en la versión alineada del esquema presentado en [67] y en particular en el análisis de convergencia de un esquema de Engquist-Osher para un sistema triangular multi-dimensional de leyes de conservación por Coclite et al. [34]. Estos análisis, y el presente tratamiento, se basan en técnicas de compacidad que utilizan desigualdades de entropía discretas y el marco de compacidad compensada.

Neethling y Cilliers [89] proporcionan un enfoque alternativo para modelar la flotación por espuma, véase también [86–88]. Este enfoque se basa fundamentalmente en las propiedades estructurales microscópicas de la espuma que consiste en películas delgadas (laminillas) que separan las burbujas entre sí. Tres de estas películas se unen para formar los llamados bordes de meseta que forman una red ramificada de canales a través de la espuma. Sin entrar en detalles, los trabajos citados brindan una descripción precisa del comportamiento de las espumas, incluida la coalescencia de las burbujas, el drenaje de líquidos y el movimiento de partículas adheridas y no adheridas a través de la espuma (ver [87,88] para más detalles). La capilaridad en el efecto espuma ha sido estudiada intensamente por Neethling y Cilliers [89,90] y Neethling y Brito-Parada [85]; ver más referencias en [95].

Organización de esta tesis

La presente tesis se organiza como sigue:

En el **Capítulo 1**, presentamos un modelo espacialmente unidimensional para la hidrodinámica de una columna de flotación basado en una fase continua, la fluida y dos fases dispersas: los agregados, es decir, burbujas cargadas con partículas valiosas hidrofóbicas, y las partículas sólidas que forman la ganga. Se considera una entrada común de alimentación para la mezcla de suspensión y gas y se supone que las burbujas están completamente agregadas con partículas hidrofóbicas a medida que ingresan a la columna. La ley de conservación de las tres fases produce un modelo expresado como un sistema de ecuaciones diferenciales parciales donde las funciones de flujo constitutivas no lineales provienen de las teorías de flujo de deriva y flujo de sólidos. Además, las funciones de flujo total son discontinuas en la coordenada espacial (altura) debido a dos entradas (lodo y agua de lavado) y salidas en la parte superior e inferior. Las soluciones estacionarias deseadas de este modelo se pueden caracterizar mediante gráficos operativos. Se utiliza un método numérico novedoso para simulaciones de la hidrodinámica bajo condiciones de operación variables, como acciones de control que conducen el proceso a los estados de operación deseados. Las simulaciones numéricas ilustran aplicaciones en el procesamiento de minerales.

Los contenidos del **Capítulo 1** corresponden al artículo [20]:

- R. Bürger, S. Diehl, M. C. Martí, Y. Vásquez, Flotation with sedimentation: Steady states and numerical simulation of transient operation, *Min. Eng.* 157 (2020), p.106419.

En el **Capítulo 2**, mostramos las aplicaciones del proceso de flotación que incluyen la flotación por aire disuelto (DAF) en el tratamiento de aguas residuales industriales y la flotación por espuma de columna (CFF, *column froth flotation*) en el tratamiento de aguas residuales y el procesamiento de minerales, como mencionamos en el Capítulo 1. El modelo unidimensional es el mismo mencionado en el capítulo anterior y un análisis de los ingredientes no lineales de las ecuaciones gobernantes ayuda a identificar las condiciones operativas de estados estacionarios deseados, esto se detalla para el proceso de espesamiento DAF. Las simulaciones dinámicas se obtienen con el método numérico desarrollado anteriormente. Las respuestas a la acción de control se demuestran con escenarios en CFF y DAF.

Los contenidos del **Capítulo 2** corresponden al artículo [28]:

- R. Bürger, S. Diehl, M. C. Martí, Y. Vásquez, Simulation and control of dissolved air flotation and column froth flotation with simultaneous sedimentation, *Water Sci. Tech.* 81 (2020), 1723–1732.

En el **Capítulo 3**, presentamos una generalización del modelo discutido en los Capítulos 1 y 2 compuesto por un sistema triangular de leyes de conservación con flujo discontinuo que surge en las aplicaciones antes mencionadas y exploramos las propiedades matemáticas del método numérico. Se formula un esquema numérico monótono para aproximar soluciones a este modelo y se prueba que satisface la propiedad de región invariante, es decir, las fracciones de volumen aproximadas de las tres fases se mantienen entre cero y uno. Se presentan algunos ejemplos numéricos, junto con estimaciones de error y orden de convergencia, para flujos en contracorriente y co-corriente de las dos fases dispersas.

El contenido del Capítulo 3 corresponde a parte del siguiente manuscrito [21]:

- R. Bürger, S. Diehl, M. C. Martí, Y. Vásquez, A difference scheme for a triangular system of conservation laws with discontinuous flux modelling three-phase flows, *in preparation*.

En el **Capítulo 4**, bajo el supuesto de flujo en una columna con área de sección transversal constante, se muestra que el esquema para la fase primaria converge a una solución de entropía. Bajo el supuesto adicional de ausencia de discontinuidades de flujo, se demuestra además, invocando argumentos de compacidad compensada, que el esquema para la fase dispersa secundaria converge a una solución débil de la ley de conservación correspondiente.

El contenido del Capítulo 4 corresponde a parte del siguiente manuscrito (ver **Capítulo 3**) [21]:

- R. Bürger, S. Diehl, M. C. Martí, Y. Vásquez, A difference scheme for a triangular system of conservation laws with discontinuous flux modelling three-phase flows, *in preparation*.

En el **Capítulo 5**, estudiamos el drenaje de líquido en el proceso de flotación debido a que la capilaridad es fundamental para la formación de una capa de espuma estable. Este efecto se incluye en un sistema hiperbólico de ecuaciones diferenciales parciales previamente formulado que se usa en el Capítulo 3 que modela las fracciones de volumen de agregados flotantes y sedimentación de sólidos hidrofílicos [R. Bürger, S. Diehl y M.C. Martí, IMA J. Appl. Math. 84 (2019) 930–973]. Se detalla la construcción de las soluciones de estado estacionario deseados con una capa de espuma y se visualizan las condiciones de viabilidad en las fracciones de volumen de alimentación y los flujos volumétricos de alimentación, subdesbordamiento y agua de lavado en los llamados gráficos operativos. Se deriva y emplea un esquema numérico monótono para simular el comportamiento dinámico de una columna de flotación. También se demuestra que, bajo una condición adecuada de Courant-Friedrichs-Lewy (CFL), las fracciones de volumen aproximadas están acotadas entre cero y uno cuando los datos iniciales lo están.

El contenido del Capítulo 5 corresponde al siguiente manuscrito sometido [19]:

- R. Bürger, S. Diehl, M. C. Martí, Y. Vásquez, A degenerating convection-diffusion system modelling froth flotation with drainage *Centro de Investigación en Ingeniería Matemática (CI^2MA)*, Preprint 2022, Universidad de Concepción, Chile 2022.

CHAPTER 1

Flotation with sedimentation: steady states and numerical simulation of transient operation

1.1 Introduction

1.1.1 Scope

In this chapter, we summarize from [18] the derivation of the governing triangular PDE system (2), present a new numerical method, and give examples on control actions for obtaining desired steady states. These are time-independent (stationary) solutions of (2). Among the variety of theoretically possible steady states we select those for discussion that are most relevant for practical applications, namely those that have a high concentration of aggregates at the top, the foam and no bubbles at the lower part of the column, and conversely for the solids gangue. These steady states represent the stationary modes of operation of a flotation column without changing control parameters. It turns out that such desired steady states need some wash water to be injected, i.e., $Q_{\mathrm{W}} > 0$. We provide conditions (for steady-state operation) on how much wash water can be used for the process to be efficient, i.e., how much can flow down through the foam. Applying more wash water will only mean that it is wasted through the effluent.

Both transient and stationary solutions have layers of different concentrations of bubbles (foam) and particles separated by discontinuities in concentration. Equation (2a) depends only on the unknown ϕ. Our approach is to solve each equation locally as a scalar conservation law with discontinuous flux. The feasible steady states relevant for operation in real applications can be visualized by so-called *operating charts* that illustrate the necessary constraints for the control of the volumetric flows.

We present here a new numerical scheme for (2), which is easier to implement than the one presented by [18]. The numerical scheme produces approximate solutions that take physically relevant values only (volume fractions between zero and one). It is the purpose of this chapter to demonstrate that the model and numerical scheme provide a useful tool for the simulation

of the operation of a flotation column in the case of a common feed inlet of the three phases and when no aggregation occurs in the column. In particular, responses of the unit to changes in operating conditions (such as the rates and composition of feed flows) are illustrated.

1.1.2 Outline of the chapter

The remainder of the chapter is organized as follows. The mathematical model is outlined in Section 1.2, starting with some general assumptions (in Section 1.2.1) and a description of the batch-drift and batch-settling flux functions (Section 1.2.2), which introduce nonlinearity into the fluxes J and F. Then, in Section 1.2.3, we outline the derivation of the governing equations (2) from the conservation of mass equations of the gas (aggregates), the solid and the fluid. The existence of stationary and transient solutions depends on geometric properties of the nonlinear flux functions, such as the locations of extrema and inflection points, which are outlined in Section 1.2.4. In Section 1.2.5 we briefly comment on the condition imposed at the effluent level z_{E}. In Section 1.3, the desired steady states and their characterization are presented. We extract in Section 1.3.1 the most interesting and usable results. The most desired steady states and their *operating charts* for given values on ϕ_{F} and ψ_{F} are presented in Section 1.3.2. The new numerical scheme is summarized in Section 1.4. In Section 1.5, we present numerical solutions of (2) that illustrate the transient behaviour of the model. After stating some preliminaries (in Section 1.5), we present in Sections 1.5.2 to 1.5.3 two examples of simulations that illustrate the model predictions, in particular the formation of and transitions between steady states and the response of the system to changes of operating conditions.

1.2 Mathematical model

1.2.1 Assumptions

Figure 1 shows the flotation column studied in this chapter and introduces the distinguished heights z_{U}, z_{F}, z_{W} and z_{E} along with the associated volume flows Q_{U}, Q_{F}, Q_{W} and Q_{E}. The volumetric feed flows of wash water, $Q_{\mathrm{W}} \geq 0$, and of feed slurry, $Q_{\mathrm{F}} > 0$, are given functions of time, as is the volumetric underflow rate $Q_{\mathrm{U}} \geq 0$. The resulting effluent volumetric overflow $Q_{\mathrm{E}} = Q_{\mathrm{W}} + Q_{\mathrm{F}} - Q_{\mathrm{U}}$ is assumed to be nonnegative, $Q_{\mathrm{E}} \geq 0$, so that the mixture is conserved and the vessel is always completely filled with mixture.

To model a feed inlet pipe located in the upper part and centre of a cylindrical column, the cross-sectional area $A = A(z)$ is assumed to have a discontinuity at the feed inlet (Figure 1):

$$A(z) := \begin{cases} A_{\mathrm{E}} & \text{for } z \geq z_{\mathrm{F}}, \\ A_{\mathrm{U}} & \text{for } z < z_{\mathrm{F}}, \end{cases} \quad \text{where } A_{\mathrm{E}} \leq A_{\mathrm{U}}. \tag{1.1}$$

We mention that our numerical method can handle any other variation in the cross-sectional area, for example, a conical bottom.

We distinguish three phases: the *fluid phase* (index f), the *solid phase* (index s), which models solid particles that are suspended in the fluid, and the *aggregate phase* (index a), which models gas bubbles fully loaded with hydrophobic particles. We let $\phi_i = \phi_i(z,t)$ denote the volume fraction of phase $i \in \{\mathrm{a},\mathrm{f},\mathrm{s}\}$, where $\phi_\mathrm{a} + \phi_\mathrm{f} + \phi_\mathrm{s} \equiv 1$. The maximum volume fraction for any phase is one. In what follows, we will use the simpler notation $\phi := \phi_\mathrm{a}$ and $\psi := \phi_\mathrm{s}$; cf. (2). Furthermore, we assume constant phase densities $\rho_\mathrm{a} < \rho_\mathrm{f} < \rho_\mathrm{s}$, consistently with the assumption that bubbles rise (float) and particles settle (sink). Finally, the aggregate bubbles and the solid particles are assumed to be monosized. We also suppose that gas bubbles do not coalesce or break.

1.2.2 Batch-drift- and batch-settling-flux functions

The drift-flux and the solids-flux theories stipulate a batch-drift-flux function $j_\mathrm{b}(\phi)$ and a batch-settling-flux function $f_\mathrm{b}(\varphi)$, respectively:

$$j_\mathrm{b}(\phi) = \phi v_{\mathrm{term,a}} V_\mathrm{a}(\phi), \tag{1.2}$$

$$f_\mathrm{b}(\varphi) = \varphi v_{\mathrm{term,s}} V_\mathrm{s}(\varphi), \tag{1.3}$$

where $v_{\mathrm{term,a}}$ and $v_{\mathrm{term,s}}$ are the terminal velocities of a single aggregate and a single solid particle, respectively, in an unbounded fluid, and V_a and V_s are dimensionless hindered bubbling and settling functions, respectively. The fluxes $j_\mathrm{b}(\phi)$ and $f_\mathrm{b}(\varphi)$ express the movement ("drift") of bubbles relative to the bulk motion of the solid-fluid-gas mixture and the movement of solid particles relative to the motion of the solid-fluid suspension that fills the interstices between the gas bubbles, respectively. The discussion of the velocities $v_{\mathrm{term,a}}$ and $v_{\mathrm{term,s}}$ is beyond our focus (but see Stevenson et al., 2008 [106]); here it suffices to assume that $v_{\mathrm{term,a}} > 0$ and $v_{\mathrm{term,s}} > 0$ are set constants for a given material. (Both these constants are assumed positive while aggregates usually float upward and solid particles settle downward. That these directions are opposed will eventually be handled by the different signs associated with the $\partial/\partial z(\dots)$ terms in (2a) and (2b), respectively.)

The functions j_b and f_b are assumed to have the same qualitative properties, namely $j_\mathrm{b}(0) = j_\mathrm{b}(1) = 0$, and we assume that there exists precisely one inflection point ϕ_infl such that $j_\mathrm{b}''(\phi) < 0$ for $0 < \phi < \phi_\mathrm{infl}$ and $j_\mathrm{b}''(\phi) > 0$ for $\phi_\mathrm{infl} < \phi < 1$. We also assume that $j_\mathrm{b}'(1) = 0$. In particular, these assumptions are satisfied for the fluxes (1.2) and (1.3) and the functions V_a and V_s given by the Richardson-Zaki (1954) expression

$$\begin{aligned} V_\mathrm{a}(\phi) &= (1-\phi)^{n_\mathrm{a}} \quad \text{for } 0 \le \phi \le 1,\ n_\mathrm{a} > 1, \\ V_\mathrm{s}(\varphi) &= (1-\varphi)^{n_\mathrm{s}} \quad \text{for } 0 \le \varphi \le 1,\ n_\mathrm{s} > 1. \end{aligned} \tag{1.4}$$

Realistic values of the parameter n_a range from 2 to 3.2 [38, 54, 91, 111]. We use $n_\mathrm{a} = 3.2$ and $v_{\mathrm{term,a}} = 2.7\,\mathrm{cm/s}$ for all plots and simulations in the present chapter along with $n_\mathrm{s} = 2.5$ [38]

and $v_{\text{term,s}} = 0.5\,\text{cm/s}$. That said, we emphasize that our approach is by no means tied to the use of the functions (1.4) and these parameters; other functions could be used as long as the resulting functions j_b and f_b have the properties stated above.

Inside the column, the aggregates and hydrophilic solids are transported by both the local bulk flow and the batch fluxes relative to the bulk flow. Outside the flotation column, we assume that all three phases have the same velocity, i.e., the particles are transported only by the bulk flow. Mathematically, this means that our problem can be defined on the real line z with batch fluxes j_b and f_b present only for $z_\text{U} < z < z_\text{E}$.

1.2.3 Governing equations

Conservation of mass for each phase implies the following system of balance equations,

$$\frac{\partial}{\partial t}\big(A(z)\phi\big) + \frac{\partial}{\partial z}\big(A(z)\phi v_\text{a}\big) = Q_\text{F}\phi_\text{F}\delta(z - z_\text{F}), \tag{1.5}$$

$$\frac{\partial}{\partial t}\big(A(z)\psi\big) + \frac{\partial}{\partial z}\big(A(z)\psi v_\text{s}\big) = Q_\text{F}\psi_\text{F}\delta(z - z_\text{F}), \tag{1.6}$$

$$\frac{\partial}{\partial t}\big(A(z)\phi_\text{f}\big) + \frac{\partial}{\partial z}\big(A(z)\phi_\text{f} v_\text{f}\big) = Q_\text{F}\phi_{\text{f,F}}\delta(z - z_\text{F}) + Q_\text{W}\phi_{\text{f,W}}\delta(z - z_\text{W}), \tag{1.7}$$

where the right-hand sides contain Dirac functions, volumetric flows and the incoming volume fractions of aggregates ϕ_F, solids ψ_F and fluid $\phi_{\text{f,W}} \equiv 1$. We assume that $\phi_\text{F} + \psi_\text{F} + \phi_{\text{f,F}} \equiv 1$ with $0 < \phi_\text{F}, \psi_\text{F}, \phi_{\text{f,F}} < 1$. In terms of the volume-average velocity, or bulk velocity, of the mixture $q := \phi v_\text{a} + \psi v_\text{s} + \phi_\text{f} v_\text{f}$, the sum of (1.5)–(1.7) can be written as

$$\frac{\partial}{\partial z}\big(A(z)q\big) = Q_\text{F}\delta(z - z_\text{F}) + Q_\text{W}\delta(z - z_\text{W}). \tag{1.8}$$

Consequently, in the flotation column, q varies with height z because of the two inlet flows and (1.1). Since $A(z)q(z,t) = -Q_\text{U}(t)$ for $z < z_\text{F}$, we can integrate (1.8) to obtain

$$q(z,t) = \begin{cases} q_1 := -Q_\text{U}/A_\text{U} & \text{in the underflow zone and zone 1,} \\ q_2 := (-Q_\text{U} + Q_\text{F})/A_\text{E} & \text{in zone 2,} \\ q_3 := (-Q_\text{U} + Q_\text{F} + Q_\text{W})/A_\text{E} & \text{in zone 3 and the effluent zone.} \end{cases} \tag{1.9}$$

Hence, this identity replaces (1.7). We recall that $Q_\text{U} \geq 0$, $Q_\text{F} > 0$, and $Q_\text{W} \geq 0$, with the additional assumption that $Q_\text{E} = Q_\text{W} + Q_\text{F} - Q_\text{U} \geq 0$ (see Section 1.2.1), such that $q_1 \leq 0$, q_2 may have either sign, and $q_3 \geq 0$.

We may now rewrite the fluxes ϕv_a and ψv_s in (1.5) and (1.6) in terms of q and the two constitutive functions j_b and f_b, and obtain the following expressions inside the vessel:

$$\begin{aligned} \phi v_\text{a} &= \phi q + j_\text{b}(\phi) =: J(\phi, z, t), \\ \psi v_\text{s} &= (1-\phi)\varphi q - (1-\phi) f_\text{b}(\varphi) - \varphi j_\text{b}(\phi) =: -F(\varphi, \phi, z, t), \end{aligned} \tag{1.10}$$

where the minus sign is to have F positive in the direction of sedimentation. (A full derivation of (1.10), based on appropriate definitions of relative velocities, is provided in [18].) Inserting these expressions into (1.5) and (1.6) we get a system of PDEs in a zone *within* the vessel. With the assumptions in Section 1.2.2 that all relative velocities are zero outside the vessel, i.e., in the effluent and underflow zones of the mathematical model, the relative fluxes j_b and f_b are set to zero there. We can now state the total flux functions of the model (2). The total flux function of the first equation (2a) is given by

$$J(\phi,z,t) = \begin{cases} j_\mathrm{E}(\phi,t) := q_3(t)\phi & \text{in the effluent zone,} \\ j_3(\phi,t) := q_3(t)\phi + j_\mathrm{b}(\phi) & \text{in zone 3,} \\ j_2(\phi,t) := q_2(t)\phi + j_\mathrm{b}(\phi) & \text{in zone 2,} \\ j_1(\phi,t) := q_1(t)\phi + j_\mathrm{b}(\phi) & \text{in zone 1,} \\ j_\mathrm{U}(\phi,t) := q_1(t)\phi & \text{in the underflow zone.} \end{cases} \tag{1.11}$$

In zone k, the aggregate flux j_k (positive upwards) consists of the hindered drift-flux j_b relative to the bulk flow and the bulk flow component $q_k\phi$. The total flux function in (2b) is given by

$$F(\varphi,\phi,z,t) = \begin{cases} f_\mathrm{E}(\varphi,\phi,t) := -(1-\phi)q_3(t)\varphi & \text{in the effluent zone,} \\ f_3(\varphi,\phi,t) & \text{in zone 3,} \\ f_2(\varphi,\phi,t) & \text{in zone 2,} \\ f_1(\varphi,\phi,t) & \text{in zone 1,} \\ f_\mathrm{U}(\varphi,\phi,t) := -(1-\phi)q_1(t)\varphi & \text{in the underflow zone,} \end{cases} \tag{1.12}$$

where the zone fluxes (positive downwards) are given by

$$\begin{aligned} f_k(\varphi,\phi,t) :=& (1-\phi)f_\mathrm{b}(\varphi) + \big(j_\mathrm{b}(\phi) - (1-\phi)q_k(t)\big)\varphi \\ =& (1-\phi)f_\mathrm{b}(\varphi) + \big(j_k(\phi,t) - q_k(t)\big)\varphi, \quad k = 1,2,3. \end{aligned}$$

The first term, $(1-\phi)f_\mathrm{b}(\varphi)$, is the hindered-settling flux of solids relative to the bulk movement outside the aggregates, which explains the factor $(1-\phi)$. The second term is the bulk flux of solids downwards, which has the overall bulk flow component $-q_k$ enhanced by the aggregate movement upwards that forces the surrounding suspension to move downwards with the velocity j_k.

1.2.4 Zone flux functions

The zone flux functions, j for the aggregates and $f(\cdot,\phi)$ for the solids, have an additional linear term due to the bulk velocity of the zone, see Figure 1.1. We temporarily skip the time dependence (that is, we treat q as a constant) and let $j(\phi) = j_\mathrm{b}(\phi) + q\phi$ denote a general zone flux function. (The case for the settling zone flux function $f(\cdot,\phi)$ is similar; however, with an additional dependence on ϕ.) The flux function j has the following distinguished values; see Figure 1.1:

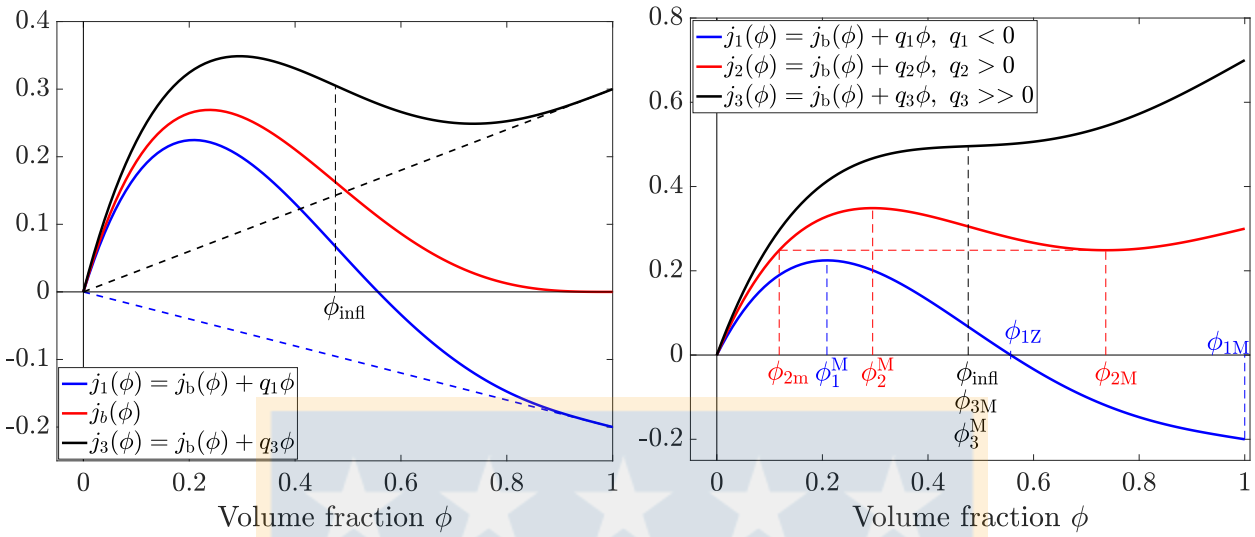

Figure 1.1: Flux functions of the aggregate phase and specific volume fractions. Left: Drift-flux function j_b and flux curves for zones 1 and 3. Right: In red colour, the local minimum ϕ_{2M} and the lower volume fraction ϕ_{2m} with the same flux value (see (1.13)) for the flux j_2 in zone 2 where $q_2 > 0$. In blue colour, the local maximum ϕ_1^M and zero ϕ_{1Z} for flux j_1 with $q_1 < 0$. In black we have represented a zone flux j_3 with a higher value of $q_3 > 0$, so that $\phi_{3M} = \phi_3^M = \phi_{infl}$. In these and other plots, we have used the expression (1.4) with $v_{term,a} = 2.7\,cm/s$ and $n_a = 3.2$ in the drift-flux function j_b. The unit on the vertical axis is cm/s.

- The flux $j(\phi)$ has the same inflection point ϕ_{infl} as $j_b(\phi)$ for any value of q.
- If $j(\phi)$ has a zero in the interval $(0, 1)$, which happens only for $q < 0$, we denote it by $\phi_Z = \phi_Z(q)$. If $j(\phi) < 0$ for all $\phi \in (0, 1]$, we set $\phi_Z := 0$.
- There is a local minimum point $\phi_M = \phi_M(q)$ in the interval $(\phi_{infl}, 1)$, which decreases with increasing $q > 0$ until ϕ_M reaches the inflection point. For higher values of q, $j(\phi)$ is an increasing function and we define $\phi_M := \phi_{infl}$. For $q < 0$, we set $\phi_M := 1$.
- Given ϕ_M and $q \geq 0$, we define $\phi_m = \phi_m(q)$ as the unique value satisfying

$$j(\phi_m) = j(\phi_M), \quad \text{where } 0 \leq \phi_m \leq \phi_{infl}. \tag{1.13}$$

- For realistic values of q, there is a local maximum $\phi^M = \phi^M(q)$ in the interval $[0, \phi_{infl})$.

Sometimes we write out the dependence on q of the flux function, i.e. $j(\phi; q)$ and $f(\varphi, \phi; q)$.

1.2.5 A comment on the condition at effluent level

We comment that there is no explicit boundary condition for the bubble volume fraction ϕ associated with the effluent level z_E other than the change from the flux $J = j_3$, corresponding

to zone 3, to the convective flux $J = j_{\mathrm{E}}$ in the (one-sidedly unbounded) effluent region, see (1.11). This jump in the algebraic definition in combination with the continuity of the aggregate flux J means that if we denote by $\phi(z_{\mathrm{E}}^-, t)$ and $\phi(z_{\mathrm{E}}^+, t)$ the limits of $\phi(\cdot, t)$ at $z = z_{\mathrm{E}}$ from below (zone 3) and above (effluent zone), respectively, then for the corresponding limits of J must satisfy $J(\phi(z_{\mathrm{E}}^-, t), z_{\mathrm{E}}^-, t) = J(\phi(z_{\mathrm{E}}^+, t), z_{\mathrm{E}}^+, t)$ at all times. In light of the definition of J, (1.11), this means that

$$q_3(t)\phi(z_{\mathrm{E}}^-, t) + j_{\mathrm{b}}\big(\phi(z_{\mathrm{E}}^-, t)\big) = q_3(t)\phi(z_{\mathrm{E}}^+, t),$$

such that

$$q_3(t)\big(\phi(z_{\mathrm{E}}^+, t) - \phi(z_{\mathrm{E}}^-, t)\big) = j_{\mathrm{b}}\big(\phi(z_{\mathrm{E}}^-, t)\big) \geq 0. \tag{1.14}$$

Since $q_3(t) \geq 0$, (1.14) means that $\phi(z_{\mathrm{E}}^-, t) \leq \phi(z_{\mathrm{E}}^+, t)$, that is, the aggregate volume fraction ϕ increases (upward) across the effluent level z_{E}. If we (for simplicity) assume that no hydrophilic solids are present in zone 3 and the effluent zone (this is usually the case under standard operating conditions), then we conclude that the fluid content $1-\phi$ decreases upward across z_{E}, i.e.,

$$\phi_{\mathrm{f}}(z_{\mathrm{E}}^-, t) = 1 - \phi(z_{\mathrm{E}}^-, t) \geq 1 - \phi(z_{\mathrm{E}}^+, t) = \phi_{\mathrm{f}}(z_{\mathrm{E}}^+, t). \tag{1.15}$$

We come back to the significance of this observation in conclusions.

1.3 Steady states

1.3.1 Desired steady states

Generally, a steady-state solution consists of piecewise constant values of ϕ and φ (or, equivalently ψ), generally with discontinuities at the locations of the inlet and outlets, and in each zone there is at most one discontinuity. We are only interested in the desired steady states that have a high concentration of aggregates at the top, so that a layer of foam exists, and zero at the bottom. Furthermore, in a desired steady state, we require in addition that the hydrophilic solids settle directly and be present only below the feed level. The different steady states depend on the values of the feed input volume fractions of the aggregates ϕ_{F} and the solids ψ_{F}, and on the volumetric flow rates Q_{F}, Q_{U} and Q_{W}. There are several equalities and inequalities involving these variables and the nonlinear flux functions j_{b} and f_{b}. We will state the conditions that are needed here and refer to [18] for all details. Theoretically, there exist many steady states; however, a main conclusion is that all desired steady states that should be able to exist for all volumetric feed flows $Q_{\mathrm{F}} > 0$ require wash water, i.e., $Q_{\mathrm{W}} > 0$. It turns out that the desired aggregate steady states that are possible for a range of volumetric flows down to zero are those described in Table 1.1. They differ only in zone 2, where the solution ϕ can

Table 1.1: Desired aggregate steady states that are possible for a range of volumetric flows down to zero. The states differ only in zone 2, where the solution ϕ can be constant low (SSl), constant high (SSh), or have a discontinuity separating these two values (SSd). Here, ϕ_3 denotes a constant solution in the entire zone 3, $\phi_{3\mathrm{M}}$ is the minimum point of $j_3(\phi)$, and $\phi_2^{\uparrow}$ and $\phi_2^{\downarrow}$ denote the values above and below, respectively, a discontinuity located at $z = z_\mathrm{d}$ within zone 2.

	$\phi_{\mathrm{SSl}}(z)$	$\phi_{\mathrm{SSh}}(z)$	$\phi_{\mathrm{SSd}}(z)$
effluent zone	$\phi_\mathrm{E} = A_\mathrm{E} j_3(\phi_3)/Q_\mathrm{E} \geq \phi_{3\mathrm{M}}$		
zone 3	$\phi_3 = \phi_{3\mathrm{M}} \geq \phi_2$		
zone 2	$\phi_2 \in [\phi_{2\mathrm{m}}, \phi_2^{\mathrm{M}}]$	$\phi_2 \in [\phi_2^{\mathrm{M}}, \phi_{2\mathrm{M}}]$	$\begin{cases} \phi_2^{\uparrow} \in [\phi_2^{\mathrm{M}}, \phi_{2\mathrm{M}}] & \text{for } z \geq z_\mathrm{d}, \\ \phi_2^{\downarrow} \in [\phi_{2\mathrm{m}}, \phi_2^{\mathrm{M}}] & \text{for } z < z_\mathrm{d} \end{cases}$
zone 1 & underflow zone	0		

be constant low (SSl), constant high (SSh), or have a discontinuity separating these two values (SSd).

For the solids, the following steady state is the most interesting one:

$$\varphi_{\mathrm{SS}}(z) := \begin{cases} 0 & \text{in the effluent zone and zones 2 and 3,} \\ \varphi_1 \in [0, \varphi_{1\mathrm{m}}] & \text{in zone 1,} \\ \varphi_\mathrm{U} = \varphi_1 + A_\mathrm{U} f_\mathrm{b}(\varphi_1)/Q_\mathrm{U} & \text{in the underflow zone.} \end{cases} \tag{1.16}$$

The necessary conditions for these steady states to exist involve the following conditions, where we now write out the dependencies on the volumetric flow rates; see (1.9). The conservation of mass across the feed and wash water levels yields the following jump conditions:

$$Q_\mathrm{F}\phi_\mathrm{F} = A_\mathrm{E} j_2(\phi_2; q_2), \tag{FJC}$$

$$Q_\mathrm{F}\psi_\mathrm{F} = A_\mathrm{U} f_1(\varphi_1, 0; q_1), \tag{FJCs}$$

$$A_\mathrm{E} j_2(\phi_2; q_2) = A_\mathrm{E} j_3(\phi_3; q_3). \tag{WJC}$$

(Since $\varphi_{\mathrm{SS}} = 0$ above and below $z = z_\mathrm{W}$, the jump condition there for the solid phase is always satisfied.) For ϕ_{SSd}, ϕ_2 should be replaced by $\phi_2^{\downarrow}$ in (FJC) and by $\phi_2^{\uparrow}$ in (WJC). We note that for given feed volume fractions ϕ_F and ψ_F, and volumetric flows Q_U and Q_F, the values ϕ_2 (or $\phi_2^{\downarrow}$ or $\phi_2^{\uparrow}$) and φ_1 are uniquely given by (FJC) and (FJCs), respectively, for the restrictions given in the solutions $\phi_{\mathrm{SSl}}(z)$, $\phi_{\mathrm{SSh}}(z)$ and $\phi_{\mathrm{SSd}}(z)$ given in Table 1.1 and $\varphi_{\mathrm{SS}}(z)$ given in (1.16). Then Q_W is given as the unique solution of the following equation (cf. (FJC) and (WJC)):

$$A_\mathrm{E} j_3\left(\phi_\mathrm{M}\left(\frac{-Q_\mathrm{U} + Q_\mathrm{F} + Q_\mathrm{W}}{A_\mathrm{E}}\right); \frac{-Q_\mathrm{U} + Q_\mathrm{F} + Q_\mathrm{W}}{A_\mathrm{E}}\right) = Q_\mathrm{F}\phi_\mathrm{F}. \tag{1.17}$$

(The function $\phi_{\mathrm{M}}(q)$ is defined in Section 1.2.4.) Then $\phi_3 = \phi_{3\mathrm{M}}(q_3)$ is uniquely determined. The choices of Q_{U} and Q_{F} are given by (some of, depending on the steady state; see Section 1.3.2) the following inequalities:

$$A_{\mathrm{E}} j_2(\phi_2^{\mathrm{M}}(q_2); q_2) \geq Q_{\mathrm{F}}\phi_{\mathrm{F}}, \tag{FIa}$$
$$\phi_2 \leq \phi_{1\mathrm{Z}}(q_1), \quad \text{where } \phi_2 \leq \phi_2^{\mathrm{M}}(q_2) \text{ is defined by (FJC)}, \tag{FIb}$$
$$A_{\mathrm{E}} j_2(\phi_{2\mathrm{M}}(q_2); q_2) \leq Q_{\mathrm{F}}\phi_{\mathrm{F}}, \tag{FIIa}$$
$$\phi_2 \leq \phi_{1\mathrm{Z}}(q_1), \quad \text{where } \phi_2 \in [\phi_2^{\mathrm{M}}(q_2), \phi_{2\mathrm{M}}(q_2)] \text{ is defined by (FJC)}, \tag{FIIb}$$
$$Q_{\mathrm{U}} > Q_{\mathrm{F}}(1 - \phi_{\mathrm{F}}), \tag{CFIIIa}$$
$$A_{\mathrm{U}} f_1(\varphi_{1\mathrm{M}}(q_1), 0; q_1) \geq Q_{\mathrm{F}}\psi_{\mathrm{F}}. \tag{FIas}$$

If Q_{U} and Q_{F} are chosen so that condition (CFIIIa) is satisfied (and other conditions depending on the feed volume fractions), then the wash water injected at the rate Q_{W} calculated by (1.17) is effective in the meaning that it flows downwards through the foam. Furthermore, $Q_{\mathrm{E}} > 0$.

1.3.2 Operating charts

Case SSl: ϕ_{SSl} and φ_{SS}

The necessary conditions are (FIa), (FIb), (FIas) and (CFIIIa) along with the jump conditions. The first four conditions involve only Q_{U} and Q_{F}, and these conditions are visualized in Figure 1.2 for $\phi_{\mathrm{F}} = 0.3$ and $\psi_{\mathrm{F}} = 0.1$. The white region in the fifth subplot of Figure 1.2 shows the possible values for $(Q_{\mathrm{U}}, Q_{\mathrm{F}})$. In each such point, there is a unique value of Q_{W}. In the fifth subplot of Figure 1.2, we have drawn red dashed curves; each for a fixed value of $Q_{\mathrm{W}} = 0, 10, 20, \ldots$ cm^3/s, defined by (1.17). The value of Q_{W} for a specific curve can be read off at the intersection of the curve with the Q_{U}-axis. This is because $Q_{\mathrm{F}} = 0$ in (1.17) gives $\phi_{\mathrm{M}}((-Q_{\mathrm{U}} + Q_{\mathrm{W}})/A_{\mathrm{U}}) = \phi_{\max}$, which is equivalent to $Q_{\mathrm{W}} = Q_{\mathrm{U}}$.

Case SSh: ϕ_{SSh} and φ_{SS}

The conditions are (FIa), (FIIa), (FIIb), (FIas) and (CFIIIa) and the jump conditions. For $\phi_{\mathrm{F}} = 0.3$ and $\psi_{\mathrm{F}} = 0.1$ we get the regions shown in Figure 1.3, where we show the new conditions that are not shown in Figure 1.2.

Case SSd: ϕ_{SSd} and φ_{SS}

The necessary conditions for this solution are the same as in case SSh; hence, the operating charts coincide with those in Figure 1.3.

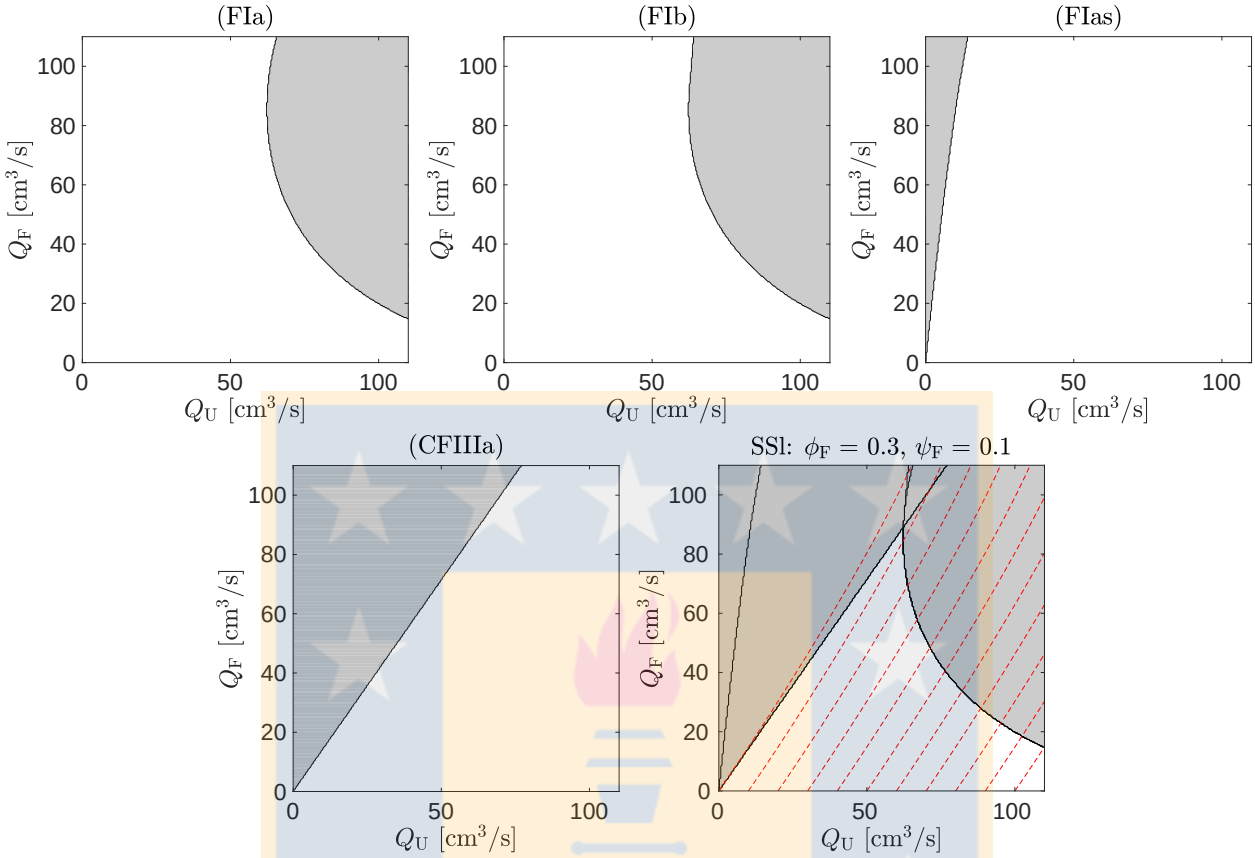

Figure 1.2: Operating charts in the case SSl with $\phi_F = 0.3$ and $\psi_F = 0.1$. The four first plots show where each condition is satisfied (white regions). The last plot shows all four conditions superimposed and curves (red dashed) along which Q_W (obtained from (1.17)) is constant with $Q_W = 0, 10, 20, \ldots$ cm^3/s. The value of Q_W can be read off on the Q_U-axis. (In this and other figures, the values $n_a = 3.2$, $v_{term,a} = 2.7\,\text{cm/s}$, $n_s = 2.5$ and $v_{term,s} = 0.5\,\text{cm/s}$ have been used for the drift-flux j_b and hindered-settling flux f_b functions.)

1.4 Numerical scheme

For the numerical simulation of nonlinear hyperbolic systems of PDEs like (2), which have coefficients that depend discontinuously on space, there exists no standard textbook method. We present here a new explicit numerical scheme for obtaining approximate solutions of the model (2) expressed in the conservative variables ϕ and ψ:

$$A(z)\frac{\partial \phi}{\partial t} + \frac{\partial}{\partial z}\big(A(z)J(\phi, z, t)\big) = Q_F(t)\phi_F(t)\delta(z - z_F), \tag{1.18a}$$

$$A(z)\frac{\partial \psi}{\partial t} + \frac{\partial}{\partial z}\big(A(z)\tilde{F}(\psi, \phi, z, t)\big) = Q_F(t)\psi_F(t)\delta(z - z_F), \tag{1.18b}$$

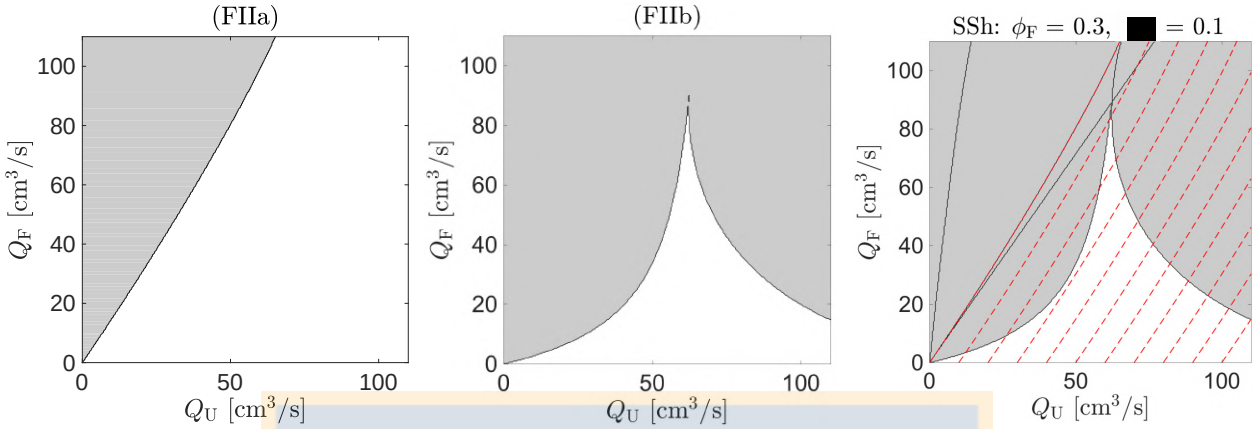

Figure 1.3: Operating charts in the cases SSh and SSd with $\phi_F = 0.3$ and $\psi_F = 0.1$. The conditions (FIIa) and (FIIb) are shown (see Figure 1.2 for the others), and in the third plot all conditions together with the red dashed lines showing the values of $Q_W = 0, 10, 20, \ldots$ cm^3/s.

where

$$\tilde{F}(\psi,\phi,z,t) := \begin{cases} -F\left(\dfrac{\psi}{1-\phi},\phi,z,t\right) & \text{if } 0 \le \phi < 1, \\ 0 & \text{if } \phi = 1, \end{cases}$$

$$-F\left(\frac{\psi}{1-\phi},\phi,z,t\right) = \psi q - \gamma(z)\left(\psi V\left(\frac{\psi}{1-\phi}\right) + \frac{\psi\phi W(\phi)}{1-\phi}\right),$$

and (cf. (1.2) and (1.3))

$$W(\phi) := v_{\text{term,a}} V_a(\phi), \qquad V(\varphi) := v_{\text{term,s}} V_s(\varphi). \tag{1.19}$$

The discretization of the system of balance laws (1.18) exploits that this is triangular. We first obtain discrete values $\phi_i^n \approx \phi(z_i, t_n)$, which approximate the solution ϕ of (1.18a) as a piecewise constant function in space and time. This is then used as a known function in (1.18b), which solution is approximated by the values $\psi_i^n \approx \psi(z_i, t_n)$. We have a proof (not yet published) that the first update formula produces discrete values $0 \le \phi_i^n \le 1$, and that the second one implies $\psi_i^n \ge 0$ and $0 \le \phi_i^n + \psi_i^n \le 1$. This property reflects that only physically relevant discrete solution values are generated, since from the natural bounds $0 \le \phi \le 1$ and $0 \le \varphi \le 1$ (see Section 1.1.1) at every point (z,t) and the relation (1) we obtain that $\phi + \psi$ satisfies $0 \le \phi + \psi = \phi + (1-\phi)\varphi \le \phi + 1 - \phi = 1$.

1.4.1 Spatial discretization

We define a computational domain of N cells by covering the vessel with $N-2$ cells and placing one cell each below and above for the calculation of the outlet volume fractions; see

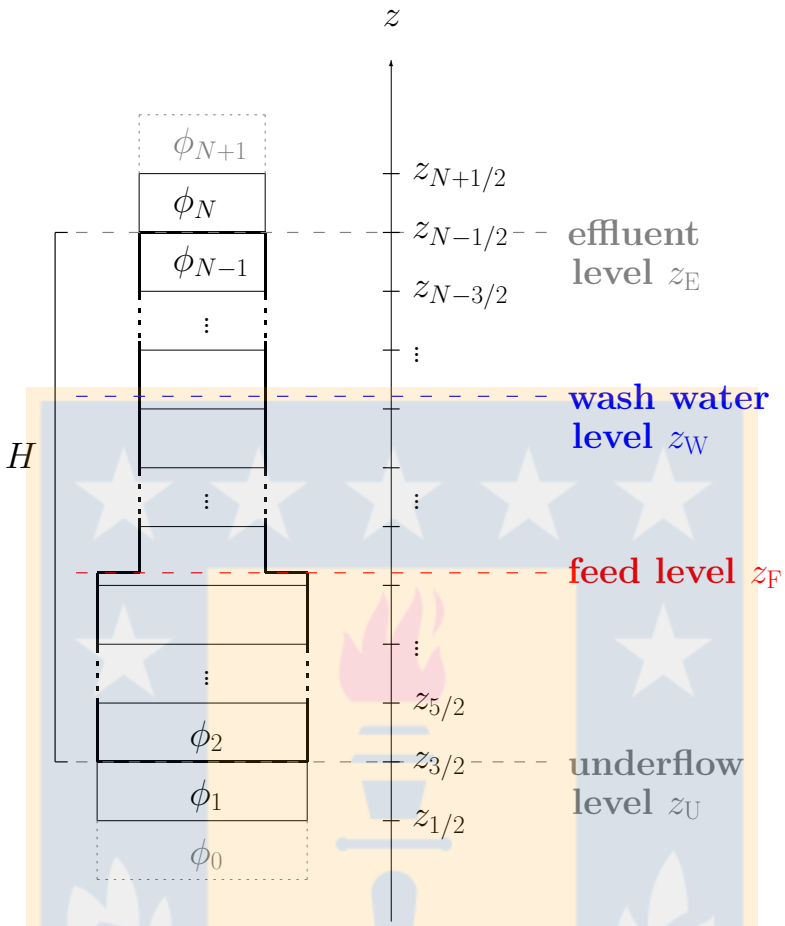

Figure 1.4: Grid defined for the discretization of the flotation column. Both inlets z_F and z_W are fixed inside a cell while the outlets, z_U and z_E, are on the boundary of a cell. The grid for the discretization of ψ is the same.

Figure 1.4. Given the column height H, we define $\Delta z := H/(N-2)$ the cell boundaries $z_{i+1/2} := i\Delta z$, $i = 0, 1, \ldots, N$, and the cell intervals $[z_{i-1/2}, z_{i+1/2})$. We place the column between $z_U := \Delta z = z_{3/2}$ and $z_E := z_U + H = (N-1)\Delta z = z_{N-1/2}$. Each of the injection points z_F and z_W is assumed to belong to one interval $[z_{i-1/2}, z_{i+1/2})$ and we define the dimensionless symbol

$$\delta_{F,i} := \int_{z_{i-1/2}}^{z_{i+1/2}} \delta_{z_F}(z)\,\mathrm{d}z := \begin{cases} 1 & \text{if } z_F \in [z_{i-1/2}, z_{i+1/2}), \\ 0 & \text{otherwise.} \end{cases}$$

The cross-sectional area $A = A(z)$, which is allowed to have a finite number of discontinuities, is discretized by cell-wise averages, namely we calculate

$$A_i := \frac{1}{\Delta z}\int_{z_{i-1/2}}^{z_{i+1/2}} A(z)\,\mathrm{d}z, \qquad A_{i+1/2} := \frac{1}{\Delta z}\int_{(i-1/2)\Delta z}^{(i+1/2)\Delta z} A(z)\,\mathrm{d}z. \tag{1.20}$$

Furthermore, we determine from these values the constants

$$M := \max_{i=1,2,\dots,N} \left\{ \frac{A_{i-1/2}}{A_i}, \frac{A_{i+1/2}}{A_i} \right\}, \qquad A_{\min} := \min_{i=1,2,\dots,N} A_i. \tag{1.21}$$

1.4.2 Time discretization

We use the uniform step length Δt and simulate N_T time steps up to the final time $T := N_T \Delta t$, and we set $t_n := n\Delta t$ for $n = 0, 1, \dots, N_T$. The time step Δt should satisfy the Courant-Friedrichs-Lewy (CFL) condition

$$\Delta t \left(\frac{2\|Q\|_{\infty,T}}{A_{\min}} + M \Big(\max\{V(0), \|V'\|_\infty\} + \|W\|_\infty + \|W'\|_\infty \Big) \right) \le \Delta z, \tag{1.22}$$

where the constants are given by (1.21) and

$$\|Q\|_{\infty,T} := \max_{0\le t\le T} \big(Q_{\mathrm{F}}(t) + Q_{\mathrm{W}}(t) \big), \qquad \|V'\|_\infty := \max_{0\le \phi\le 1} |V'(\phi)|.$$

The CFL condition (1.22) is a well-known stability condition that usually arises in the context of explicit discretizations of time-dependent PDEs (see, e.g., [77]) and limits Δt for given Δz.

The time-dependent feed functions are discretized as

$$Q_{\mathrm{F}}^n := \frac{1}{\Delta t} \int_{t_n}^{t_{n+1}} Q_{\mathrm{F}}(t)\, \mathrm{d}t, \qquad \phi_{\mathrm{F}}^n := \frac{1}{\Delta t} \int_{t_n}^{t_{n+1}} \phi_{\mathrm{F}}(t)\, \mathrm{d}t,$$

and the same is made for the other volumetric flows and ψ.

1.4.3 Marching formula

Assume that Δz is the spatial mesh width ("layer thickness") specified above and Δt is the time step chosen such that (1.22) is in effect. The numerical approximations of the PDE solutions are defined as follows. Firstly, the initial data are discretized by

$$\phi_i^0 := \frac{1}{A_i \Delta z} \int_{z_{i-1/2}}^{z_{i+1/2}} \phi(z,0) A(z)\, \mathrm{d}z, \qquad \psi_i^0 := \frac{1}{A_i \Delta z} \int_{z_{i-1/2}}^{z_{i+1/2}} \psi(z,0) A(z)\, \mathrm{d}z.$$

To advance from t_n to t_{n+1}, we assume that ϕ_i^n, $i = 1, \dots, N$, are given and set the boundary values

$$\begin{aligned} \phi_0^n &:= \phi_1^n, \quad \phi_{N+1}^n := \phi_N^n, \\ \psi_0^n &:= \psi_1^n, \quad \psi_{N+1}^n := \psi_N^n. \end{aligned}$$

To present the final marching formula, we calculate (for $i = 0, \dots, N$)

$$\psi_{\max,i+1/2}^n := \min\{1 - \phi_i^n, 1 - \phi_{i+1}^n\} = 1 - \max\{\phi_i^n, \phi_{i+1}^n\}. \tag{1.23}$$

For the calculation of some numerical fluxes, we define the function

$$f^n_{i+1/2}(\psi) =: \psi \widetilde{V}\left(\frac{\psi}{\psi^n_{\max,i+1/2}}\right), \quad \widetilde{V}(u) := \begin{cases} V(u) & \text{if } u < 1, \\ 0 & \text{if } u \geq 1. \end{cases} \tag{1.24}$$

We denote by $\hat{\psi}^n_{i+1/2}$ the (unique) maximum point of the function $f^n_{i+1/2}$ Then we calculate (the Godunov numerical flux on the function $f^n_{i+1/2}$) [56]

$$G^n_{i+1/2} := \min\{f^n_{i+1/2}(\min\{\psi^n_i, \hat{\psi}^n_{i+1/2}\}), f^n_{i+1/2}(\max\{\psi^n_{i+1}, \hat{\psi}^n_{i+1/2}\})\}. \tag{1.25}$$

We use the notation $\gamma_{i+1/2} := \gamma(z_{i+1/2})$ and $Q(z,t) := A(z)q(z,t)$, where q is defined by (1.9). The marching formulas are the following (for $i = 1, \ldots, N$):

$$\begin{aligned}
\phi^{n+1}_i = \phi^n_i + \frac{\Delta t}{A_i \Delta z}\Big(&\phi^n_{i-1} \max\{Q^n_{i-1/2}, 0\} + \phi^n_i \min\{Q^n_{i-1/2}, 0\} \\
&- \phi^n_i \max\{Q^n_{i+1/2}, 0\} - \phi^n_{i+1} \min\{Q^n_{i+1/2}, 0\} \\
&+ A_{i-1/2}\gamma_{i-1/2}\phi^n_{i-1} W(\phi^n_i) - A_{i+1/2}\gamma_{i+1/2}\phi^n_i W(\phi^n_{i+1}) + Q^n_{\mathrm{F}}\phi^n_{\mathrm{F}}\delta_{\mathrm{F},i}\Big), \\
\psi^{n+1}_i = \psi^n_i + \frac{\Delta t}{A_i \Delta z}\Bigg(&\psi^n_{i-1} \max\{Q^n_{i-1/2}, 0\} + \psi^n_i \min\{Q^n_{i-1/2}, 0\} \\
&- \psi^n_i \max\{Q^n_{i+1/2}, 0\} - \psi^n_{i+1} \min\{Q^n_{i+1/2}, 0\} \\
&- A_{i-1/2}\gamma_{i-1/2}\left(G^n_{i-1/2} + \phi^n_{i-1}\frac{\psi^n_i}{1-\phi^n_i} W(\phi^n_i)\right) \\
&+ A_{i+1/2}\gamma_{i+1/2}\left(G^n_{i+1/2} + \phi^n_i \frac{\psi^n_{i+1}}{1-\phi^n_{i+1}} W(\phi^n_{i+1})\right) + Q^n_{\mathrm{F}}\psi^n_{\mathrm{F}}\delta_{\mathrm{F},i}\Bigg).
\end{aligned}$$

Finally, the underflow and effluent concentrations are obtained by

$$\phi^n_{\mathrm{U}} := \phi^n_1, \qquad \phi^n_{\mathrm{E}} := \phi^n_N.$$

1.5 Numerical simulations

1.5.1 Preliminaries

In our examples we will use the dimensions of the flotation column that is part of the Reflux Flotation Cell used in [38, 54]. The flotation column is $H = 1\,\mathrm{m}$ high with $A_{\mathrm{U}} = 83.65\,\mathrm{cm}^2$. Feed slurry and gas bubbles are pumped through a downcomer of external diameter 3.81 cm, which forms an annulus around a 2.54 cm-diameter tube incorporating a porous sparger for bubble creation. Hence, the effective horizontal cross-sectional area above the feed inlet is $A_{\mathrm{E}} = 72.25\,\mathrm{cm}^2$. The outlet of the downcomer is positioned 66.7 cm below the top of the vessel, hence a vertical distance of 33.3 cm separates the downcomer outlet from the bottom of the

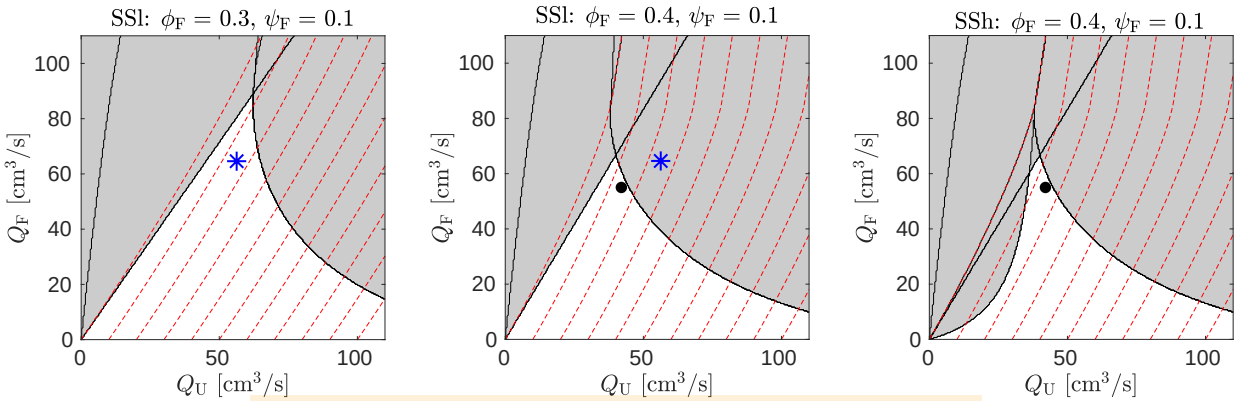

Figure 1.5: Examples 1.1 and 1.2. Operating charts for a steady state of type SSl with $\phi_F = 0.3$, $\psi_F = 0.1$ (left) and $\phi_F = 0.4$, $\psi_F = 0.1$ (middle) and for a steady state of type SSh with $\phi_F = 0.4$, $\psi_F = 0.1$ (right). The point $(Q_U, Q_F) = (56.3, 64.6)\,\mathrm{cm}^3/\mathrm{s}$ is marked in blue (asterisk) while $(Q_U, Q_F) = (42, 55)\,\mathrm{cm}^3/\mathrm{s}$ is marked in black (solid point). The red dashed curves correspond to constant values of $Q_W = 0, 10, 20, \ldots\,\mathrm{cm}^3/\mathrm{s}$ where the washing process is effective.

column. The new numerical method used for the simulations is given in Section 1.4. All the numerical results have been obtained with a spatial discretization of $N = 1600$ computational cells, which means a spatial step size $\Delta z = 0.0626\,\mathrm{cm}$ and a time step $\Delta t = 0.004\,\mathrm{s}$ satisfying the CFL condition (1.22). Note that for the three-dimensional plots in Figures 1.6, 1.7, 1.8, 1.9, 1.11, and 1.12, we have used a visual grid of only 100 spatial points.

1.5.2 Example 1.1

We start from a tank filled only with fluid at time $t = 0\,\mathrm{s}$, when we start pumping aggregates, solids, fluid and wash water, with $\phi_F = 0.3$ and $\psi_F = 0.1$. From the corresponding operating chart, see Figure 1.5 (left), we choose the operating point of volumetric flows $(Q_U, Q_F) = (56.3, 64.6)\,\mathrm{cm}^3/\mathrm{s}$ lying in the white region and choose $Q_W = 15.3\,\mathrm{cm}^3/\mathrm{s}$ by (1.17) to guarantee effective washing, i.e., this is the maximum flow of wash water injected that will flow downwards; applying a higher value will mean an overflow through the effluent. Then a steady-state of type SSl is feasible with the effluent volumetric flow $Q_E = 23.6\,\mathrm{cm}^3/\mathrm{s}$.

As can be seen in Figure 1.6, a first steady state arises after about $t = 130\,\mathrm{s}$ with a low concentration of aggregates in zones 2 and 3; hence, there is no foam and this is an undesired solution. To obtain the desired steady state ϕ_{SSl}, we 'close' the top of the tank at $t = 150\,\mathrm{s}$ by setting $Q_U = Q_F + Q_W = 79.9\,\mathrm{cm}^3/\mathrm{s}$, so that $Q_E = 0\,\mathrm{cm}^3/\mathrm{s}$. Then aggregates accumulate at the top forming a layer of foam which grows downwards. After 80 s, at $t = 230\,\mathrm{s}$, the top of the column is opened again and a desired steady state of type SSl is reached after $t = 530\,\mathrm{s}$.

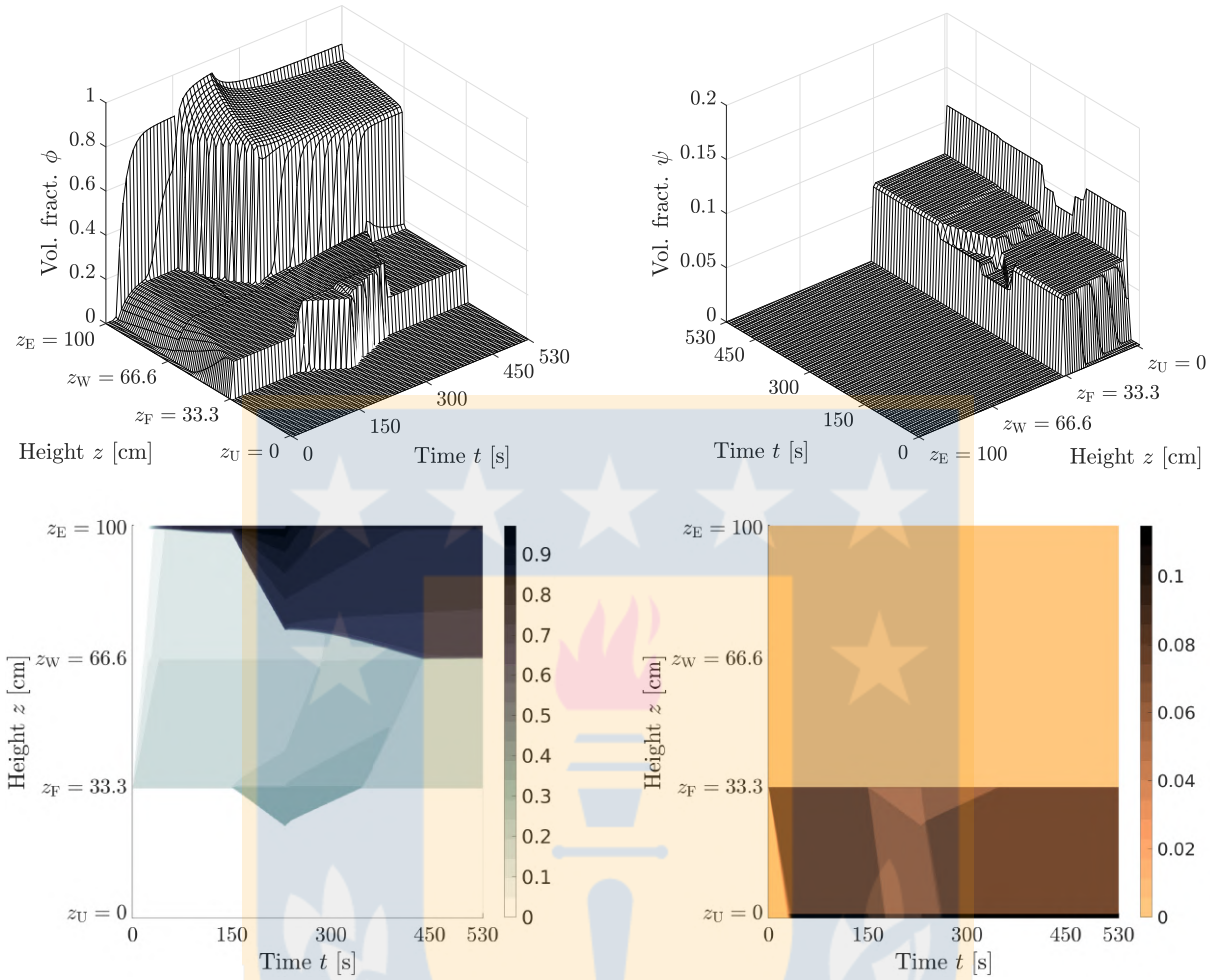

Figure 1.6: Example 1.1. Time evolution from $t = 0$ to $t = 530\,\text{s}$ of the volume fraction profiles of aggregates ϕ (left) and solids ψ (right). As it can be seen, the inlets are located at $z_F = 33.3\,\text{cm}$ and $z_W = 66.6\,\text{cm}$.

Example 1.1a (no control action)

Once the system is in steady state, we assume that, at $t = 530\,\text{s}$, the feed volume fraction of aggregates changes from $\phi_F = 0.3$ to 0.4, and simulate first the reaction of the system without making any control action. In the corresponding operating chart for this new set of variables, the point $(Q_U, Q_F) = (56.3, 64.6)\,\text{cm}^3/\text{s}$ is no longer in the white region; see Figure 1.5 (middle), and no steady state of type SSl is feasible.

Figure 1.7 shows in detail the dynamics from $t = 530\,\text{s}$ to $830\,\text{s}$, while the system evolves from a desired steady state to a non-desired one. The aggregates fill the column downwards through zones 2 and 1 until they leave the tank through the underflow outlet, reaching a non-desired steady state. It can also be seen how the solids volume fraction adapts to the movement of

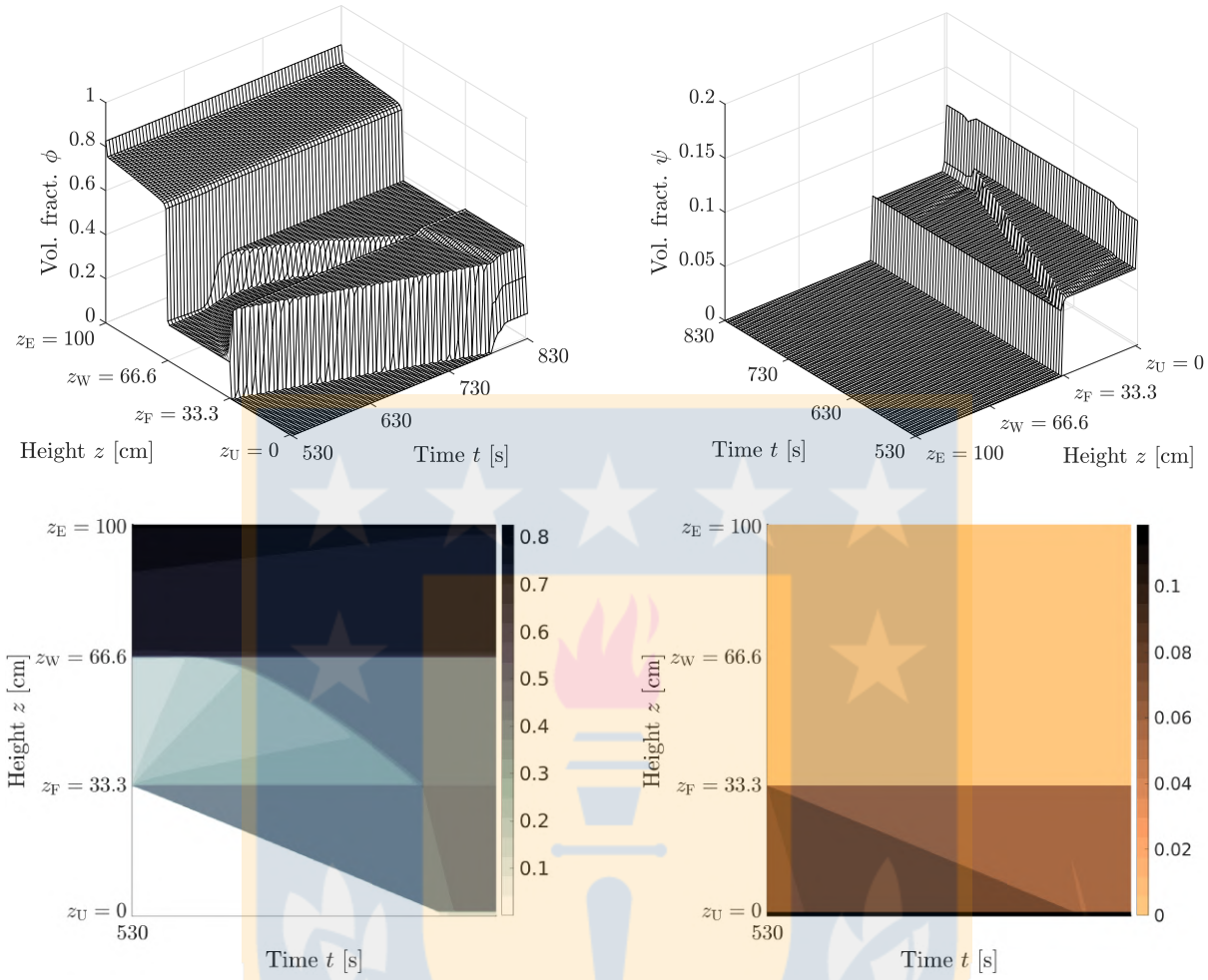

Figure 1.7: Example 1.1a. Time evolution from $t = 530$ to $t = 830\,\mathrm{s}$ of the volume fraction profiles of aggregates ϕ (left) and solids ψ (right) after a change in the feed volume fraction of aggregates from $\phi_F = 0.3$ to 0.4.

aggregates in zone 1.

Example 1.1b (with control action)

To avoid losing aggregates through the underflow, we simulate also the case when we make a control action directly at $t = 530\,\mathrm{s}$ as a response to the change of the feed volume fraction of aggregates from $\phi_F = 0.3$ to 0.4. We close the top of the tank for only 4.5 s and then, at $t = 534.5\,\mathrm{s}$, change the volumetric flows so that the new point $(Q_U, Q_F) = (42, 55)\,\mathrm{cm}^3/\mathrm{s}$ lies inside the white region of the corresponding operating chart in Figure 1.5 (middle), with $Q_W = 14.3\,\mathrm{cm}^3/\mathrm{s}$ given by (1.17). Figure 1.8 shows that a second steady state of type SSl is reached after $t = 834.5\,\mathrm{s}$. The entire simulation with the control action is shown in Figures 1.9

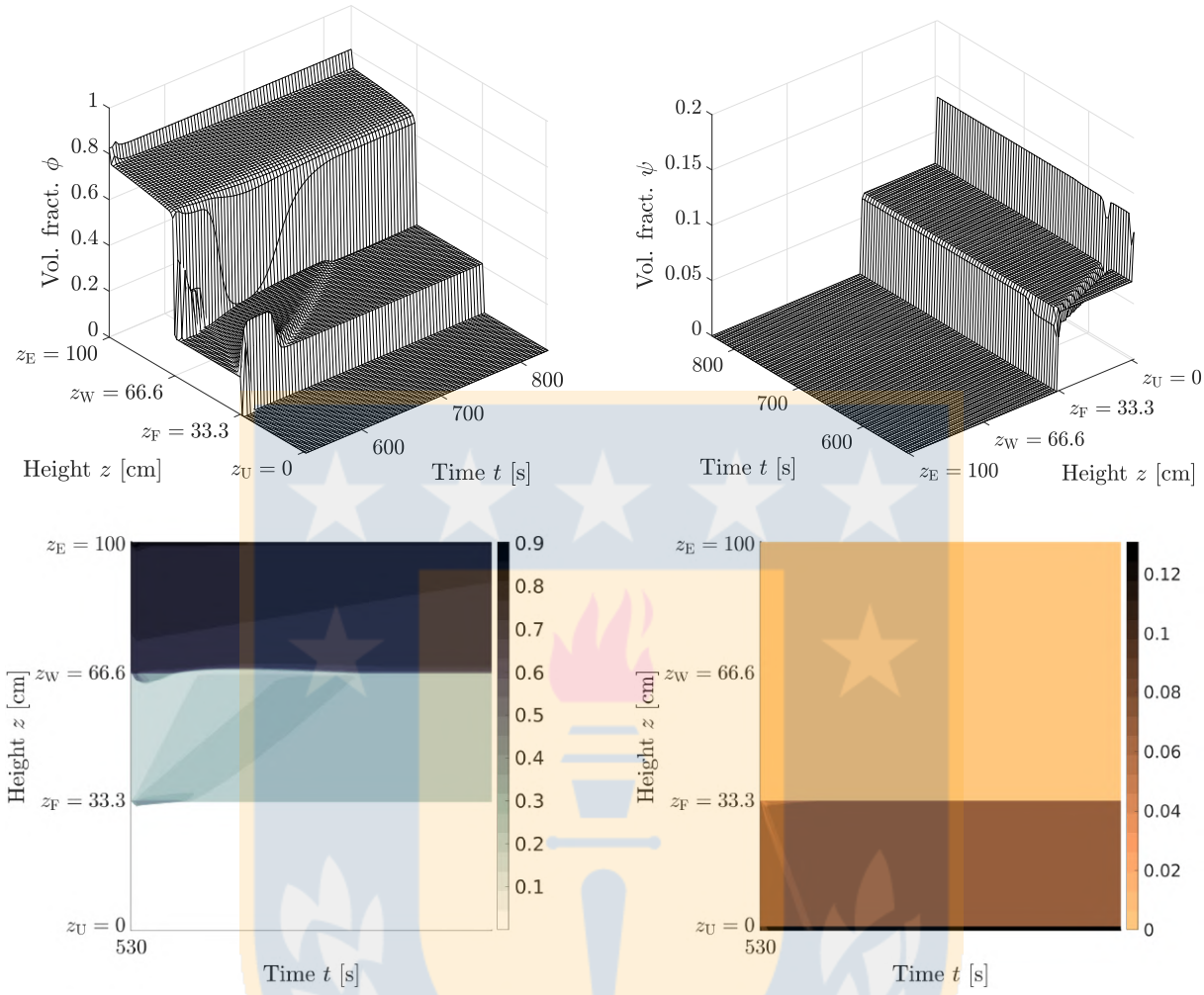

Figure 1.8: Example 1.1b. Time evolution of the volume fraction profiles of aggregates ϕ (left), and solids ψ (right) from time $t = 530\,\mathrm{s}$ to $834.5\,\mathrm{s}$, after making a control action.

and Figure 1.10.

1.5.3 Example 1.2

We demonstrate the cases SSd and SSh. In Figure 1.5 (middle) and (right), we see that the point $(Q_U, Q_F) = (42, 55)\,\mathrm{cm}^3/\mathrm{s}$ lies in the white regions of both feasible steady states SSl and SSh (and SSd). We consider the simulation in Example 1 up to $t = 530\,\mathrm{s}$ when a first desired steady state of type SSl is reached.

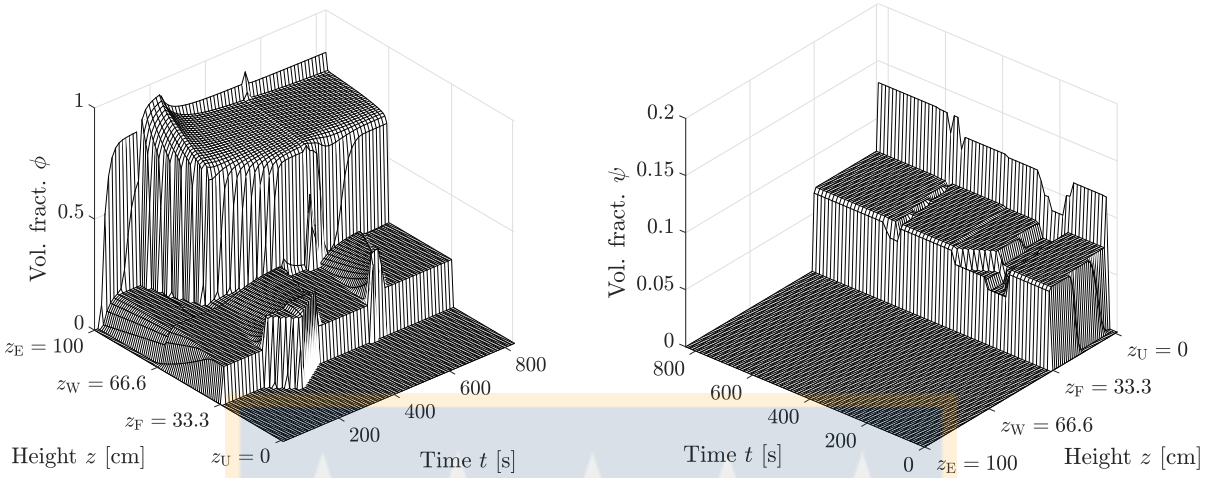

Figure 1.9: Example 1.1b. Time evolution of the volume fraction profiles of aggregates ϕ (left), and solids ψ (right) from $t = 0\,\mathrm{s}$ to $834.5\,\mathrm{s}$.

Example 1.2a (demonstration of SSd)

At that time point, we close the top of the tank for a longer period (15 s) than we did in Example 1.1, until $t = 545\,\mathrm{s}$, when we simultaneously change the feed volume fraction of aggregates from $\phi_F = 0.3$ to 0.4 and adjust the volumetric flows as in Example 1.1b. Figure 1.11 shows that a steady state of type SSd is reached after $t = 845\,\mathrm{s}$, with a stationary discontinuity in zone 2 at $z_d \approx 42\,\mathrm{cm}$, above and below which the volume fractions are

$$\begin{cases} \phi_2^{\uparrow} = 0.3382 \in [\phi_2^{M}, \phi_{2M}] = [0.2697, 0.8032] & \text{for } z > z_d, \\ \phi_2^{\downarrow} = 0.2104 \in [\phi_{2m}, \phi_2^{M}] = [0.0665, 0.2697] & \text{for } z < z_d, \end{cases}$$

satisfying $j_2(\phi_2^{\uparrow}) = j_2(\phi_2^{\downarrow})$.

Example 1.2b (demonstration of SSh)

If we perform the same actions except that the top is closed for 18 s instead of 15 s, then a steady state of type SSh is reached after $t = 848\,\mathrm{s}$; see Figure 1.12. The entire simulation for this case is shown in Figure 1.13. The "stationary" value of the effluent volume fraction of aggregates can be calculated to $\phi_E = Q_F\phi_F/Q_E = 0.8212$ before the disturbance and 0.8061 after.

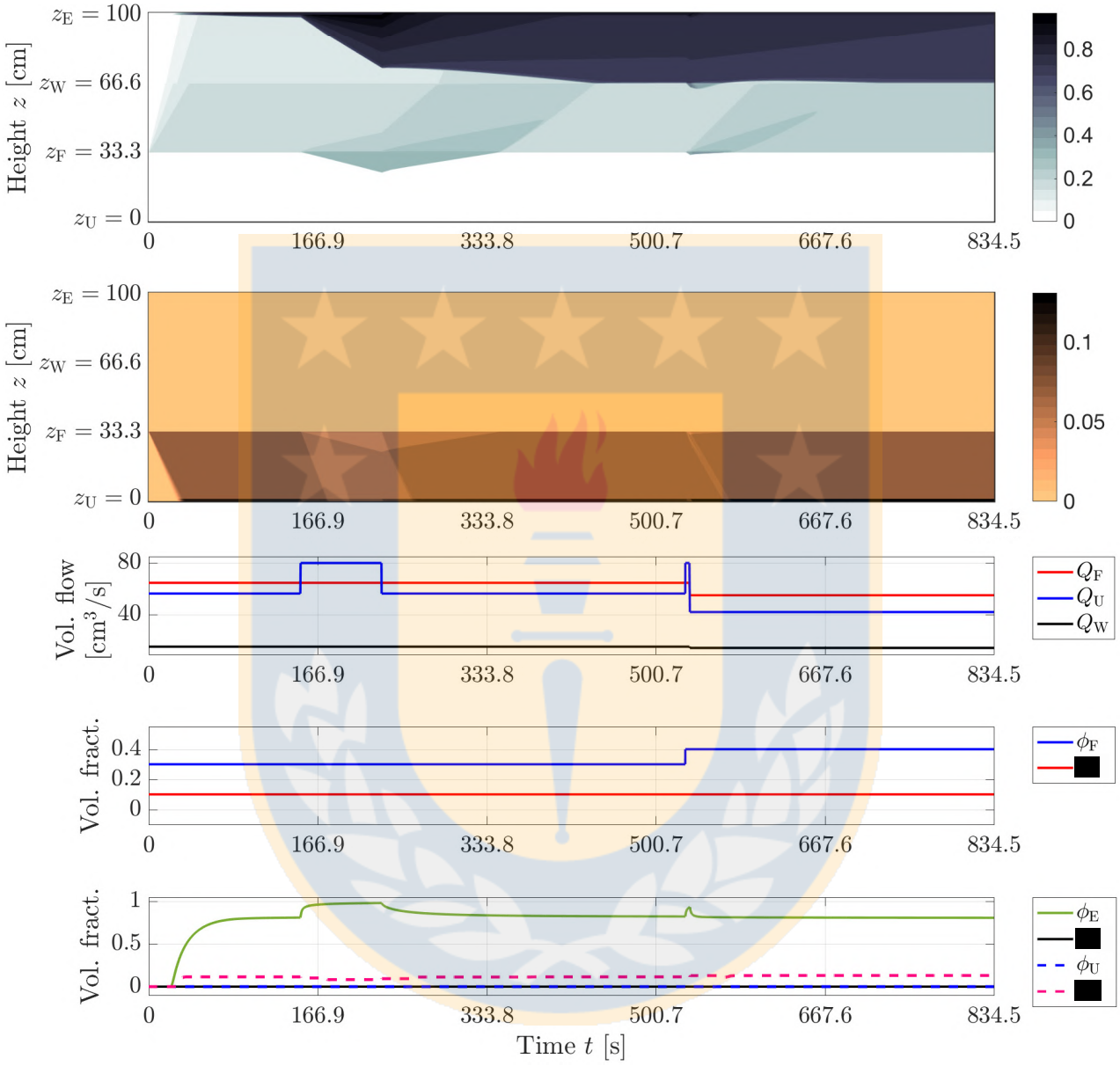

Figure 1.10: Example 1.1b. Dynamics of the entire simulation during 834.5 s with a control action at $t = 530$ s. Here and in Figure 1.13, the panels show (from top to bottom) the aggregate volume fraction ϕ; the solids volume fraction ψ; the volumetric flows Q_U, Q_F and Q_W; the volume fractions of aggregates and solids of the feed (ϕ_F and ψ_F); and the volume fractions of aggregates and solids of the underflow (ϕ_U and ψ_U) and the effluent (ϕ_E and ψ_E).

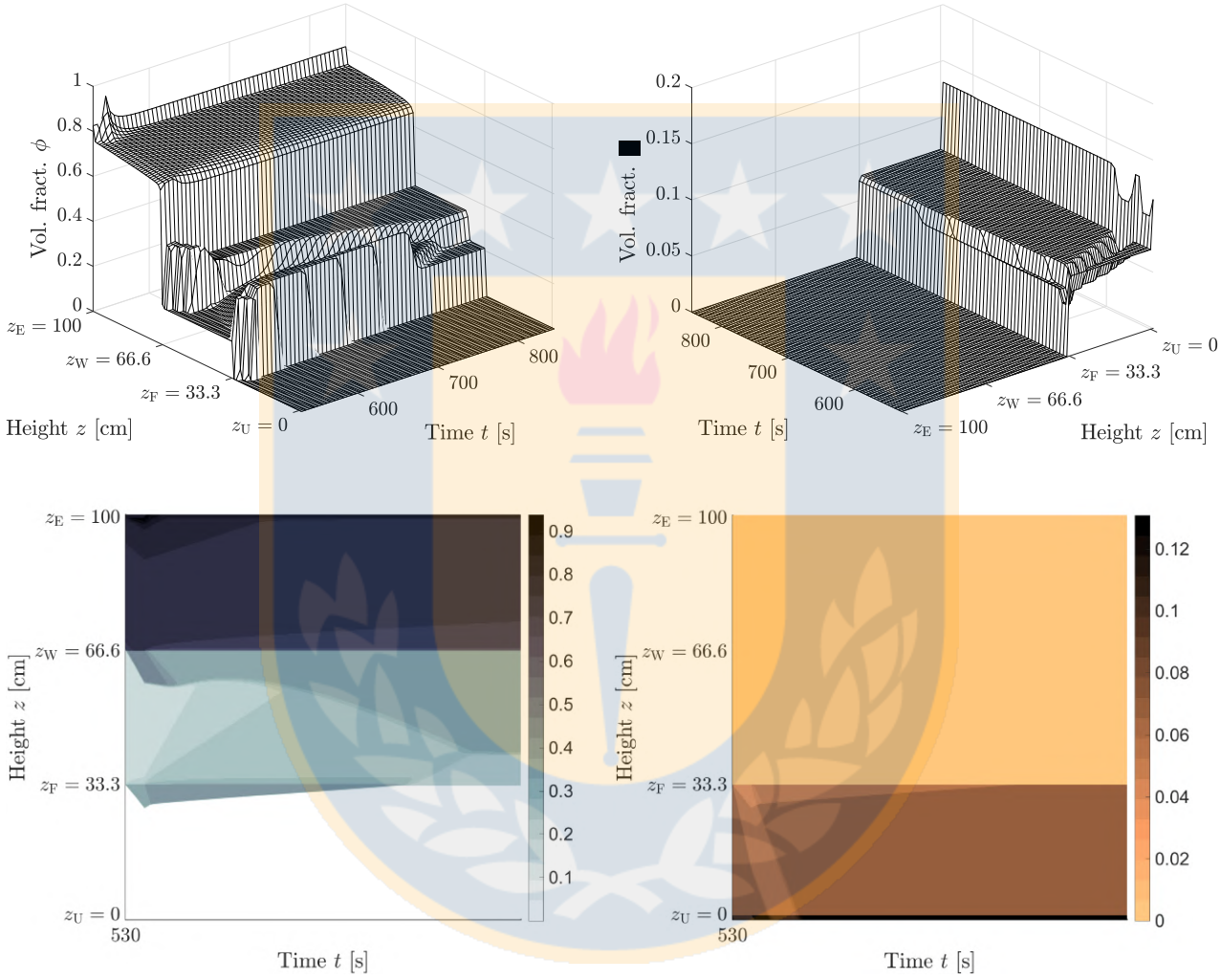

Figure 1.11: Example 1.2a. Transient solution between the steady states SSl and SSd, where the latter has a discontinuity in the aggregate volume fraction in zone 2. The location of this discontinuity depends on the transient solution before, hence, on the control actions made.

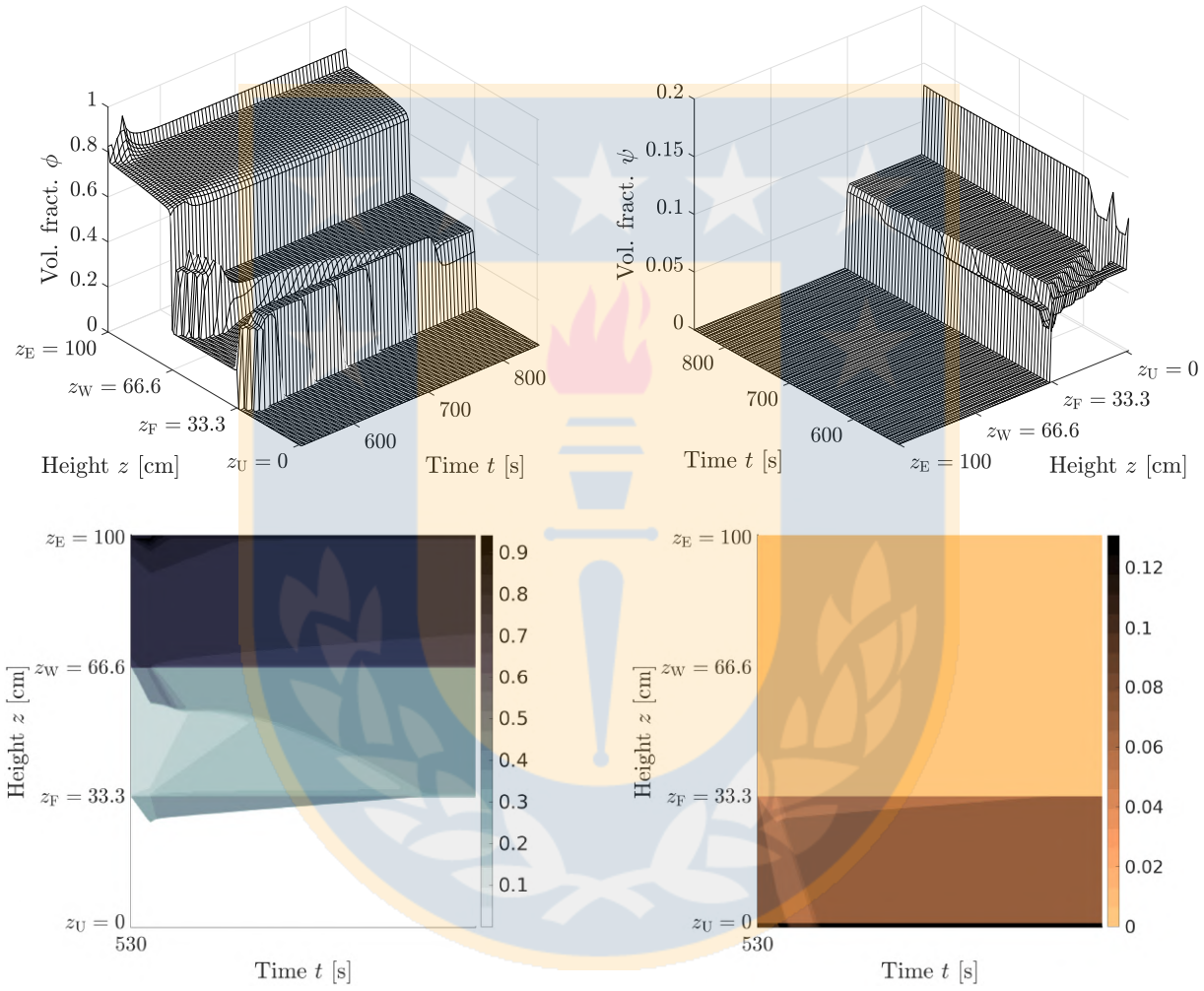

Figure 1.12: Example 1.2b. Transient solution between the steady states SSl and SSh.

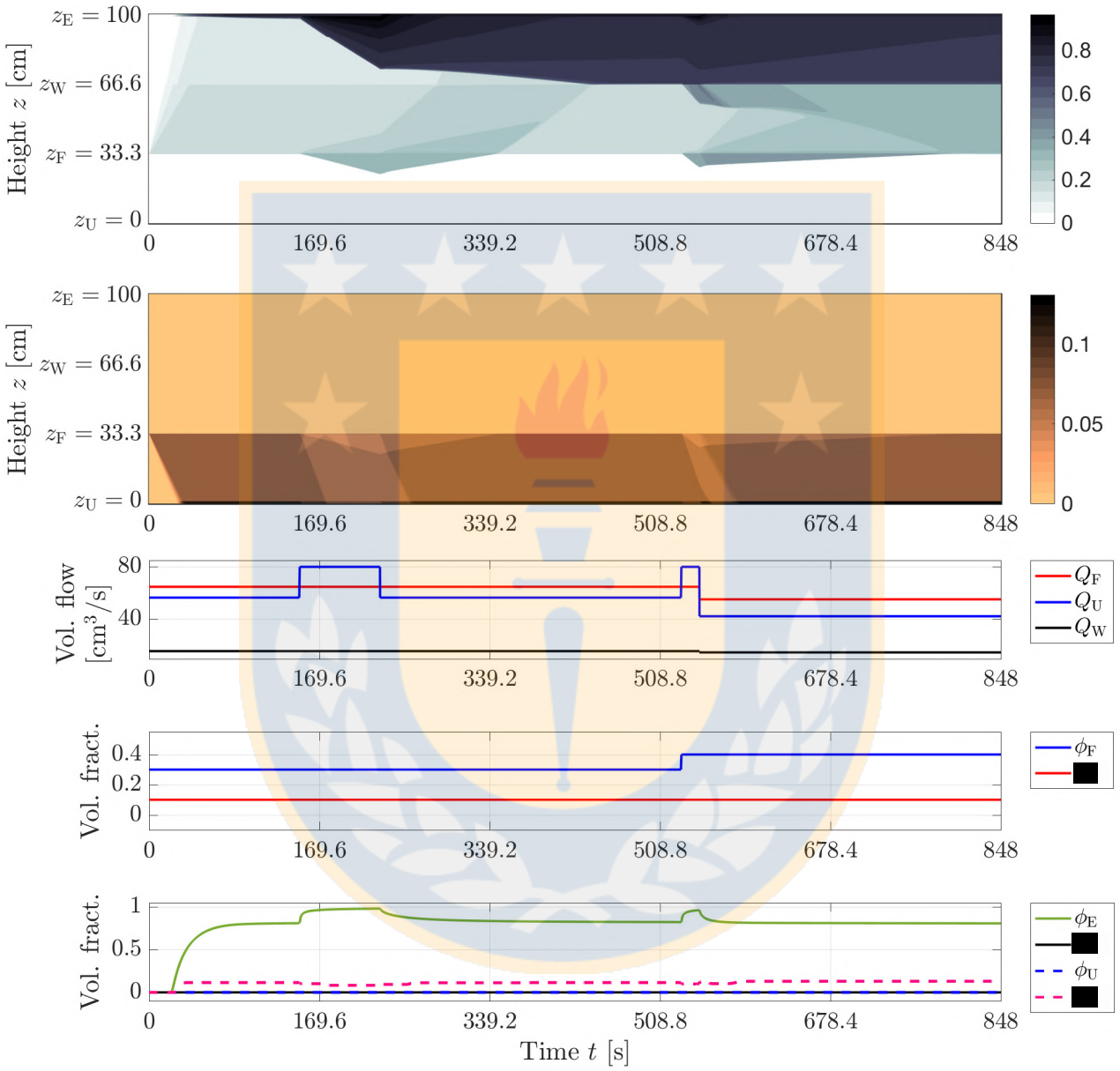

Figure 1.13: Example 1.2b. Dynamics of various variables from the initial time $t = 0\,\mathrm{s}$ to $t = 848\,\mathrm{s}$.

CHAPTER 2

Simulation and control of dissolved air flotation and column froth flotation with simultaneous sedimentation

2.1 Introduction

2.1.1 Scope

Gas flotation is a process to separate particles or droplets from a suspension when the particles/droplets are either too small or have a density too close to that of water to settle efficiently. The gas bubbles and particles/droplets form aggregates which rise to the top of a flotation tank where a layer of froth is skimmed off; see Figures 2.1 and 2.2 for two applications. The suspension may also contain hydrophilic particles that do not attach to bubbles and, if their density is larger than that of water, settle to the bottom where they are removed in the underflow.

In column froth flotation (CFF), a stable foam or froth at the top is required; see Figure 2.1. This can be utilized in the removal of metal ions from wastewater [8, 79, 93, 100], removal of emulsified oil from wastewater [32], or recovery of riboflavin from wastewater [94]. Another application is mineral processing as we mentioned in **Chapter 1**. In the process of DAF thickening, no stable foam layer is needed; however, while WAS (waste activated sludge) floats, grit and other substances may settle simultaneously [31, 114]; see Figure 2.2. Small air bubbles are trapped with the larger WAS flocs, which then float. In other applications, very small hydrophobic oil droplets attach to the air bubbles, while the grit settles. Remember that the simultaneous flotation–sedimentation process means that three phases are involved: liquid, buoyant aggregates and settling solids.

In this chapter we demostrate that the three-phase flow PDE model mentioned in Section 1.2 of **Chapter 1** for one-dimensional (1D) modelling of simultaneous flotation and sedimentation can be utilized for different flotation applications with or without a layer of froth at the top. We refer to Bürger et al. (2019) [18] for the derivation of the PDE model, the mathematical and numerical analyses behind the steady states and the numerical method. Our purpose

is thus not to fit the model to specific data in a specific application. While **Chapter 1** focus on the application to CFF in mineral processing, we present here new results for the DAF thickening process with the possible simultaneous sedimentation of solid particles. In particular, we present a new operating chart for the control of steady states of DAF thickening with sedimentation. The designs of flotation columns and DAF tanks are variable and since the purpose here is to advance a conceptual general model, we demonstrate its applicability to two different dimensioned tanks shown in Figures 2.1 and 2.2, and drift- and settling-flux functions in agreement with literature on CFF [38, 54].

To put this contribution into the proper perspective, we mention that 1D models of flotation columns for the two–phase flow of aggregates and fluid have been based on the drift-flux theory [38,113], or empirical relationships [12], which can model steady-state situations only. Dynamic models of flotation are few in the literature. The two–phase PDE framework by Bascur (1991) [6] is applicable to one of the zones of the column (Figure 2.1) and was extend [7] by several empirical equations for subprocesses, such as attachment and detachment in the froth and pulp regions.

The present approach differs from the models referred to above. Apart from the tank dimensions, the only model inputs in our 1D model are two constitutive functions for the aggregate rise velocity and the particle sedimentation velocity, respectively. An advantage of this model is that the interfaces of pulp/froth and liquid/particles appear naturally as discontinuities in the solution and need not be tracked explicitly. The description of the rise of aggregates in a fluid is conceptually similar to the settling of particles described by a batch settling–flux function. Widely accepted dynamic 1D simulation models for continuous sedimentation based on PDEs have been developed since the 1990s ([16,39,46]). This contrasts with the case of flotation, for which the potential of 1D PDE-based models has not yet been exploited fully.

Many of the properties defined in **Chapter 1** will be used in this chapter.

2.1.2 Outline of the chapter

The remainder of the chapter is organized as follows. Some general assumptions of the PDE model is presented in Section 2.2. In Section 2.3, the necessary conditions for the desired steady states solutions and their operating charts are given for the DAF thickening case. In Section 2.4, we present numerical solutions of (2.1) for CFF and DAF applications that illustrate the behaviour of the model using the numerical scheme mentioned in **Chapter 1**.

2.2 PDE model and dynamic solutions

We assume that all aggregation of (hydrophobic) particles and bubbles occurs before the slurry is fed into the column, e.g. in the incoming pipe [54]. This assumption is also consistent

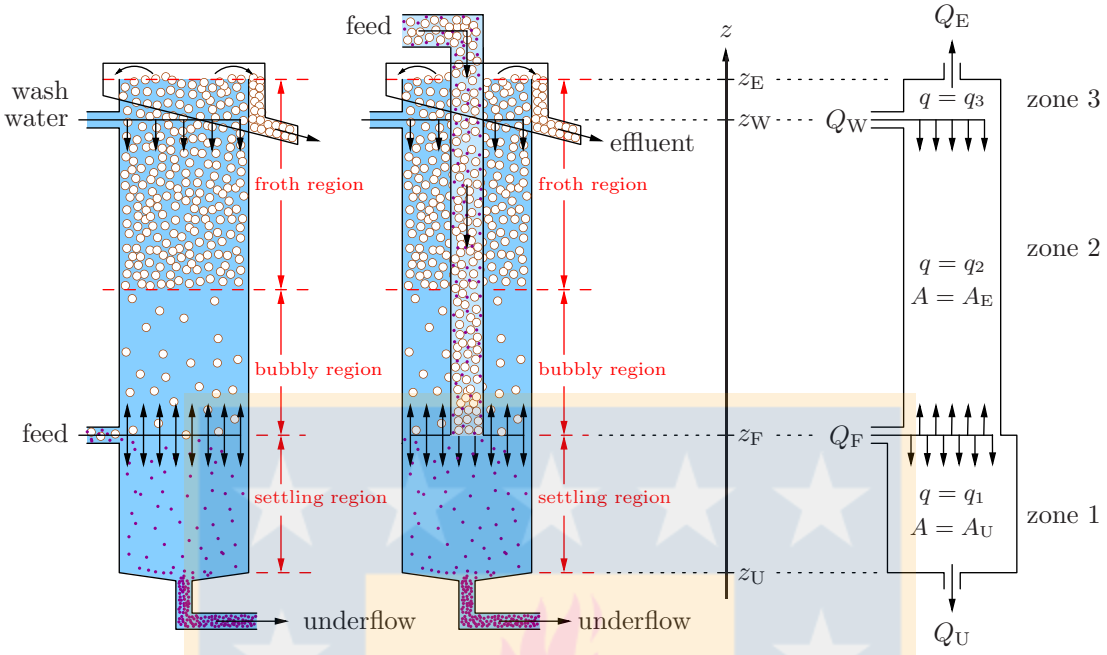

Figure 2.1: Schematic of CFF with a feed inlet for slurry mixture and gas (cf. [18]). At the top, wash water can be injected for desliming of unwanted particles. We simulate here the second column where the fluid-gas-particle slurry is fed through a downcomer pipe, which makes the cross-sectional area vary with height z.

with the principle of operation of *dissolved* air flotation (i.e. there is one feed stream that also contains the air in dissolved form), as opposed to *dispersed* air flotation. The distinction between both is clearly made, for instance, by Metcalf and Eddy [81]. Figure 2.1 shows a typical vessel for froth flotation, where wash water can be injected at the top, while Figure 2.2 shows a DAF thickener which has no wash water. Remember that the system of PDEs of the conservation of mass for the three phases of aggregates, fluid and (hydrophilic) settling solids as we mentioned in **Chapter 1** is:

$$A(z)\frac{\partial \phi}{\partial t} + \frac{\partial}{\partial z}\big(A(z)J(\phi, z, t)\big) = Q_{\mathrm{F}}(t)\phi_{\mathrm{F}}(t)\delta(z - z_{\mathrm{F}}), \tag{2.1a}$$

$$A(z)\frac{\partial}{\partial t}\big((1-\phi)\varphi\big) - \frac{\partial}{\partial z}\big(A(z)F(\varphi, \phi, z, t)\big) = Q_{\mathrm{F}}(t)\psi_{\mathrm{F}}(t)\delta(z - z_{\mathrm{F}}). \tag{2.1b}$$

The unknowns ϕ and φ depend on height z and time t. The volume fractions of aggregates are ϕ and solids ψ, respectively. The variable $\varphi = \psi/(1-\phi)$ is the volume fraction of settling solids within the suspension. The cross–sectional area $A(z)$ may depend on z in any way; however, for the scenarios here we let it be piecewise constant and take at most two values (A_{U} and A_{E}); see Figure 2.1. With the given inlet volumetric flows Q_{F} and Q_{W}, we then define the zone bulk velocities $q_1 = -Q_{\mathrm{U}}/A_{\mathrm{U}}$, $q_2 = (-Q_{\mathrm{U}} + Q_{\mathrm{F}})/A_{\mathrm{E}}$ and $q_3 = (-Q_{\mathrm{U}} + Q_{\mathrm{F}} + Q_{\mathrm{W}})/A_{\mathrm{E}}$ for

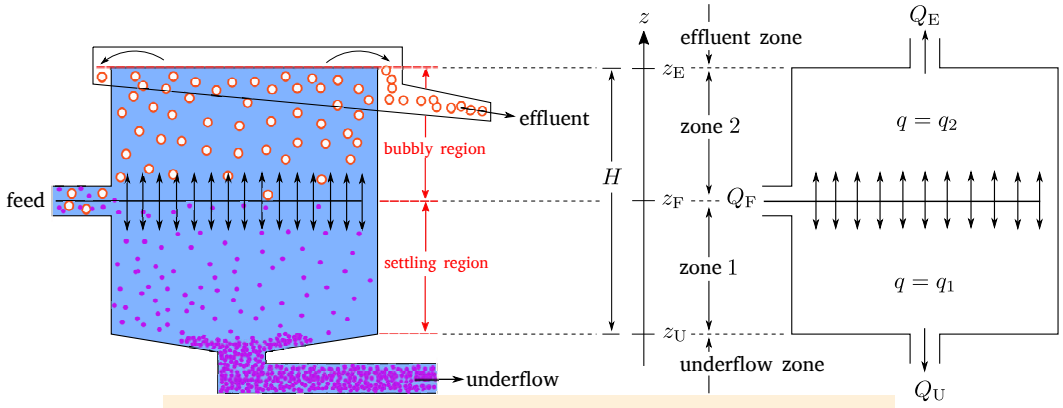

Figure 2.2: Schematic of a DAF thickener (cf. [114]) with constant cross-sectional area and two zones.

CFF (Figure 2.1). For DAF (Figure 2.2), we let $A = A_U = A_E$. The total flux functions for the rising aggregates $J(\phi, z, t)$ and settling solids $F(\varphi, \phi, z, t)$ are given by (1.11) and (1.12), respectively.

In Section 1.2.2 we defined the batch drift-flux function $j_b(\phi)$ for the rising aggregates and the batch settling-flux function $f_b(\varphi)$ for the settling solids contained in the total flux functions J and F. Both functions principally have the same concave–convex form with one inflection point. The choice of explicit expression (polynomial, exponential, power law, etc.) for $j_b(\phi)$ and $f_b(\varphi)$ depends on the materials and belongs to the model calibration step. The choice does not influence the qualitative behaviour of the process.

For the batch-drift-flux function $j_b(\phi)$ the terminal velocity of a single bubble in water is $v_{term,a} = 2.7\,\mathrm{cm/s}$ and the dimensionless parameter n_a is chosen here as $n_a = 3.2$ [38]. For the batch-settling flux $f_b(\varphi)$, we have chosen $v_{term,s} = 0.5\,\mathrm{cm/s}$ (Scenario DAF1), $v_{term,s} = 0.1\,\mathrm{cm/s}$ (Scenario DAF2), and $n_s = 2.5$. We neglect, for simplicity, compression effects.

We utilize the triangular property of the system (2.1) in the classification of desired steady states for the derivation of operating charts and the numerical method for the PDE system. The latter has been adapted from a general treatment by Karlsen et al. [67]. The numerical method is the same as the one presented in Section 1.4 and has been implemented in MATLAB (2019).

2.3 Steady states and construction of an operating chart for DAF

The analysis of the stationary solutions of (2.1a) and (2.1b) is delicate and invokes a so-called entropy condition [39] to obtain physically correct solutions. For given feed volume fractions ϕ_F

and ψ_{F}, several nonlinear conditions on the volumetric flows have to be satisfied for a certain steady state to exist because of the feed inlets and discontinuities of the solution. The local maxima and minima of the zone flux functions appear in the inequalities (see [18] and Section 1.3 for all details). The nonlinear conditions can be visualized in operating charts (cf. Figures 2.3 and 2.6), where an operating point $(Q_{\mathrm{U}}, Q_{\mathrm{F}})$ in the admissible white region means that all conditions are satisfied. For CFF with wash water, the value of Q_{W} is calculated from a global mass balance. An operating chart depends on the values of ϕ_{F} and ψ_{F}, as can be seen from the difference between the left and right plots in Figure 2.3. We emphasize that the conditions for obtaining a certain steady state are only necessary; the actual state depends also on the dynamic history of the process.

A desired steady-state solution in DAF thickening (where there is no wash water), is one where aggregates are only present above the feed level and settling solids only below. The necessary conditions on the operating point $(Q_{\mathrm{U}}, Q_{\mathrm{F}})$ in the DAF case are four inequalities, which we now state and which are visualized in Figure 2.6. We assume, for simplicity, that the cross-sectional area A is constant. The fluid flow in zone 2 above the feed inlet should be upwards. This first constraint can be written as

$$Q_{\mathrm{F}} - Q_{\mathrm{U}} - \phi Q_{\mathrm{F}} > 0 \tag{2.2}$$

and for given ϕ_{F} this means an (upper left) triangular region in the operating chart; see two such in Figure 2.6. For the derivation of (2.2), we refer to [18]; see condition (FIIIa) therein. Condition (2.2) implies that the effluent volumetric flow satisfies $Q_{\mathrm{E}} = Q_{\mathrm{F}} - Q_{\mathrm{U}} > 0$. The other three curves that define the white region in the operating chart are given by the following nonlinear inequalities ([18]: conditions FIa, FIb and FIas (Section 1.3.1)):

$$\begin{aligned} & j_b(\phi_2^{\mathrm{M}}(q_2)) + q_2\phi_2^{\mathrm{M}}(q_2) \geq \frac{Q_{\mathrm{F}}\phi_{\mathrm{F}}}{A}, \\ & \phi_2 \leq \phi_{1\mathrm{Z}}, \\ & f_b(\varphi_{1\mathrm{M}}(q_1)) - q_1\varphi_{1\mathrm{M}}(q_1) \geq \frac{Q_{\mathrm{F}}\psi_{\mathrm{F}}}{A}. \end{aligned}$$

These formulas involve four volume fractions that are calculated as follows:

- $\phi_2^{\mathrm{M}}(q_2)$ is the local maximum point (located below the inflection point) of the function $j_b(\phi) + q_2\phi$,
- ϕ_2 is the solution (located to the left of the maximum point $\phi_2^{\mathrm{M}}(q_2)$ of the equation $j_b(\phi) + q_2\phi = Q_{\mathrm{F}}\phi_{\mathrm{F}}/A$,
- $\phi_{1\mathrm{Z}}$ is the solution of the equation $j_b(\phi) + q_1\phi = 0$,
- $\varphi_{1\mathrm{M}}(q_1)$ is the local minimum point (located to the right of the inflection point) of the function $f_b(\varphi) + q_1\varphi$

where we recall that $q_1 = -Q_{\mathrm{U}}/A$ and $q_2 = (-Q_{\mathrm{U}} + Q_{\mathrm{F}})/A$.

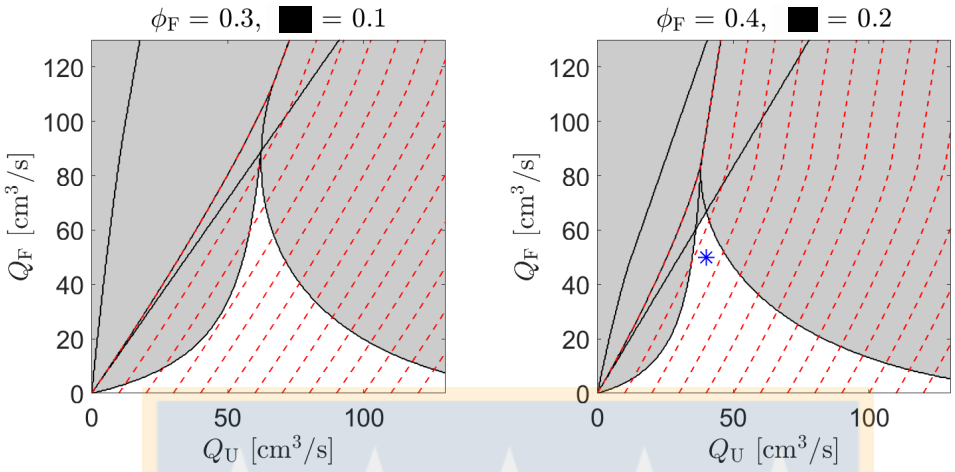

Figure 2.3: Example 2.1: Scenario CFF. Operating charts for CFF showing the intersection of several nonlinear inequalities for given feed volume fractions of aggregates ϕ_F and solids ψ_F. The white region shows the values of (Q_U, Q_F) that can be chosen to obtain a desired steady state. The top corner of the white region indicates the maximum possible value for Q_F, which is the optimal handling capacity. Along each dashed curve the volumetric wash water flow Q_W is constant and its value can be read off on the Q_U-axis. That is, on the leftmost curve $Q_W = 0\,\text{cm}^3/\text{s}$, on the next one $Q_W = 10\,\text{cm}^3/\text{s}$, etc.

2.4 Numerical simulations

2.4.1 Preliminaries

For the case study of CFF in Figure 2.1, we have used the values $A_E = 72.25\,\text{cm}^2$ and $A_U = 83.65\,\text{cm}^2$, and consider a laboratory scale column of height 1 m with $z_F = 33\,\text{cm}$ and $z_W = 90\,\text{cm}$. Two operating charts are shown in Figure 2.3 for a desired steady-state solution having a layer of froth in zone 3, a possible froth discontinuity in zone 2, and solids only in zone 1 ([18]: case SS31).

For the case study of a DAF thickener in Figure 2.2, we have used the constant cross-sectional area $A = \pi 2.5^2\,\text{m}^2 = 19.635\,\text{m}^2$, height $H = 2\,\text{m}$ and feed inlet at $z_F = 1\,\text{m}$.

2.4.2 Example 2.1: Scenario CFF

We assume that the feed volume fractions are $\phi_F = 0.4$ and $\psi_F = 0.2$. In Figure 2.3 (right), we choose the operating point $(Q_U, Q_F) = (40, 50)\,\text{cm}^3/\text{s}$ in the white region; see the asterisk. The wash water volumetric flow is calculated to $Q_W = 14.46\,\text{cm}^3/\text{s}$, which is the maximum that can flow downwards through the foam. A larger value would cause an overflow of wash

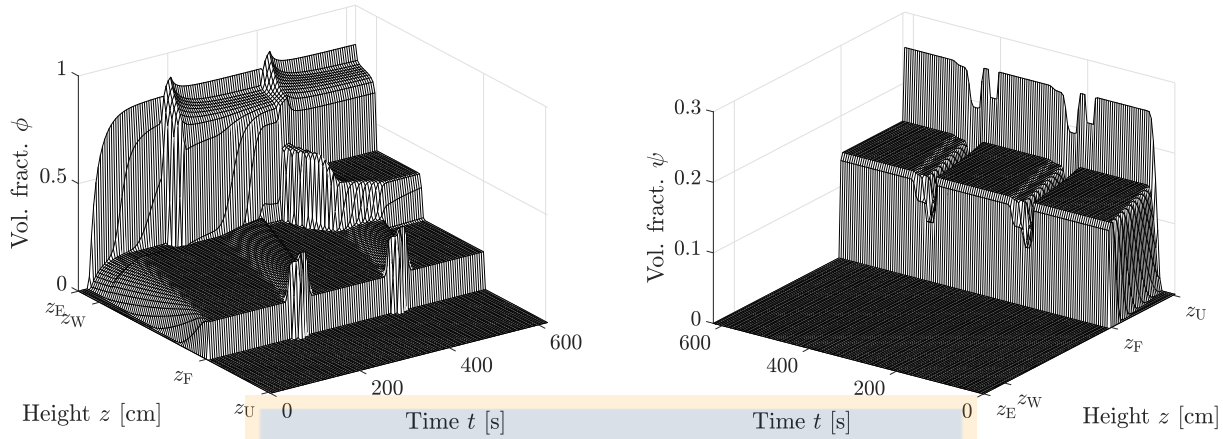

Figure 2.4: Example 2.1: Scenario CFF. Simulation results with volume fractions of aggregates (left) and solids (right) as functions of height z [cm] and time t [s].

water through the effluent. Figures 2.4 and 2.5 show a simulation when the column initially contains only water. Very quickly, a steady state is reached at $t = 180\,\mathrm{s}$; see Figures 2.4 (left) and 2.5(a). This has a low concentration of aggregates at the top and we perform some control actions. At $t = 180\,\mathrm{s}$, the top is closed until $t = 200\,\mathrm{s}$ by temporarily setting $Q_\mathrm{U} = 64.46\,\mathrm{cm}^3/\mathrm{s}$ (so that the effluent volumetric flow is $Q_\mathrm{E} = 0\,\mathrm{cm}^3/\mathrm{s}$). Aggregates will then accumulate at the top of the column and around the feed inlet. At $t = 200\,\mathrm{s}$, we reopen the effluent by setting back $Q_\mathrm{U} = 40\,\mathrm{cm}^3/\mathrm{s}$. The aggregates then move upwards; compare Figure 2.5(b) and 2.5(c). At about $t = 400\,\mathrm{s}$, an approximate steady state is reached (Figure 2.5(d)), which has a high concentration of froth only in the small zone 3. If we close the top of the tank again during 20 s more, another steady state is reached at about $t = 620\,\mathrm{s}$ with a high froth concentration also in the upper part of zone 2, which is a desired steady state in mineral processing.

2.4.3 Example 2.2: Scenario DAF1

We simulate a DAF tank that initially contains only water and the feed volume fractions are $\phi_\mathrm{F} = 0.2$ and $\psi_\mathrm{F} = 0.2$. The operating chart can be seen in Figure 2.6 (left). Choosing the operating point $(Q_\mathrm{U}, Q_\mathrm{F}) = (300, 450)\,\mathrm{m}^3/\mathrm{h}$ in the white region, one gets the simulation shown in Figure 2.7. A first desired steady state, with aggregates only above the feed inlet and solids only below it, appears quickly after about $t = 0.07\,\mathrm{h} = 4.2\,\mathrm{min}$. Then, we change the feed volume fraction of aggregates from $\phi_\mathrm{F} = 0.2$ to $\phi_\mathrm{F} = 0.4$ and simulate the reaction of the system; see Figure 2.7(a) and 2.7(b). As Figure 2.7(a) shows, aggregates accumulate at the top of the vessel and a growing layer reaches and passes below the feed point. In the corresponding operating chart for this new set of variables, in Figure 2.6 (right), the operating point, marked with a blue asterisk, lies now outside the admissible white region. To avoid this situation, we resimulate the scenario and perform a control action at $t = 0.27\,\mathrm{h} = 16.2\,\mathrm{min}$ by choosing a new

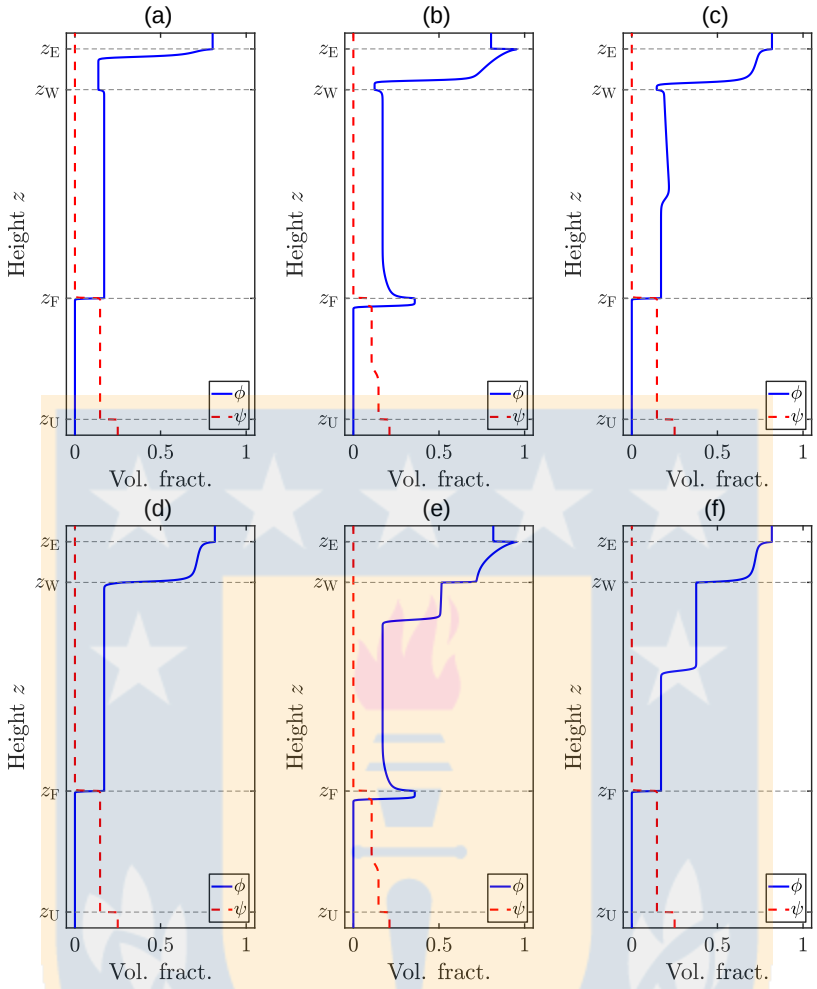

Figure 2.5: Example 2.1: Scenario CFF. Snapshots of the simulation shown in Figure 2.4 at $t = 180,\ 200,\ 300,\ 400,\ 420$ and $620\,\mathrm{s}$ for the volume fractions of the aggregates ϕ_F (solid) and solids ψ_F (dashed).

operating point $(Q_U, Q_F) = (250, 600)\,\mathrm{m}^3/\mathrm{h}$ inside the white area in Figure 2.6 (right), marked with a red point. In Figure 2.7(c) and 2.7(d) the reaction of the system is shown. The layer of aggregates that was increasing downwards now turns upwards, eventually leaving through the effluent. In this case, a desired steady state is finally reached after $t = 0.5\,\mathrm{h} = 30\,\mathrm{min}$.

2.4.4 Example 2.3: Scenario DAF2

In this example, we focus on the solids behaviour. We consider solid particles whose density is slightly larger than that of water so they can easily be caught in an upstream towards the effluent. To simulate this, we choose the lower value $v_{\mathrm{term,s}} = 0.1\,\mathrm{cm/s}$ and consider a tank initially filled with water when aggregates and solids are fed with volume fractions $\phi_F = 0.3$ and

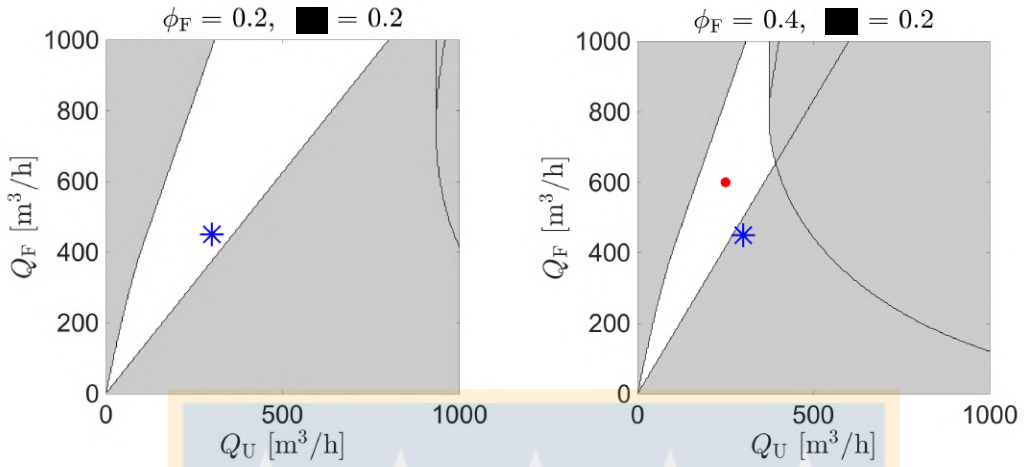

Figure 2.6: Example 2.2: Scenario DAF1. Operating charts before $t = 0.27\,\mathrm{h} = 16.2\,\mathrm{min}$ (left) and after (right), where the feed volume fractions ϕ_F and ψ_F make a step change. The blue asterisk marks the first operating point and the red dot the second one considered after the control action at $t = 0.27\,\mathrm{h} = 16.2\,\mathrm{min}$.

$\psi = 0.1$. The point $(Q_U, Q_F) = (100, 400)\,\mathrm{m}^3/\mathrm{h}$ is chosen in the white region of the operating chart in Figure 2.8, which is a necessary condition for a desired steady state, but not sufficient, as can be seen for small times in the simulation result in Figure 2.9. A steady state is quickly reached for the aggregates while solid particles start settling but also move upwards, leaving through the effluent after $t = 0.2\,\mathrm{h} = 12\,\mathrm{min}$. This is not a desired steady state. Therefore, at $t = 0.2\,\mathrm{h} = 12\,\mathrm{min}$ we make a control action by setting $(Q_U, Q_F) = (250, 400)\,\mathrm{m}^3/\mathrm{h}$. Figure 2.9 shows how the aggregates quickly reach a desired steady state with a high concentration in the effluent while the solids that where on the upper part of the tank slowly settle to the bottom, reaching a steady state with solids present only below the feed inlet after $t = 2\,\mathrm{h}$.

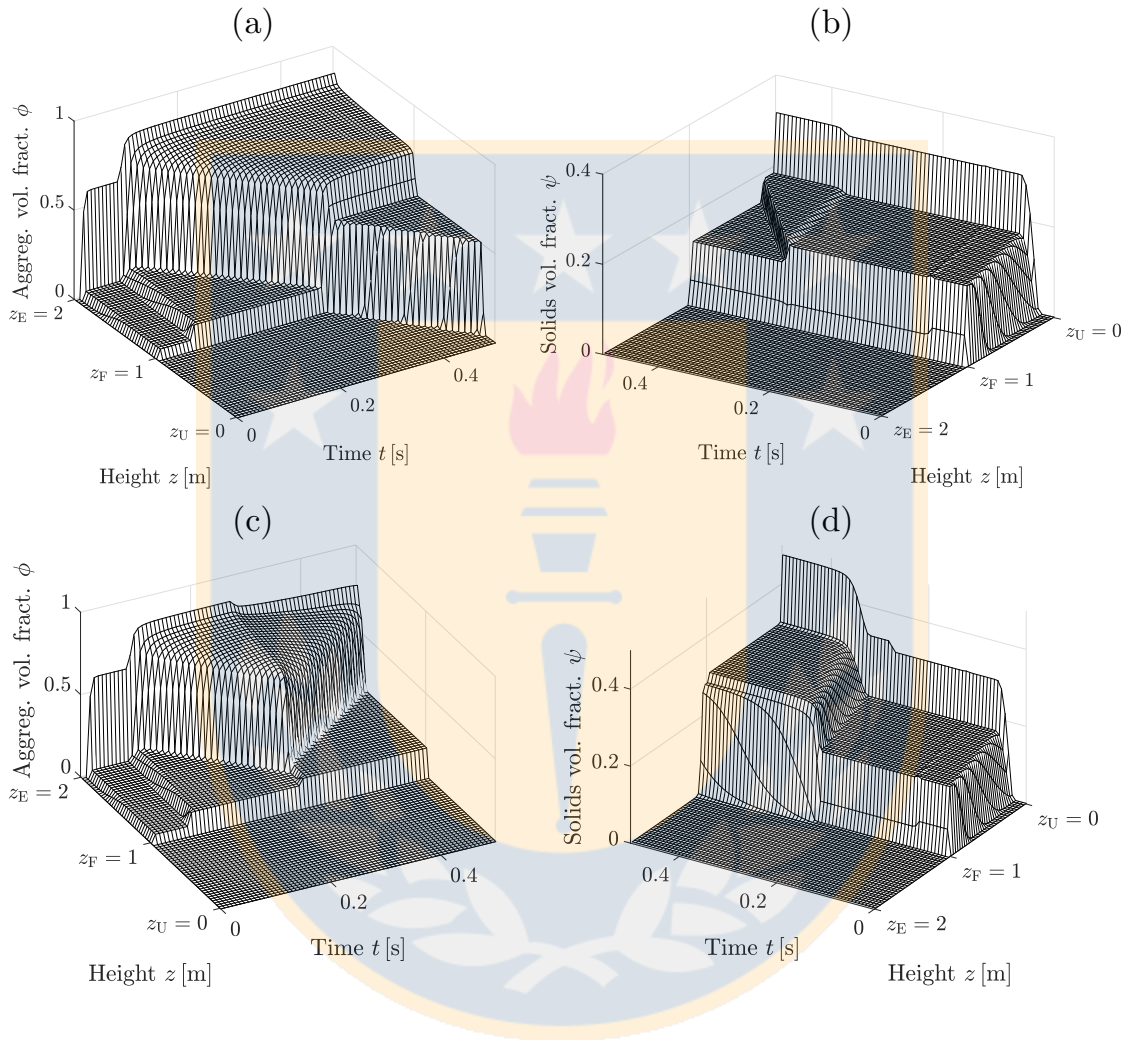

Figure 2.7: Example 2.2: Scenario DAF1. The first row shows a simulation of aggregates (a) and solids (b) volume fraction without control action. A layer of aggregates is built up and grows into the thickening zone below the feed level (zone 1). The second row (c, d) shows a simulation with control action at $t = 0.27\,\mathrm{h} = 16.2\,\mathrm{min}$.

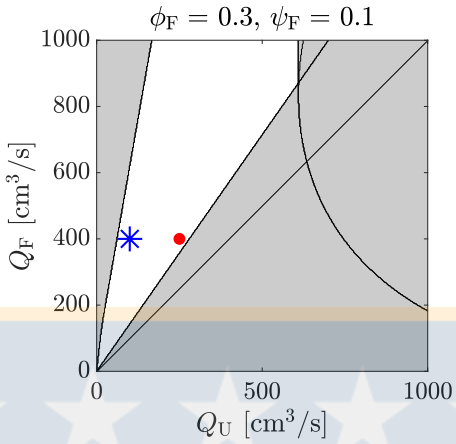

Figure 2.8: Example 2.3: Scenario DAF2. Operating chart for feed volume fractions of aggregates $\phi_F = 0.3$ and solids $\psi = 0.1$. The blue asterisk marks the first operating point and the red dot the second one considered after the control action.

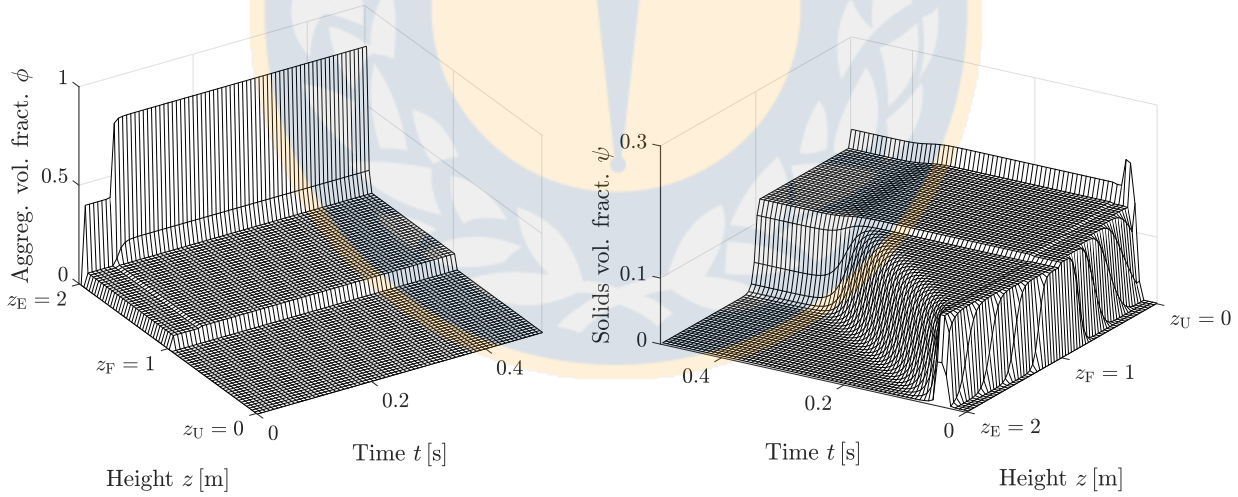

Figure 2.9: Example 2.3: Scenario DAF2. Simulation of aggregates (left) and solids (right) volume fraction with a control action taken at $t = 0.2\,\text{h} = 12\,\text{min}$. The final steady state has a desired large jump in the volume fraction of aggregates at the top of the tank and all slowly settling particles leave through the underflow.

CHAPTER 3

A difference scheme for a triangular system of conservation laws with discontinuous flux modeling three-phase flows

3.1 Introduction

3.1.1 Scope

It is the purpose of this chapter and **Chapter** 4 to generalize, and in part analyze, the numerical scheme for a system of conservation laws with source terms of the type presented in **Chapter** 1

$$\partial_t \left(A(z) \begin{pmatrix} \phi \\ \psi \end{pmatrix} \right) + \partial_z \left(A(z) \begin{pmatrix} J(\phi, z, t) \\ \tilde{F}(\phi, \psi, z, t) \end{pmatrix} \right) = \sum_{k=1}^{K} Q_{\mathrm{F},k}(t) \begin{pmatrix} \phi_{\mathrm{F},k}(t) \\ \psi_{\mathrm{F},k}(t) \end{pmatrix} \delta(z - z_{\mathrm{F},k}), \tag{3.1}$$

where t is time, z is spatial position, ϕ is the concentration (volume fraction or density) of the primary disperse phase, and ψ is the volume fraction of the secondary disperse phase. Both disperse phases move within the continuous phase of the one-dimensional flow. We let $A(z)$ denote a variable cross-sectional area, and assume that $z = z_{\mathrm{U}} < z_{\mathrm{F},1} < \cdots < z_{\mathrm{F},K} < z_{\mathrm{E}}$ are positions across which the flux functions J and $\tilde{F}$ are discontinuous. These fluxes contain the constitutive assumptions of the model and therefore are nonlinear functions of ϕ and ψ. The right-hand side of (3.1) describes the effect of singular sources located at $z = z_{\mathrm{F},k}$, $k = 1, \ldots, K$, and is composed of given functions. It is assumed that $Q_{\mathrm{F},k}(t)$ is the volumetric bulk flow of the mixture (the continuous and the two disperse phases) injected at $z = z_{\mathrm{F},k}$, and that $\phi_{\mathrm{F},k}(t)$ and $\psi_{\mathrm{F},k}(t)$ are the volume fractions of the primary and secondary disperse phases in the feed flow, respectively. System (3.1) is posed on the domain $\Pi_T := \mathbb{R} \times (0, T)$ together with initial conditions

$$\phi(z, 0) = \phi_0(z) \quad \text{for all } z \in \mathbb{R}, \tag{3.2a}$$

$$\psi(z, 0) = \psi_0(z) \quad \text{for all } z \in \mathbb{R}, \tag{3.2b}$$

where we assume that

$$0 \leq \phi_0(z) \leq 1, \quad 0 \leq \psi_0(z) \leq 1 - \phi_0(z) \quad \text{for all } z \in \mathbb{R}. \tag{3.3}$$

Likewise, we assume that

$$0 \leq \phi_{\mathrm{F},k}(t) \leq 1, \quad 0 \leq \psi_{\mathrm{F},k}(t) \leq 1 - \phi_{\mathrm{F},k}(t) \quad \text{for all } k = 1, \ldots, K \text{ and } t \in [0, T]. \tag{3.4}$$

System (3.1) models the flow of three phases, namely the continuous phase and two disperse phases. If θ denotes the volume fraction of the continuous phase, then we assume that

$$0 \leq \phi, \psi, \theta \leq 1; \quad \phi + \psi + \theta = 1, \tag{3.5}$$

which motivates assumptions (3.3) and (3.4). (Of course, satisfaction of (3.5) by exact or numerical solutions of (3.1), (3.2) on Π_T needs to be proved; this issue is addressed within this chapter.)

System (3.1) could also apply to other unit operations and, as we mentioned in **Chapters 1–2**, it serves as a model of a flotation column [17, 18], where ϕ denotes the volume fraction of bubbles (specifically, aggregate bubbles) and ψ that of solid particles (Figure 3.1). The bottom of the column has the coordinate z_{U} (the underflow) and the top z_{E} (the effluent). The primary phase of bubbles is assumed to flow through the suspension of solid particles and liquid independently of the volume fraction of solids. The solid particles move in the remaining space outside the bubbles and make up the secondary phase. If the solid particles of the secondary phase have a density larger than that of the fluid, we have counter-current flow of the two phases; otherwise co-current flow. The distinction between primary and secondary disperse phase also becomes evident in the components of the flux functions: the flux J of the primary phase depends on ϕ only (besides z and t), while that of the secondary phase, $\tilde{F}$, depends both on ϕ and its own volume fraction ψ. Thus, the system (3.1) is triangular; however, it is generally non-strictly hyperbolic; see [18], which presents the counter-current model of the form (3.1).

The main contribution of this chapter is an easily implemented explicit numerical scheme for (3.1) that provably satisfies an invariant-region property, namely that the volume fractions of the three phases stay between zero and one.

3.1.2 Outline of the chapter

The remainder of this chapter is organized as follows. In Section 3.2, the model from [18] is written in a slightly more general form. We outline the derivation of the fluxes of the governing PDE system (3.1) from the balance equations of the three phases.

In Section 3.3 the proposed numerical method is detailed. The discretization of the model is introduced in Section 3.3.1 while the numerical fluxes and update formulas for both disperse

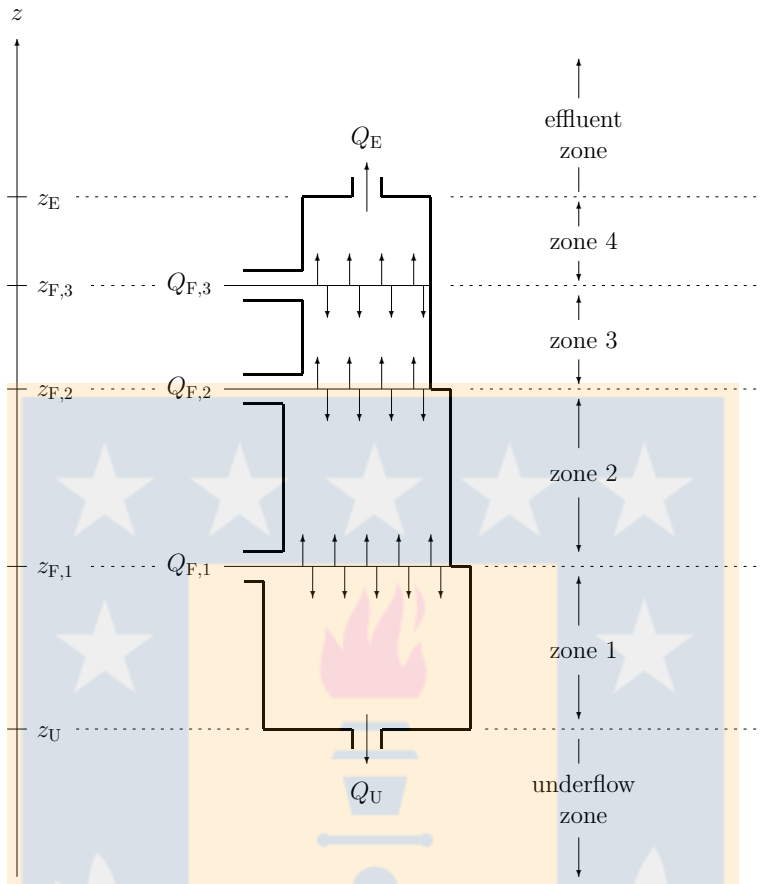

Figure 3.1: Schematic of a one-dimensional column with $K = 3$ inlets and $K + 1 = 4$ zones, where Q_U is the downwards volumetric outflow, $Q_{F,j}$ is the volumetric flow at the inlet $z_{F,j}$, for each $j = 1, \ldots, K$, and Q_E is the upwards volumetric outflow. Note that the distances between the inlets/outlets are arbitrary and the cross-sectional area $A = A(z)$ may vary piecewise continuously (although the figure shows a piecewise constant example).

phases are described in Sections 3.3.2 and 3.3.3. In Section 3.3.4, we prove that the numerical method is monotone and that the approximated solutions obtained by the numerical method proposed in this work satisfy a so-called invariant-region property, i.e., the approximations of both phases ϕ and ψ are bounded between zero and one, given that the initial data also satisfy this.

Estimations of errors and convergence order of the numerical method can be found in Section 3.4.1. Some numerical examples are presented in Section 3.4. First, in Section 3.4.3, we use a smooth solution to estimate the order of convergence. Later on, we present two numerical examples that illustrate the model predictions for counter-current (Section 3.4.4) and co-current flows (Section 3.4.5).

3.2 Three-phase flow model

The density of each phase is assumed constant, so the conservation of mass of each phase can be expressed as the system of balance equations

$$\partial_t\big(A(z)\phi\big) + \partial_z\big(A(z)\phi v_\phi\big) = \sum_{k=1}^{K} Q_{\mathrm{F},k}(t)\phi_{\mathrm{F},k}(t)\delta(z - z_{\mathrm{F},k}), \tag{3.6}$$

$$\partial_t\big(A(z)\psi\big) + \partial_z\big(A(z)\psi v_\psi\big) = \sum_{k=1}^{K} Q_{\mathrm{F},k}(t)\psi_{\mathrm{F},k}(t)\delta(z - z_{\mathrm{F},k}), \tag{3.7}$$

$$\partial_t\big(A(z)\theta\big) + \partial_z\big(A(z)\theta v_\theta\big) = \sum_{k=1}^{K} Q_{\mathrm{F},k}(t)\big(1 - \phi_{\mathrm{F},k}(t) - \psi_{\mathrm{F},k}(t)\big)\delta(z - z_{\mathrm{F},k}), \tag{3.8}$$

where the right-hand sides contain Dirac functions, the feed volume fractions $\phi_{\mathrm{F},k}$ and $\psi_{\mathrm{F},k}$ of the disperse phases, and the corresponding volume fraction $1-\phi_{\mathrm{F},k}(t)-\psi_{\mathrm{F},k}(t)$ of the continuous phase, at the inlet located at $z = z_{\mathrm{F},k}$, $k = 1, \dots, K$.

We define the volume-average velocity, or bulk velocity, of the mixture by

$$q := \phi v_\phi + \psi v_\psi + \theta v_\theta,$$

and replace (3.8) by the sum of (3.6)–(3.8), which is

$$\partial_z\big(A(z)q\big) = \sum_{k=1}^{K} Q_{\mathrm{F},k}(t)\delta(z - z_{\mathrm{F},k}). \tag{3.9}$$

Consequently, within the unit q varies with distance z due to the K inlet flows and the variable cross-sectional area. We define $Q(z,t) := A(z)q(z,t)$ and integrate (3.9) from any point $z_0 < z_{\mathrm{U}}$ to obtain

$$Q(z,t) = Q(z_0,t) + \sum_{k=1}^{K} Q_{\mathrm{F},k}(t)H(z - z_{\mathrm{F},k}),$$

where $H(\cdot)$ is the Heaviside function. If the volumetric underflow $Q_{\mathrm{U}}(t)$ is given, then $Q(z,t) = -Q_{\mathrm{U}}(t)$ for $z < z_{\mathrm{U}}$, and

$$Q(z,t) = -Q_{\mathrm{U}}(t) + \sum_{k=1}^{K} Q_{\mathrm{F},k}(t)H(z - z_{\mathrm{F},k}) = -Q_{\mathrm{U}}(t) + \sum_{k:z_{\mathrm{F},k}\geq z} Q_{\mathrm{F},k}(t).$$

This is the continuity equation of the mixture, which replaces (3.8). We next rewrite (3.6) and (3.7) in terms of q and two constitutive functions. We refer to the continuous phase and the secondary disperse phase as "secondary mixture", and define the volume fraction of the secondary disperse phase within the secondary mixture as

$$\varphi := \frac{\psi}{\psi + \theta} = \frac{\psi}{1 - \phi} \quad (\text{when } \phi < 1),$$

where $0 \le \varphi \le 1$ by (3.5). The volume-average velocity of the secondary mixture is

$$q_{\mathrm{s}} := \frac{\psi v_\psi + \theta v_\theta}{\psi + \theta} = \varphi v_\psi + \frac{1-\phi-\psi}{1-\phi} v_\theta = \varphi v_\psi + (1-\varphi) v_\theta.$$

It is then assumed that within $[z_{\mathrm{U}}, z_{\mathrm{E}})$, the relative velocity $v_{\phi\mathrm{s}} := v_\phi - q_{\mathrm{s}}$ of the primary disperse phase with respect to the secondary mixture is a given constitutive function $\tilde{v}_{\phi\mathrm{s}}(\phi)$, while outside that interval, both phases move at the same velocity, so their velocity difference is zero. Thus, defining the characteristic function

$$\gamma(z) := \chi_{[z_{\mathrm{U}}, z_{\mathrm{E}})}(z) = \begin{cases} 1 & \text{for } z \in [z_{\mathrm{U}}, z_{\mathrm{E}}), \\ 0 & \text{for } z \notin [z_{\mathrm{U}}, z_{\mathrm{E}}), \end{cases}$$

we have $v_{\phi\mathrm{s}} = \gamma(z)\tilde{v}_{\phi\mathrm{s}}(\phi)$. Within $[z_{\mathrm{U}}, z_{\mathrm{E}})$, the relative velocity of the secondary disperse phase with respect to the continuous phase $v_{\psi\theta} := v_\psi - v_\theta$ is supposed to be a given function $\tilde{v}_{\psi\theta}$ of φ, that is, we employ $v_{\psi\theta} = \gamma(z)\tilde{v}_{\psi\theta}(\varphi)$.

The definitions of all velocities imply the identities

$$\begin{aligned} \phi v_\phi &= \phi q + \gamma(z)\phi(1-\phi)\tilde{v}_{\phi\mathrm{s}}(\phi), \\ \psi v_\psi &= \psi q + \gamma(z)\psi\big((1-\varphi)\tilde{v}_{\psi\theta}(\varphi) - \phi\tilde{v}_{\phi\mathrm{s}}(\phi)\big). \end{aligned} \tag{3.10}$$

for the (unweighted) fluxes ϕv_ϕ and ψv_ψ arising in (3.6) and (3.7), respectively. It is then useful to introduce the velocity and flux functions

$$\begin{aligned} W(\phi) &:= (1-\phi)\tilde{v}_{\phi\mathrm{s}}(\phi), & V(\varphi) &:= \sigma(1-\varphi)\tilde{v}_{\psi\theta}(\varphi), \\ j(\phi) &:= \phi W(\phi), & f(\varphi) &:= \varphi V(\varphi), \end{aligned} \tag{3.11}$$

where $\sigma = \pm 1$ is chosen depending on the application such that $V(\varphi), f(\varphi) \ge 0$ (for standard convenience, e.g., when plotting their graphs); $\sigma = 1$ for co-current flows (upwards) and $\sigma = -1$ for counter-current flows. The velocity and flux of the secondary phase with respect to the z-coordinate are therefore $\sigma V(\varphi)$ and $\sigma f(\varphi)$, respectively. We assume that $W', V' \le 0$ and $V(1) = W(1) = 0$, as well as that

$$f \text{ has one local maximum } \omega \text{ and one inflection point } \tilde{\omega},\ 0 < \omega < \tilde{\omega} < 1. \tag{3.12}$$

Combining (3.10) and (3.11) yields the expressions

$$\begin{aligned} \phi v_\phi &= \phi q + \gamma(z)\phi W(\phi) =: J(\phi, z, t), \\ \psi v_\psi &= (1-\phi)\varphi q + \gamma(z)\big((1-\phi)\varphi\sigma V(\varphi) - \varphi\phi W(\phi)\big) =: F(\varphi, \phi, z, t) \end{aligned} \tag{3.13}$$

for the total fluxes of (3.6) and (3.7). For $\phi < 1$, we define the final flux function

$$\tilde{F}(\phi, \psi, z, t) := F\left(\phi, \frac{\psi}{1-\phi}, \phi, z, t\right) = \psi q + \gamma(z)\left(\psi\sigma V\left(\frac{\psi}{1-\phi}\right) - \frac{\psi\phi W(\phi)}{1-\phi}\right), \tag{3.14}$$

whereas for $\phi = 1$, we set $\tilde{F}(\psi, 1, z, t) := 0$ (since $F(\varphi, 1, z, t) = 0$ for all $\varphi \in [0, 1]$). Substituting (3.13) and (3.14) into (3.6) and (3.7), respectively, yields the final governing PDE system (3.1).

For illustrations and numerical examples, we use the Richardson-Zaki expressions [98]

$$W(\phi) = v_{\text{term,p}}(1-\phi)^{n_\text{p}} \quad \text{for } 0 \le \phi \le 1, \quad n_\text{p} > 1, \tag{3.15}$$

$$V(\varphi) = v_{\text{term,s}}(1-\varphi)^{n_\text{s}} \quad \text{for } 0 \le \varphi \le 1, \quad n_\text{s} > 1, \tag{3.16}$$

where $v_{\text{term,p}}$ and $v_{\text{term,s}}$ are the terminal velocities of a single particle of the primary and secondary phases, respectively, in an unbounded fluid.

In Figure 3.2, we illustrate the non-linearities of the flux functions $J(\phi, z, t)$ and $\tilde{F}(\phi, \psi, z, t)$ in the different zones of the column. We set $n_\text{p} = 3.2$ and $v_{\text{term,p}} = 2.7\,\text{cm/s}$ for the primary phase velocity function W and $n_\text{s} = 2.5$ and $v_{\text{term,s}} = 0.5\,\text{cm/s}$ for the secondary phase velocity function V and consider $\sigma = -1$. The values choosen here are used in Examples 3.2 and 3.3 in Section 3.4.

3.3 Numerical method

3.3.1 Discretization and CFL condition

The discretization of the model is based on the triangularity of the system of conservation laws (3.1). The numerical fluxes are based on the particular treatment of conservation laws arising in kinematic modelling with fluxes having an explicit "concentration times velocity" structure [23] and obtain an approximate solution ϕ of the first PDE of (3.1). Then ϕ is used as a given piecewise constant function in space and time in the second PDE of (3.1), which is updated accordingly.

We define a computational domain $[0, z_\text{end})$ (to be used for the error calculation; see Section 3.4.1) consisting of N cells by covering the vessel with $N-2$ cells and placing one cell each below and above; see Figure 3.3. This setup, with a finite spatial domain, is introduced for practical reasons and is the minimal spatial domain that captures the interior of the tank and the concentrations found in the underflow and effluent zones. The formulation of the scheme and subsequent proof of invariant region property are referred to this computational domain.

Given the column height H, we define $\Delta z := H/(N-2)$ and the cell boundaries $z_i := i\Delta z$, $i = 0, 1, \ldots, N$. Furthermore, we define the cell intervals $I_{i-1/2} := [z_{i-1}, z_i)$ and $I_i := [z_{i-1/2}, z_{i+1/2})$. We place the column between $z_\text{U} := \Delta z = z_1$ and $z_\text{E} := z_\text{U} + H = (N-1)\Delta z = z_{N-1}$. Then the length of the interval of error calculation is $z_\text{end} := H + 2\Delta z = N\Delta z$. Each injection point $z_{\text{F},k}$ is assumed to belong to one cell $I_{i-1/2}$ and we define the dimensionless function

$$\delta_{k,i-1/2} := \int_{I_{i-1/2}} \delta_{z_{\text{F},k}}(z)\,\mathrm{d}z := \begin{cases} 1 & \text{if } z_{\text{F},k} \in I_{i-1/2}, \\ 0 & \text{otherwise.} \end{cases} \tag{3.17}$$

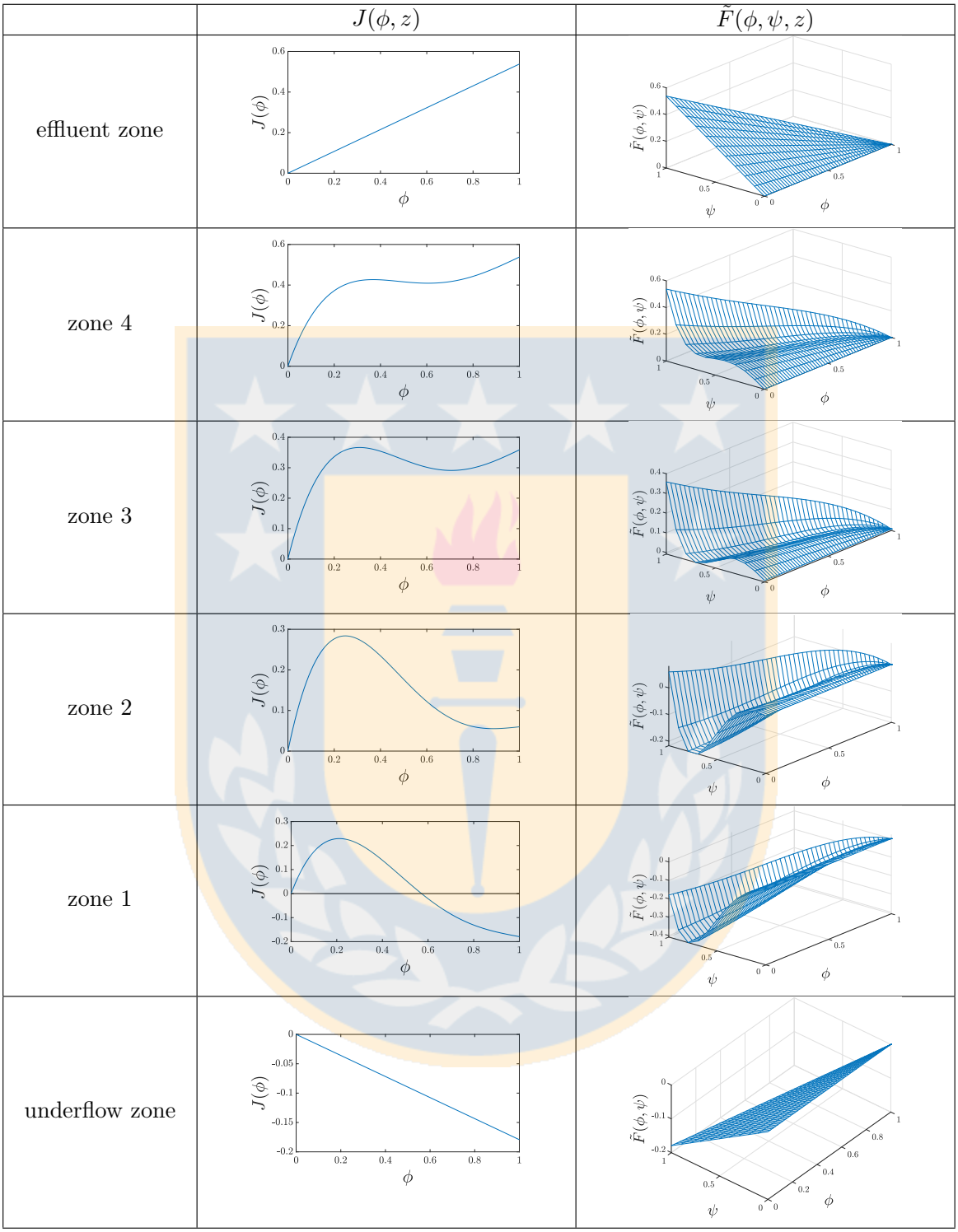

Figure 3.2: Illustration of the non-linearities of the flux functions $J(\phi, z)$ and $\tilde{F}(\phi, \psi, z)$ in the different zones of the column at a fixed z in each zone.

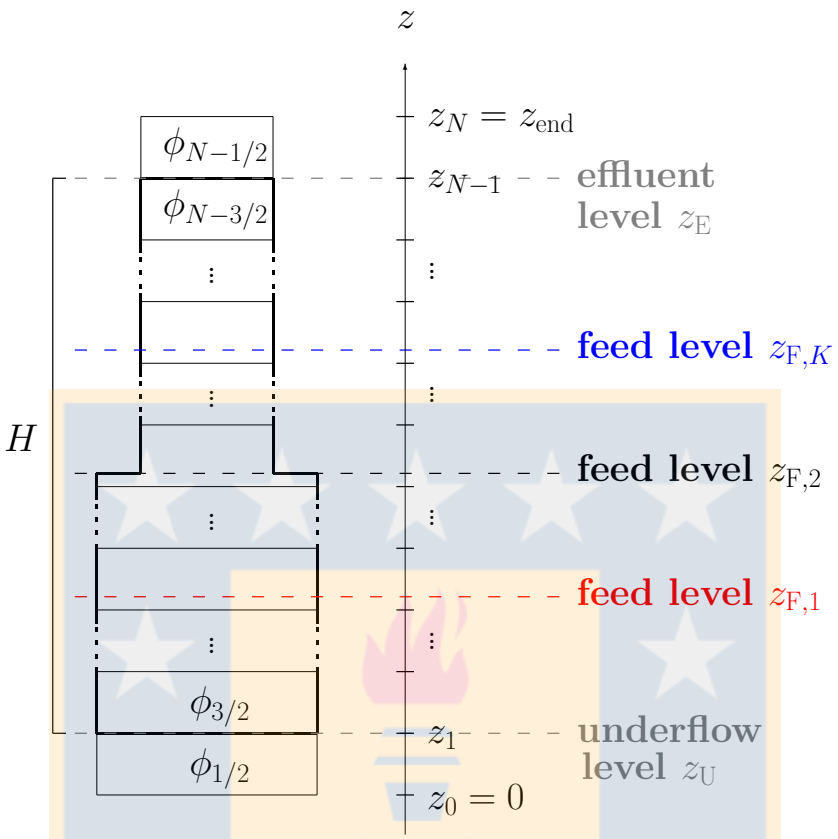

Figure 3.3: Grid for the discretization of ϕ and ψ in the application to flotation, where the height of the vessel is $H = z_{\text{E}} - z_{\text{U}}$, there are K inlets, and we exemplify here with a cross-sectional area $A(z)$ with two values separated by a discontinuity at $z = z_{\text{F},2}$; cf. the examples in Sections 3.4.4 and 3.4.5.

The cross-sectional area $A = A(z)$ is allowed to have a finite number of discontinuities and it is discretized by

$$A_i := \frac{1}{\Delta z}\int_{I_i} A(z)\,\mathrm{d}z, \qquad A_{i+1/2} := \frac{1}{\Delta z}\int_{I_{i+1/2}} A(z)\,\mathrm{d}z.$$

We simulate N_T time steps up to the final time $T := N_T\Delta t$, with the fixed time step Δt satisfying the Courant-Friedrichs-Lewy (CFL) condition

$$\Delta t\left(\frac{2\|Q\|_{\infty,T}}{A_{\min}} + M\big(\max\{V(0), \|V'\|_\infty\} + \|W\|_\infty + \|W'\|_\infty\big)\right) \leq \Delta z, \quad (3.18)$$

where

$$M := \max_{i=1,2,\ldots,N}\left\{\frac{A_{i-1}}{A_{i-1/2}}, \frac{A_i}{A_{i-1/2}}\right\}, \quad A_{\min} := \min_{k=0,1/2,1,3/2,\ldots,N} A_k,$$

$$\|Q\|_{\infty,T} := \max_{0\leq t\leq T}\sum_{k=1}^{K} Q_{\text{F},k}(t), \quad \|W'\|_\infty := \max_{0\leq\phi\leq 1}|W'(\phi)|.$$

Finally, we set $t^n := n\Delta t$ for $n = 0, 1, \dots, N_T$.

The time-dependent feed functions are discretized as

$$Q^n_{\mathrm{F},k} := \frac{1}{\Delta t}\int_{t^n}^{t^{n+1}} Q_{\mathrm{F},k}(t)\,\mathrm{d}t, \qquad \phi^n_{\mathrm{F},k} := \frac{1}{\Delta t}\int_{t^n}^{t^{n+1}} \phi_{\mathrm{F},k}(t)\,\mathrm{d}t,$$

for $k = 1, \dots, K$, and the same is made for $\psi_{\mathrm{F},k}$.

3.3.2 Update of ϕ

The first equation of (3.1) depends only on ϕ and is discretized by a scheme that combines upwind discretizations of the term $q\phi$ with the particular numerical scheme proposed in [23] suitable for kinematic flow models with a "concentration times velocity" flux, as is the case for the term $\phi W(\phi)$.

The initial data are discretized by

$$\phi^0_{i-1/2} := \frac{1}{A_{i-1/2}\Delta z}\int_{I_{i-1/2}} \phi(z,0)A(z)\,\mathrm{d}z.$$

To advance from t^n to t^{n+1}, we assume that $\phi^n_{i-1/2}$, $i = 1, \dots, N$, are given. With the notation

$$a^+ := \max\{a, 0\}, \quad a^- := \min\{a, 0\}, \quad \gamma_i := \gamma(z_i), \quad \text{and} \quad q^{n+}_i := (q(z_i, t^n))^+,$$

we define the numerical flux at $z = z_i$ by

$$\mathcal{J}^n_i := \begin{cases} \phi^n_{1/2} q^{n-}_0 & \text{for } i = 0, \\ \phi^n_{i-1/2} q^{n+}_i + \phi^n_{i+1/2} q^{n-}_i + \gamma_i \phi^n_{i-1/2} W(\phi^n_{i+1/2}) & \text{for } i = 1, \dots, N-1, \\ \phi^n_{N-1/2} q^{n+}_N & \text{for } i = N. \end{cases} \tag{3.19}$$

Since the bulk fluxes above and below the tank are directed away from it, we have

$$\phi^n_{-1/2} q^{n+}_0 = 0 \quad \text{and} \quad \phi^n_{N+1/2} q^{n-}_N = 0 \quad \text{for any values of } \phi^n_{-1/2} \text{ and } \phi^n_{N+1/2}.$$

To simplify the presentation, we use the middle line of (3.19) as the definition of $\mathcal{J}^n_i$ together with $\phi^n_{-1/2} := 0$ and $\phi^n_{N+1/2} := 0$. With the notation $\lambda := \Delta t/\Delta z$ and $Q^{n+}_i := A_i q^{n+}_i$ etc., the conservation law on $I_{i-1/2}$ implies the update formula

$$\begin{aligned} \phi^{n+1}_{i-1/2} &= \phi^n_{i-1/2} + \frac{\lambda}{A_{i-1/2}}\left(A_{i-1}\mathcal{J}^n_{i-1} - A_i \mathcal{J}^n_i + \sum_{k=1}^{K} Q^n_{\mathrm{F},k}\phi^n_{\mathrm{F},k}\delta_{k,i-1/2}\right) \\ &=: \mathcal{H}_{i-1/2}\big(\phi^n_{i-3/2}, \phi^n_{i-1/2}, \phi^n_{i+1/2}\big), \quad i = 1, \dots, N. \end{aligned} \tag{3.20}$$

Then we define the piecewise constant approximate solution $\phi^{\Delta z}$ on $\mathbb{R} \times [0, T)$ by

$$\phi^{\Delta z}(z,t) := \sum_{i,n} \chi_{I_{i-1/2}}(z)\chi_{[t^n, t^{n+1})}(t)\phi^n_{i-1/2},$$

where χ_Ω denotes the characteristic function of the set Ω.

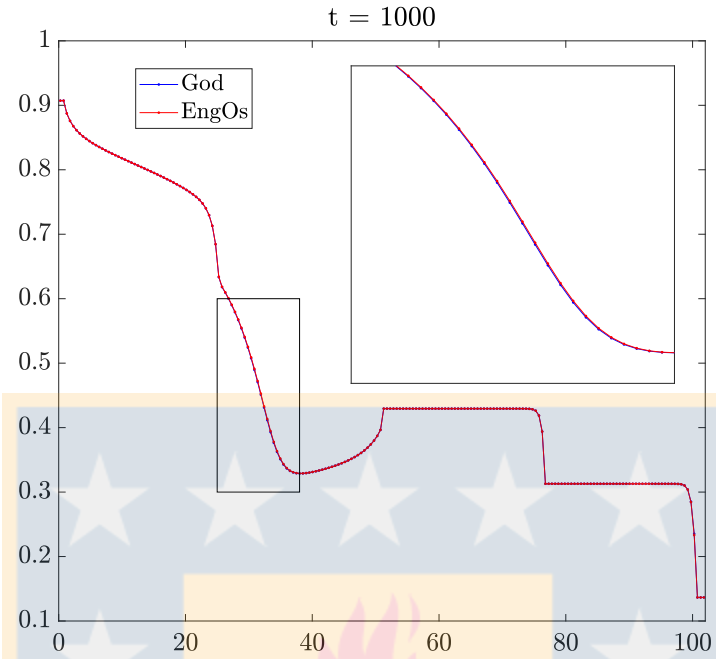

Figure 3.4: Comparison of the results obtained by the Godunov and Engquist-Osher methods operating under the same CFL condition. We can see that the results are quite similar.

3.3.3 Update of ψ

We discretize the initial data by

$$\psi^0_{i-1/2} := \frac{1}{A_{i-1/2}\Delta z}\int_{I_{i-1/2}} \psi(z,0)A(z)\,\mathrm{d}z.$$

For the invariat-region proof in Section 3.3.4 we use the well-known Engquist-Osher numerical flux [51] for a given continuous, piecewise differentiable flux function g and real values a and b on the left/right is given by

$$\mathcal{G}(g;a,b) := g(0) + \int_0^a \max\{0, g'(s)\}\,\mathrm{d}s + \int_0^b \min\{0, g'(s)\}\,\mathrm{d}s. \tag{3.21}$$

instead the Godunov numerical flux (1.25) used in **Chapter 1**, Figure 3.4 shows that this change does not affect our results.

Then a consistent numerical flux corresponding to (3.14) is, for $i = 0, \ldots, N$,

$$\begin{aligned}\mathcal{F}^n_i &:= \psi^n_{i-1/2}q^{n+}_i + \psi^n_{i+1/2}q^{n-}_i \\ &\quad + \gamma_i\left(G^n_i\left(\psi^n_{i-1/2}, \psi^n_{i+1/2}\right) - \phi^n_{i-1/2}\frac{\psi^n_{i+1/2}}{1-\phi^n_{i+1/2}}W(\phi^n_{i+1/2})\right),\end{aligned}$$

where we set $\psi^n_{-1/2} := 0$ and $\psi^n_{N+1/2} := 0$ with the same motivation as for ϕ above (these values are irrelevant). Here

$$G^n_i\left(\psi^n_{i-1/2}, \psi^n_{i+1/2}\right) := \mathcal{G}\left(\sigma f^n_i; \psi^n_{i-1/2}, \psi^n_{i+1/2}\right) \tag{3.22}$$

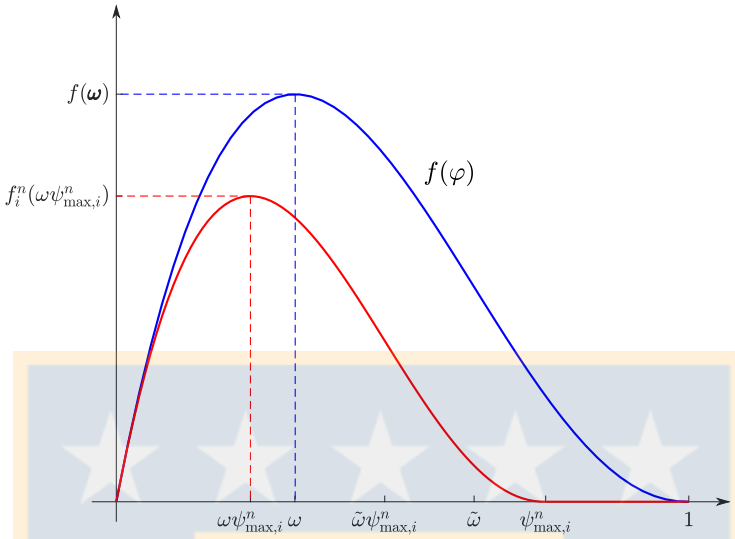

Figure 3.5: Graphical representation of Lemma 3.1.

is the Engquist-Osher numerical flux associated with the function

$$\sigma f_i^n(\psi) := \sigma\psi\tilde{V}\left(\frac{\psi}{\psi^n_{\max,i}}\right), \quad \tilde{V}(u) := \begin{cases} V(u) & \text{for } u < 1, \\ 0 & \text{for } u \geq 1, \end{cases} \tag{3.23}$$

where we define

$$\psi^n_{\max,i} := \min\{1-\phi^n_{i-1/2}, 1-\phi^n_{i+1/2}\} = 1 - \max\{\phi^n_{i-1/2}, \phi^n_{i+1/2}\}.$$

The function $\psi \mapsto \sigma f_i^n(\psi)$ is unimodal. Let $\hat{\psi}_i^n$ denote the maximum point of f_i^n. For a given function $\tilde{V}$ the values $\hat{\psi}_i^n$ and $\psi^n_{\max,i}$ are related by the following lemma.

Lemma 3.1. *Assume that $0 < \omega < \tilde{\omega} < 1$ are the unique local maximum and inflection point, respectively, of $f(\varphi) = \varphi V(\varphi)$ (cf. (3.12)). Then $\hat{\psi}_i^n = \omega\psi^n_{\max,i}$ for all i and n and all possible values $0 \leq \psi^n_{\max,i} \leq 1$. Moreover, the unique inflection point $\psi^n_{\text{infl},i} \in (\hat{\psi}_i^n, \psi^n_{\max,i})$ of f_i^n satisfies $\psi^n_{\text{infl},i} = \tilde{\omega}\psi^n_{\max,i}$ for all i and n and all possible values $0 \leq \psi^n_{\max,i} \leq 1$. (See Figure 3.5.)*

Proof. Assume that $0 < \psi^n_{\max,i} \leq 1$. Since $\hat{\psi}_i^n$ is the unique solution $\hat{\psi}_i^n < \psi^n_{\max,i}$ of

$$\frac{\mathrm{d}}{\mathrm{d}\psi}\left(\psi\tilde{V}\left(\frac{\psi}{\psi^n_{\max,i}}\right)\right) = 0 \quad \Leftrightarrow \quad \tilde{V}\left(\frac{\psi}{\psi^n_{\max,i}}\right) + \frac{\psi}{\psi^n_{\max,i}}\tilde{V}'\left(\frac{\psi}{\psi^n_{\max,i}}\right) = 0,$$

it follows that ω is the unique solution in $(0,1)$ of $\tilde{V}(\omega) + \omega\tilde{V}'(\omega) = 0$ (cf. (3.12)). By a similar argument, $\tilde{\omega}$ is the unique solution of $2\tilde{V}'(\tilde{\omega}) + \tilde{\omega}\tilde{V}''(\tilde{\omega}) = 0$. □

The Engquist-Osher numerical flux (3.22) can now be computed as follows, where we recall that $f_i^n(0) = 0$. For $\sigma = 1$ we get

$$\begin{aligned}\int_0^{\psi_{i-1/2}^n} \max\{0, (f_i^n)'(s)\}\,\mathrm{d}s &= \begin{cases} f_i^n(\psi_{i-1/2}^n) & \text{if } \psi_{i-1/2}^n \le \hat{\psi}_i^n, \\ f_i^n(\hat{\psi}_i^n) & \text{if } \psi_{i-1/2}^n > \hat{\psi}_i^n, \end{cases} \\ \int_0^{\psi_{i+1/2}^n} \min\{0, (f_i^n)'(s)\}\,\mathrm{d}s &= \begin{cases} 0 & \text{if } \psi_{i+1/2}^n \le \hat{\psi}_i^n, \\ f_i^n(\psi_{i+1/2}^n) - f_i^n(\hat{\psi}_i^n) & \text{if } \psi_{i+1/2}^n > \hat{\psi}_i^n, \end{cases}\end{aligned} \tag{3.24}$$

hence

$$\begin{aligned}&\mathcal{G}(f_i^n; \psi_{i-1/2}^n, \psi_{i+1/2}^n) \\ &= \begin{cases} f_i^n(\psi_{i-1/2}^n) & \text{if } \psi_{i-1/2}^n \le \hat{\psi}_i^n \text{ and } \psi_{i+1/2}^n \le \hat{\psi}_i^n, \\ f_i^n(\psi_{i-1/2}^n) + f_i^n(\psi_{i+1/2}^n) - f_i^n(\hat{\psi}_i^n) & \text{if } \psi_{i-1/2}^n \le \hat{\psi}_i^n \text{ and } \psi_{i+1/2}^n > \hat{\psi}_i^n, \\ f_i^n(\hat{\psi}_i^n) & \text{if } \psi_{i-1/2}^n > \hat{\psi}_i^n \text{ and } \psi_{i+1/2}^n \le \hat{\psi}_i^n, \\ f_i^n(\psi_{i+1/2}^n) & \text{if } \psi_{i-1/2}^n > \hat{\psi}_i^n \text{ and } \psi_{i+1/2}^n > \hat{\psi}_i^n. \end{cases}\end{aligned} \tag{3.25}$$

By analogous reasoning we obtain for $\sigma = -1$

$$\begin{aligned}&\mathcal{G}(-f_i^n; \psi_{i-1/2}^n, \psi_{i+1/2}^n) \\ &= \begin{cases} -f_i^n(\psi_{i+1/2}^n) & \text{if } \psi_{i-1/2}^n \le \hat{\psi}_i^n \text{ and } \psi_{i+1/2}^n \le \hat{\psi}_i^n, \\ -f_i^n(\hat{\psi}_i^n) & \text{if } \psi_{i-1/2}^n \le \hat{\psi}_i^n \text{ and } \psi_{i+1/2}^n > \hat{\psi}_i^n, \\ f_i^n(\hat{\psi}_i^n) - f_i^n(\psi_{i-1/2}^n) - f_i^n(\psi_{i+1/2}^n) & \text{if } \psi_{i-1/2}^n > \hat{\psi}_i^n \text{ and } \psi_{i+1/2}^n \le \hat{\psi}_i^n, \\ -f_i^n(\psi_{i-1/2}^n) & \text{if } \psi_{i-1/2}^n > \hat{\psi}_i^n \text{ and } \psi_{i+1/2}^n > \hat{\psi}_i^n. \end{cases}\end{aligned} \tag{3.26}$$

The marching formula is (for $i = 1, \dots, N$)

$$\begin{aligned}\psi_{i-1/2}^{n+1} &= \psi_{i-1/2}^n + \frac{\lambda}{A_{i-1/2}} \left(A_{i-1}\mathcal{F}_{i-1}^n - A_i \mathcal{F}_i^n + \sum_{k=1}^{K} Q_{\mathrm{F},k}^n \psi_{\mathrm{F},k}^n \delta_{k,i-1/2} \right) \\ &= \psi_{i-1/2}^n - \frac{\lambda}{A_{i-1/2}} \Bigg(\Delta_- \Bigg(\psi_{i-1/2}^n Q_i^{n+} + \psi_{i+1/2}^n Q_i^{n-} \\ &\quad + (A\gamma)_i \left(G_i^n\left(\psi_{i-1/2}^n, \psi_{i+1/2}^n\right) - \phi_{i-1/2}^n \frac{\psi_{i+1/2}^n}{1 - \phi_{i+1/2}^n} W(\phi_{i+1/2}^n) \right) \Bigg) \\ &\quad - \sum_{k=1}^{K} Q_{\mathrm{F},k}^n \psi_{\mathrm{F},k}^n \delta_{k,i-1/2} \Bigg).\end{aligned} \tag{3.27}$$

Then we define the piecewise constant approximate solution $\psi^{\Delta z}$ on $\mathbb{R} \times [0, T)$ by

$$\psi^{\Delta z}(z,t) := \sum_{i,n} \chi_{I_{i-1/2}}(z) \chi_{[t^n, t^{n+1})}(t) \psi_{i-1/2}^n. \tag{3.28}$$

3.3.4 Monotonicity and invariant-region principle

We prove that the update formulas (3.20) and (3.27) are monotone, a property which then is used to prove the invariant-region property that the approximate solutions are positive and bounded.

Theorem 3.1. *If the CFL condition (3.18) is satisfied, then the update formula for ϕ (3.20) is monotone and*

$$0 \le \phi^n_{i-1/2} \le 1 \quad \text{for } i = 1, \dots, N \text{ and } n = 1, \dots, N_T.$$

Proof. We recall that the initial function ϕ_0 is assumed to satisfy (3.3). We first prove monotonicity of the three-point scheme for ϕ (3.20), i.e, that $\partial\phi^{n+1}_{i-1/2}/\partial\phi^n_{k-1/2} \ge 0$ for all $i = 1, \dots, N$ and $k = i-1, i, i+1$. We have

$$\begin{aligned}
\frac{\partial \phi^{n+1}_{i-1/2}}{\partial \phi^n_{i-3/2}} &= \frac{\lambda}{A_{i-1/2}} \left(Q^{n+}_{i-1} + (A\gamma)_{i-1} W(\phi^n_{i-1/2})\right) \ge 0, \\
\frac{\partial \phi^{n+1}_{i-1/2}}{\partial \phi^n_{i+1/2}} &= \frac{\lambda}{A_{i-1/2}} \left(-Q^{n-}_{i} - (A\gamma)_{i} \phi^n_{i-1/2} W'(\phi^n_{i+1/2})\right) \ge 0, \\
\frac{\partial \phi^{n+1}_{i-1/2}}{\partial \phi^n_{i-1/2}} &= 1 + \frac{\lambda}{A_{i-1/2}} \Big(Q^{n-}_{i-1} + (A\gamma)_{i-1} \phi^n_{i-3/2} W'(\phi^n_{i-1/2}) \\
&\qquad\qquad - Q^{n+}_{i} - (A\gamma)_{i} W(\phi^n_{i+1/2})\Big) \\
&\ge 1 - \lambda \left(\frac{2\|Q\|_{\infty,T}}{A_{\min}} + M\big(\|W'\|_\infty + \|W\|_\infty\big)\right) \ge 0,
\end{aligned}$$

where we have used the CFL condition (3.18).

We now prove that if $0 \le \phi^n_{i-1/2} \le 1$ for all i, then $0 \le \phi^{n+1}_{i-1/2} \le 1$ for all i. Clearly, (3.3) implies that $0 \le \phi^0_{i-1/2} \le 1$ for all i. Since the scheme (3.20) is monotone, $\mathcal{H}_{i-1/2}$ is non-decreasing in each argument. Since by assumption $W(1) = 0$, we get the following estimation (where we use $a^+ + a^- = a$):

$$\begin{aligned}
0 &\le \frac{\lambda}{A_{i-1/2}} \sum_{k=1}^K Q^n_{\mathrm{F},k} \phi^n_{\mathrm{F},k} \delta_{k,i-1/2} = \mathcal{H}_{i-1/2}(0,0,0) \le \phi^{n+1}_{i-1/2} \\
&= \mathcal{H}_{i-1/2}\big(\phi^n_{i-3/2}, \phi^n_{i-1/2}, \phi^n_{i+1/2}\big) \le \mathcal{H}_{i-1/2}(1,1,1) \\
&= 1 + \frac{\lambda}{A_{i-1/2}} \left(\big(Q^n_{i-1} - Q^n_i\big) + \sum_{k=1}^K Q^n_{\mathrm{F},k} \phi^n_{\mathrm{F},k} \delta_{k,i-1/2} \right) \\
&\le 1 + \frac{\lambda}{A_{i-1/2}} \left(\sum_{k=1}^K \big(-Q^n_{\mathrm{F},k}\big) \delta_{k,i-1/2} + \sum_{k=1}^K Q^n_{\mathrm{F},k} \delta_{k,i-1/2} \right) = 1.
\end{aligned}$$

□

Lemma 3.2. *The function f_i^n defined by (3.23) satisfies*

$$\|(f_i^n)'\|_\infty \le \max\{V(0), \|V'\|_\infty\}.$$

Proof. By (3.12), the function $f(\varphi) = \varphi V(\varphi)$ has a single inflection point $\tilde\omega \in (0,1)$ and by Lemma 3.1, f_i^n has the inflection point $\tilde\omega\psi^n_{\max,i} \in (0, \psi^n_{\max,i})$. We have $(f_i^n)'(0) = V(0)$, $(f_i^n)'(\varphi) = 0$ for $\psi^n_{\max,i} \le \varphi \le 1$ and the lowest (and negative) value of $(f_i^n)'$ is obtained at its only critical point $\tilde\omega\psi^n_{\max,i}$, for which

$$(f_i^n)'(\tilde\omega\psi^n_{\max,i}) = \tilde V(\tilde\omega) + \tilde\omega\tilde V'(\tilde\omega) \ge -\|V'\|_\infty.$$

This concludes the proof of the lemma. □

Lemma 3.3. *There holds $G_i^n(1-\phi^n_{i-1/2}, 1-\phi^n_{i+1/2}) = 0$ for all i and n.*

Proof. Assume that $0 < \psi^n_{\max,i} = (1-\phi^n_{i-1/2}) \wedge (1-\phi^n_{i+1/2}) \le 1$. By Lemma 3.1, $\hat\psi_i^n < \psi^n_{\max,i}$, hence (3.25), (3.26), and

$$\tilde V\big((1-\phi^n_{i-1/2})/\psi^n_{\max,i}\big) = \tilde V\big((1-\phi^n_{i+1/2})/\psi^n_{\max,i}\big) = 0$$

imply that

$$G_i^n\big(1-\phi^n_{i-1/2}, 1-\phi^n_{i+1/2}\big) = \begin{cases} f_i^n(1-\phi^n_{i+1/2}) = 0 & \text{if } \sigma = 1, \\ -f_i^n(1-\phi^n_{i-1/2}) = 0 & \text{if } \sigma = -1. \end{cases}$$

□

Theorem 3.2. *Under the assumptions of Theorem 3.1, the update formula for ψ (3.27) is monotone and along with (3.20) produces approximate solutions that satisfy*

$$0 \le \psi^n_{i-1/2} \le 1 - \phi^n_{i-1/2} \quad \text{for all } i \text{ and } n.$$

Proof. By assumptions (3.3) and (3.4), we may assert that $0 \le \psi^0_{i-1/2} \le 1 - \phi^0_{i-1/2}$ for all i and

$$\psi^n_{\mathrm{F},k} \le 1 - \phi^n_{\mathrm{F},k} \quad \text{for all } n. \tag{3.29}$$

To prove that the scheme (3.27) is monotone, we write (3.27) as

$$\psi^{n+1}_{i-1/2} = \mathcal{K}^n_{i-1/2}\big(\psi^n_{i-3/2}, \psi^n_{i-1/2}, \psi^n_{i+1/2}\big) \tag{3.30}$$

and show that this expression is non-decreasing in each of its arguments.

Since $0 \le \phi^n_{i-1/2} \le 1$ for a given n and all i, and appealing to the definition of the Engquist-Osher flux (3.21), we have

$$\frac{\partial\psi^{n+1}_{i-1/2}}{\partial\psi^n_{i-3/2}} = \frac{\lambda}{A_{i-1/2}}\left(Q^{n+}_{i-1} + (A\gamma)_{i-1}\frac{\partial G^n_{i-1}}{\partial\psi^n_{i-3/2}}\right) \ge 0,$$

$$\frac{\partial \psi_{i-1/2}^{n+1}}{\partial \psi_{i+1/2}^{n}} = \frac{\lambda}{A_{i-1/2}}\left(-Q_i^{n-} - (A\gamma)_i \frac{\partial G_i^n}{\partial \psi_{i+1/2}^n} + (A\gamma)_i \frac{\phi_{i-1/2}^n}{1-\phi_{i+1/2}^n} W(\phi_{i+1/2}^n)\right) \geq 0,$$

$$\begin{aligned}\frac{\partial \psi_{i-1/2}^{n+1}}{\partial \psi_{i-1/2}^{n}} &= 1 + \frac{\lambda}{A_{i-1/2}}\Bigg(Q_{i-1}^{n-} - Q_i^{n+} \\ &\quad + (A\gamma)_{i-1}\left(\frac{\partial G_{i-1}^n}{\partial \psi_{i-1/2}^n} - \frac{\phi_{i-3/2}^n W(\phi_{i-1/2}^n)}{1-\phi_{i-1/2}^n}\right) - (A\gamma)_i \frac{\partial G_i^n}{\partial \psi_{i-1/2}^n}\Bigg) \\ &\geq 1 - \lambda\left(\frac{2\|Q\|_{\infty,T}}{A_{\min}} + M\left(\frac{\partial G_i^n}{\partial \psi_{i-1/2}^n} - \frac{\partial G_{i-1}^n}{\partial \psi_{i-1/2}^n} + \frac{W(\phi_{i-1/2}^n)}{1-\phi_{i-1/2}^n}\right)\right).\end{aligned}$$

By (3.21) and Lemma 3.2 we also obtain

$$\begin{aligned}\frac{\partial G_i^n}{\partial \psi_{i-1/2}^n} - \frac{\partial G_{i-1}^n}{\partial \psi_{i-1/2}^n} &= (f_i^n)'\big(\psi_{i-1/2}^n\big)^+ - (f_i^n)'\big(\psi_{i-1/2}^n\big)^- = \big|(f_i^n)'\big(\psi_{i-1/2}^n\big)\big| \\ &\leq \|(f_i^n)'\|_\infty \leq \max\{V(0), \|V'\|_\infty\},\end{aligned}$$

and for the remaining term, we use that $W(1) = 0$ and the mean-value theorem to get, for some $\xi \in (\phi_{i-1/2}^n, 1)$,

$$\frac{W(\phi_{i-1/2}^n)}{1-\phi_{i-1/2}^n} = -\frac{W(1) - W(\phi_{i-1/2}^n)}{1-\phi_{i-1/2}^n} = -W'(\xi) \leq \|W'\|_\infty.$$

Hence, the CFL condition (3.18) implies

$$\frac{\partial \psi_{i-1/2}^{n+1}}{\partial \psi_{i-1/2}^{n}} \geq 1 - \lambda\left(\frac{2\|Q\|_{\infty,T}}{A_{\min}} + M\big(\max\{V(0), \|V'\|_\infty\} + \|W'\|_\infty\big)\right) \geq 0.$$

The inequalities proved imply that $\mathcal{K}_{i-1/2}^n$ is non-decreasing in each of its arguments. Now we use that $0 \leq \psi_{i-1/2}^n \leq 1 - \phi_{i-1/2}^n$ for all i and Lemma 3.3 to obtain

$$\begin{aligned}0 &\leq \frac{\lambda}{A_{i-1/2}} \sum_{k=1}^{K} Q_{\mathrm{F},k}^n \psi_{\mathrm{F},k}^n \delta_{k,i-1/2} = \mathcal{H}_{i-1/2}(0,0,0) \leq \psi_{i-1/2}^{n+1} \\ &= \mathcal{H}_{i-1/2}(\psi_{i-3/2}^n, \psi_{i-1/2}^n, \psi_{i+1/2}^n) \leq \mathcal{H}_{i-1/2}(1-\phi_{i-3/2}^n, 1-\phi_{i-1/2}^n, 1-\phi_{i+1/2}^n) \\ &= 1 - \phi_{i-1/2}^n + \frac{\lambda}{A_{i-1/2}}\Bigg(A_{i-1}\mathcal{F}_{i-1}^n(1-\phi_{i-3/2}^n, 1-\phi_{i-1/2}^n) \\ &\quad - A_i \mathcal{F}_i^n(1-\phi_{i-1/2}^n, 1-\phi_{i+1/2}^n) + \sum_{k=1}^{K} Q_{\mathrm{F},k}^n \psi_{\mathrm{F},k}^n \delta_{k,i-1/2}\Bigg) \\ &= 1 - \phi_{i-1/2}^n + \frac{\lambda}{A_{i-1/2}}\Bigg((1-\phi_{i-3/2}^n)Q_{i-1}^{n+} + (1-\phi_{i-1/2}^n)Q_{i-1}^{n-} \\ &\quad - (A\gamma)_{i-1}\phi_{i-3/2}^n W(\phi_{i-1/2}^n) - (1-\phi_{i-1/2}^n)Q_i^{n+} - (1-\phi_{i+1/2}^n)Q_i^{n-}\end{aligned}$$

$$+ (A\gamma)_i \phi^n_{i-1/2} W(\phi^n_{i+1/2}) + \sum_{k=1}^{K} Q^n_{\mathrm{F},k} \psi^n_{\mathrm{F},k} \delta_{k,i-1/2} \Bigg).$$

Appealing to (3.29) and the update formula for ϕ (3.20), we get

$$\begin{aligned}\psi^{n+1}_{i-1/2} &\le 1 - \phi^{n+1}_{i-1/2} + \frac{\lambda}{A_{i-1/2}} \left(Q^{n+}_{i-1} + Q^{n-}_{i-1} - Q^{n+}_i - Q^{n-}_i + \sum_{k=1}^{K} Q^n_{\mathrm{F},k} \delta_{k,i-1/2} \right) \\ &= 1 - \phi^{n+1}_{i-1/2} + \frac{\lambda}{A_{i-1/2}} \left\{ Q^n_{i-1} - Q^n_i + \sum_{k=1}^{K} Q^n_{\mathrm{F},k} \delta_{k,i-1/2} \right\} = 1 - \phi^{n+1}_{i-1/2}.\end{aligned}$$

The last equality holds since $\{\dots\} = 0$ irrespective of whether there is a source in the cell; $Q^n_{i-1} - Q^n_i + Q^n_{\mathrm{F},k} = 0$, or not; $Q^n_{i-1} - Q^n_i = 0$. □

We here conclude the discussion of the schemes for the full problem (3.1), (3.2).

3.4 Numerical results

3.4.1 Approximate numerical error

As it can be seen in Figure 3.3, the grid we have considered in our numerical scheme satisfies that the boundaries of the tank agree with the boundaries of a cell. This will simplify the error estimations.

Since an exact solution is frequently difficult to obtain, we use an approximate reference solution obtained with a large number N_{ref} cells against which we measure the error of other simulated solutions with $N < N_{\mathrm{ref}}$. The error is estimated on a fixed interval $[0, z_{\mathrm{end}})$ a little wider than the column of height H so that the outflow volume fractions are included. Given H, we define the coarsest grid of N_0 cells with $\Delta z_0 := H/(N_0 - 2)$ and place the column between $z_{\mathrm{U}} := \Delta z_0$ and $z_{\mathrm{E}} := z_{\mathrm{U}} + H = (N_0 - 1)\Delta z_0$. This corresponds to what is shown in Figure 3.3 with $N = N_0$. We define the length of the interval of error estimation as $z_{\mathrm{end}} := H + 2\Delta z_0 = N_0 \Delta z_0$.

To estimate the convergence order, we perform simulations with $N_k = 2^k N_0$ cells, $k = 0, \dots, k_{\mathrm{ref}} - 1$, where k_{ref} is an integer that defines the number of cells $N_{\mathrm{ref}} := N_{k_{\mathrm{ref}}} := 2^{k_{\mathrm{ref}}} N_0$ we use for the reference solution. Then we define $\Delta z_k := z_{\mathrm{end}}/N_k$, $\Delta z^{\mathrm{r}} := \Delta z_{k_{\mathrm{ref}}} := z_{\mathrm{end}}/N_{k_{\mathrm{ref}}} = \Delta z_0 / 2^{k_{\mathrm{ref}}}$ and the factor of refinement from N_k cells to N_{ref} as $m_k := \Delta z_k / \Delta z^{\mathrm{r}} = N_{k_{\mathrm{ref}}}/N_k = 2^{k_{\mathrm{ref}} - k}$. We note that $z_{N_k} := N_k \Delta z_k = z_{\mathrm{end}}$ for all k.

We will now measure the error between the piecewise constant numerical solution obtained by $N = N_k$ cells (we skip the index k for a moment) and the reference solution obtained with N_{ref} cells on the grid refined by a factor $m = \Delta z / \Delta z^{\mathrm{r}}$. The refined grid satisfies $z^{\mathrm{r}}_0 := z_0 = 0$ and we have $z_i = i\Delta z = im\Delta z^{\mathrm{r}} =: z^{\mathrm{r}}_{im}$. The corresponding numerical solutions on the refined

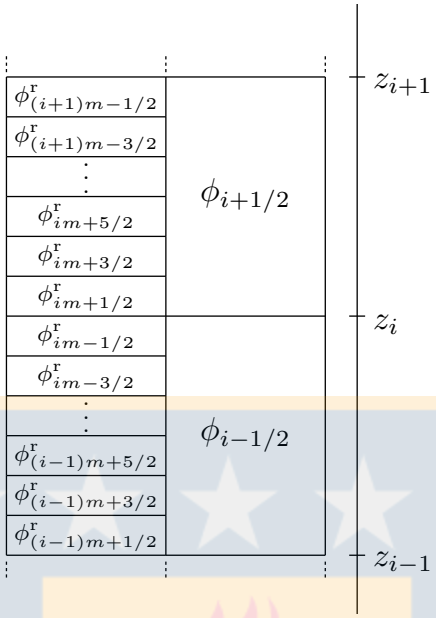

Figure 3.6: The cell division for error calculations with a refined grid on the left and the coarsest grid on the right.

grids are denoted by (skipping the time index n) $\phi^{\mathrm{r}}_{i+1/2}$, $\psi^{\mathrm{r}}_{i+1/2}$, etc., where $A^{\mathrm{r}}_{i+1/2}$ are defined by means of Δz^{r}. The numbering of the refined cells is defined such that the first cell for ϕ above $z^{\mathrm{r}}_0 = 0$ contains the value $\phi^{\mathrm{r}}_{1/2}$. Then $z_{\mathrm{end}} = Nm\Delta z^{\mathrm{r}}$. This means that the cells within $[0, z_{\mathrm{end}})$ contain the values $\phi^{\mathrm{r}}_{1/2}, \ldots, \phi^{\mathrm{r}}_{Nm-1/2}$, and analogously for ψ. See Figure 3.6 for a schematic of the refined mesh compared with the coarsest one.

Note that the location of the spatial discontinuities z_{U} and z_{E} will coincide with a cell boundary for any mesh considered in the refinement process while the locations of the inlets $z_{\mathrm{F},1}$, etc. will be chosen so that each of them lays inside a cell for the finest grid; hence, they do this for all the coarser meshes. In this way, the numerical fluxes at cell boundaries are well defined.

We compute the estimated error at a time point $t = T$ and define

$$\left\|\phi^{\Delta z}(\cdot, T)\right\| := \int_0^{z_{\mathrm{end}}} A(z)\left|\phi^{\Delta z}(z, T)\right| \mathrm{d}z.$$

The L^1-difference between two numerical solutions computed on grids with cell sizes Δz and Δz^{r} is calculated as follows for ϕ:

$$E^{\phi}(\Delta z, \Delta z^{\mathrm{r}}, T) := \left\|\phi^{\Delta z}(\cdot, t) - \phi^{\Delta z^{\mathrm{r}}}(\cdot, T)\right\| = \sum_{i=0}^{N-1} I^{\phi}_{i+1/2}(T)$$

with the subintegrals defined by

$$I^{\phi}_{i+1/2}(T) = \int_{z_i}^{z_{i+1}} A(z)\left|\phi^{\Delta z}(z, T) - \phi^{\Delta z^{\mathrm{r}}}(z, T)\right| \mathrm{d}z$$

$$= \sum_{k=0}^{m-1} \int_{z^{\mathrm{r}}_{im+k}}^{z^{\mathrm{r}}_{im+k+1}} A(z) \big| \phi_{i+1/2} - \phi^{\mathrm{r}}_{im+1/2+k} \big| \, \mathrm{d}z$$
$$= \Delta z^{\mathrm{r}} \sum_{k=0}^{m-1} A^{\mathrm{r}}_{im+1/2+k} \big| \phi_{i+1/2} - \phi^{\mathrm{r}}_{im+1/2+k} \big|.$$

The approximate relative error for ϕ in the interval $[0, z_{\mathrm{end}})$ is then defined as

$$e^{\phi}_{N_k}(T) := \frac{E^{\phi}(\Delta z_k, \Delta z^{\mathrm{r}}, T)}{\|\phi^{\Delta z^{\mathrm{r}}}(\cdot, T)\|} = \frac{\|\phi^{\Delta z_k}(\cdot, T) - \phi^{\Delta z^{\mathrm{r}}}(\cdot, T)\|}{\|\phi^{\Delta z^{\mathrm{r}}}(\cdot, T)\|}.$$

We define $e^{\psi}_{N}(t)$ analogously and hence, the total relative error can be defined as

$$e^{\mathrm{tot}}_{N_k}(T) := e^{\phi}_{N_k}(T) + e^{\psi}_{N_k}(T)$$

and the observed convergence order between two discretizations N_{k-1} and N_k, with $k = 1, \ldots, k_{\mathrm{ref}} - 1$, as

$$\Theta_k(T) := -\frac{\log(e^{\mathrm{tot}}_{N_{k-1}}(T)/e^{\mathrm{tot}}_{N_k}(T))}{\log(N_{k-1}/N_k)}.$$

For smooth solutions, we can use an alternative way of calculating approximate errors and convergence orders in which a reference solution is not needed. In [11], the authors proposed to use cubic interpolation to compute the quantities $\tilde{\phi}^{\Delta z_k}_{i+1/2}$ from a grid with $N_{k+1} = 2\,N_k$ cells, $k = 0, \ldots, \hat{k}$, with $\hat{k}$ an integer, taking into consideration that $z^{k}_{i+1/2} = (z^{k+1}_{2i+1/2} + z^{k+1}_{2i+3/2})/2$. Then, $\tilde{\phi}^{\Delta z_k}_{i+1/2}$ is given by

$$\tilde{\phi}^{\Delta z_k}_{i+1/2} = \frac{9}{16}\big(\phi^{\Delta z_{k+1}}_{2i+3/2} + \phi^{\Delta z_{k+1}}_{2i+1/2}\big) - \frac{1}{16}\big(\phi^{\Delta z_{k+1}}_{2i+5/2} + \phi^{\Delta z_{k+1}}_{2i-1/2}\big), \quad i = 1, \ldots, N_k.$$

The alternative approximate relative L^1-error for ϕ can then be calculated as

$$\hat{e}^{\phi}_{N_k}(T) := \frac{1}{N_k} \sum_{i=1}^{N_k} \big| \tilde{\phi}^{\Delta z_k}_{i+1/2}(\cdot, T) - \phi^{\Delta z_k}_{i+1/2}(\cdot, T) \big|.$$

We can define $\tilde{\psi}^{N_k}_{i+1/2}$ and $\hat{e}^{\psi}_{N_k}(T)$ analogously, and define the alternative total approximate L^1-error as

$$\hat{e}^{\mathrm{tot}}_{N_k}(T) := \hat{e}^{\phi}_{N_k}(T) + \hat{e}^{\psi}_{N_k}(T).$$

Finally, the alternative convergence order can be computed by

$$\hat{\Theta}_k(T) := \log_2(\hat{e}^{\mathrm{tot}}_{N_k}(T)/\hat{e}^{\mathrm{tot}}_{N_{k+1}}(T)) \quad \text{for } k = 0, \ldots, \hat{k}.$$

3.4.2 Preliminaries for numerical tests

For the first example, in Section 3.4.3, we use a smooth solution away from spatial discontinuities, to estimate the order of convergence of the numerical scheme. For this example, we use $N_0 = 500$, $N_k = 2^k N_0$ for $k = 0, 1, \ldots, 5$ and $k_{\text{ref}} = 8$; hence, $N_5 = 16\,000$ and $N_{\text{ref}} = 128\,000$.

In Sections 3.4.4 and 3.4.5, we exemplify counter- and co-current flows of the primary and secondary phases, respectively. For these two examples, we use $N_0 = 100$, and $k_{\text{ref}} = 7$. We set three inlets $z_{\text{F},1}$, $z_{\text{F},2}$ and $z_{\text{F},3}$ dividing the tank into four equal parts each with the height $H/4$, where $H = 1\,\text{m}$ is used. These three inlets are defined so that they lie inside a cell for any mesh size considered. A fixed quantity of the primary phase is introduced through inlet $z_{\text{F},1}$, a fixed quantity of the secondary phase through inlet $z_{\text{F},2}$ and some wash water through inlet $z_{\text{F},3}$.

Tables 3.1, 3.2 and 3.3 show the estimated errors and convergence orders for the three escenarios studied. In the calculations of the alternative approximate error $\hat{e}^{\text{tot}}_{N_k}(T)$ and convergence order $\hat{\Theta}_k(T)$ in Table 3.1, we use $\hat{k} = 6$.

For all examples the column flotation is $H = 100\,\text{cm}$ high.

3.4.3 Example 3.1: Smooth solution

For this first example, we consider a vessel with a constant cross-sectional area of $A(z) = 83.65\,\text{cm}^2$, and we set all inlet and outlet volumetric flows to zero, i.e, $Q_{\text{F},1} = Q_{\text{F},2} = Q_{\text{F},3} = Q_{\text{U}} = Q_{\text{E}} = 0\,\text{cm}^3/\text{s}$. For the velocity functions W and V, given by (3.15) and (3.16), respectively, we use the parameters $n_{\text{p}} = 2.2$, $v_{\text{term,p}} = 1.5\,\text{cm/s}$, $n_{\text{s}} = 2.2$ and $v_{\text{term,s}} = 1.5\,\text{cm/s}$, and consider $\sigma = -1$ (counter-current flow). As initial data, we choose a sinusoidal function for both phases with support in the interval $]z_{\text{U}}, z_{\text{E}}[$; see Figure 3.7.

We simulate a short time, until $t = 9\,\text{s}$, before the first discontinuity appears. Figure 3.8 shows the time evolution of the primary and secondary phases for $N = 1000$ in the first row. In the second row, we compare two approximate solutions obtained with a coarse mesh with $N = 500$ and a finer one with $N = 8000$.

Table 3.1 shows the estimated errors and convergence orders. We observe that both $\Theta_k(T)$ and $\hat{\Theta}_{N_k}(T)$ assume values close to one as N_k increases, as it was expected, confirming that the scheme is first-order accurate for smooth solution.

3.4.4 Example 3.2: Counter-current fluxes

We consider now a full tank with $\sigma = -1$; hence, the primary phase will move upwards and the secondary phase downwards with respect to the volume average velocity q of the mixture. A straightforward interpretation of this scenario is the flotation process used in the mineral industry to recover valuable minerals from crushed ore; see the model in [17,18]. In that model,

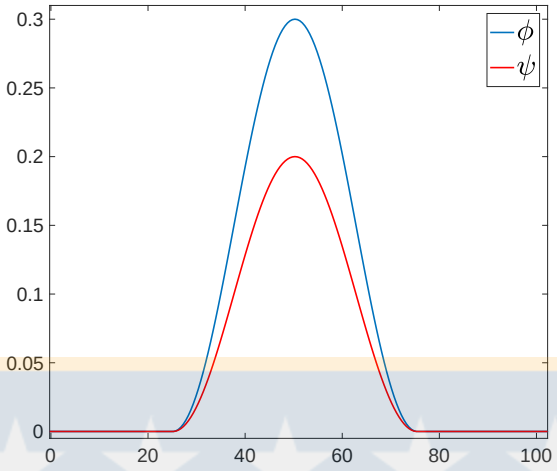

Figure 3.7: Example 3.1: Simulation of a smooth solution. Smooth initial data for the example in Section 3.4.3.

Table 3.1: Example 3.1: Simulation of a smooth solution. Total estimated relative L^1-error $e^{\mathrm{tot}}_{N_k}(T)$ and alternative $\hat{e}^{\mathrm{tot}}_{N_k}(T)$ and estimated convergence order $\Theta_k(T)$ and its alternative counterpart $\hat{\Theta}_k(T)$, calculated with $N_{\mathrm{ref}} = 128\,000$ and $T = 9\,\mathrm{s}$.

N_k	$e^{\mathrm{tot}}_{N_k}(T)$	$\Theta_k(T)$	$\hat{e}^{\mathrm{tot}}_{N_k}(T)$	$\hat{\Theta}_k(T)$
500	3.7212×10^{-2}	–	1.3041×10^{-3}	0.9513
1000	1.8985×10^{-2}	0.9709	6.7443×10^{-4}	0.9657
2000	9.5710×10^{-3}	0.9881	3.4533×10^{-4}	0.9781
4000	4.7582×10^{-3}	1.0083	1.7531×10^{-4}	0.9870
8000	2.3174×10^{-3}	1.0379	8.8448×10^{-5}	0.9927
16000	1.0867×10^{-3}	1.0926	4.4447×10^{-5}	–

the primary phase consists of aggregates, which are air bubbles fully loaded with hydrophobic minerals, and the secondary phase is the tailings, consisting of hydrophilic particles suspended in the fluid that do not attach to air bubbles.

Following the numerical experiments carried out in [17,18], we set here $n_{\mathrm{p}} = 3.2$ and $v_{\mathrm{term,p}} = 2.7\,\mathrm{cm/s}$ for the primary phase (aggregates) velocity function W and $n_{\mathrm{s}} = 2.5$ and $v_{\mathrm{term,s}} = 0.5\,\mathrm{cm/s}$ for the secondary phase (solids) velocity function V; see (3.15) and (3.16). We consider three inlets $z_{\mathrm{F},1}$, $z_{\mathrm{F},2}$ and $z_{\mathrm{F},3}$, dividing the tank into four regions with equal height. At $z_{\mathrm{F},1}$, only gas is fed, at $z_{\mathrm{F},3}$ only wash water, while at $z_{\mathrm{F},2}$ a slurry of solids and water is fed into the column.

The cross-sectional area of the tank is discontinuous because of a centered pipe going from

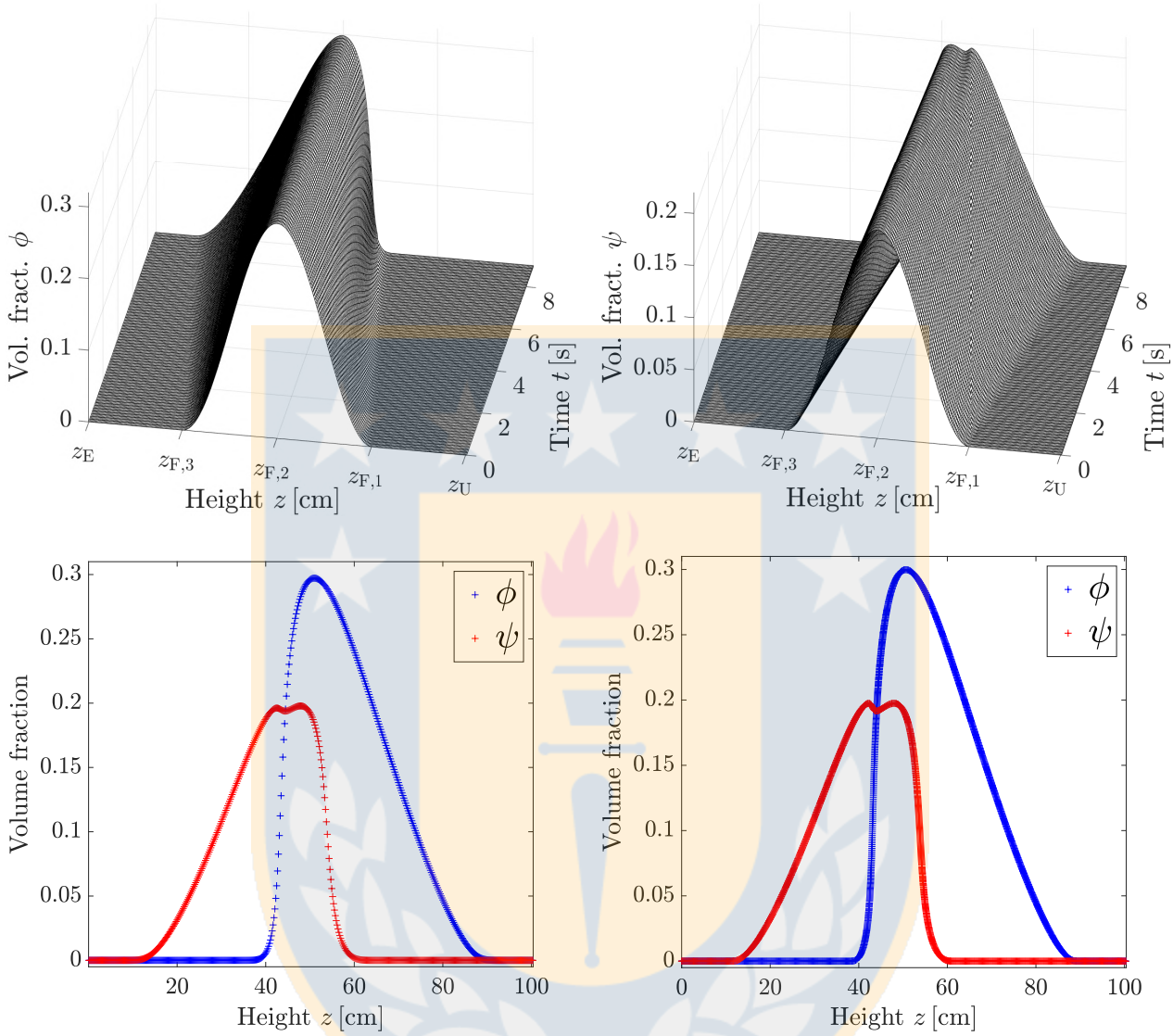

Figure 3.8: Example 3.1: Simulation of a smooth solution. First row: Time evolution of the volume fraction of the primary phase ϕ (left) and the secondary phase ψ (right) from time $t = 0\,\mathrm{s}$ to $t = 9\,\mathrm{s}$. Second row: Approximate solutions at time $t = 9\,\mathrm{s}$ computed with $N = 500$ (left) and $N = 8000$ (right).

the top down to $z_{\mathrm{F},2}$; cf. Figure 3.3, introducing material into the tank. It is defined by

$$A(z) = \begin{cases} 72.25\,\mathrm{cm}^2 & \text{for } z \geq z_{\mathrm{F},2}, \\ 83.65\,\mathrm{cm}^2 & \text{for } z < z_{\mathrm{F},2}. \end{cases}$$

These measurements come from the Reflux Flotation Cell developed by Galvin and Dickinson [54].

We consider that the column is filled only with fluid at time $t = 0\,\mathrm{s}$, hence $\phi(z, 0) = \psi(z, 0) =$

Table 3.2: Example 3.2: Counter-current flows. Total estimated relative L^1-error, $e^{\text{tot}}_{N_k}(T)$, and estimated convergence orders, $\Theta_k(T)$, calculated between consecutive values of N_k, with $N_{\text{ref}} = 12\,800$, $T = 350\,\text{s}$.

N_k	$e^{\text{tot}}_{N_k}(T)$	$\Theta_k(T)$
100	4.2032×10^{-1}	–
200	2.5992×10^{-1}	0.6934
400	1.5820×10^{-1}	0.7163
800	9.4139×10^{-2}	0.7489
1600	5.3953×10^{-2}	0.8031
3200	2.8018×10^{-2}	0.9453

0 for all z, when we start pumping aggregates and solids with concentrations $\phi_{\text{F},1} = 1.0$, $\psi_{\text{F},1} = 0$, $\phi_{\text{F},2} = 0$, $\psi_{\text{F},2} = 0.4$, $\phi_{\text{F},3} = 0$ and $\psi_{\text{F},3} = 0$, along with fluid and/or wash water. We choose the volumetric flows $(Q_{\text{U}}, Q_{\text{F},1}, Q_{\text{F},2}, Q_{\text{F},3}) = (5, 15, 25, 10)\,\text{cm}^3/\text{s}$, so that the mixture flows in zones 2 and 3 are positive, i.e., directed upwards: $Q_{\text{F},1} - Q_{\text{U}} = 10\,\text{cm}^3/\text{s}$ in zone 2 and $Q_{\text{F},2} + Q_{\text{F},1} - Q_{\text{U}} = 35\,\text{cm}^3/\text{s}$ in zone 3.

Figure 3.9 shows the time evolution of the volume fractions of ϕ and ψ. It can be seen that the aggregates rise fast to the top, while the solids are travelling both up and down the vessel, leaving through the effluent and the underflow.

At time $t = 350\,\text{s}$, we change the volumetric flow from $Q_{\text{F},2} = 25\,\text{cm}^3/\text{s}$ to $Q_{\text{F},2} = 7\,\text{cm}^3/\text{s}$. After this change, the solids settle and we obtain a steady state. We mention that this is not a desired steady state in the mining industry (the capacity of the device is not fully used); see [18] for more examples.

Table 3.2 shows the estimated errors and convergence orders for this simulation. As in the smooth example in Section 3.4.3, the convergence orders tend to one as N_k increases.

3.4.5 Example 3.3: Co-current fluxes

For the last example, we consider $\sigma = 1$, which means that both the primary and secondary phases have less density than the water and therefore move upwards relative the mixture motion. An interpretation of this scenario is a flotation process with two buoyant phases differing in density and possibly also in size.

We consider here the same flotation column as in Example 3.2 and choose the values $n_{\text{p}} = 3.2$ and $v_{\text{term,p}} = 2.5\,\text{cm/s}$ for the primary phase and $n_{\text{s}} = 2.5$ and $v_{\text{term,s}} = 1.5\,\text{cm/s}$ for the secondary phase so that we have two buoyant phases with different (upwards-directed) velocities relative to the mixture. As in the previous example, only the primary phase is fed into the tank at $z_{\text{F},1}$ and only the secondary at $z_{\text{F},2}$.

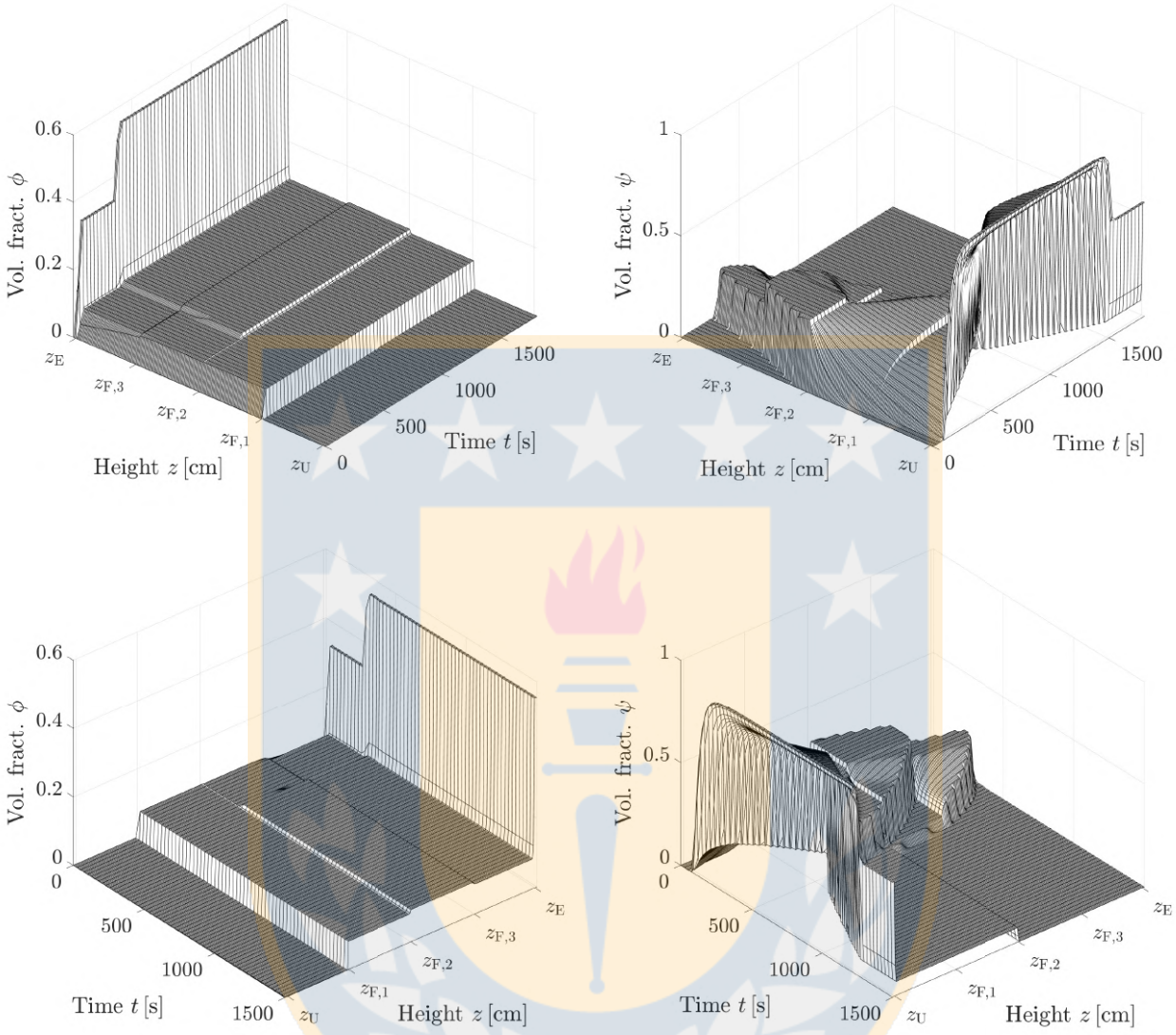

Figure 3.9: Example 3.2: Counter-current flows. Time evolution of the volume fraction profiles of the primary phase ϕ (left) and secondary phase ψ (right) from time $t = 0\,\mathrm{s}$ to $t = 1800\,\mathrm{s}$ seen from two different angles (first and second rows).

The column is initially filled with only fluid at time $t = 0\,\mathrm{s}$, hence $\phi(z,0) = \psi(z,0) = 0$ for all z, when we start pumping both phases with the following volume fractions: $\phi_{\mathrm{F},1} = 1.0$, $\psi_{\mathrm{F},1} = 0.0$, $\phi_{\mathrm{F},2} = 0.0$, $\psi_{\mathrm{F},2} = 0.6$, $\phi_{\mathrm{F},3} = 0$ and $\psi_{\mathrm{F},3} = 0$. We choose the volumetric flows $(Q_{\mathrm{U}}, Q_{\mathrm{F},1}, Q_{\mathrm{F},2}, Q_{\mathrm{F},3}) = (15, 30, 20, 10)\,\mathrm{cm}^3/\mathrm{s}$, so that the volumetric flows in the tank are positive in all zones but no in zone 1.

Figure 3.10 shows the time evolution of the volume fractions of both phases. It can be seen that, for times $t < 350\,\mathrm{s}$, the primary phase is leaving the tank through both the underflow and effluent outlets, while the secondary phase have quickly risen to the top part of the tank and

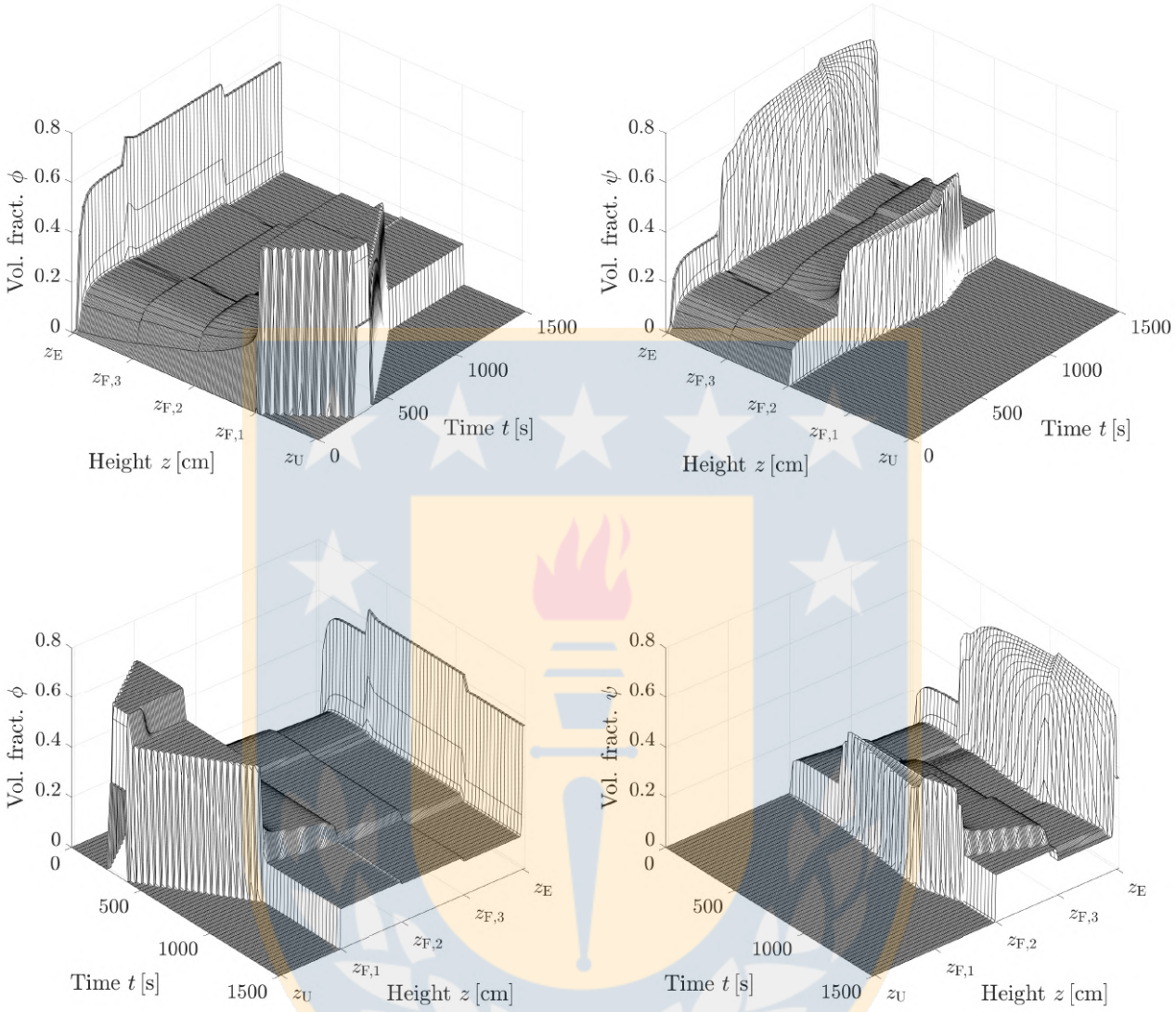

Figure 3.10: Example 3.3: Co-current flows. Time evolution of the volume fraction profiles of primary phase ϕ (left) and secondary phase ψ(right) from time $t = 0\,\mathrm{s}$ to $t = 1500\,\mathrm{s}$ seen from two different angles (first and second rows).

is leaving it just through the effluent outlet.

At $t = 350\,\mathrm{s}$, we change the volumetric flow of the inlet $z_{\mathrm{F},1}$ from $Q_{\mathrm{F},1} = 30$ to $Q_{\mathrm{F},1} = 20\,\mathrm{cm}^3/\mathrm{s}$, maintaining the other volumetric flows. As a consequence we can see that the primary phase ϕ rises and leaves zone 1, exiting the tank only through the effluent while the secondary phase maintains the same behaviour as before and is present only above the feed level $z_{\mathrm{F},2}$.

Table 3.3 shows the estimated errors and convergence orders for this simulation, which have the same behaviour as the ones showed in the numerical examples in Sections 3.4.3 and 3.4.4.

Table 3.3: Example 3.3: Co-current flows. Total estimated relative L^1-error, $e^{\mathrm{tot}}_{N_k}(T)$, and estimated convergence orders, $\Theta_k(T)$, calculated between consecutive values of N_k, with $N_{\mathrm{ref}} = 12\,800$, $T = 500\,\mathrm{s}$.

N_k	$e^{\mathrm{tot}}_{N_k}(T)$	$\Theta_k(T)$
100	2.7733×10^{-1}	–
200	1.7102×10^{-1}	0.6974
400	1.0504×10^{-1}	0.7032
800	6.2422×10^{-2}	0.7508
1600	3.4649×10^{-2}	0.8492
3200	1.6926×10^{-2}	1.0336

CHAPTER 4

Convergence analysis of a difference scheme for a triangular system of conservation laws with discontinuous flux in a column with constant cross-sectional area

4.1 Introduction

The purpose of this chapter is to contribute to the mathematical analysis of the numerical scheme presented in **Chapter 3**, focusing on the structure of the numerical fluxes of the ϕ– and ψ–schemes that satisfy the region-invariant property and also allow the application of the compensated compactness theory.

The steps of the convergence analysis are based on additional simplifying assumptions, namely those of a constant cross-sectional area A and constant bulk and feed flows Q_{U}, $Q_{\mathrm{F},k}$, $\phi_{\mathrm{F},k}$ and $\psi_{\mathrm{F},k}$ $(k = 1, \ldots, K)$. We can then prove convergence of the ϕ-scheme (Section 4.2) and L^1 Lipschitz continuity of the ψ-scheme (Section 4.3). If in addition all z-dependent flux discontinuities are removed, we may apply compensated compactness techniques to prove convergence of the ψ-scheme (Section 4.4), to do this, it is used that the scheme converges to the only entropy solution in the sense of Kružkov. For the simplified problems, we assume that the model is posed as initial value problem (3.1), (3.2) with the initial data posed on the real line and assumptions (3.3) and (3.4) are imposed, so Theorems 3.1 and 3.2 remain in effect.

For ease of the argument, let us focus on the case of a constant interior cross-sectional area A. That is, we assume

$$A \equiv \text{const.}, \quad A > 0. \tag{4.1}$$

In addition, we assume that the feed volume flows and concentrations $Q^n_{\mathrm{F},k}$, $\phi^n_{\mathrm{F},k}$, and $\psi^n_{\mathrm{F},k}$ $(k = 1, \ldots, K)$ are constant and therefore do not depend on n. The same is assumed for the

underflow volume rate Q_{U}. Then (3.20) and (3.27) take the forms

$$\phi_{i-1/2}^{n+1} = \phi_{i-1/2}^{n} - \lambda\Delta_{-}\big(\phi_{i-1/2}^{n} q_i^{+} + \phi_{i+1/2}^{n} q_i^{-} + \gamma_i \phi_{i-1/2}^{n} W\big(\phi_{i+1/2}^{n}\big)\big) + \lambda \sum_{k=1}^{K} \frac{Q_{\mathrm{F},k}}{A} \phi_{\mathrm{F},k} \delta_{k,i-1/2}, \tag{4.2}$$

$$\begin{aligned}\psi_{i-1/2}^{n+1} = \psi_{i-1/2}^{n} - \lambda\Delta_{-}\Bigg(&\psi_{i-1/2}^{n} q_i^{+} + \psi_{i+1/2}^{n} q_i^{-} \\ &+ \gamma_i \Bigg(G_i^{n}\big(\psi_{i-1/2}^{n}, \psi_{i+1/2}^{n}\big) - \phi_{i-1/2}^{n} \frac{\psi_{i+1/2}^{n} W(\phi_{i+1/2}^{n})}{1-\phi_{i+1/2}^{n}}\Bigg)\Bigg) + \lambda \sum_{k=1}^{K} \frac{Q_{\mathrm{F},k}}{A} \psi_{\mathrm{F},k}^{n} \delta_{k,i-1/2}.\end{aligned} \tag{4.3}$$

Furthermore, to be able to properly embed the treatment into available analyses of schemes for conservation laws with discontinuous flux, we absorb the feed term into the numerical flux. That is, we define $i = i_k$ if $\delta_{k,i-1/2} = 1$ (see (3.17)). Then

$$q_i = \begin{cases} -q_{\mathrm{U}} & \text{if } i \le i_1 - 1, \\ -q_{\mathrm{U}} + q_{\mathrm{F},1} + \cdots + q_{\mathrm{F},l} & \text{if } i_l \le i \le i_{l+1} - 1,\ l = 1, \ldots, K-1, \\ -q_{\mathrm{U}} + q_{\mathrm{F},1} + \cdots + q_{\mathrm{F},K} & \text{for } i \ge i_K. \end{cases} \tag{4.4}$$

Furthermore, we define the feed flux

$$h_{\mathrm{F},i} = \begin{cases} 0 & \text{if } i \le i_1 - 1, \\ q_{\mathrm{F},1}\phi_{\mathrm{F},1} + \cdots + q_{\mathrm{F},l}\phi_{\mathrm{F},l} & \text{if } i_l \le i \le i_{l+1} - 1,\ l = 1, \ldots, K-1, \\ q_{\mathrm{F},1}\phi_{\mathrm{F},1} + \cdots + q_{\mathrm{F},K}\phi_{\mathrm{F},K} & \text{for } i \ge i_K, \end{cases} \tag{4.5}$$

such that

$$h_{\mathrm{F},i} - h_{\mathrm{F},i-1} = -\sum_{k=1}^{K} \frac{Q_{\mathrm{F},k}}{A} \phi_{\mathrm{F},k} \delta_{k,i-1/2}.$$

Consequently, we may write the scheme as

$$\phi_{i-1/2}^{n+1} = \phi_{i-1/2}^{n} - \lambda\Delta_{-}\big(\phi_{i+1/2}^{n} q_i^{-} + \phi_{i-1/2}^{n} q_i^{+} + \gamma_i \phi_{i-1/2}^{n} W(\phi_{i+1/2}^{n}) + h_{\mathrm{F},i}\big). \tag{4.6}$$

For later use we define the function

$$h(z, v, u) := q^{-}(z)v + q^{+}(z)u + \gamma(z)uW(v) + h_{\mathrm{F}}(z) \tag{4.7}$$

that allows us to write (4.6) as

$$\phi_{i-1/2}^{n+1} = \phi_{i-1/2}^{n} - \lambda\Delta_{-} h\big(z_i, \phi_{i+1/2}^{n}, \phi_{i-1/2}^{n}\big). \tag{4.8}$$

4.2 Convergence of the ϕ-scheme

The partial differential equation for ϕ, under the present simplification (4.1), is the conservation law

$$\partial_t \phi + \partial_z J(\phi, z) = 0, \quad (z,t) \in \Pi_T \tag{4.9}$$

with discontinuous flux

$$J(\phi,z) = \begin{cases} \left(-q_{\mathrm{U}} + \sum_{k=1}^{K} q_{\mathrm{F},k}\right)\phi + \sum_{k=1}^{K} q_{\mathrm{F},k}\phi_{\mathrm{F},k} & \text{for } z > z_{\mathrm{E}}, \\ \left(-q_{\mathrm{U}} + \sum_{k=1}^{K} q_{\mathrm{F},k}\right)\phi + \sum_{k=1}^{K} q_{\mathrm{F},k}\phi_{\mathrm{F},k} + j(\phi) & \text{for } z_{\mathrm{F},K} < z < z_{\mathrm{E}}, \\ \left(-q_{\mathrm{U}} + \sum_{k=1}^{l} q_{\mathrm{F},k}\right)\phi + \sum_{k=1}^{l} q_{\mathrm{F},k}\phi_{\mathrm{F},k} + j(\phi) & \text{for } z_{\mathrm{F},l} < z < z_{\mathrm{F},l+1}, \\ & l = 1,\dots,K-1, \\ -q_{\mathrm{U}}\phi + j(\phi) & \text{for } z_{\mathrm{U}} < z < z_{\mathrm{F},1}, \\ -q_{\mathrm{U}}\phi & \text{for } z < z_{\mathrm{U}}. \end{cases} \tag{4.10}$$

posed along with the initial condition (3.2a).

The choice of the appropriate solution concept for weak solutions, and the ways we may relate the model to the available mathematical theory of conservation laws with discontinuous flux, requires that we verify whether $J(\phi,z)$ as given by (4.10) satisfies the so-called "crossing condition" across each discontinuity $z \in \mathcal{Z} := \{z_{\mathrm{U}}, z_{\mathrm{F},1}, \dots, z_{\mathrm{F},K}, z_{\mathrm{E}}\}$. Certain early well-posedness (existence, stability, and uniqueness) results for conservation laws with discontinuous flux (and related equations) rely on satisfaction of this condition (cf., e.g., [69]), although later developments advance solution concepts that do not rely on satisfaction of the crossing condition (see [2,66,82]).

In the present context this condition is satisfied for a particular discontinuity at z if the adjacent fluxes to the right and the left, $J(\phi, z^+)$ and $J(\phi, z^-)$, satisfy

$$\forall \phi_1, \phi_2 \in [0,1] : J(\phi_1, z^+) - J(\phi_1, z^-) < 0 < J(\phi_2, z^+) - J(\phi_2, z^-) \Rightarrow \phi_1 < \phi_2, \tag{4.11}$$

which means either the graphs of $J(\cdot, z^-)$ and $J(\cdot, z^+)$ do not intersect, or if they do, there is at most one flux crossing ϕ_χ and the graph of $J(\cdot, z^-)$ lies above that of $J(\cdot, z^+)$ to the left of ϕ_χ. For $J(\phi,z)$ as given by (4.10) this condition is clearly satisfied for $z \in \{z_{\mathrm{E}}, z_{\mathrm{U}}\}$ (considering that $j(\phi) > 0$ for $0 < \phi < 1$ implies that $J(\cdot, z^-)$ and $J(\cdot, z^+)$ do not intersect in this case), while

$$J(\phi, z_{\mathrm{F},l}^+) - J(\phi, z_{\mathrm{F},l}^-) = q_{\mathrm{F},l}(\phi - \phi_{\mathrm{F},l}) \quad \text{for } l = 1,\dots,K.$$

Thus, the crossing condition is satisfied also for $z = z_{\mathrm{F},l}$, $l = 1,\dots,K$, since either $\phi_{\mathrm{F},l} = 0$ and the adjacent fluxes do not intersect in $(0,1)$, or the intersection takes place at $\phi_\chi = \phi_{\mathrm{F},l}$ and

(4.11) holds since $q_{\mathrm{F},l} > 0$ for all l. The preceding consideration is analogous to the one for the simpler clarifier-thickener model (equivalent to the case $K = 1$ in the present notation) studied e.g. in [24, 25]. With the present analysis it is clear that the crossing condition is satisfied at each flux discontinuity $z \in \mathcal{Z}$.

Some of the available analyses refer to initial-value problems of the type

$$\begin{aligned} \partial_t u + \partial_x \mathcal{F}(u,x) &= 0 \quad \text{for } (x,t) \in \Pi_T, \\ u(x,0) &= u_0(x) \quad \text{for } x \in \mathbb{R}, \\ \text{where} \quad \mathcal{F}(u,x) &:= H(-x)g(u) + H(x)f(u) \end{aligned} \tag{4.12}$$

where f and g are Lipschitz continuous functions of u denoting the "right" and "left" flux adjacent to a flux discontinuity across $x = 0$ and H denotes the Heavyside function. The model problem (4.12) features, of course, only one flux discontinuity (sitting at $x = 0$), while (4.10), (3.2a) includes several of them at separate spatial locations. The study of (4.12) is, however, sufficient for the analysis of each single flux discontinuity.

Here we start from the concept of *entropy solutions of type* $\mathcal{V}$ introduced by Karlsen and Towers [70]. This concept does not appeal to the existence of traces of the unknown with respect to the interfaces $z \in \mathcal{Z}$ across which $J(\phi, z)$ is discontinuous. To state its adaptation to the situation at hand, we define the sets

$$\begin{aligned} \Pi_T^{(K+3/2)} &:= (z_{\mathrm{E}}, \infty) \times (0,T), \\ \Pi_T^{(K+1/2)} &:= (z_{\mathrm{F},K}, z_{\mathrm{E}}) \times (0,T), \\ \Pi_T^{(k-1/2)} &:= (z_{\mathrm{F},k-1}, z_{\mathrm{F},k}) \times (0,T), \quad k = 2, \dots, K, \\ \Pi_T^{(1/2)} &:= (z_{\mathrm{U}}, z_{\mathrm{F},1}) \times (0,T), \\ \Pi_T^{(-1/2)} &:= (-\infty, z_{\mathrm{U}}) \times (0,T). \end{aligned}$$

Definition 4.2.1. *A measurable function $\phi = \phi(z,t) \in L^1(\Pi_T)$ is an* entropy solution of type $\mathcal{V}$ *of the initial-value problem (4.9), (3.2a) if it satisfies the following conditions:*

(i) *The function ϕ belongs to $L^\infty(\Pi_T)$; for a.e. $(z,t) \in \Pi_T$ there holds $\phi(z,t) \in [0,1]$.*

(ii) *The function ϕ is a weak solution of (4.9), i.e., for all smooth test functions ζ with compact support in Π_T,*

$$\iint_{\Pi_T} \big(\phi \partial_t \zeta + J(\phi, z) \partial_z \zeta\big) \,\mathrm{d}z \,\mathrm{d}t = 0. \tag{4.13}$$

(iii) *For all $l = 0, \dots, K+2$, for any nonnegative smooth test function $\zeta^{(l)}$ with compact support in $\Pi_T^{(l)}$ and all $c \in [0,1]$ there holds*

$$\begin{aligned} &\iint_{\Pi_T} \Big(|\phi - c| \partial_t \zeta^{(l)} + \operatorname{sgn}(\phi - c) \big(J(\phi,z) - J(c,z)\big) \partial_z \zeta^{(l)} \Big) \,\mathrm{d}z \,\mathrm{d}t \\ &+ \int_{\mathbb{R}} |\phi_0 - c| \, \zeta^{(l)}(z,0) \,\mathrm{d}t \geq 0. \end{aligned} \tag{4.14}$$

(iv) *The following Kružkov-type [72] entropy inequality holds for all nonnnegative smooth test functions ζ with compact support in Π_T and all constants $c \in \mathbb{R}$:*

$$\begin{aligned}&\iint_{\Pi_T} \Big(|\phi - c| \partial_t \zeta + \operatorname{sgn}(\phi - c) \big(J(\phi, z) - J(c, z) \big) \partial_z \zeta \Big) \, \mathrm{d}z \, \mathrm{d}t \\ &+ \int_0^T \sum_{z \in \mathcal{Z}} \big| J(c, z^+) - J(c, z^-) \big| \, \zeta(z, t) \, \mathrm{d}t \geq 0.\end{aligned} \tag{4.15}$$

Notice that the entropy inequality (4.15) does not imply the weak formulation (4.13). The standard derivation of the weak formulation from the Kružkov entropy inequality (cf., e.g., [60, Sect. 2.1]) cannot be applied here since some of the flux differences $|J(c, z^+) - J(c, z^-)|$ are not compactly supported with respect to c, see [24, Rem. 1.1].

Lemma 4.1. *There exists a constant C_1, depending on $\mathrm{TV}(\phi_0)$, such that*

$$\Delta z \sum_{i \in \mathbb{Z}} \big| \phi^{n+1}_{i-1/2} - \phi^n_{i-1/2} \big| \leq \Delta z \sum_{i \in \mathbb{Z}} \big| \phi^1_{i-1/2} - \phi^0_{i-1/2} \big| \leq C_1 \Delta t.$$

Proof. Subtracting from (4.2) its version from the previous time step, we get

$$\begin{aligned}\phi^{n+1}_{i-1/2} - \phi^n_{i-1/2} = &\big(\phi^n_{i-3/2} - \phi^{n-1}_{i-3/2} \big) \lambda B^n_{i-1/2} \\ &+ \big(\phi^n_{i-1/2} - \phi^{n-1}_{i-1/2} \big) \big\{ 1 - \lambda B^n_{i+1/2} + \lambda C^n_{i-1/2} \big\} \\ &+ \big(\phi^n_{i+1/2} - \phi^{n-1}_{i+1/2} \big) \{ -\lambda C^n_{i+1/2} \},\end{aligned}$$

where we define

$$B^n_{i-1/2} := q^+_{i-1} + \gamma_{i-1} W\big(\phi^n_{i-1/2} \big),$$

$$C^n_{i+1/2} := \begin{cases} q^-_i + \gamma_i \phi^{n-1}_{i-1/2} \dfrac{W(\phi^n_{i+1/2}) - W(\phi^{n-1}_{i+1/2})}{\phi^n_{i+1/2} - \phi^{n-1}_{i+1/2}} & \text{if } \phi^n_{i+1/2} \neq \phi^{n-1}_{i+1/2}, \\ 0 & \text{otherwise.} \end{cases}$$

Clearly $B^n_{i-1/2} \geq 0$, $C^n_{i+1/2} \leq 0$, and due to the CFL condition,

$$1 - \lambda B^n_{i+1/2} + \lambda C^n_{i-1/2} \geq 0,$$

hence taking absolute values and summing over $i \in \mathbb{Z}$ we get, by appealing to standard arguments, that

$$\Delta z \sum_{i \in \mathbb{Z}} \big| \phi^{n+1}_{i-1/2} - \phi^n_{i-1/2} \big| \leq \Delta z \sum_{i \in \mathbb{Z}} \big| \phi^n_{i-1/2} - \phi^{n-1}_{i-1/2} \big| \leq \Delta z \sum_{i \in \mathbb{Z}} \big| \phi^1_{i-1/2} - \phi^0_{i-1/2} \big|.$$

Furthermore, following the lines e.g. of the proof of [24, Lemma 3.2], we get that there exists a constant C_2 that is independent of $(\Delta t, \Delta z)$ such that

$$\sum_{i \in \mathbb{Z}} \big| \phi^1_{i-1/2} - \phi^0_{i-1/2} \big| \leq C_2 \big(\mathrm{TV}(\phi^0) + \mathrm{TV}(q) + \mathrm{TV}(\gamma) \big),$$

which completes the proof. □

A straightforward calculation yields that we can write the scheme in the form

$$\phi_{i-1/2}^{n+1} = \phi_{i-1/2}^n + C_i^n \Delta_+ \phi_{i-1/2}^n - D_{i-1}^n \Delta_- \phi_{i-1/2}^n - \theta_i^n,$$

where we define

$$\begin{aligned} C_i^n &:= \begin{cases} -\lambda q_i^- - \lambda \gamma_{i-1} \phi_{i-3/2}^n \dfrac{\Delta_- W(\phi_{i+1/2}^n)}{\Delta_+ \phi_{i-1/2}^n} & \text{if } \Delta_+ \phi_{i-1/2}^n \neq 0, \\ -\lambda q_i^- & \text{otherwise,} \end{cases} \\ D_{i-1}^n &:= \lambda q_i^+ + \lambda \gamma_{i-1} W(\phi_{i+1/2}^n), \\ \theta_i^n &:= \lambda \big(\phi_{i-1/2}^n \Delta_- q_i^- + \phi_{i-3/2}^n \Delta_- q_i^+ + \phi_{i-1/2}^n W(\phi_{i+1/2}^n) \Delta_- \gamma_i - \Delta_- h_{\mathrm{F},i} \big). \end{aligned}$$

The incremental coefficients satisfy $C_i^n \geq 0$ and $D_i^n \geq 0$; furthermore, the CFL condition ensures that $C_i^n + D_i^n \leq 1$ (in all cases for all i and n). Notice that $\theta_i^n = 0$ with the possible exception for those indices i at which $\Delta_- q_i^- \neq 0$, $\Delta_- q_i^+ \neq 0$, or $\Delta_- \gamma_i \neq 0$. According to the definition of γ_i and that of q_i, see (4.4), this may occur at most at a finite number of indices. Precisely, we may assert that

$$\theta_i^n = 0 \quad \text{if } z_{i-1}, z_i \notin \mathcal{Z},$$

hence for all indices i with the exception of finitely many indices i such that $|z_j - \zeta| \leq \Delta z$ for some $\zeta \in \mathcal{Z}$, the scheme is given by the incremental form

$$\phi_{i-1/2}^{n+1} = \phi_{i-1/2}^n + C_i^n \Delta_+ \phi_{i-1/2}^n - D_{i-1}^n \Delta_- \phi_{i-1/2}^n$$

with incremental coefficients $C_i^n \geq 0$, $D_i^n \geq 0$, and $C_i^n + D_i^n \leq 1$. This property, in conjunction with Lemma 4.1, shows that we may apply [27, Lemma 5.3] (which is essentially Lemma 4.2 of [23], where a proof can be found) to the situation at hand. We have therefore proved the following lemma, where $V_a^b(g)$ denotes the total variation of a function $z \mapsto g(z)$ over the interval (a, b).

Lemma 4.2. *For any interval $[a, b]$ such that $[a, b] \cap \mathcal{Z} = \varnothing$ and any $t \in [0, T]$ there exists a total variation bound of the form*

$$V_a^b\big(\phi^{\Delta z}(\cdot, t)\big) \leq C(a, b),$$

where $C(a, b)$ is independent of $(\Delta x, \Delta t)$ and t for $t \in [0, T]$.

Finally, we have shown in Theorem 3.1 that the scheme (3.20) is monotone. This applies, in particular, to the reduced scheme (4.2) or equivalently, (4.6) or (4.8). Thus, the scheme satisfies a discrete entropy inequality. The proof of the following lemma is identical to that of [70, Lemma 5.2], and is therefore omitted.

Lemma 4.3. *The scheme (4.8) satisfies the following entropy inequality for any $c_{i-3/2}, c_{i-1/2}, c_{i+1/2} \in [0,1]$:*

$$\begin{aligned}\left|\phi^{n+1}_{i-1/2} - c_{i-1/2}\right| \le \left|\phi^{n}_{i-1/2} - c_{i-1/2}\right| - \lambda\Delta_- H^n_i \\ - \lambda \operatorname{sgn}\left(\phi^{n+1}_{i-1/2} - c_{i-1/2}\right)\Delta_- h\left(z_i, \phi^n_{i+1/2}, \phi^n_{i-1/2}\right),\end{aligned}$$

where the numerical entropy flux H^n_i is defined by

$$\begin{aligned}H^n_i := h\left(z_i, \phi^n_{i+1/2} \vee c_{i+1/2}, \phi^n_{i-1/2} \vee c_{i-1/2}\right) \\ - h\left(z_i, \phi^n_{i+1/2} \wedge c_{i+1/2}, \phi^n_{i-1/2} \wedge c_{i-1/2}\right).\end{aligned}$$

We now may appeal to the results of [70] and argue as follows. Theorem 3.1 and Lemmas 4.1, 4.2 and 4.3 ensure convergence of the functions ϕ^Δ to a weak solution of (4.9), (3.2a) that satisfies items (i), (ii) and (iii) of Definition 4.2.1. It also satisfies the entropy inquality (4.15) arising in part (iv) of that definition by utilizing the discrete entropy inequality stated in Lemma 4.3.

4.3 L^1 Lipschitz continuity in time of the ψ-scheme

Next, we deal with the marching formula (4.3). To this end, we define a feed flux $\tilde{h}_{\mathrm{F},i}$ exactly as in (4.5) but with $\phi_{\mathrm{F},i}$ replaced by $\psi_{\mathrm{F},i}$ for $i = 1, \dots, K$. Furthermore, we recall that $\tilde{v}_{\phi\mathrm{s}}(\phi) = W(\phi)/(1-\phi)$. Thus, the scheme can be written as

$$\begin{aligned}\psi^{n+1}_{i-1/2} = \psi^n_{i-1/2} - \lambda\Delta_-\Big(\tilde{h}_{\mathrm{F},i} + \psi^n_{i-1/2} q_i^+ + \psi^n_{i+1/2} q_i^- \\ + \gamma_i\left(G^n_i\left(\psi^n_{i-1/2}, \psi^n_{i+1/2}\right) - \phi^n_{i-1/2}\tilde{v}_{\phi\mathrm{s}}\left(\phi^n_{i+1/2}\right)\psi^n_{i+1/2}\right)\Big).\end{aligned} \tag{4.16}$$

Lemma 4.4 (Crandall and Tartar [35])**.** *Assume that (Ω, μ) is some measure space and assume that D is a subset of $L^1(\Omega)$ with the property that if $u, v \in D$, then $(u \vee v) \in D$. Assume that T is a map $T : D \ni u \mapsto T(u) \in D$ such that*

$$\int_\Omega T(u)\,\mathrm{d}\mu = \int_\Omega u\,\mathrm{d}\mu \quad \text{for all } u \in D.$$

Then the following statements, valid for all $u, v \in D$, are equivalent:

(i) *If $u \le v$, then $T(u) \le T(v)$.*

(ii) $\int_\Omega ((T(u) - T(v)) \vee 0)\,\mathrm{d}\mu \le \int_\Omega ((u-v) \vee 0)\,\mathrm{d}\mu$.

(iii) $\int_\Omega |T(u) - T(v)|\,\mathrm{d}\mu \le \int_\Omega |u - v|\,\mathrm{d}\mu$.

Following, for instance, [34], we utilize Lemma 4.4 for the following mapping. Assume that $D \subset L^1(\mathbb{R})$ is the set of piecewise constant functions and that are constant on the intervals $I_{i-1/2}$ for $i \in \mathbb{Z}$, and that with the marching formula (3.30) we associate an operator $\mathcal{K}^n : D \to D$ such that if $\psi^{\Delta z}(\cdot, t^n)$ is the piecewise constant function defined by (3.28) for $t = t_n$, we may write the scheme as

$$\psi^{\Delta z}(\cdot, t_{n+1}) = \mathcal{K}^n\big(\psi^{\Delta z}(\cdot, t_n)\big).$$

Clearly, the monotonicity of the scheme implies that if $u, v \in D$, then

$$u \le v \Rightarrow \mathcal{K}^n(u) \le \mathcal{K}^n(v).$$

Thus, Lemma 4.4 (i) holds. For $u = \psi^{\Delta z}(\cdot, t_n)$ and $v = \psi^{\Delta z}(\cdot, t_{n-1})$, Lemma 4.4 (iii) implies that

$$\begin{aligned}\Delta z \sum_{i\in\mathbb{Z}} \big|\psi^{n+1}_{i-1/2} - \psi^{n}_{i-1/2}\big| &= \int_{\mathbb{R}} \big|\psi^{\Delta z}(z, t_{n+1}) - \psi^{\Delta z}(z, t_n)\big|\,\mathrm{d}z \\ \le \int_{\mathbb{R}} \big|\psi^{\Delta z}(z, t_n) - \psi^{\Delta z}(z, t_{n-1})\big|\,\mathrm{d}z &= \Delta z \sum_{i\in\mathbb{Z}} \big|\psi^{n}_{i-1/2} - \psi^{n-1}_{i-1/2}\big|\end{aligned}$$

and therefore

$$\Delta z \sum_{i\in\mathbb{Z}} \big|\psi^{n+1}_{i-1/2} - \psi^{n}_{i-1/2}\big| \le \Delta z \sum_{i\in\mathbb{Z}} \big|\psi^{1}_{i-1/2} - \psi^{0}_{i-1/2}\big|.$$

However, we may assert that there exists a constant C_3, which is independent of $(\Delta t, \Delta x)$, such that

$$\begin{aligned}\sum_{i\in\mathbb{Z}} \big|\psi^{1}_{i-1/2} - \psi^{0}_{i-1/2}\big| = \sum_{i\in\mathbb{Z}} \Big| \Delta_- \Big(&\psi^0_{i-1/2} q_i^+ + \psi^0_{i+1/2} q_i^- \\ &+ \gamma_i \Big(G_i^0\big(\psi^0_{i-1/2}, \psi^0_{i+1/2}\big) - \phi^n_{i-1/2} \frac{\psi^0_{i+1/2} W(\phi^0_{i+1/2})}{1 - \phi^0_{i+1/2}} \Big) \Big) \\ &- \lambda \sum_{k=1}^{K} \frac{Q_{\mathrm{F},k}}{A} \psi^0_{\mathrm{F},k} \delta_{k,i-1/2} \Big| \le C_3.\end{aligned}$$

A sufficient condition for this bound on the initial discrete divergence to hold is

$$\mathrm{TV}(\phi^0) < \infty, \quad \mathrm{TV}(\psi^0) < \infty.$$

Thus,

$$\Delta z \sum_{i\in\mathbb{Z}} \big|\psi^{n+1}_{i-1/2} - \psi^{n}_{i-1/2}\big| \le \Delta z C_3 = \frac{\Delta t}{\lambda} C_3.$$

Consequently, we have proved the following lemma.

Lemma 4.5. *There exists a constant C_4 that is independent of $(\Delta t, \Delta z)$ such that*

$$\Delta z \sum_{i\in\mathbb{Z}} \big|\psi^{n+1}_{i-1/2} - \psi^{n}_{i-1/2}\big| \le C_4 \Delta t.$$

4.4 Compensated compactness

To write down the scheme in the simplest setting possible, we consider the model and numerical scheme under the assumptions before, and additionally assume the case of a constant bulk velocity q, assume that the feed terms (giving rise to the singular source) are zero, and that γ plays the role of a parameter that can be either 0 or 1. Thus, the model reduces to the triangular system of conservation laws

$$\partial_t \phi + \partial_z J(\phi) = 0, \tag{4.17}$$

$$\partial_t \psi + \partial_z \tilde{F}(\phi, \psi) = 0, \quad (z,t) \in \Pi_T, \tag{4.18}$$

where J and $\tilde{F}$ are defined as before and we assume that (4.17), (4.18) is equipped with the initial conditions (3.2), where we assume that assumptions (3.3) are in effect. For ease of reference we state the definition of a weak solution of the initial-value problem (4.17), (4.18), (3.2).

Definition 4.4.1. *The pair (ϕ, ψ) is called a* weak solution *of the initial-value problem (4.17), (4.18), (3.2) if*

(i) *The functions ϕ and ψ belong to $L^\infty(\Pi_T)$.*

(ii) *The functions ϕ and ψ satisfy (4.17), (4.18), (3.2) in the sense of distributions on Π_T, that is, for each smooth test function ζ with compact support in Π_T, the following identities hold:*

$$\iint_{\Pi_T} \big(\phi \partial_t \zeta + J(\phi) \partial_z \zeta\big) \,\mathrm{d}z \,\mathrm{d}t + \int_{\mathbb{R}} \phi_0(z) \,\mathrm{d}z = 0, \tag{4.19}$$

$$\iint_{\Pi_T} \big(\psi \partial_t \zeta + \tilde{F}(\phi, \psi) \partial_z \zeta\big) \,\mathrm{d}z \,\mathrm{d}t + \int_{\mathbb{R}} \psi_0(z) \,\mathrm{d}z = 0. \tag{4.20}$$

(iii) *The function ϕ is an entropy solution of the single conservation law (4.17), that is, for each smooth and nonnegative test function ζ with compact support in Π_T, the following inequality holds for all $c \in \mathbb{R}$:*

$$\begin{aligned} &\iint_{\Pi_T} \big(|\phi - c| \partial_t \zeta + \operatorname{sgn}(\phi - c)\big(J(\phi) - J(k)\big) \partial_z \zeta\big) \,\mathrm{d}z \,\mathrm{d}t \\ &\quad + \int_{\mathbb{R}} \big|\phi_0(z) - c\big| \,\mathrm{d}z \geq 0. \end{aligned} \tag{4.21}$$

Assume now that $\eta = \eta(\psi)$ is a smooth convex entropy function and $Q = Q(\phi, \psi)$ is the corresponding compatible entropy flux compatible with (4.18), i.e., the function Q satisfies

$$\partial_\psi Q(\phi, \psi) = \eta'(\psi) \partial_\psi \tilde{F}(\phi, \psi). \tag{4.22}$$

In what follows, we refer to (η, Q) as an *entropy pair* for (4.18). In particular we denote by (η_0, Q_0) the Kružkov entropy pair [72], that is

$$\eta_0(\psi) = |\psi - c|, \quad Q_0(\phi, \psi) = \operatorname{sgn}(\psi - c)\big(\tilde{F}(\phi, \psi) - \tilde{F}(\phi, c)\big), \tag{4.23}$$

where $c \in \mathbb{R}$ is a constant.

The convergence proof is based on the following lemma, slightly adapted from [34, Lemma 2.2], which in turn is an adaptation of [92, Theorem 5].

Lemma 4.6. *Let ϕ be the unique entropy solution of the initial-value problem (4.17), (3.2a), and assume that $\{\psi^\nu\}_{\nu>0}$ is a family of functions defined on Π_T. If $\{\psi^\nu\}$ is bounded in $L^\infty(\Pi_T)$ and*

$$\big\{\partial_t \eta_0(\psi^\nu) + \partial_z Q_0(u, \psi^\nu)\big\}_{\nu>0}$$

lies in a compact set of $H^{-1}_{\mathrm{loc}}(\Pi_T)$ for all constants c (cf. (4.23)), then there exists a sequence $\{\nu_n\}_{n\in\mathbb{N}}$ such that $\nu_n \to 0$ as $n \to \infty$ and a function $\psi \in L^\infty(\Pi_T)$ such that

$$\psi^{\nu_n} \to \psi \quad \text{a.e. and in } L^p_{\mathrm{loc}}(\Pi_T),\ 1 \le p < \infty.$$

Consistently with (4.7), (4.8) we assume that the scheme employed to approximate entropy solutions of (4.17) is

$$\phi^{n+1}_{i-1/2} = \phi^n_{i-1/2} - \lambda \Delta_- h\big(\phi^n_{i+1/2}, \phi^n_{i-1/2}\big). \tag{4.24}$$

with the numerical flux

$$h(z, v, u) := q^- v + q^+ u + \gamma u W(v). \tag{4.25}$$

Clearly, under a suitable CFL condition, the scheme converges to the unique entropy solution of (4.17), (3.2a). Our goal is to establish convergence of the corresponding scheme for ψ. We here write the scheme as

$$\begin{aligned} \psi^{n+1}_{i-1/2} &= \psi^n_{i-1/2} - \lambda \Delta_- \mathcal{F}\big(\phi^n_{i-1/2}, \phi^n_{i+1/2}, \psi^n_{i-1/2}, \psi^n_{i+1/2}\big) \\ &\equiv \psi^n_{i-1/2} - \lambda \Delta_- \mathcal{F}(\boldsymbol{\phi}^n_i, \boldsymbol{\psi}^n_i), \end{aligned} \tag{4.26}$$

where we define the four-argument numerical flux

$$\mathcal{F}(a, b, u, v) := q^+ u + q^- v + \gamma\big(G(a, b, u, v) - a\tilde{v}_{\phi\mathrm{s}}(b)v\big), \tag{4.27}$$

and denote pairs of neighboring ϕ- and ψ-values by

$$\boldsymbol{\phi}^n_i := \big(\phi^n_{i-1/2}, \phi^n_{i+1/2}\big) \quad \text{and} \quad \boldsymbol{\psi}^n_i := \big(\psi^n_{i-1/2}, \psi^n_{i+1/2}\big),$$

and replace the arguments "$\phi^n_{i-1/2}, \phi^n_{i+1/2}$" by $\boldsymbol{\phi}^n_i$ (analogously for ψ). In (4.27) a and b play the roles of $\phi^n_{i-1/2}$ and $\phi^n_{i+1/2}$, and u and v those of $\psi^n_{i-1/2}$ and $\psi^n_{i+1/2}$, respectively, and we define $G(a,b,u,v)$ as follows. Let

$$f(a,b,\psi) := \psi \tilde{V}\left(\frac{\psi}{1-(a\vee b)}\right)$$

(see (1.24)), then $G(a,b,\cdot,\cdot)$ is the Engquist-Osher numerical flux [51] associated with $f(a,b,\cdot)$.

We multiply the scheme (4.26) by $\eta'(\psi^{n+1}_{i-1/2})$, where η is a smooth convex entropy function, and utilize the Taylor expansion

$$\eta'\big(\psi^{n+1}_{i-1/2}\big)\big(\psi^{n+1}_{i-1/2}-\psi^n_{i-1/2}\big) = \eta\big(\psi^{n+1}_{i-1/2}\big)-\eta\big(\psi^n_{i-1/2}\big)+\frac{1}{2}\eta''\big(\xi^{n+1/2}_{i-1/2}\big)\big(\psi^{n+1}_{i-1/2}-\psi^n_{i-1/2}\big)^2,$$

where $\xi^{n+1/2}_{i-1/2}$ is an intermediate value between $\psi^n_{i-1/2}$ and $\psi^{n+1}_{i-1/2}$. Then we get

$$\begin{aligned}
&\eta\big(\psi^{n+1}_{i-1/2}\big)-\eta\big(\psi^n_{i-1/2}\big)+\frac{1}{2}\eta''\big(\xi^{n+1/2}_{i-1/2}\big)\big(\psi^{n+1}_{i-1/2}-\psi^n_{i-1/2}\big)^2\\
&= -\lambda\eta'\big(\psi^{n+1}_{i-1/2}\big)\Delta_-\mathcal{F}(\boldsymbol{\phi}^n_i,\boldsymbol{\psi}^n_i)\\
&= -\lambda\eta'\big(\psi^n_{i-1/2}\big)\Delta_-\mathcal{F}(\boldsymbol{\phi}^n_i,\boldsymbol{\psi}^n_i)-\lambda\big(\eta'\big(\psi^{n+1}_{i-1/2}\big)-\eta'\big(\psi^n_{i-1/2}\big)\big)\Delta_-\mathcal{F}(\boldsymbol{\phi}^n_i,\boldsymbol{\psi}^n_i).
\end{aligned} \tag{4.28}$$

We now define the functions $\hat{f}$ and $\check{f}$ as the partial derivatives

$$\begin{aligned}
\hat{f}(a,b,u) &:= \partial_u\mathcal{F}(a,b,u,v) = q^+ + \partial_u G(a,b,u,v) \geq 0,\\
\check{f}(a,b,v) &:= \partial_v\mathcal{F}(a,b,u,v) = q^- + \partial_v G(a,b,u,v) - a\tilde{v}_{\phi s}(b) \leq 0.
\end{aligned}$$

The dependence of $\partial_u\mathcal{F}(a,b,u,v)$ and $\partial_v\mathcal{F}(a,b,u,v)$ on u and v only, respectively, is crucial for the subsequent analysis. We define the functions

$$\hat{\mathcal{F}}(a,b,u) := \int_0^u \hat{f}(a,b,s)\,\mathrm{d}s, \quad \check{\mathcal{F}}(a,b,v) := \int_0^v \check{f}(a,b,s)\,\mathrm{d}s$$

and note that

$$\mathcal{F}(a,b,u,v) = \hat{\mathcal{F}}(a,b,u) + \check{\mathcal{F}}(a,b,v). \tag{4.29}$$

Next, we define

$$\begin{aligned}
\mathcal{Q}^+(a,b,\psi) &:= \int_0^\psi \eta'(u)\hat{f}(a,b,u)\,\mathrm{d}u, \quad \mathcal{Q}^-(a,b,\psi) := \int_0^\psi \eta'(v)\check{f}(a,b,v)\,\mathrm{d}v,\\
\mathcal{Q}(a,b,\psi_1,\psi_2) &:= \mathcal{Q}^+(a,b,\psi_1)+\mathcal{Q}^-(a,b,\psi_2).
\end{aligned} \tag{4.30}$$

The function $\mathcal{Q}$ is a consistent numerical entropy flux for the scheme (4.26) for the entropy function η since

$$\mathcal{Q}(a,a,\psi,\psi) = \int_0^\psi \eta'(u)\big(\hat{f}(a,a,u)+\check{f}(a,a,u)\big)\,\mathrm{d}u$$

$$= \int_0^\psi \eta'(u)\partial_u \mathcal{F}(a,a,u,u)\,\mathrm{d}u = \int_0^\psi \eta'(u)\tilde{F}(a,u)\,\mathrm{d}u = Q(a,\psi).$$

Furthermore, integration by parts yields

$$\begin{aligned}
&\mathcal{Q}^+(a,b,\psi) - \mathcal{Q}^+(a,b,\tilde{\psi}) \\
&= \eta'(\psi)\big(\hat{\mathcal{F}}(a,b,\psi) - \hat{\mathcal{F}}(a,b,\tilde{\psi})\big) - \int_{\tilde{\psi}}^{\psi} \eta''(u)\big(\hat{\mathcal{F}}(a,b,u) - \hat{\mathcal{F}}(a,b,\tilde{\psi})\big)\,\mathrm{d}u, \qquad (4.31)\\
&\mathcal{Q}^-(a,b,\psi) - \mathcal{Q}^-(a,b,\tilde{\psi}) \\
&= \eta'(\psi)\big(\check{\mathcal{F}}(a,b,\psi) - \check{\mathcal{F}}(a,b,\tilde{\psi})\big) - \int_{\tilde{\psi}}^{\psi} \eta''(u)\big(\check{\mathcal{F}}(a,b,u) - \check{\mathcal{F}}(a,b,\tilde{\psi})\big)\,\mathrm{d}u \qquad (4.32)\\
&= \eta'(\tilde{\psi})\big(\check{\mathcal{F}}(a,b,\psi) - \check{\mathcal{F}}(a,b,\tilde{\psi})\big) - \int_{\tilde{\psi}}^{\psi} \eta''(u)\big(\check{\mathcal{F}}(a,b,u) - \check{\mathcal{F}}(a,b,\psi)\big)\,\mathrm{d}u. \qquad (4.33)
\end{aligned}$$

Now, denoting by Δ_-^ϕ and Δ_-^ψ difference operators that act on both ϕ- and ψ-arguments only, respectively (leaving the two others unchanged), we observe that

$$\Delta_- \mathcal{F}(\boldsymbol{\phi}_i^n, \boldsymbol{\psi}_i^n) = \Delta_-^\psi \mathcal{F}(\boldsymbol{\phi}_i^n, \boldsymbol{\psi}_i^n) + \Delta_+^\phi \mathcal{F}(\boldsymbol{\phi}_{i-1}^n, \boldsymbol{\psi}_{i-1}^n). \qquad (4.34)$$

Utilizing (4.31) and (4.33) we can then write

$$\begin{aligned}
&\eta'\big(\psi_{i-1/2}^n\big)\Delta_-^\psi \mathcal{F}(\boldsymbol{\phi}_i^n, \boldsymbol{\psi}_i^n) \\
&= \mathcal{Q}^+\big(\boldsymbol{\phi}_i^n, \psi_{i-1/2}^n\big) - \mathcal{Q}^+\big(\boldsymbol{\phi}_i^n, \psi_{i-3/2}^n\big) + \mathcal{Q}^-\big(\boldsymbol{\phi}_i^n, \psi_{i+1/2}^n\big) - \mathcal{Q}^-\big(\boldsymbol{\phi}_i^n, \psi_{i-1/2}^n\big) \\
&\quad - \Bigg(\eta'(\psi_{i-1/2}^n)\big(\hat{\mathcal{F}}(\boldsymbol{\phi}_i^n, \psi_{i-1/2}^n) - \hat{\mathcal{F}}(\boldsymbol{\phi}_i^n, \psi_{i-3/2}^n)\big) \\
&\qquad\quad - \int_{\psi_{i-3/2}^n}^{\psi_{i-1/2}^n} \eta''(u)\big(\hat{\mathcal{F}}(\boldsymbol{\phi}_i^n, u) - \hat{\mathcal{F}}(\boldsymbol{\phi}_i^n, \psi_{i-3/2}^n)\big)\,\mathrm{d}u\Bigg) \\
&\quad - \Bigg(\eta'(\psi_{i-1/2}^n)\big(\check{\mathcal{F}}(\boldsymbol{\phi}_i^n, \psi_{i+1/2}^n) - \check{\mathcal{F}}(\boldsymbol{\phi}_i^n, \psi_{i-1/2}^n)\big) \\
&\qquad\quad + \int_{\psi_{i+1/2}^n}^{\psi_{i-1/2}^n} \eta''(u)\big(\check{\mathcal{F}}(\boldsymbol{\phi}_i^n, u) - \check{\mathcal{F}}(\boldsymbol{\phi}_i^n, \psi_{i+1/2}^n)\big)\,\mathrm{d}u\Bigg) \\
&\quad + \eta'\big(\psi_{i-1/2}^n\big)\big(\hat{\mathcal{F}}\big(\boldsymbol{\phi}_i^n, \psi_{i-1/2}^n\big) - \hat{\mathcal{F}}\big(\boldsymbol{\phi}_i^n, \psi_{i-3/2}^n\big) \\
&\qquad\quad + \check{\mathcal{F}}\big(\boldsymbol{\phi}_i^n, \psi_{i+1/2}^n\big) - \check{\mathcal{F}}\big(\boldsymbol{\phi}_i^n, \psi_{i-1/2}^n\big)\big) \\
&= \mathcal{Q}\big(\boldsymbol{\phi}_i^n, \psi_{i-1/2}^n, \psi_{i+1/2}^n\big) - \mathcal{Q}\big(\boldsymbol{\phi}_i^n, \psi_{i-3/2}^n, \psi_{i-1/2}^n\big) + \Theta_{i-1/2}^n \\
&= \Delta_-^\psi \mathcal{Q}(\boldsymbol{\phi}_i^n, \boldsymbol{\psi}_i^n) + \Theta_{i-1/2}^n, \qquad (4.35)
\end{aligned}$$

where the notation for evaluations and differences for $\mathcal{Q}$ is the same as for $\mathcal{F}$ and

$$\Theta_{i-1/2}^n := (\Theta_{i-1}^n)^+ + (\Theta_i^n)^-,$$

where

$$(\Theta_{i-1}^n)^+ := \int_{\psi_{i-3/2}^n}^{\psi_{i-1/2}^n} \eta''(u)\big(\hat{\mathcal{F}}\big(\boldsymbol{\phi}_i^n, u\big) - \hat{\mathcal{F}}\big(\boldsymbol{\phi}_i^n, \psi_{i-3/2}^n\big)\big)\,\mathrm{d}u,$$
$$(\Theta_i^n)^- := -\int_{\psi_{i+1/2}^n}^{\psi_{i-1/2}^n} \eta''(u)\big(\check{\mathcal{F}}\big(\boldsymbol{\phi}_i^n, u\big) - \check{\mathcal{F}}\big(\boldsymbol{\phi}_i^n, \psi_{i+1/2}^n\big)\big)\,\mathrm{d}u.$$

Since $\hat{\mathcal{F}}$ is increasing and $\check{\mathcal{F}}$ is decreasing in the respective third argument, there holds

$$(\Theta_{i-1}^n)^+, (\Theta_i^n)^- \geq 0$$

and therefore $\Theta_{i-1/2}^n \geq 0$. Furthermore, we notice that

$$\eta'\big(\psi_{i-1/2}^n\big)\Delta_+^\phi \mathcal{F}(\boldsymbol{\phi}_{i-1}^n, \boldsymbol{\psi}_{i-1}^n) = \Delta_+^\phi\big(\eta'\big(\psi_{i-1/2}^n\big)\mathcal{F}(\boldsymbol{\phi}_{i-1}^n, \boldsymbol{\psi}_{i-1}^n)\big). \tag{4.36}$$

From (4.34) we obtain by taking into account (4.35) and (4.36)

$$\begin{aligned}
&\eta'\big(\psi_{i-1/2}^n\big)\Delta_- \mathcal{F}(\boldsymbol{\phi}_i^n, \boldsymbol{\psi}_i^n)\\
&= \Delta_-^\psi \mathcal{Q}(\boldsymbol{\phi}_i^n, \boldsymbol{\psi}_i^n) + \eta'\big(\psi_{i-1/2}^n\big)\Delta_+^\phi \mathcal{F}(\boldsymbol{\phi}_{i-1}^n, \boldsymbol{\psi}_{i-1}^n) + \Theta_{i-1/2}^n\\
&= \Delta_- \mathcal{Q}(\boldsymbol{\phi}_i^n, \boldsymbol{\psi}_i^n) - \Delta_+^\phi \mathcal{Q}(\boldsymbol{\phi}_{i-1}^n, \boldsymbol{\psi}_{i-1}^n) + \eta'\big(\psi_{i-1/2}^n\big)\Delta_+^\phi \mathcal{F}(\boldsymbol{\phi}_{i-1}^n, \boldsymbol{\psi}_{i-1}^n) + \Theta_{i-1/2}^n\\
&= \Delta_- \mathcal{Q}(\boldsymbol{\phi}_i^n, \boldsymbol{\psi}_i^n) + \Delta_+^\phi\big(\eta'\big(\psi_{i-1/2}^n\big)\mathcal{F}(\boldsymbol{\phi}_{i-1}^n, \boldsymbol{\psi}_{i-1}^n) - \mathcal{Q}(\boldsymbol{\phi}_{i-1}^n, \boldsymbol{\psi}_{i-1}^n)\big) + \Theta_{i-1/2}^n.
\end{aligned}$$

Consequently, (4.28) can be written as

$$\begin{aligned}
&\eta\big(\psi_{i-1/2}^{n+1}\big) - \eta\big(\psi_{i-1/2}^n\big) + \frac{1}{2}\eta''\big(\xi_{i-1/2}^{n+1/2}\big)\big(\psi_{i-1/2}^{n+1} - \psi_{i-1/2}^n\big)^2 + \lambda\Theta_{i-1/2}^n\\
&= -\lambda\Delta_- \mathcal{Q}(\boldsymbol{\phi}_i^n, \boldsymbol{\psi}_i^n) - \lambda\big(\eta'\big(\psi_{i-1/2}^{n+1}\big) - \eta'\big(\psi_{i-1/2}^n\big)\big)\Delta_- \mathcal{F}(\boldsymbol{\phi}_i^n, \boldsymbol{\psi}_i^n)\\
&\quad - \lambda\Delta_+^\phi\big(\eta'\big(\psi_{i-1/2}^n\big)\mathcal{F}(\boldsymbol{\phi}_{i-1}^n, \boldsymbol{\psi}_{i-1}^n) - \mathcal{Q}(\boldsymbol{\phi}_{i-1}^n, \boldsymbol{\psi}_{i-1}^n)\big).
\end{aligned} \tag{4.37}$$

Multiplying (4.37) by Δz and summing over $(n, i) \in \mathcal{I}_1$, where

$$\mathcal{I}_k := \{(n, i) \mid n = 0, \ldots, N_T - k,\ i \in \mathbb{Z}\},$$

we get

$$\begin{aligned}
&\Delta z \sum_{i\in\mathbb{Z}} \eta\big(\psi_{i-1/2}^N\big) - \Delta z \sum_{i\in\mathbb{Z}} \eta\big(\psi_{i-1/2}^0\big) + \frac{\Delta z}{2}\sum_{\mathcal{I}_1} \eta''\big(\xi_{i-1/2}^{n+1/2}\big)\big(\psi_{i-1/2}^{n+1} - \psi_{i-1/2}^n\big)^2\\
&+ \lambda\Delta z \sum_{\mathcal{I}_1} \Theta_{i-1/2}^n\\
&= -\lambda\Delta z \sum_{\mathcal{I}_1} \Delta_- \mathcal{Q}(\boldsymbol{\phi}_i^n, \boldsymbol{\psi}_i^n) - \lambda\Delta z \sum_{\mathcal{I}_1}\big(\eta'\big(\psi_{i-1/2}^{n+1}\big) - \eta'\big(\psi_{i-1/2}^n\big)\big)\Delta_- \mathcal{F}(\boldsymbol{\phi}_i^n, \boldsymbol{\psi}_i^n)\\
&\quad - \lambda\Delta z \sum_{\mathcal{I}_1} \Delta_+^\phi\big(\eta'\big(\psi_{i-1/2}^n\big)\mathcal{F}(\boldsymbol{\phi}_{i-1}^n, \boldsymbol{\psi}_{i-1}^n) - \mathcal{Q}(\boldsymbol{\phi}_{i-1}^n, \boldsymbol{\psi}_{i-1}^n)\big),
\end{aligned}$$

which implies the inequality

$$\begin{aligned}
&\Delta z\sum_{i\in\mathbb{Z}}\eta\big(\psi^N_{i-1/2}\big)+\frac{\Delta z}{2}\sum_{\mathcal{I}_1}\eta''\big(\xi^{n+1/2}_{i-1/2}\big)\big(\psi^{n+1}_{i-1/2}-\psi^n_{i-1/2}\big)^2+\lambda\Delta z\sum_{\mathcal{I}_1}\Theta^n_{i-1/2}\\
&\le\Delta z\sum_{i\in\mathbb{Z}}\eta\big(\psi^0_{i-1/2}\big)+2\|\eta'\|_{L^\infty}\Delta z\Delta t\sum_{\mathcal{I}_1}\frac{1}{\Delta z}\big|\Delta_-\mathcal{F}(\boldsymbol{\phi}^n_i,\boldsymbol{\psi}^n_i)\big|\\
&\quad+C\Delta z\Delta t\sum_{\mathcal{I}_1}\frac{1}{\Delta z}\big|\Delta^\phi_+\big(\eta'\big(\psi^n_{i-1/2}\big)\mathcal{F}(\boldsymbol{\phi}^n_{i-1},\boldsymbol{\psi}^n_{i-1})-\mathcal{Q}(\boldsymbol{\phi}^n_{i-1},\boldsymbol{\psi}^n_{i-1})\big)\big|.
\end{aligned}$$

The last term on the right-hand side is uniformly bounded since we know that $\phi^{\Delta z}$ has bounded variation. Now let us choose $\eta(v)=v^2$ and take into account (cf. [65]) that there exists a constant $C_{\mathcal{F}}$ such that

$$(\Theta^n_{i-1})^+\ge\frac{1}{C_{\mathcal{F}}}\Big(\Delta^\psi_-\hat{\mathcal{F}}\big(\boldsymbol{\phi}^n_i,\psi_{i-1/2}\big)\Big)^2,\quad(\Theta^n_i)^-\ge\frac{1}{C_{\mathcal{F}}}\Big(\Delta^\psi_+\check{\mathcal{F}}\big(\boldsymbol{\phi}^n_i,\psi_{i-1/2}\big)\Big)^2.$$

Noticing that Lemma 4.5, applied to the present scheme, implies the bound on the discrete divergence of the numerical flux

$$\Delta z\sum_{i\in\mathbb{Z}}\frac{1}{\Delta z}\big|\Delta_-\mathcal{F}_i(\boldsymbol{\phi}^n,\boldsymbol{\psi}^n)\big|\le C,\tag{4.38}$$

we obtain from (4.37)

$$\begin{aligned}
&\Delta z\sum_{i\in\mathbb{Z}}\eta\big(\psi^N_{i-1/2}\big)+\Delta z\sum_{\mathcal{I}_1}\big(\psi^{n+1}_{i-1/2}-\psi^n_{i-1/2}\big)^2\\
&+\frac{\lambda}{C_{\mathcal{F}}}\Delta z\sum_{\mathcal{I}_1}\Big(\big(\Delta^\psi_-\hat{\mathcal{F}}\big(\boldsymbol{\phi}^n_i,\psi_{i-1/2}\big)\big)^2+\big(\Delta^\psi_+\check{\mathcal{F}}\big(\boldsymbol{\phi}^n_i,\psi^n_{i-1/2}\big)\big)^2\Big)\\
&\le\Delta z\sum_{i\in\mathbb{Z}}\big(\psi^0_{i-1/2}\big)^2+C_T.
\end{aligned}\tag{4.39}$$

Inequality (4.39) implies the following estimate.

Lemma 4.7. *There exists a constant C_7 that is independent of $(\Delta z,\Delta t)$ such that*

$$\Delta t\Delta z\sum_{n=0}^{N_T-1}\sum_{i\in\mathbb{Z}}\big(\psi^{n+1}_{i-1/2}-\psi^n_{i-1/2}\big)^2\le C_7\Delta z.\tag{4.40}$$

Proof. The estimate for the "time variation" of $\psi^{\Delta z}$, (4.40), follows immediately from (4.39) if we consider that its right-hand side is uniformly bounded. □

Before proceeding, we prove the following lemma.

Lemma 4.8. *There exist constants C_8 and C_9 that are independent of $(\Delta z,\Delta t)$ such that for all i,*

$$\big|\Delta_-\mathcal{Q}(\boldsymbol{\phi}^n_i,\boldsymbol{\psi}^n_i)\big|\le C_8\big|(\Delta^{(3)}_-+\Delta^{(4)}_-)\mathcal{F}(\boldsymbol{\phi}^n_i,\boldsymbol{\psi}^n_i)\big|+C_9\big(\big|\Delta_-\phi^n_{i-1/2}\big|+\big|\Delta_+\phi^n_{i-1/2}\big|\big).\tag{4.41}$$

Proof. We note that

$$\Delta_- \mathcal{Q}(\boldsymbol{\phi}_i^n, \boldsymbol{\psi}_i^n) = \Delta_-^{\psi} \mathcal{Q}(\boldsymbol{\phi}_i^n, \boldsymbol{\psi}_i^n) + \Delta_+^{\phi} \mathcal{Q}(\boldsymbol{\phi}_{i-1}^n, \boldsymbol{\psi}_{i-1}^n). \tag{4.42}$$

For ease of notation we denote the difference operatos $\Delta_\pm^{(3)}$ and $\Delta_\pm^{(4)}$ that only act on the third or fourth argument of a function, respectively. We first discuss the term

$$\Delta_-^{(3)} \mathcal{Q}(\boldsymbol{\phi}_i^n, \boldsymbol{\psi}_i^n) = \Delta_-^{(3)} \mathcal{Q}^+\big(\boldsymbol{\phi}_i^n, \psi_{i-1/2}^n\big) + \Delta_-^{(3)} \mathcal{Q}^-\big(\boldsymbol{\phi}_i^n, \psi_{i+1/2}^n\big).$$

From (4.31) we get

$$\begin{aligned}
&\big|\Delta_-^{\psi} \mathcal{Q}^+\big(\boldsymbol{\phi}_i^n, \psi_{i-1/2}^n\big)\big| \\
&= \left|\eta'\big(\psi_{i-1/2}^n\big)\Delta_-^{(3)} \mathcal{F}(\boldsymbol{\phi}_i^n, \boldsymbol{\psi}_i^n) - \int_{\psi_{i-3/2}^n}^{\psi_{i-1/2}^n} \eta''(u)\Big(\hat{\mathcal{F}}\big(\boldsymbol{\phi}_i^n, u\big) - \hat{\mathcal{F}}\big(\boldsymbol{\phi}_i^n, \psi_{i-1/2}^n\big)\Big)\,\mathrm{d}u\right| \\
&\le \big|\eta'\big(\psi_{i-1/2}^n\big)\big|\big|\Delta_-^{(3)} \mathcal{F}(\boldsymbol{\phi}_i^n, \boldsymbol{\psi}_i^n)\big| + \left|\int_{\psi_{i-3/2}^n}^{\psi_{i-1/2}^n} \eta''(u)\,\mathrm{d}u\right|\big|\Delta_-^{(3)} \mathcal{F}(\boldsymbol{\phi}_i^n, \boldsymbol{\psi}_i^n)\big| \\
&\le 3\|\eta'\|_{L^\infty(0,1)}\big|\Delta_-^{(3)} \mathcal{F}(\boldsymbol{\phi}_i^n, \boldsymbol{\psi}_i^n)\big|
\end{aligned}$$

and analogously

$$\big|\Delta_-^{(3)} \mathcal{Q}^-\big(\boldsymbol{\phi}_i^n, \psi_{i+1/2}^n\big)\big| \le 3\|\eta'\|_{L^\infty(0,1)}\big|\Delta_-^{(4)} \mathcal{F}(\boldsymbol{\phi}_i^n, \boldsymbol{\psi}_i^n)\big|,$$

hence

$$\big|\Delta_-^{\psi} \mathcal{Q}(\boldsymbol{\phi}_i^n, \boldsymbol{\psi}_i^n)\big| \le 3\|\eta'\|_{L^\infty(0,1)}\big|\big(\Delta_-^{(3)} + \Delta_-^{(4)}\big)\mathcal{F}(\boldsymbol{\phi}_i^n, \boldsymbol{\psi}_i^n)\big|. \tag{4.43}$$

On the other hand, we take into account that

$$\Delta_+^{\phi} \mathcal{Q}(\boldsymbol{\phi}_{i-1}^n, \boldsymbol{\psi}_{i-1}^n) = \Delta_+^{\phi} \mathcal{Q}^+\big(\boldsymbol{\phi}_{i-1}^n, \psi_{i-3/2}^n\big) + \Delta_+^{\phi} \mathcal{Q}^-\big(\boldsymbol{\phi}_{i-1}^n, \psi_{i-1/2}^n\big).$$

Now

$$\begin{aligned}
\Delta_+^{\phi} \mathcal{Q}^+\big(\boldsymbol{\phi}_{i-1}^n, \psi_{i-3/2}^n\big) &= \int_0^{\psi_{i-3/2}^n} \eta'(u)\big(\hat{f}\big(\boldsymbol{\phi}_i^n, u\big) - \hat{f}\big(\boldsymbol{\phi}_{i-1}^n, u\big)\big)\,\mathrm{d}u \\
&= \Big[\eta'(u)\big(\hat{\mathcal{F}}\big(\boldsymbol{\phi}_i^n, u\big) - \hat{\mathcal{F}}\big(\boldsymbol{\phi}_{i-1}^n, u\big)\big)\Big]_{u=0}^{u=\psi_{i-3/2}^n} \\
&\quad - \int_0^{\psi_{i-3/2}^n} \eta''(u)\big(\hat{\mathcal{F}}(\boldsymbol{\phi}_i^n, u) - \hat{\mathcal{F}}\big(\boldsymbol{\phi}_{i-1}^n, u\big)\big)\,\mathrm{d}u
\end{aligned} \tag{4.44}$$

and analogously

$$\begin{aligned}
\Delta_+^{\phi} \mathcal{Q}^-\big(\boldsymbol{\phi}_{i-1}^n, \psi_{i-1/2}^n\big) &= \int_0^{\psi_{i-1/2}^n} \eta'(u)\big(\check{f}\big(\boldsymbol{\phi}_i^n, v\big) - \check{f}\big(\boldsymbol{\phi}_{i-1}^n, v\big)\big)\,\mathrm{d}v \\
&= \Big[\eta'(v)\big(\check{\mathcal{F}}\big(\boldsymbol{\phi}_i^n, v\big) - \check{\mathcal{F}}\big(\boldsymbol{\phi}_{i-1}^n, v\big)\big)\Big]_{v=0}^{v=\psi_{i-1/2}^n}
\end{aligned}$$

$$- \int_0^{\psi^n_{i-1/2}} \eta''(v)\big(\check{\mathcal{F}}(\boldsymbol{\phi}^n_i, v) - \check{\mathcal{F}}(\boldsymbol{\phi}^n_{i-1}, v)\big)\,\mathrm{d}v.$$

Consequently,

$$\big|\Delta^\phi_+ \mathcal{Q}^+\big(\boldsymbol{\phi}^n_{i-1}, \psi^n_{i-3/2}\big)\big| \le 3\|\eta'\|_{L^\infty(0,1)} \max_{0\le u\le \psi^n_{i-3/2}} \big|\hat{\mathcal{F}}\big(\boldsymbol{\phi}^n_i, u\big) - \hat{\mathcal{F}}\big(\boldsymbol{\phi}^n_{i-1}, u\big)\big|, \tag{4.45}$$

and by analogous reasoning for $\mathcal{Q}^-$,

$$\big|\Delta^\phi_+ \mathcal{Q}^-\big(\boldsymbol{\phi}^n_{i-1}, \psi^n_{i-1/2}\big)\big| \le 3\|\eta'\|_{L^\infty(0,1)} \max_{0\le v\le \psi^n_{i-1/2}} \big|\check{\mathcal{F}}\big(\boldsymbol{\phi}^n_i, v\big) - \check{\mathcal{F}}\big(\boldsymbol{\phi}^n_{i-1}, v\big)\big|. \tag{4.46}$$

To estimate the right-hand side of (4.45), we recall that

$$\hat{\mathcal{F}}\big(\boldsymbol{\phi}^n_i, u\big) - \hat{\mathcal{F}}\big(\boldsymbol{\phi}^n_{i-1}, u\big) = \int_0^u \big(((f^n_i)')^+(s) - ((f^n_{i-1})')^+(s)\big)\,\mathrm{d}s =: \hat{\mathcal{D}}^n_{i-1/2}.$$

We now assume that $\sigma = 1$ and use (3.24). To estimate $\hat{\mathcal{D}}^n_{i-1/2}$, we will appeal to the trivial but useful inequality

$$\big|(\alpha \vee x) - (\beta \vee y)\big| \le |\alpha - \beta| + |x - y|.$$

We proceed by discussing all possible cases of the location of u in relation to the extrema $\hat{\psi}^n_i$ and $\hat{\psi}^n_{i-1}$ of f^n_i and f^n_{i-1}, respectively, and assume that $\sigma = 1$.

1. Assume that $u \le \hat{\psi}^n_i \wedge \hat{\psi}^n_{i-1}$. Since $\hat{\psi}^n_i \le \psi^n_{\max,i}$ and $\hat{\psi}^n_{i-1} \le \psi^n_{\max,i-1}$, in this case $\hat{\mathcal{D}}^n_{i-1/2} = 0$ if $\psi^n_{\max,i} = \psi^n_{\max,i-1}$ and otherwise

$$\begin{aligned}\big|\hat{\mathcal{D}}^n_{i-1/2}\big| &= \big|f^n_i(u) - f^n_{i-1}(u)\big| = u\big|\tilde{V}\big(u/\psi^n_{\max,i}\big) - \tilde{V}\big(u/\psi^n_{\max,i-1}\big)\big| \\ &\le \frac{u^2}{\psi^n_{\max,i}\psi^n_{\max,i-1}}\|\tilde{V}'\|_\infty|\psi^n_{\max,i} - \psi^n_{\max,i-1}| \\ &\le \|\tilde{V}'\|_\infty\big|\psi^n_{\max,i} - \psi^n_{\max,i-1}\big|.\end{aligned}$$

   Noticing that

$$\begin{aligned}\big|\psi^n_{\max,i} - \psi^n_{\max,i-1}\big| &= \big|\phi^n_{i-1/2} \vee \phi^n_{i+1/2} - \phi^n_{i-3/2} \vee \phi^n_{i-1/2}\big| \\ &\le \big|\Delta_-\phi^n_{i-1/2}\big| + \big|\Delta_+\phi^n_{i-1/2}\big|,\end{aligned} \tag{4.47}$$

   we conclude that

$$\big|\hat{\mathcal{D}}^n_{i-1/2}\big| \le \|\tilde{V}'\|_\infty\big(\big|\Delta_-\phi^n_{i-1/2}\big| + \big|\Delta_+\phi^n_{i-1/2}\big|\big).$$

2. If $\hat{\psi}^n_i < u < \hat{\psi}^n_{i-1}$ then

$$\big|\hat{\mathcal{D}}^n_{i-1/2}\big| = \big|f^n_i\big(\hat{\psi}^n_i\big) - f^n_{i-1}(u)\big|$$

$$\leq \big|f_i^n(\hat\psi_i^n) - f_{i-1}^n(\hat\psi_{i-1}^n)\big| + \big|f_{i-1}^n(\hat\psi_{i-1}^n) - f_{i-1}^n(u)\big|.$$

Since $f_i^n(\hat\psi_i^n) = \psi_{\max,i}^n \omega \tilde V(\omega)$ for all i, we conclude that

$$\begin{aligned}\big|f_i^n(\hat\psi_i^n) - f_{i-1}^n(\hat\psi_{i-1}^n)\big| &\leq \omega\|\tilde V\|_\infty \big|\psi_{\max,i}^n - \psi_{\max,i-1}^n\big| \\ &\leq \|\tilde V\|_\infty\big(\big|\Delta_-\phi_{i-1/2}^n\big| + \big|\Delta_+\phi_{i-1/2}^n\big|\big).\end{aligned} \tag{4.48}$$

On the other hand, in the present case

$$\big|f_{i-1}^n(\hat\psi_{i-1}^n) - f_{i-1}^n(u)\big| = f_{i-1}^n(\hat\psi_{i-1}^n) - f_{i-1}^n(u) \leq f_{i-1}^n(\hat\psi_{i-1}^n) - f_{i-1}^n(\hat\psi_i^n).$$

Since for $s \in [0, \hat\psi_{i-1}^n]$ there holds $(f_{i-1}^n)'(s) \leq (f_{i-1}^n)'(0) = \tilde V(0)$, we get

$$\begin{aligned}\big|f_{i-1}^n(\hat\psi_{i-1}^n) - f_{i-1}^n(u)\big| &= \int_u^{\hat\psi_{i-1}^n} (f_{i-1}^n)'(s)\,\mathrm{d}s \leq \int_{\hat\psi_i^n}^{\hat\psi_{i-1}^n} (f_{i-1}^n)'(s)\,\mathrm{d}s \\ &\leq \tilde V(0)\big(\hat\psi_{i-1}^n - \hat\psi_i^n\big)\end{aligned}$$

Lemma 3.1 (a) implies that

$$\big|\hat\psi_i^n - \hat\psi_{i-1}^n\big| = \omega\big|\psi_{\max,i}^n - \psi_{\max,i-1}^n\big|, \tag{4.49}$$

hence

$$\big|\hat{\mathcal{D}}_{i-1/2}^n\big| \leq 2\|\tilde V\|_\infty\big(\big|\Delta_-\phi_{i-1/2}^n\big| + \big|\Delta_+\phi_{i-1/2}^n\big|\big).$$

The same estimate holds for $\hat\psi_{i-1}^n < u < \hat\psi_i^n$.

3. If $u \geq \hat\psi_i^n \vee \hat\psi_{i-1}^n$ then utilizing (4.48) we get

$$\big|\hat{\mathcal{D}}_{i-1/2}^n\big| = \big|f_i^n(\hat\psi_i^n) - f_{i-1}^n(\hat\psi_{i-1}^n)\big| \leq \|\tilde V\|_\infty\big(\big|\Delta_-\phi_{i-1/2}^n\big| + \big|\Delta_+\phi_{i-1/2}^n\big|\big).$$

Combining all possible cases we deduce that

$$\big|\hat{\mathcal{D}}_{i-1/2}^n\big| \leq \big(\|\tilde V'\|_\infty + 2\|\tilde V\|_\infty\big)\big(\big|\Delta_-\phi_{i-1/2}^n\big| + \big|\Delta_+\phi_{i-1/2}^n\big|\big). \tag{4.50}$$

Next, we deal with (4.46), recalling that (see (4.27))

$$\check{\mathcal{F}}(\boldsymbol{\phi}_i^n, v) - \check{\mathcal{F}}(\boldsymbol{\phi}_{i-1}^n, v) = \check{\mathcal{D}}_{i-1/2}^n + \mathcal{E}_{i-1/2}^n,$$

where we define

$$\begin{aligned}\check{\mathcal{D}}_{i-1/2}^n &:= \int_0^v \big(((f_i^n)')^-(s) - ((f_{i-1}^n)')^-(s)\big)\,\mathrm{d}s, \\ \mathcal{E}_{i-1/2}^n &:= \big(\phi_{i-1/2}^n \tilde v_{\phi\mathrm{s}}(\phi_{i+1/2}^n) - \phi_{i-3/2}^n \tilde v_{\phi\mathrm{s}}(\phi_{i-1/2}^n)\big)v.\end{aligned}$$

The discussion of all possible cases of the location of v in relation to $\hat\psi_i^n$ and $\hat\psi_{i-1}^n$ gives rise to the following cases for the estimation of $\check{\mathcal{D}}_{i-1/2}^n$.

1. If $v \le \hat\psi_i^n \wedge \hat\psi_{i-1}^n$ or $v \ge \psi_{\max,i}^n \vee \psi_{\max,i-1}^n$ then $\check{\mathcal{D}}_{i-1/2}^n = 0$.

2. To handle the case $\hat\psi_i^n \wedge \hat\psi_{i-1}^n \le v \le \hat\psi_i^n \vee \hat\psi_{i-1}^n$ we assume that $\hat\psi_i^n < \hat\psi_{i-1}^n$ and $\hat\psi_i^n \le v \le \hat\psi_{i-1}^n$. Then

$$\begin{aligned}\big|\check{\mathcal{D}}_{i-1/2}^n\big| &= \big|f_i^n(v) - f_i^n\big(\hat\psi_i^n\big)\big| = \left|\int_{\hat\psi_i^n}^{v} ((f_i^n)')^-(s)\,\mathrm{d}s\right| \\ &\le \max_{\hat\psi_i^n \le s \le \hat\psi_{i-1}^n} \big|((f_i^n)')^-(s)\big|\big|\hat\psi_i^n - \hat\psi_{i-1}^n\big| \\ &\le \big|(f_i^n)'(\psi_{\mathrm{infl},i}^n)\big|\big|\hat\psi_i^n - \hat\psi_{i-1}^n\big|.\end{aligned}$$

   By Lemma 3.1 (ii),

$$(f_i^n)'(\psi_{\mathrm{infl},i}^n) = (f_i^n)'(\tilde\omega\phi_{\max,i}^n) = \tilde V(\tilde\omega) + \tilde\omega\tilde V'(\tilde\omega),$$

   so $(f_i^n)'(\psi_{\mathrm{infl},i}^n)$ does not depend on $\phi_{\max,i}^n$ and we conclude that

$$\big|\check{\mathcal{D}}_{i-1/2}^n\big| \le \big(\|\tilde V\|_\infty + \|\tilde V'\|_\infty\big)\big|\hat\psi_i^n - \hat\psi_{i-1}^n\big|.$$

   Applying the argument of (4.47) and (4.49) yields

$$\big|\check{\mathcal{D}}_{i-1/2}^n\big| \le \big(\|\tilde V\|_\infty + \|\tilde V'\|_\infty\big)\big(\big|\Delta_-\phi_{i-1/2}^n\big| + \big|\Delta_+\phi_{i-1/2}^n\big|\big).$$

   The same inequality is also valid if $\hat\psi_{i-1}^n < \hat\psi_i^n$ and $\hat\psi_{i-1}^n \le v \le \hat\psi_i^n$.

3. Finally, assume that $v > \hat\psi_i^n \vee \hat\psi_{i-1}^n$. In this case

$$\begin{aligned}\big|\check{\mathcal{D}}_{i-1/2}^n\big| &= \big|f_i^n(v) - f_{i-1}^n(v) - f_i^n\big(\hat\psi_i^n\big) + f_{i-1}^n\big(\hat\psi_{i-1}^n\big)\big| \\ &\le \big|f_i^n(v) - f_{i-1}^n(v)\big| + \big|f_i^n\big(\hat\psi_i^n\big) - f_{i-1}^n\big(\hat\psi_{i-1}^n\big)\big|.\end{aligned}$$

   Taking into account that $f_i^n(\hat\psi_i^n) = \psi_{\max,i}^n\omega\tilde V(\omega)$, we get

$$\begin{aligned}\big|f_i^n\big(\hat\psi_i^n\big) - f_{i-1}^n\big(\hat\psi_{i-1}^n\big)\big| &= \omega\tilde V(\omega)\,\big|\psi_{\max,i}^n - \psi_{\max,i-1}^n\big| \\ &\le \|\tilde V\|_\infty\big(\big|\Delta_-\phi_{i-1/2}^n\big| + \big|\Delta_+\phi_{i-1/2}^n\big|\big).\end{aligned} \tag{4.51}$$

   If $v > \psi_{\max,i}^n \vee \psi_{\max,i-1}^n$, then $f_i^n(v) = f_{i-1}^n(v) = 0$, hence (4.51) means that

$$\big|\check{\mathcal{D}}_{i-1/2}^n\big| \le \|\tilde V\|_\infty\big(\big|\Delta_-\phi_{i-1/2}^n\big| + \big|\Delta_+\phi_{i-1/2}^n\big|\big).$$

   Suppose now that

$$\hat\psi_i^n \vee \hat\psi_{i-1}^n \le \psi_{\max,i}^n \le v \le \psi_{\max,i-1}^n. \tag{4.52}$$

   Since we know that $v = \psi_{i+1/2}^n \le 1 - \phi_{i+1/2}^n$, the inequality $\psi_{\max,i}^n \le v$ can only be satisfied if

$$\psi_{\max,i}^n = (1 - \phi_{i-1/2}^n) \wedge (1 - \phi_{i+1/2}^n) = 1 - \phi_{i-1/2}^n.$$

On the other hand,

$$\psi^n_{\max,i-1} = (1-\phi^n_{i-1/2}) \wedge (1-\phi^n_{i-3/2}) \le 1-\phi^n_{i-1/2},$$

so (4.52) is only possible when $\psi^n_{\max,i} = v = \psi^n_{\max,i-1} = 1-\phi^n_{i-1/2}$, which means that $\check{\mathcal{D}}^n_{i-1/2} = 0$.

If instead of (4.52) we have

$$\hat{\psi}^n_i \vee \hat{\psi}^n_{i-1} \le \psi^n_{\max,i-1} \le v \le \psi^n_{\max,i}, \tag{4.53}$$

then $1/\psi^n_{\max,i-1} \le 1/(\omega\psi^n_{\max,i})$ implies

$$\begin{aligned}\big|f^n_i(v) - f^n_{i-1}(v)\big| &= v\big|\tilde{V}\big(v/\psi^n_{\max,i}\big) - \tilde{V}\big(v/\psi^n_{\max,i-1}\big)\big| \\ &\le v^2\|\tilde{V}'\|_\infty \frac{|\psi^n_{\max,i} - \psi^n_{\max,i-1}|}{\psi^n_{\max,i}\psi^n_{\max,i-1}} \le \frac{\|\tilde{V}'\|_\infty}{\omega}\big|\psi^n_{\max,i} - \psi^n_{\max,i-1}\big|.\end{aligned}$$

The remainder of the estimate is based on (4.47). Since $\omega < 1$, we conclude that if (4.52) holds, then

$$\big|f^n_i(v) - f^n_{i-1}(v)\big| \le \frac{\|\tilde{V}'\|_\infty}{\omega}\big(\big|\Delta_-\phi^n_{i-1/2}\big| + \big|\Delta_+\phi^n_{i-1/2}\big|\big).$$

In combination with (4.51) we obtain in this case

$$\big|\check{\mathcal{D}}^n_{i-1/2}\big| \le \left(\|\tilde{V}\|_\infty + \frac{\|\tilde{V}'\|_\infty}{\omega}\right)\big(\big|\Delta_-\phi^n_{i-1/2}\big| + \big|\Delta_+\phi^n_{i-1/2}\big|\big). \tag{4.54}$$

Next, suppose that instead of (4.52) or (4.53) there holds

$$\hat{\psi}^n_i \le \psi^n_{\max,i} \le \hat{\psi}^n_{i-1} \le v \le \psi^n_{\max,i-1},$$

then the discussion of (4.52) can be applied again and we get that this ordering is only feasible if all terms are equal and zero, and therefore $\check{\mathcal{D}}^n_{i-1/2} = 0$. On the other hand, let us assume that

$$\hat{\psi}^n_{i-1} \le \psi^n_{\max,i-1} \le \hat{\psi}^n_i \le v \le \psi^n_{\max,i}.$$

In this case there exists $\xi \in [\hat{\psi}^n_i, v]$ such that

$$\begin{aligned}\big|\check{\mathcal{D}}^n_{i-1/2}\big| &= \left|\int_0^v ((f^n_i)')^-(s)\,\mathrm{d}s\right| = \left|\int_{\hat{\psi}^n_i}^v ((f^n_i)')^-(s)\,\mathrm{d}s\right| \\ &\le \int_{\hat{\psi}^n_i}^v \big|((f^n_i)')^-(s)\big|\,\mathrm{d}s \\ &\le \int_{\psi^n_{\max,i-1}}^{\psi^n_{\max,i}} \big|(f^n_i)'\big|\,\mathrm{d}s \le \big(\|\tilde{V}\|_\infty + \|\tilde{V}'\|_\infty\big)\big(\psi^n_{\max,i} - \psi^n_{\max,i-1}\big)\end{aligned}$$

$$\leq \big(\|\tilde V\|_\infty + \|\tilde V'\|_\infty\big)\big(\big|\Delta_-\phi^n_{i-1/2}\big| + \big|\Delta_+\phi^n_{i-1/2}\big|\big).$$

It remains to treat the case $\hat\psi^n_i \vee \hat\psi^n_{i-1} \leq v \leq \psi^n_{\max,i} \wedge \psi^n_{\max,i-1}$. We then have $v^2/(\psi^n_{\max,i-1}\psi^n_{\max,i}) \leq 1$, and analogously to the derivation of (4.54) we get

$$\big|\check{\mathcal{D}}^n_{i-1/2}\big| \leq \big(\|\tilde V\|_\infty + \|\tilde V'\|_\infty\big)\big(\big|\Delta_-\phi^n_{i-1/2}\big| + \big|\Delta_+\phi^n_{i-1/2}\big|\big).$$

Collecting all estimates for $\check{\mathcal{D}}^n_{i-1/2}$, we see that

$$\big|\check{\mathcal{D}}^n_{i-1/2}\big| \leq \big(3\|\tilde V\|_\infty + (1+1/\omega)\|\tilde V'\|_\infty\big)\big(\big|\Delta_-\phi^n_{i-1/2}\big| + \big|\Delta_+\phi^n_{i-1/2}\big|\big). \tag{4.55}$$

Furthermore, we obtain

$$\big|\mathcal{E}^n_{i-1/2}\big| \leq \|\tilde v'_{\phi\mathrm{s}}\|_\infty\big|\Delta_+\phi^n_{i-1/2}\big| + \|\tilde v_{\phi\mathrm{s}}\|_\infty\big|\Delta_-\phi^n_{i-1/2}\big|. \tag{4.56}$$

Combining the estimates (4.50), (4.55) and (4.56), we obtain from (4.45) and (4.46) the bounds

$$\begin{aligned}&\big|\hat{\mathcal{F}}(\boldsymbol{\phi}^n_i, u) - \hat{\mathcal{F}}(\boldsymbol{\phi}^n_{i-1}, u)\big|,\ \big|\check{\mathcal{F}}(\boldsymbol{\phi}^n_i, v) - \check{\mathcal{F}}(\boldsymbol{\phi}^n_{i-1}, v)\big| \\ &\leq C_{10}\big(\big|\Delta_-\phi^n_{i-1/2}\big| + \big|\Delta_+\phi^n_{i-1/2}\big|\big)\end{aligned} \tag{4.57}$$

and therefore

$$\big|\Delta^\phi_- \mathcal{Q}(\boldsymbol{\phi}^n_i, \boldsymbol{\psi}^n_i)\big| \leq C_{11}\big(\big|\Delta_-\phi^n_{i-1/2}\big| + \big|\Delta_+\phi^n_{i-1/2}\big|\big).$$

with constants C_{10} and C_{11}. Combining the last inequality with (4.42) and (4.43) we arrive at the desired estimate (4.41). □

From (4.41), and considering that $0 \leq \phi^n_{i-1/2} \leq 1$ for all i and n, we obtain

$$\begin{aligned}\big(\Delta_- Q(\boldsymbol{\phi}^n_i, \boldsymbol{\psi}^n_i)\big)^2 &\leq 2C_8^2\big((\Delta^{(3)}_- + \Delta^{(4)}_-)\mathcal{F}(\boldsymbol{\phi}^n_i, \boldsymbol{\psi}^n_i)\big)^2 + 2C_9^2\big(\big|\Delta_-\phi^n_{i-1/2}\big| + \big|\Delta_+\phi^n_{i-1/2}\big|\big)^2 \\ &\leq 4C_8^2\Big(\big(\Delta^{(3)}_-\mathcal{F}(\boldsymbol{\phi}^n_i, \boldsymbol{\psi}^n_i)\big)^2 + \big(\Delta^{(4)}_-\mathcal{F}(\boldsymbol{\phi}^n_i, \boldsymbol{\psi}^n_i)\big)^2\Big) \\ &\quad + 4C_9^2\big(\big|\Delta_-\phi^n_{i-1/2}\big|^2 + \big|\Delta_+\phi^n_{i-1/2}\big|^2\big) \\ &\leq C_{12}\Big(\big(\Delta^{(3)}_-\mathcal{F}(\boldsymbol{\phi}^n_i, \boldsymbol{\psi}^n_i)\big)^2 + \big(\Delta^{(4)}_-\mathcal{F}(\boldsymbol{\phi}^n_i, \boldsymbol{\psi}^n_i)\big)^2 + \big|\Delta_-\phi^n_{i-1/2}\big| + \big|\Delta_+\phi^n_{i-1/2}\big|\Big).\end{aligned}$$

Summing over $(i,n) \in \mathcal{I}_0$ we get

$$\begin{aligned}\sum_{\mathcal{I}_0}\big(\Delta_- Q(\boldsymbol{\phi}^n_i, \boldsymbol{\psi}^n_i)\big)^2 &\leq C_{12}\sum_{\mathcal{I}_0}\Big(\big(\Delta^{(3)}_-\mathcal{F}(\boldsymbol{\phi}^n_i, \boldsymbol{\psi}^n_i)\big)^2 + \big(\Delta^{(4)}_-\mathcal{F}(\boldsymbol{\phi}^n_i, \boldsymbol{\psi}^n_i)\big)\Big)^2 + 2C_{12}\sum_{\mathcal{I}_1}\big|\Delta_+\phi^n_{i-1/2}\big| \\ &\leq C_{12}\sum_{\mathcal{I}_0}\Big(\big(\Delta^{(3)}_-\mathcal{F}(\boldsymbol{\phi}^n_i, \boldsymbol{\psi}^n_i)\big)^2 + \big(\Delta^{(4)}_-\mathcal{F}(\boldsymbol{\phi}^n_i, \boldsymbol{\psi}^n_i)\big)^2\Big)^2 + 2C_{12}\sum_{n=0}^{N}\mathrm{TV}(\boldsymbol{\phi}^n).\end{aligned}$$

Multiplying this inequality by $\Delta t\Delta z$ and taking into account (4.39) and the uniform bound on $\mathrm{TV}(\boldsymbol{\phi}^n)$ we have proved the following lemma.

Lemma 4.9. *There exists a constant $C = C(T)$ that is independent on Δt or Δz such that the following estimate holds:*

$$\Delta t \Delta z \sum_{n=0}^{N_T} \sum_{i \in \mathbb{Z}} \big(\Delta_- \mathcal{Q}(\boldsymbol{\phi}_i^n, \boldsymbol{\psi}_i^n)\big)^2 \leq C(T) \Delta z. \tag{4.58}$$

In part following the proofs of Lemmas 5.5 and 5.9 in [67] and Lemma 3.4 in [34] we now prove the H^{-1}_{loc} compactness result.

Lemma 4.10. *Assume that $\psi^{\Delta z}$ is generated by the scheme (4.26), and that ϕ is the unique entropy solution of (4.17), (3.2a) on Π_T. Furthermore, we denote by (η_0, Q_0) the Kružkov entropy pair (4.23), and the distribution*

$$\mu^{\Delta z} := \partial_t \eta_0(\psi^{\Delta z}) + \partial_z Q_0(\phi^{\Delta z}, \psi^{\Delta z}). \tag{4.59}$$

Then the sequence $\{\mu^{\Delta z}\}_{\Delta z > 0}$ belongs to a compact subset of $H^{-1}_{\mathrm{loc}}(\Pi_T)$.

Proof. Following [34], we work with smooth entropies instead of η_0, so we denote by $\eta_{\Delta z}$ a smooth convex approximation to η_0, so that $\eta_{\Delta z}(0) = 0$ and $|\eta_{\Delta z}| \leq 1$, and $\|\eta_{\Delta z} - \eta_0\|_{L^\infty} \leq \Delta z$. Moreover, if $Q_{\Delta z}$ is the entropy flux associated with $\eta_{\Delta z}$, then there also holds $\|Q_{\Delta z} - Q_0\|_{L^\infty} \to 0$ as $\Delta z \to 0$. Then we split $\mu^{\Delta z}$ as $\mu^{\Delta z} = \mu_1^{\Delta z} + \mu_2^{\Delta z}$, where we define

$$\begin{aligned} \mu_1^{\Delta z} &:= \partial_t \big(\eta_0(\psi^{\Delta z}) - \eta_{\Delta z}(\psi^{\Delta z})\big), \\ \mu_2^{\Delta z} &:= \partial_t \eta_{\Delta z}(\psi^{\Delta z}) + \partial_z Q_0(\phi^{\Delta z}, \psi^{\Delta z}). \end{aligned}$$

If $\zeta \in C_0^1(\Pi_T)$ denotes a test function with compact support, then as in [34], one verifies that

$$\begin{aligned} \big|\langle \mu_1^{\Delta z}, \zeta \rangle\big| &\leq \iint_{\Pi_T} \big|\eta_{\Delta z}(\psi^{\Delta z}) - \eta_0(\psi^{\Delta z})\big| |\zeta_t| \,\mathrm{d}z \,\mathrm{d}t \\ &\leq C_{21} \|\zeta_t\|_{L^2(\Pi_T)} \|\eta_{\Delta z} - \eta_0\|_{L^\infty} \to 0 \quad \text{as } \Delta z \to 0, \end{aligned}$$

hence $\{\mu_1^{\Delta z}\}_{\Delta z > 0}$ is compact in $H^{-1}_{\mathrm{loc}}(\Pi_T)$. By an integration by parts we get

$$\begin{aligned} \langle \mu_2^{\Delta z}, \zeta \rangle &= -\iint_{\Pi_T} \big(\eta_{\Delta z}(\psi^{\Delta z}) \zeta_t + Q_0(\phi^{\Delta z}, \psi^{\Delta z}) \zeta_z\big) \,\mathrm{d}z \,\mathrm{d}t \\ &= -\sum_{n=1}^{N_T - 1} \int_{\mathbb{R}} \int_{t_n}^{t_{n+1}} \eta_{\Delta z}(\psi^{\Delta z}) \zeta_t \,\mathrm{d}t \,\mathrm{d}z - \sum_{n=1}^{N_T - 1} \int_{t_n}^{t_{n+1}} \int_{\mathbb{R}} Q_0(\phi^{\Delta z}, \psi^{\Delta z}) \zeta_z \,\mathrm{d}z \,\mathrm{d}t \\ &= -\sum_{n=0}^{N_T - 1} \int_{\mathbb{R}} \eta_{\Delta z}\big(\psi^{\Delta z}(z, t_n)\big) \big(\zeta(z, t_{n+1}) - \zeta(z, t_n)\big) \,\mathrm{d}z \\ &\quad - \sum_{n=1}^{N_T - 1} \sum_{i \in \mathbb{Z}} \int_{t_n}^{t_{n+1}} Q_0\big(\phi_{i-1/2}^n, \psi_{i-1/2}^n\big) \big(\zeta(z_i, t) - \zeta(z_{i-1}, t)\big) \,\mathrm{d}z \,\mathrm{d}t, \end{aligned}$$

so we may finally write

$$\begin{aligned}\langle \mu_2^{\Delta z}, \zeta\rangle = &\sum_{n=0}^{N_T-2}\sum_{i\in\mathbb{Z}}\big(\eta_{\Delta z}(\psi_{i-1/2}^{n+1})-\eta_{\Delta z}(\psi_{i-1/2}^{n})\big)\int_{I_{i-1/2}}\zeta(z,t_{n+1})\,\mathrm{d}z\\ &+\sum_{n=1}^{N_T-1}\sum_{i\in\mathbb{Z}}\big(\Delta_+ Q_0(\phi_{i-1/2}^{n},\psi_{i-1/2}^{n})\big)\int_{t_n}^{t_{n+1}}\zeta(z_i,t)\,\mathrm{d}t.\end{aligned} \tag{4.60}$$

We define the cell average

$$\zeta_{i-1/2}^{n} := \frac{1}{\Delta z\Delta t}\iint_{I_{j-1/2}^{n}}\zeta(z,t)\,\mathrm{d}z\,\mathrm{d}t. \tag{4.61}$$

Replacing the integral in the first term of the right-hand side of (4.60) by $\Delta z\zeta_{i-1/2}^{n}$ produces the following error, where we follow the derivation of (3.27) in [34]:

$$\begin{aligned}&\left|\sum_{\mathcal{I}_2}\big(\eta_{\Delta z}(\psi_{i-1/2}^{n+1})-\eta_{\Delta z}(\psi_{i-1/2}^{n})\big)\left(\int_{I_{i-1/2}}\zeta(z,t_{n+1})\,\mathrm{d}z-\Delta z\zeta_{i-1/2}^{n}\right)\right|\\
&\le \|\eta'_{\Delta z}\|_{L^\infty}\sum_{\mathcal{I}_2}\big|\psi_{i-1/2}^{n+1}-\psi_{i-1/2}^{n}\big|\frac{1}{\Delta t}\iint_{I_{j-1/2}^{n}}\big|\zeta(z,t_{n+1})-\zeta(z,t)\big|\,\mathrm{d}z\,\mathrm{d}t\\
&\le \sum_{n,i}\big|\psi_{i-1/2}^{n+1}-\psi_{i-1/2}^{n}\big|\frac{1}{\Delta t}\iint_{I_{j-1/2}^{n}}\int_{t}^{t_{n+1}}\big|\zeta_t(z,s)\big|\,\mathrm{d}s\,\mathrm{d}z\,\mathrm{d}t\\
&\le \sum_{\mathcal{I}_2}\big|\psi_{i-1/2}^{n+1}-\psi_{i-1/2}^{n}\big|\frac{1}{\Delta t}\iint_{I_{j-1/2}}\int_{t_n}^{t_{n+1}}(t_{n+1}-t)^{1/2}\left(\int_{t_n}^{t_{n+1}}\big|\zeta_t(z,s)\big|^2\,\mathrm{d}s\right)^{1/2}\mathrm{d}z\,\mathrm{d}t\\
&\le \frac{2}{3}\sum_{\mathcal{I}_2}\big|\psi_{i-1/2}^{n+1}-\psi_{i-1/2}^{n}\big|\Delta t^{1/2}\int_{I_{i-1/2}}\left(\int_{t_n}^{t_{n+1}}\big|\zeta_t(z,s)\big|^2\,\mathrm{d}s\right)^{1/2}\mathrm{d}z\\
&\le \frac{2}{3}\sum_{\mathcal{I}_2}\big|\psi_{i-1/2}^{n+1}-\psi_{i-1/2}^{n}\big|\Delta z^{1/2}\Delta t^{1/2}\left(\iint_{I_{i-1/2}^{n}}\big(\zeta_t(z,s)\big)^2\,\mathrm{d}z\,\mathrm{d}t\right)^{1/2}\\
&\le \frac{2}{3}\left(\Delta z\Delta t\sum_{n,i}\big(\psi_{i-1/2}^{n+1}-\psi_{i-1/2}^{n}\big)^2\right)^{1/2}\left(\sum_{\mathcal{I}_2}\iint_{I_{i-1/2}^{n}}\big(\zeta_t(z,s)\big)^2\,\mathrm{d}z\,\mathrm{d}t\right)^{1/2}\\
&\le \frac{2}{3}(C_7\Delta z)^{1/2}\|\zeta\|_{H^1(\Pi_T)}\end{aligned}$$

(see (4.40)). By similar arguments we obtain the bound

$$\begin{aligned}&\left|\sum_{\mathcal{I}_1}\big(\Delta_+ Q_0(\phi_{i-1/2}^{n},\psi_{i-1/2}^{n})\big)\left(\int_{t_n}^{t_{n+1}}\zeta(z_{i+1/2},t)\,\mathrm{d}t-\Delta t\zeta_{i-1/2}^{n}\right)\right|\\
&\le \tilde{C}_T\Delta z^{1/2}\|\zeta\|_{H^1(\Pi_T)}.\end{aligned}$$

Consequently, and further following [34], we have shown that

$$\langle \mu_2^{\Delta z}, \zeta\rangle = \Delta z\Delta t\sum_{\mathcal{I}_1}\left\{\frac{\eta_{\Delta z}(\psi_{i-1/2}^{n+1})-\eta_{\Delta z}(\psi_{i-1/2}^{n})}{\Delta t}+\frac{\Delta_+ Q_0(\phi_{i-1/2}^{n},\psi_{i-1/2}^{n})}{\Delta z}\right\}\zeta_{i-1/2}^{n}$$

$$+\text{ terms which are compact in } H^{-1}_{\mathrm{loc}}(\Pi_T).$$

We now utilize the "scheme for η", (4.37), to rewrite the term in curled brackets as

$$\{\dots\} = \mathcal{A}^n_{i-1/2} + \mathcal{B}^n_{i-1/2} + \mathcal{C}^n_{i-1/2} + \mathcal{D}^n_{i-1/2},$$

where we define

$$\begin{aligned}
\mathcal{A}^n_{i-1/2} &:= -\frac{1}{2\Delta t}\eta''_{\Delta z}\big(\xi^{n+1/2}_{i-1/2}\big)\big(\psi^{n+1}_{i-1/2} - \psi^n_{i-1/2}\big)^2 - \frac{1}{\Delta z}\Theta^n_{i-1/2},\\
\mathcal{B}^n_{i-1/2} &:= -\frac{1}{\Delta z}\big(\eta'\big(\psi^{n+1}_{i-1/2}\big) - \eta'\big(\psi^n_{i-1/2}\big)\big)\Delta_-\mathcal{F}(\boldsymbol{\phi}^n_i, \boldsymbol{\psi}^n_i),\\
\mathcal{C}^n_{i-1/2} &:= -\frac{1}{\Delta z}\Delta^\phi_+\big(\eta'\big(\psi^n_{i-1/2}\big)\mathcal{F}(\boldsymbol{\phi}^n_{i-1}, \boldsymbol{\psi}^n_{i-1}) - \mathcal{Q}(\boldsymbol{\phi}^n_{i-1}, \boldsymbol{\psi}^n_{i-1})\big),\\
\mathcal{D}^n_{i-1/2} &:= -\frac{1}{\Delta z}\big(\Delta_-\mathcal{Q}(\boldsymbol{\phi}^n_i, \boldsymbol{\psi}^n_i) - \Delta_+ Q_0\big(\phi^n_{i-1/2}, \psi^n_{i-1/2}\big)\big).
\end{aligned} \tag{4.62}$$

Thus, $\langle \mu_2^{\Delta z}, \zeta\rangle = \langle \mathcal{A}, \zeta\rangle + \langle \mathcal{B}, \zeta\rangle + \langle \mathcal{C}, \zeta\rangle + \langle \mathcal{D}, \zeta\rangle + \text{compact terms}$, where

$$\langle \mathcal{A}, \zeta\rangle = \Delta z \Delta t \sum_{n,i} \mathcal{A}^n_{i-1/2}\zeta^n_{i-1/2}$$

and $\langle \mathcal{B}, \zeta\rangle$, $\langle \mathcal{C}, \zeta\rangle$, and $\langle \mathcal{D}, \zeta\rangle$ are defined analogously. In view of Lemma 4.7, we get

$$\begin{aligned}
\big|\langle \mathcal{A}, \zeta\rangle\big| &\le \|\zeta\|_{L^\infty(\Pi_T)}\bigg(\frac{\Delta z}{2}\sum_{\mathcal{I}_1}\eta''_{\Delta z}\big(\xi^{n+1/2}_{i-1/2}\big)\big(\psi^{n+1}_{i-1/2} - \psi^n_{i-1/2}\big)^2 + \Delta t\sum_{\mathcal{I}_1}\Theta^n_{i-1/2}\bigg)\\
&\le C_T\|\zeta\|_{L^\infty(\Pi_T)},
\end{aligned}$$

and therefore $\mathcal{A} \in \mathcal{M}_{\mathrm{loc}}(\Pi_T)$. Appealing to the divergence bound of the numerical flux (4.38) and taking into account the BV bound on $\phi^{\Delta z}$ it also follows that $|\langle \mathcal{B}+\mathcal{C}, \zeta\rangle| \le C_T\|\zeta\|_{L^\infty(\Pi_T)}$, and therefore $\mathcal{B}+\mathcal{C} \in \mathcal{M}_{\mathrm{loc}}(\Pi_T)$.

Finally, to deal with $\langle \mathcal{D}, \zeta\rangle$ we consider first $\varepsilon > 0$ and let Q_ε, $\mathcal{Q}^\pm_\varepsilon$ and $\mathcal{Q}_\varepsilon$ denote the entropy and numerical entropy fluxes calculated from (4.22) and (4.30), respectively, where $\eta = \eta_\varepsilon$. Since $\mathcal{Q}_\varepsilon$ is consistent with Q_ε,

$$\begin{aligned}
&\mathcal{Q}_\varepsilon(\phi,\phi,\psi_1,\psi_2) - Q_\varepsilon(\phi,\psi_2)\\
&= \mathcal{Q}_\varepsilon(\phi,\phi,\psi_1,\psi_2) - \mathcal{Q}_\varepsilon(\phi,\phi,\psi_2,\psi_2) = \int_{\psi_2}^{\psi_1}\eta'_\varepsilon(s)\check{f}(\phi,\phi,s)\,\mathrm{d}s\\
&= \eta'_\varepsilon(\psi_1)\big(\check{\mathcal{F}}(\phi,\phi,\psi_1) - \check{\mathcal{F}}(\phi,\phi,\psi_2)\big) - \int_{\psi_2}^{\psi_1}\eta''_\varepsilon(s)\big(\check{\mathcal{F}}(\phi,\phi,s) - \check{\mathcal{F}}(\phi,\phi,\psi_1)\big)\,\mathrm{d}s
\end{aligned}$$

(cf. (4.32)). By using the monotonicity of $\check{\mathcal{F}}$ with respect to its ψ-argument we get

$$\begin{aligned}
\big|\mathcal{Q}_\varepsilon(\phi,\phi,\psi_1,\psi_2) - Q_\varepsilon(\phi,\psi_2)\big| &\le 3\|\eta'_\varepsilon\|_{L^\infty}\big|\check{\mathcal{F}}(\phi,\phi,\psi_2) - \check{\mathcal{F}}(\phi,\phi,\psi_1)\big|\\
&\le 3\big|\check{\mathcal{F}}(\phi,\phi,\psi_2) - \check{\mathcal{F}}(\phi,\phi,\psi_1)\big|,
\end{aligned}$$

so in the limit $\varepsilon \to 0$,

$$\big|\mathcal{Q}(\phi,\phi,\psi_1,\psi_2) - Q_0(\phi,\psi_2)\big| \le 3\big|\check{\mathcal{F}}(\phi,\phi,\psi_2) - \check{\mathcal{F}}(\phi,\phi,\psi_1)\big|. \tag{4.63}$$

Noticing that

$$\begin{aligned}\Delta_-\mathcal{Q}(\boldsymbol{\phi}_i^n,\boldsymbol{\psi}_i^n) - \Delta_+ Q_0\big(\phi_{i-1/2}^n,\psi_{i-1/2}^n\big) &= \Delta_-\big(\mathcal{Q}\big(\boldsymbol{\phi}_i^n,\psi_{i-1/2}^n,\psi_{i+1/2}^n\big) - Q_0(\phi_{i+1/2}^n,\psi_{i+1/2}^n)\big)\\ &= \Delta_-\big(\mathcal{Q}\big(\phi_{i+1/2}^n,\phi_{i+1/2}^n,\boldsymbol{\psi}_i^n\big) - Q_0(\phi_{i+1/2}^n,\psi_{i+1/2}^n)\big)\\ &\quad + \Delta_-\big(\mathcal{Q}\big(\boldsymbol{\phi}_i^n,\boldsymbol{\psi}_i^n\big) - \mathcal{Q}\big(\phi_{i+1/2}^n,\phi_{i+1/2}^n,\boldsymbol{\psi}_i^n\big)\big)\end{aligned}$$

we get from (4.62)

$$\begin{aligned}&\left|\Delta z\Delta t\sum_{\mathcal{I}_1}\mathcal{D}_{i-1/2}^n\zeta_{i-1/2}^n\right|\\ &\le \left|\Delta z\Delta t\sum_{\mathcal{I}_1}\frac{1}{\Delta z}\Delta_-\big(\mathcal{Q}\big(\phi_{i+1/2}^n,\phi_{i+1/2}^n,\boldsymbol{\psi}_i^n\big) - Q_0(\phi_{i+1/2}^n,\psi_{i+1/2}^n)\big)\zeta_{i-1/2}^n\right|\\ &\quad + \left|\Delta z\Delta t\sum_{\mathcal{I}_1}\frac{1}{\Delta z}\Delta_-\big(\mathcal{Q}\big(\boldsymbol{\phi}_i^n,\boldsymbol{\psi}_i^n\big) - \mathcal{Q}\big(\phi_{i+1/2}^n,\phi_{i+1/2}^n,\boldsymbol{\psi}_i^n\big)\big)\zeta_{i-1/2}^n\right| =: |\mathcal{S}_1| + |\mathcal{S}_2|.\end{aligned}$$

By a summation by parts and applying (4.63) we get

$$\begin{aligned}|\mathcal{S}_1| &= \left|\Delta z\Delta t\sum_{\mathcal{I}_1}\big(\mathcal{Q}\big(\phi_{i+1/2}^n,\phi_{i+1/2}^n,\boldsymbol{\psi}_i^n\big) - Q_0(\phi_{i+1/2}^n,\psi_{i+1/2}^n)\big)\frac{\Delta_+\zeta_{i-1/2}^n}{\Delta z}\right|\\ &\le 3\Delta z\Delta t\sum_{\mathcal{I}_1}\big|\Delta_+^{(3)}\check{\mathcal{F}}\big(\phi_{i+1/2}^n,\phi_{i+1/2}^n,\psi_{i-1/2}^n\big)\big|\frac{|\Delta_+\zeta_{i-1/2}^n|}{\Delta z}.\end{aligned} \tag{4.64}$$

We now write

$$\Delta_+^{(3)}\check{\mathcal{F}}\big(\phi_{i+1/2}^n,\phi_{i+1/2}^n,\psi_{i-1/2}^n\big) = \Delta_+^{(3)}\check{\mathcal{F}}\big(\boldsymbol{\phi}_i^n,\psi_{i-1/2}^n\big) + \mathcal{Y}_{i+1/2}^n - \mathcal{Y}_{i-1/2}^n,$$

where

$$\mathcal{Y}_{i\pm1/2}^n := \check{\mathcal{F}}\big(\phi_{i+1/2}^n,\phi_{i+1/2}^n,\psi_{i\pm1/2}^n\big) - \check{\mathcal{F}}\big(\boldsymbol{\phi}_i^n,\psi_{i\pm1/2}^n\big).$$

From (4.57), and considering $\phi_{i-3/2}^n = \phi_{i-1/2}^n$ in that bound, we deduce there exists a constant C such that $|\mathcal{Y}_{i\pm1/2}^n| \le C|\Delta_+\phi_{i-1/2}^n|$, therefore there exists (another) constant C such that

$$\big|\mathcal{Y}_{i+1/2}^n - \mathcal{Y}_{i-1/2}^n\big| \le C\big|\Delta_+\phi_{i-1/2}^n\big|. \tag{4.65}$$

Consequently, from (4.64) we deduce that

$$|\mathcal{S}_1| \le 3\Delta z\Delta t\left(\sum_{\mathcal{I}_1}\big|\Delta_+^{(3)}\check{\mathcal{F}}\big(\boldsymbol{\phi}_i^n,\psi_{i-1/2}^n\big)\big|\frac{|\Delta_+\zeta_{i-1/2}^n|}{\Delta z} + \sum_{\mathcal{I}_1}\big|\Delta_+\phi_{i-1/2}^n\big|\frac{|\Delta_+\zeta_{i-1/2}^n|}{\Delta z}\right)$$

$$\leq 3\left(\Delta z\Delta t\left(\sum_{\mathcal{I}_1}\big(\Delta_+^{(3)}\check{\mathcal{F}}\big(\phi^n_{i+1/2},\phi^n_{i+1/2},\psi^n_{i-1/2}\big)\big)^2+C\sum_n \mathrm{TV}(\boldsymbol{\phi}^n)\right)\right)^{1/2}\times$$
$$\times\left(\Delta z\Delta t\sum_{\mathcal{I}_1}\left(\frac{|\Delta_+\zeta^n_{i-1/2}|}{\Delta z}\right)^2\right)^{1/2}.$$

From (4.39) we infer that there exists a constant C_T such that

$$\Delta t\sum_{\mathcal{I}_1}\big(\Delta_+^{(3)}\check{\mathcal{F}}\big(\phi^n_{i+1/2},\phi^n_{i+1/2},\psi^n_{i-1/2}\big)\big)^2\leq C_T.$$

Noticing that also

$$\Delta t\sum_n \mathrm{TV}(\boldsymbol{\phi}^n)\leq C_{t_N},$$

we conclude that there exists a constant C_{t_N} such that

$$\big|\langle\mathcal{S}_1,\zeta\rangle\big|\leq C_{T_N}\Delta z^{1/2}\|\partial_z\zeta\|_{L^2(\Pi_T)}.$$

Next, we deal with $\mathcal{S}_2$. Applying again a summation by parts yields

$$|\mathcal{S}_2|=\left|\Delta z\Delta t\sum_{n,i}\big(\mathcal{Q}\big(\boldsymbol{\phi}^n_i,\boldsymbol{\psi}^n_i\big)-\mathcal{Q}\big(\phi^n_{i+1/2},\phi^n_{i+1/2},\boldsymbol{\psi}^n_i\big)\big)\frac{\Delta_+\zeta^n_{i-1/2}}{\Delta z}\right|.$$

The definition of $\mathcal{Q}$ (see (4.30)) we get

$$\big|\mathcal{Q}\big(\boldsymbol{\phi}^n_i,\boldsymbol{\psi}^n_i\big)-\mathcal{Q}\big(\phi^n_{i+1/2},\phi^n_{i+1/2},\boldsymbol{\psi}^n_i\big)\big|\leq\big|\mathcal{Q}^+\big(\boldsymbol{\phi}^n_i,\psi^n_{i-1/2}\big)-\mathcal{Q}^+\big(\phi^n_{i+1/2},\phi^n_{i+1/2},\psi^n_{i-1/2}\big)\big|$$
$$+\big|\mathcal{Q}^-\big(\boldsymbol{\phi}^n_i,\psi^n_{i+1/2}\big)-\mathcal{Q}^-\big(\phi^n_{i+1/2},\phi^n_{i+1/2},\psi^n_{i-1/2}\big)\big|.$$

By a computation similar to (4.44) we get

$$\big|\mathcal{Q}^+\big(\boldsymbol{\phi}^n_i,\psi^n_{i-1/2}\big)-\mathcal{Q}^+\big(\phi^n_{i+1/2},\phi^n_{i+1/2},\psi^n_{i-1/2}\big)\big|\leq 3\|\eta'\|_\infty\big|\mathcal{X}^n_{i-1/2}\big|,$$

where we define

$$\mathcal{X}^n_{i-1/2}:=\hat{\mathcal{F}}\big(\boldsymbol{\phi}^n_i,\psi^n_{i-1/2}\big)-\hat{\mathcal{F}}\big(\phi^n_{i+1/2},\phi^n_{i+1/2},\psi^n_{i-1/2}\big).$$

The discussion of $\mathcal{X}^n_{i-1/2}$ is similar to that of $\mathcal{Y}^n_{i-1/2}$ above, and appealing to (4.57) we see that

$$\big|\mathcal{X}^n_{i-1/2}\big|\leq C\big|\Delta_+\phi^n_{i-1/2}\big|.$$

On the other hand, (4.65) implies that

$$\big|\mathcal{Q}^-\big(\boldsymbol{\phi}^n_i,\psi^n_{i-1/2}\big)-\mathcal{Q}^-\big(\phi^n_{i+1/2},\phi^n_{i+1/2},\psi^n_{i-1/2}\big)\big|$$
$$\leq 3\|\eta'\|_\infty\big|\check{\mathcal{F}}\big(\boldsymbol{\phi}^n_i,\psi^n_{i-1/2}\big)-\check{\mathcal{F}}\big(\phi^n_{i+1/2},\phi^n_{i+1/2},\psi^n_{i-1/2}\big)\big|\leq C\big|\Delta_+\phi^n_{i-1/2}\big|.$$

Thus

$$\big|\mathcal{Q}(\boldsymbol{\phi}_i^n, \boldsymbol{\psi}_i^n) - \mathcal{Q}\big(\phi_{i+1/2}^n, \phi_{i+1/2}^n, \boldsymbol{\psi}_i^n\big)\big| \le C\big|\Delta_+ \phi_{i-1/2}^n\big|,$$

and we deduce that $\mathcal{S}_2$ can be bounded in a similar way as $\mathcal{S}_1$. In particular,

$$|\mathcal{S}_2| \le 3\left(\Delta z \Delta t C \sum_n \mathrm{TV}(\boldsymbol{\phi}^n)\right)^{1/2}\left(\Delta z \Delta t \sum_{n,i}\left(\frac{|\Delta_+ \zeta_{i-1/2}^n|}{\Delta z}\right)^2\right)^{1/2},$$

and we conclude that also

$$\big|\langle \mathcal{S}_2, \zeta\rangle\big| \le C_T \Delta z^{1/2} \|\partial_z \zeta\|_{L^2(\mathbb{R}^2\times\mathbb{R}^+)},$$

so $\mathcal{D}$ is compact in $H^{-1}_{\mathrm{loc}}(\Pi_T)$. Thus, the sequence $\{\mu_2^{\Delta z}\}_{\Delta z>0}$, and therefore also the sequence $\{\mu^{\Delta z}\}_{\Delta z>0}$ belong to a compact subset of $H^{-1}_{\mathrm{loc}}(\Pi_T)$. □

Since $\phi^{\Delta z} \to \phi$ strongly in L^p, we obtain that there exists a constant C such that

$$\big|\big\langle \partial_z\big(Q(\phi^{\Delta z}, \psi^{\Delta z}) - Q(\phi, \psi^{\Delta z})\big), \zeta\big\rangle\big| \le C\|\phi^{\Delta z} - \phi\|_{L^2(\Pi_T)}\|\zeta\|_{H^1(\Pi_T)} \to 0 \quad \text{as } \Delta z \to 0,$$

hence the sequence $\{\tilde{\mu}^{\Delta z}\}_{\Delta z>0}$, where we define

$$\tilde{\mu}^{\Delta z} := \partial_t \eta_0(\psi^{\Delta z}) + \partial_z Q(\phi, \psi^{\Delta z}),$$

is compact in $H^{-1}_{\mathrm{loc}}(\Pi_T)$. Now, by Lemma 4.6 there exists a subsequence $\{\psi^{\Delta z}\}$ (which we do not relabel) and a function $\psi \in L^\infty(\Pi_T)$ such that

$$\psi^\Delta \to \psi \quad \text{as } \Delta z \to 0, \text{ a.e. and in } L^p_{\mathrm{loc}}(\Pi_T) \text{ for any } p \in [1,\infty). \tag{4.66}$$

Lemma 4.11. *Assume that the maps ϕ and ψ are the limit functions of $\phi^{\Delta z}$ and of $\psi^{\Delta z}$ as $\Delta z \to 0$ (the latter one being defined by (4.66)). Then (ϕ, ψ) is a weak solution of the initial-value problem (4.17), (4.18), (3.2) in the sense of Definition 4.4.1.*

Proof. The proof follows that of [34, Lemma 3.5]. We only need to verify that ψ is a weak solution of (4.18), that is, that (4.20) holds. To this end, we choose a test function $\zeta \in C_0^\infty(\Pi_T)$, recall the definition (4.61) of cell averages $\zeta_{i-1/2}^n$, multiply the ψ-scheme (4.26) by $\Delta z \zeta_{i-1/2}^n$, sum over i and n, and apply a summation by parts to obtain an identity $\mathcal{J}_0 + \mathcal{J}_1 + \mathcal{J}_2 = 0$, where

$$\mathcal{J}_0 := \Delta z \sum_{i\in\mathbb{Z}} \psi_{i-1/2}^0 \zeta_{i-1/2}^0, \quad \mathcal{J}_1 := \Delta z \sum_{i\in\mathbb{Z}}\sum_{n=1}^{N_T} \psi_{i-1/2}^n\big(\zeta_{i-1/2}^n - \zeta_{i-1/2}^{n-1}\big),$$
$$\mathcal{J}_2 := \Delta z \Delta t \sum_{n=0}^{N_T-1}\sum_{i\in\mathbb{Z}} \mathcal{F}(\boldsymbol{\phi}_i^n, \boldsymbol{\psi}_i^n)\frac{\Delta_+ \zeta_{i-1/2}^n}{\Delta z}.$$

By exactly following the estimates of terms I_0 and I_1 in the proof of [34, Lemma 3.5] and appealing to the bounded convergence theorem we may prove that

$$\lim_{\Delta z\to 0}\mathcal{J}_0=\int_{\mathbb{R}}\psi_0(z)\zeta(z,0)\,\mathrm{d}z,\quad \lim_{\Delta z\to 0}\mathcal{J}_1=\iint_{\Pi_T}\psi\partial_t\zeta\,\mathrm{d}z\,\mathrm{d}t. \tag{4.67}$$

The treatment of $\mathcal{J}_2$ differs from that of the term I_2 in [34, Lemma 3.5] since here the numerical flux depends on four arguments (not three, as in [34]). We here get

$$\mathcal{J}_2=\iint_{\Pi_T}\tilde{F}(\phi^{\Delta z},\psi^{\Delta z})\partial_z\zeta\,\mathrm{d}z\,\mathrm{d}t+\mathcal{J}_{2,1}+\mathcal{J}_{2,2}+\mathcal{J}_{2,3},$$

where we define

$$\begin{aligned}
\mathcal{J}_{2,1}&:=-\sum_{\mathcal{I}_1}\tilde{F}\big(\phi^n_{i-1/2},\psi^n_{i-1/2}\big)\iint_{I^n_{i-1/2}}\int_0^{\Delta z}\frac{\partial_z\zeta(z,t)-\partial_z\zeta(z+\xi,t)}{\Delta z}\,\mathrm{d}\xi\,\mathrm{d}z\,\mathrm{d}t,\\
\mathcal{J}_{2,2}&:=-\Delta z\Delta t\sum_{\mathcal{I}_1}\big(\tilde{F}\big(\phi^n_{i-1/2},\psi^n_{i-1/2}\big)-\mathcal{F}\big(\boldsymbol{\phi}^n_i,\psi^n_{i-1/2},\psi^n_{i-1/2}\big)\big)\frac{\Delta_+\zeta^n_{i-1/2}}{\Delta z},\\
\mathcal{J}_{2,3}&:=-\Delta z\Delta t\sum_{\mathcal{I}_1}\big(\mathcal{F}\big(\boldsymbol{\phi}^n_i,\psi^n_{i-1/2},\psi^n_{i-1/2}\big)-\mathcal{F}\big(\boldsymbol{\phi}^n_i,\boldsymbol{\psi}^n_i\big)\big)\frac{\Delta_+\zeta^n_{i-1/2}}{\Delta z}\\
&=\Delta z\Delta t\sum_{\mathcal{I}_1}\Delta^{(3)}_+\check{\mathcal{F}}\big(\boldsymbol{\phi}^n_i,\psi^n_{i-1/2}\big)\frac{\Delta_+\zeta^n_{i-1/2}}{\Delta z}.
\end{aligned}$$

The term $\mathcal{J}_{2,1}$ can be estimated by choosing a constant M such that $\zeta(z,t)=0$ for $|z|>M$ and noting that

$$|\mathcal{J}_{2,1}|\le\Delta z\|\partial_z^2\zeta\|_{L^\infty}\|\tilde{F}(\phi^\Delta,\psi^\Delta)\|_{L^1([-M,M]\times[0,T])}\ \to 0\text{ as }\Delta z\to 0. \tag{4.68}$$

Furthermore, in light of (4.29) the difference arising in $\mathcal{J}_{2,2}$ can be written as

$$\begin{aligned}
&\tilde{F}\big(\phi^n_{i-1/2},\psi^n_{i-1/2}\big)-\mathcal{F}\big(\boldsymbol{\phi}^n_i,\psi^n_{i-1/2},\psi^n_{i-1/2}\big)\\
&=\mathcal{F}\big(\phi^n_{i-1/2},\phi^n_{i-1/2},\psi^n_{i-1/2},\psi^n_{i-1/2}\big)-\mathcal{F}\big(\phi^n_{i-1/2},\phi^n_{i+1/2},\psi^n_{i-1/2},\psi^n_{i-1/2}\big)\\
&=\hat{\mathcal{F}}\big(\phi^n_{i-1/2},\phi^n_{i-1/2},\psi^n_{i-1/2}\big)-\hat{\mathcal{F}}\big(\phi^n_{i-1/2},\phi^n_{i+1/2},\psi^n_{i-1/2}\big)\\
&\quad+\check{\mathcal{F}}\big(\phi^n_{i-1/2},\phi^n_{i-1/2},\psi^n_{i-1/2}\big)-\check{\mathcal{F}}\big(\phi^n_{i-1/2},\phi^n_{i+1/2},\psi^n_{i-1/2}\big).
\end{aligned}$$

Utilizing the estimate (4.57) with $\phi^n_{i-3/2}=\phi^n_{i-1/2}$ yields that there exists a constant C_{12} such that

$$\big|\tilde{F}\big(\phi^n_{i-1/2},\psi^n_{i-1/2}\big)-\mathcal{F}\big(\boldsymbol{\phi}^n_i,\psi^n_{i-1/2},\psi^n_{i-1/2}\big)\big|\le C_{12}\big|\Delta_+\phi^n_{i-1/2}\big|,$$

hence

$$\big|\mathcal{J}_{2,2}\big|\le C_{12}\Delta z\Delta t\sum_{n=0}^{N_T-1}\mathrm{TV}(\boldsymbol{\phi}^n)\frac{\Delta_+\zeta^n_{i-1/2}}{\Delta z}\le C\Delta z\|\partial_z\zeta\|_{L^\infty}\ \to 0\text{ as }\Delta z\to 0. \tag{4.69}$$

To estimate $\mathcal{J}_{2,3}$, we utilize (4.39). Then

$$\begin{aligned} |\mathcal{J}_{2,3}| &\leq \left(\Delta z \Delta t \sum_{\mathcal{I}_1} \left(\Delta_+^{(3)} \check{\mathcal{F}}\left(\boldsymbol{\phi}_i^n, \psi_{i-1/2}^n \right) \right)^2 \right)^{1/2} \left(\Delta z \Delta t \sum_{\mathcal{I}_1} \left(\frac{\Delta_+ \zeta_{i-1/2}^n}{\Delta z} \right)^2 \right)^{1/2} \\ &\leq C_T^{1/2} \Delta z^{1/2} \|\partial_z \zeta\|_{L^2(\Pi_T)} \quad \to 0 \text{ as } \Delta z \to 0. \end{aligned} \tag{4.70}$$

From (4.68), (4.69) and (4.70) and appealing to the strong convergence of $\phi^{\Delta z}$ and $\psi^{\Delta z}$ we deduce that

$$\lim_{\Delta z \to 0} \mathcal{J}_2 = \iint_{\Pi_T} \tilde{F}(\phi, \psi) \partial_z \zeta \, \mathrm{d}z \, \mathrm{d}t. \tag{4.71}$$

The limits (4.67) and (4.71) imply that the limit ψ is a weak solution. □

CHAPTER 5

A degenerating convection-diffusion system modelling froth flotation with drainage

5.1 Introduction

5.1.1 Scope

As we stated in previous chapters, flotation is a separation process where air bubbles are used to attract hydrophobic particles or droplets from a mixture of solids in water. The process is often applied in a column to which both a mixture of particles (or droplets) and air bubbles are injected. The effluent at the top should consist of a concentrate of hydrophobic particles that are attached to the bubbles, while the hydrophilic particles settle to the bottom, where they are removed (see Figure 5.1). A layer of froth at the top is preferred since the effluent then consists of a minimum amount of water and the froth works as a filter enhancing the separation process. In our previous models of column froth flotation (with or without simultaneous sedimentation of hydrophilic particles) Bürger et al. [17, 18, 20, 28], a particular constitutive assumption on the bubble velocity leads to a hyperbolic system of partial differential equations (PDEs) that models the layer of froth with a constant horizontal average volume fraction of bubbles ϕ, or equivalently, the volume fraction $\varepsilon = 1 - \phi$ of liquid (or suspension with hydrophilic particles) that fills the interstices outside the bubbles. It is however known that ε varies with the height in the froth because of capillarity and drainage of liquid; see Neethling and Brito-Parada [85] and references therein.

It is the purpose of this chapter to extend the hyperbolic model presented in Chapter 3 to one that includes capillarity. To this end we partly generalize the well-known drainage equation to hold for all bubble volume fractions, and partly generalize our previous model of column froth flotation with simultaneous sedimentation. The latter is a nonlinear system of PDEs where the unknowns are the volume fractions of aggregates (bubbles/droplets loaded with hydrophobic particles) and solid hydrophilic particles. A numerical scheme for the new governing PDE

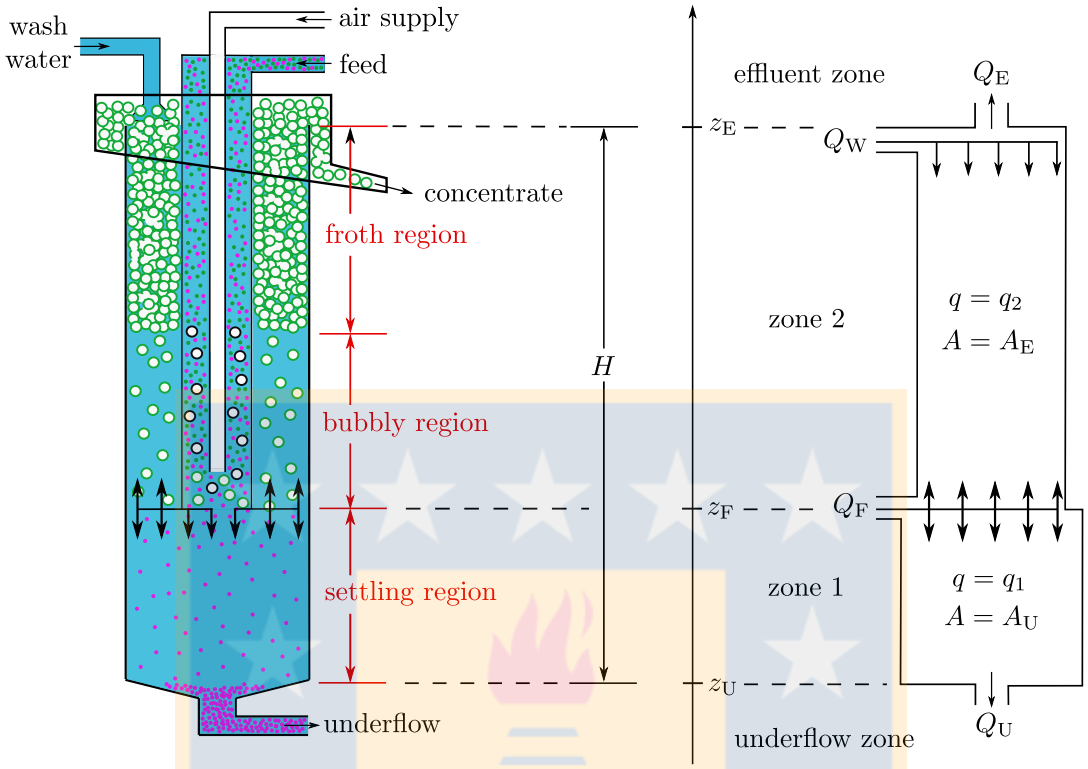

Figure 5.1: Left: Schematic of a flotation column; cf. the Reflux Flotation Cell by [38]. Right: The corresponding one-dimensional conceptual model with a non-constant cross-sectional area $A(z)$. Wash water is sprinkled at the effluent level $z = z_E$ and a mixture of aggregates and feed slurry is fed at $z = z_F$, where $z_U < z_F < z_E$ divide the real line into the zones inside the column and the underflow and effluent zones.

system is presented. We show that the approximate volume fractions stay between zero and one if a suitable Courant-Friedrichs-Lewy (CFL) condition is used. Furthermore, we construct desired steady-state solutions and provide algebraic equations and inequalities that establish the dependence of steady states on the input and control variables. Such dependences are conveniently visualized in so-called operating charts that constitute a graphical tool for controlling the process. The particular importance of steady states comes from the application under study; namely they describe the ability of the model to capture steady operation of the flotation device without the necessity of permanent control actions.

5.1.2 Some preliminaries

Froth is assumed to form when the volume fraction of bubbles ϕ is above a critical value $\phi_c = 1 - \varepsilon_c$ when the bubbles are in contact with each other. Then capillarity forces are involved, which means that the governing PDE is parabolic, whereas it is hyperbolic in regions without

froth. The present derivation is based on the traditional one by Goldfarb et al. [57], Leonard and Lemlich [76], and Verbist et al. [112], leading to the drainage equation for low liquid content ε. We then combine results of [90] and [107] to obtain a constitutive relationship between the relative fluid-gas velocity u and the liquid volume fraction $\varepsilon \leq \varepsilon_c$ when capillarity forces are present. With a compatibility condition at ε_c, we obtain a constitutive relationship of the relative fluid-bubble velocity u as a function of $\varepsilon \in [0,1]$, which for $\varepsilon > \varepsilon_c$ is the common Richardson and Zaki [98] power-law expression for separated bubbles (Galvin and Dickinson [54])‘. The resulting generalized drainage PDE is (in a closed vessel)

$$\partial_t \varepsilon - \partial_z\big(\varepsilon \tilde{v}_f(\varepsilon)\big) = \partial_z^2 \tilde{D}(\varepsilon), \tag{5.1}$$

where t is time, z is height, $\tilde{v}_f(\varepsilon)$ is a nonlinear fluid-velocity function, and $\tilde{D}(\varepsilon)$ an integrated diffusion function modelling capillarity, which is zero for $\varepsilon > \varepsilon_c$.

Equation (5.1) can alternatively be written in terms of the volume fraction of bubbles ϕ. We assume that ϕ denotes the volume fraction of aggregates, by which we mean bubbles that are fully loaded with hydrophobic particles. Under a common constitutive assumption for the settling of hydrophilic particles within the liquid outside the bubbles, the following system of PDEs models the combined flotation-drainage-sedimentation process in a vertical column with a feed inlet of air-slurry mixture at the height $z = z_F$ with the volumetric flow $Q_F(t)$ (see Figure 5.1):

$$\begin{aligned} &A(z)\partial_t \begin{pmatrix} \phi \\ \psi \end{pmatrix} + \partial_z \left(A(z) \begin{pmatrix} J(\phi, z, t) \\ -\tilde{F}(\psi, \phi, z, t) \end{pmatrix} \right) \\ &= \partial_z \left(A(z)\gamma(z)\partial_z D(\phi) \begin{pmatrix} 1 \\ -\psi/(1-\phi) \end{pmatrix} \right) + Q_F(t) \begin{pmatrix} \phi_F(t) \\ \psi_F(t) \end{pmatrix} \delta_{z_F}. \end{aligned} \tag{5.2}$$

Here, ψ is the volume fraction of solids, $A(z)$ the cross-sectional area of the tank, and J and $\tilde{F}$ are convective flux functions that depend discontinuously on z at the locations of the feed and wash water inlets and the outlets at the top and bottom. The system (5.2) is valid for $t > 0$ and all $z \in \mathbb{R}$ where the characteristic function $\gamma(z) = 1$ indicates the interior of the tank and $\gamma(z) = 0$ outside, and δ is the delta function. Outside the tank, the mixture is assumed to follow the outlet streams; consequently, boundary conditions are not needed; conservation of mass determines the outlet volume fractions in a natural way.

Similarly to the role of $\tilde{D}$ in (5.1), the nonlinear function D models the capillarity present when bubbles are in contact. Precisely, with a function $d(\phi)$ (specified later) we define

$$D(\phi) := \int_0^\phi d(s)\,\mathrm{d}s. \tag{5.3}$$

The function d is assumed to satisfy

$$d(\phi) = D'(\phi) = \begin{cases} 0 & \text{for } 0 \leq \phi \leq \phi_c, \\ > 0 & \text{for } \phi_c < \phi \leq 1. \end{cases} \tag{5.4}$$

Consequently, at each point (z,t) where $\phi(z,t) \le \phi_c$, there holds $D(\phi(z,t)) = 0$, and therefore (5.2) degenerates at such points into a first-order system of conservation laws of hyperbolic type (as was shown in [18]). Since this degeneration occurs for $0 \le \phi \le \phi_c$ and $0 \le \psi \le 1-\phi$, that is, on a set of positive two-dimensional measure, (5.2) is called *strongly* degenerate. While it is clear that the first PDE in (5.2) is parabolic for $\phi_c < \phi \le 1$ and this PDE, as well as (5.1), are scalar strongly degenerate parabolic equations, the same cannot be said about the system. We observe namely that with $A = \gamma = 1$, the diffusion term on the right-hand side can be written as

$$\partial_z\left(d(\phi)\partial_z\phi\begin{pmatrix}1\\ -\psi/(1-\phi)\end{pmatrix}\right) = \partial_z\left(\boldsymbol{B}(\phi,\psi)\begin{pmatrix}\partial_z\phi\\ \partial_z\psi\end{pmatrix}\right), \quad \boldsymbol{B}(\phi,\psi) := d(\phi)\begin{bmatrix}1 & 0\\ -\psi/(1-\phi) & 0\end{bmatrix}.$$

Since at least one of the eigenvalues of $\boldsymbol{B}(\phi,\psi)$ is always zero, we observe that even when $d(\phi) > 0$, the system (5.2) is not *strictly* parabolic.

5.1.3 Outline of the chapter

In Section 5.2, we consider a simplified two-phase bubble-fluid system in a closed vessel and derive a generalized drainage equation governing the flotation of the bubbles with formation of froth and drainage of liquid from it. In Section 5.3, we extend the equation derived to the process of column flotation with sedimentation of solid particles and with froth drainage at the top. The treatment of the feed inlets and the definition of the flux density functions in each zone (see Figure 5.1) are detailed. Section 5.4 is devoted to the construction of steady-state solutions having a froth layer at the top of the tank and bubble-free underflow. Necessary conditions for those so-called desired steady-states to appear, in terms of inequalities involving the volumetric flows Q_U, Q_F and Q_W and the incoming volume fractions of aggregates ϕ_F and solids ψ_F, are derived in Sections 5.4.4 and 5.4.5. In Section 5.5, the numerical scheme for simulation of the process is introduced. It is proven that under a CFL condition, the approximate volume fractions of aggregates and solids remain between zero and one provided that the initial data do. Some simulations are provided in Section 5.6. They show fill-up of a flotation column and froth formation, illustrating the response of the system to changes of operating conditions.

5.2 A generalized drainage equation in a closed tank

The two-phase system has bubbles of volume fraction ϕ and phase velocity v, and fluid of volume fraction $\varepsilon = 1-\phi$ and phase velocity v_f, where $0 \le \phi, \varepsilon \le 1$. When the bubbles are mono-sized and separated from each other (i.e., there is no froth), a common expression for their velocity in a closed container without any bulk flow is [91, 111]

$$v(\phi) = v_{\text{term}}(1-\phi)^{n_b} \qquad \text{(separated bubbles)},$$

where v_{term} is the velocity of a single bubble far away from others ($\phi \approx 0$) and n_{b} a dimensionless parameter (similar to the Richardson-Zaki exponent within the analogous expression for the sedimentation of mono-sized and equal-density particles in a liquid, see Section 5.3.3). We thus let velocities be positive in the upward direction of the z-axis. The relative velocity of fluid to bubbles is $u := v_{\text{f}} - v$. In a closed container, the volume-average velocity is zero; hence, $0 = \phi v + \varepsilon v_{\text{f}}$, and we get

$$u = -\frac{(1-\varepsilon)v}{\varepsilon} - v = -\frac{v}{\varepsilon} = -v_{\text{term}}\varepsilon^{n_{\text{b}}-1} \qquad \text{(separated bubbles)}, \tag{5.5}$$

which is negative because the fluid flows downwards. We also obtain the identities $v_{\text{f}} = (1-\varepsilon)u$ and $v = -(1-\phi)u$.

If ϕ exceeds a certain critical volume fraction $\phi_{\text{c}} = 1 - \varepsilon_{\text{c}}$, the bubbles touch each other and a foam is formed. The larger $\phi > \phi_{\text{c}}$, or smaller $\varepsilon < \varepsilon_{\text{c}}$, the more deformed are the bubbles. Randomly packed rigid spheres leave a volume fraction of $\varepsilon_{\text{c}} = 1 - 0.64 = 0.36$; cf. [15, Table 1]. For froth, we assume the value $\varepsilon_{\text{c}} = 0.26$ [89, Eq. (21)] and Narsimhan [84].

We discuss below the most difficult intermediate fluid volume fractions when ε is smaller than, but close to ε_{c}. We consider, however, first a layer of foam with a very low volume fraction of liquid ε and recall the derivation of the drainage equation [57, 76, 112]. In this case the deformed bubbles are separated by very thin lamellae, which are separated by channels, so called *Plateau borders*, which are connected at vertices, or nodes, so that a network is formed. It is assumed that almost all the liquid is contained in the Plateau borders, whose cross section is the plane region bounded by three externally tangential circles all of radius r. This deformed triangular-shaped region has the area

$$\mathcal{A} = C^2 r^2, \quad \text{with} \quad C := \left(\sqrt{3} - \pi/2\right)^{1/2}. \tag{5.6}$$

If the radius r changes along the Plateau border, this is related to a pressure difference according to the Young-Laplace law:

$$p_{\text{f}} = p_{\text{b}} - \frac{\gamma_{\text{w}}}{r},$$

where p_{f} and p_{b} are the fluid and bubble pressure, respectively, and γ_{w} is the surface tension of water. The bubble pressure p_{b} is assumed to be constant.

There are three forces acting per volume fraction of the Plateau border:

$$\begin{aligned} &\text{gravity:} && \rho_{\text{f}}\boldsymbol{g}, \\ &\text{dissipation:} && -\frac{C_{\text{PB}}\mu}{\mathcal{A}}\boldsymbol{u} = -\frac{C_{\text{PB}}\mu}{C^2 r^2}\boldsymbol{u}, \\ &\text{capillarity:} && -\nabla p_{\text{f}} = -\frac{\gamma_{\text{w}}}{r^2}\nabla r. \end{aligned}$$

Here, $\boldsymbol{g}$ is the gravity acceleration vector, $\boldsymbol{u}$ the fluid-bubble relative velocity, μ the fluid viscosity, and $C_{\text{PB}}$the dimensionless Plateau border drag coefficient, which can be inferred to be 49.3 from the numerical calculations by Leonard and Lemlich [76]. The value $C_{\text{PB}} = 50$ is

often used in the literature. The sum of the three forces is zero if one neglects inertial forces. Along a Plateau border tilted an angle θ from the vertical z-axis, we place a z_θ-axis with the coordinate relation $z = z_\theta \cos\theta$. The force balance along the z_θ-axis is

$$-\rho_{\mathrm{f}} g \cos\theta - \frac{C_{\mathrm{PB}}\mu}{C^2 r^2} u_\theta - \frac{\gamma_{\mathrm{w}}}{r^2}\partial_{z_\theta} r = 0,$$

where the relative fluid-gas velocity in the channel is $u_\theta = u_{\mathrm{PB}}/\cos\theta$ and u_{PB} is its vertical contribution from one Plateau border of angle θ, which thus is

$$u_{\mathrm{PB}} = -\frac{C^2 r^2}{C_{\mathrm{PB}}\mu}\left(\rho_{\mathrm{f}} g + \frac{\gamma_{\mathrm{w}}}{r^2}\partial_z r\right)\cos^2\theta.$$

Under the assumption of randomly distributed Plateau borders with respect to the angle $0 \le \theta \le \pi$, the likelihood that a Plateau border has an angle in the interval $(\theta, \theta + \mathrm{d}\theta)$ is the area $2\pi \sin\theta\,\mathrm{d}\theta$ of the circular strip of the unit sphere divided by its total area 4π. Since

$$\langle\cos^2\rangle := \int_0^\pi \cos^2\theta \,\frac{2\pi\sin\theta}{4\pi}\mathrm{d}\theta = \frac{1}{3},$$

the relative vertical velocity u is defined as the average vertical relative fluid-gas velocity for many Plateau borders:

$$u = \langle u_{\mathrm{PB}}\rangle = -\frac{C^2 r^2 \rho_{\mathrm{f}} g}{3 C_{\mathrm{PB}}\mu}\left(1 + \frac{\gamma_{\mathrm{w}}}{r^2\rho_{\mathrm{f}} g}\partial_z r\right). \tag{5.7}$$

This velocity can be expressed in $\mathcal{A}$ by (5.6), and substituting the resulting expression into the conservation law $\partial_t \mathcal{A} + \partial_z(\mathcal{A}(1-\varepsilon)u) = 0$ and setting $\varepsilon = 0$ (recall that $v_{\mathrm{f}} = (1-\varepsilon)u$) one obtains the classical drainage equation for low liquid content.

We want an equation for the volume fraction ε, which is equal to $\mathcal{A}$ times the length of Plateau borders per unit volume; cf. [85]. Then the length L and number of such channels should be estimated. Since we also want an equation for all $0 \le \varepsilon \le \varepsilon_{\mathrm{c}}$, the estimation of such numbers becomes difficult since the Plateau borders are only narrow channels for small ε, their lengths are not well defined and the volume and dissipation effect in the nodes varies. [71] presented a relationship between ε, L and r, valid for at least ε up to 0.1. They derived a generalized foam drainage equation which covers the two limiting cases of channel- and node-dominated models, respectively. To remove the variable L, Neethling et al. [90] made the common assumption that for small ε, bubbles can be assumed to have the form of a tetrakaidecahedron (Kelvin cell) and used the equation $4\pi r_{\mathrm{b}}^3/3 = (1-\varepsilon)2^{2/7}L^3$, where r_{b} is the bubble radius. Thereby, they obtained the algebraic equation

$$\varepsilon = 0.3316\left(\frac{r}{r_{\mathrm{b}}}\right)^2(1-\varepsilon)^{2/3} + 0.5402\left(\frac{r}{r_{\mathrm{b}}}\right)^3(1-\varepsilon), \tag{5.8}$$

which is implicit in all its variables. Containing these three variables, they derived a PDE valid for $0 \le \varepsilon \le \varepsilon_{\mathrm{c}}$ by considering dissipation both from the Plateau borders and the nodes. Assuming r_{b} is constant, their PDE and algebraic equation defines the unknowns ε and r.

Stevenson [104] demonstrated that the effective relative fluid-gas velocity u could be very well approximated by a power law of the type (5.5), at least for fluid volume fraction up to $\varepsilon \approx 0.2$. In particular, Stevenson and Stevanov [107] approximated Equation (5.8) by

$$\frac{r}{r_{\mathrm{b}}} = m\varepsilon^{n_{\mathrm{S}}}, \quad \text{with} \quad m = 1.28,\ n_{\mathrm{S}} = 0.46.$$

This equation can be substituted into (5.7) to give

$$u = -v_{\mathrm{drain}}\varepsilon^{2n_{\mathrm{S}}}\big(1 + d_{\mathrm{cap}}\varepsilon^{-(1+n_{\mathrm{S}})}\partial_z\varepsilon\big) \quad \text{for } 0 \le \varepsilon < \varepsilon_{\mathrm{c}}, \tag{5.9}$$

where the drainage velocity v_{drain} (with respect to gravity and dissipation) and the dimensionless capillarity-to-gravity parameter d_{cap} are given by

$$v_{\mathrm{drain}} := \frac{m^2C^2r_{\mathrm{b}}^2\rho_{\mathrm{f}}g}{3C_{\mathrm{PB}}\mu}, \qquad d_{\mathrm{cap}} := \frac{n_{\mathrm{S}}\gamma_{\mathrm{w}}}{mr_{\mathrm{b}}\rho_{\mathrm{f}}g}.$$

The derivative term in (5.9) models the capillarity that is not present for separated bubbles; see (5.5). Hence, we suggest the relative fluid-gas velocity

$$u := -\begin{cases} v_{\mathrm{drain}}\varepsilon^{2n_{\mathrm{S}}}\big(1 + d_{\mathrm{cap}}\varepsilon^{-(1+n_{\mathrm{S}})}\partial_z\varepsilon\big) & \text{for } 0 \le \varepsilon < \varepsilon_{\mathrm{c}}, \\ v_{\mathrm{term}}\varepsilon^{n_{\mathrm{b}}-1} & \text{for } \varepsilon_{\mathrm{c}} \le \varepsilon \le 1 \end{cases}$$

with the compatibility condition (continuity across $\varepsilon = \varepsilon_{\mathrm{c}}$)

$$v_{\mathrm{drain}}\varepsilon_{\mathrm{c}}^{2n_{\mathrm{S}}} = v_{\mathrm{term}}\varepsilon_{\mathrm{c}}^{n_{\mathrm{b}}-1} \quad \Leftrightarrow \quad \frac{v_{\mathrm{drain}}}{v_{\mathrm{term}}} = \varepsilon_{\mathrm{c}}^{n-1-2n_{\mathrm{S}}}. \tag{5.10}$$

Values for n_{b} in the literature range from 2 to 3.2 [38, 54, 91, 111].

Recalling once again that $v_{\mathrm{f}} = (1-\varepsilon)u$, we now define the velocity function

$$\tilde{v}_{\mathrm{f}}(\varepsilon) := \begin{cases} v_{\mathrm{drain}}(1-\varepsilon)\varepsilon^{2n_{\mathrm{S}}} & \text{for } 0 \le \varepsilon < \varepsilon_{\mathrm{c}}, \\ v_{\mathrm{term}}(1-\varepsilon)\varepsilon^{n_{\mathrm{b}}-1} & \text{for } \varepsilon_{\mathrm{c}} \le \varepsilon \le 1 \end{cases}$$

and the diffusion function

$$d_{\mathrm{f}}(\varepsilon) := \begin{cases} v_{\mathrm{drain}}d_{\mathrm{cap}}(1-\varepsilon)\varepsilon^{n_{\mathrm{S}}} & \text{for } 0 \le \varepsilon < \varepsilon_{\mathrm{c}}, \\ 0 & \text{for } \varepsilon_{\mathrm{c}} \le \varepsilon \le 1, \end{cases}$$

so that the liquid flux (in a closed vessel) becomes

$$\varepsilon v_{\mathrm{f}} = \varepsilon(1-\varepsilon)u = -\varepsilon\tilde{v}_{\mathrm{f}}(\varepsilon) - d_{\mathrm{f}}(\varepsilon)\partial_z\varepsilon = -\varepsilon\tilde{v}_{\mathrm{f}}(\varepsilon) - \partial_z\tilde{D}(\varepsilon), \tag{5.11}$$

where the integrated diffusion function is

$$\tilde{D}(\varepsilon) := \int_0^{\varepsilon} d_{\mathrm{f}}(\xi)\,\mathrm{d}\xi = \begin{cases} v_{\mathrm{drain}}d_{\mathrm{cap}}\left(\dfrac{\varepsilon^{n_{\mathrm{S}}+1}}{n_{\mathrm{S}}+1} - \dfrac{\varepsilon^{n_{\mathrm{S}}+2}}{n_{\mathrm{S}}+2}\right) & \text{for } 0 \le \varepsilon < \varepsilon_{\mathrm{c}}, \\ v_{\mathrm{drain}}d_{\mathrm{cap}}\left(\dfrac{\varepsilon_{\mathrm{c}}^{n_{\mathrm{S}}+1}}{n_{\mathrm{S}}+1} - \dfrac{\varepsilon_{\mathrm{c}}^{n_{\mathrm{S}}+2}}{n_{\mathrm{S}}+2}\right) & \text{for } \varepsilon_{\mathrm{c}} \le \varepsilon \le 1. \end{cases}$$

(Notice that $\tilde{D}(\varepsilon)$ is constant, and therefore $\tilde{D}'(\varepsilon) = 0$, for $\varepsilon_{\mathrm{c}} \le \varepsilon \le 1$.) Inserting the expression (5.11) into the conservation law for the fluid phase $\partial_t\varepsilon + \partial_z(\varepsilon v_{\mathrm{f}}) = 0$, we obtain the generalized Equation (5.1) modelling both rising bubbles and drainage of froth in a closed container.

5.3 A model of flotation including froth drainage

5.3.1 Assumption on the tank and mixture

We use a one-dimensional setup of the Reflux Flotation Cell by Dickinson and Galvin [38]; see Figure 5.1. A mixture of slurry and aggregates is fed at the height $z = z_{\mathrm{F}}$ at the volumetric flow $Q_{\mathrm{F}} > 0$ and wash water is injected at the top effluent level $z = z_{\mathrm{E}}$ at $Q_{\mathrm{W}} \geq 0$. At $z = z_{\mathrm{U}}$, a volumetric flow $Q_{\mathrm{U}} \geq 0$ is taken out. In the one-dimensional model on the real line, there are four zones, two inside the vessel plus the underflow and effluent zones. The resulting effluent volumetric overflow $Q_{\mathrm{E}} := Q_{\mathrm{W}} + Q_{\mathrm{F}} - Q_{\mathrm{U}}$ is assumed to be positive so that the mixture is conserved and the vessel is always completely filled. In comparison to the previous treatments [18, 20], here we do not separate the wash water inlet and the effluent level, i.e., $z_{\mathrm{W}} = z_{\mathrm{E}}$. The cross-sectional area is assumed to satisfy

$$A(z) = \begin{cases} A_{\mathrm{E}} & \text{for } z \geq z_{\mathrm{F}}, \\ A_{\mathrm{U}} & \text{for } z < z_{\mathrm{F}}. \end{cases}$$

Particles trapped in the froth region influence the drainage of fluid [3,59], but for simplicity we nevertheless assume that the volume fraction of aggregates (bubbles with attached hydrophobic particles) can be determined as a function of height and time by a single equation. Thus, the suspension in the interstices outside the bubbles is assumed to behave independently of the volume fraction of (hydrophilic) particles. Such particles may however settle within the suspension, which undergoes bulk transport. From now on we denote by $\phi = 1 - \varepsilon$ the volume fraction of aggregates. As a first approximation in a closed vessel, ϕ can be obtained by solving (5.1) for ε and setting $\phi = 1 - \varepsilon$, but we proceed to derive an explicit equation for ϕ since that will be extended to the more complicated model of a flotation column with in- and outlets.

5.3.2 Equation for aggregates with froth drainage in a closed tank

We recall the gas-phase velocity $v = -(1-\phi)u$ and the compatibility condition (5.10), and define

$$\tilde{v}(\phi) := \begin{cases} v_{\mathrm{term}}(1-\phi)^{n_{\mathrm{b}}} & \text{for } 0 \leq \phi \leq \phi_{\mathrm{c}}, \\ v_{\mathrm{drain}}(1-\phi)^{2n_{\mathrm{S}}+1} = v_{\mathrm{term}} \dfrac{(1-\phi)^{2n_{\mathrm{S}}+1}}{(1-\phi_{\mathrm{c}})^{2n_{\mathrm{S}}+1-n_{\mathrm{b}}}} & \text{for } \phi_{\mathrm{c}} < \phi \leq 1, \end{cases} \tag{5.12}$$

$$d(\phi) := \begin{cases} 0 & \text{for } 0 \leq \phi \leq \phi_{\mathrm{c}}, \\ v_{\mathrm{drain}} d_{\mathrm{cap}} \phi (1-\phi)^{n_{\mathrm{S}}} = v_{\mathrm{term}} d_{\mathrm{cap}} \dfrac{\phi(1-\phi)^{n_{\mathrm{S}}}}{(1-\phi_{\mathrm{c}})^{2n_{\mathrm{S}}+1-n_{\mathrm{b}}}} & \text{for } \phi_{\mathrm{c}} < \phi \leq 1. \end{cases} \tag{5.13}$$

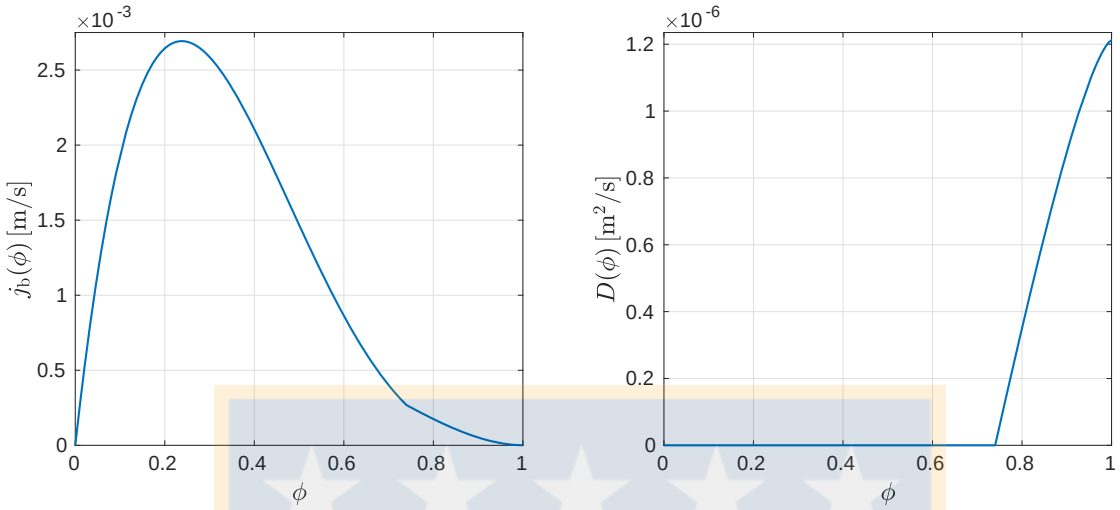

Figure 5.2: Left: function $j_b(\phi) = \phi\tilde{v}(\phi)$. Right: diffusion function $D(\phi)$ modelling capillarity. Note the behaviour of these functions at the critical concentration $\phi_c = 0.74$.

With the batch-drift flux function $j_b(\phi) := \phi\tilde{v}(\phi)$, where $\tilde{v}(\phi)$ is given by (5.12), we can write the aggregate-phase flux (in a closed container) as

$$\phi v = -\phi(1-\phi)u = \phi\tilde{v}(\phi) + d(\phi)\partial_z(1-\phi) = \phi\tilde{v}(\phi) - d(\phi)\partial_z\phi = j_b(\phi) - \partial_z D(\phi),$$

where $D(\phi)$ is defined by (5.3). In light of (5.13) we obtain

$$D(\phi) = \begin{cases} 0 & \text{for } 0 \le \phi \le \phi_c, \\ v_{\text{drain}} d_{\text{cap}} \dfrac{\omega(\phi_c) - \omega(\phi)}{(n_S+1)(n_S+2)} & \text{for } \phi_c < \phi \le 1, \end{cases} \tag{5.14}$$

where $\omega(\phi) := (1-\phi)^{n_S+1}((n_S+1)\phi+1)$ and we reconfirm the property (5.4). The conservation law $\partial_t\phi + \partial_z(\phi v) = 0$ now yields the following equation for the volume fraction $\phi = \phi(z,t) \in [0,1]$ of aggregates in a closed vessel:

$$\partial_t\phi + \partial_z j_b(\phi) = \partial_z^2 D(\phi). \tag{5.15}$$

The graphs of the constitutive functions $j_b(\phi)$ and $D(\phi)$ are drawn in Figure 5.2.

5.3.3 Three phases and constitutive assumptions

The three phases and their volume fractions are the fluid ϕ_f, the solids ψ, and the aggregates ϕ, where $\phi_f + \psi + \phi = 1$. By suspension we mean the fluid and solid phases. The volume fraction of solids *within the suspension* φ is defined by

$$\varphi := \frac{\psi}{\psi + \phi_f} = \frac{\psi}{1-\phi}.$$

The drift-flux and solids-flux theories utilize constitutive functions for the aggregate upward batch flux $j_{\mathrm{b}}(\phi)$ and the solids batch sedimentation flux $f_{\mathrm{b}}(\varphi) := \varphi v_{\mathrm{hs}}(\varphi)$, where $v_{\mathrm{hs}}(\varphi)$ is the hindered-settling function. For simplicity, we employ the common expression [98]

$$v_{\mathrm{hs}}(\varphi) = v_\infty(1-\varphi)^{n_{\mathrm{RZ}}}, \quad \text{where } n_{\mathrm{RZ}} > 1. \tag{5.16}$$

Applying the conservation of mass to each of the three phases, introducing the volume-average velocity, or bulk velocity, of the mixture q and the relative velocities of both the aggregate-suspension and the solid-fluid, Bürger et al. [18] derived the PDE model (5.2) without the capillarity function $D(\phi)$. In particular, the volumetric flows in and out of the flotation column define explicitly

$$q(z,t) := \begin{cases} q_{\mathrm{E}} := (-Q_{\mathrm{U}} + Q_{\mathrm{F}} + Q_{\mathrm{W}})/A_{\mathrm{E}} & \text{for } z \geq z_{\mathrm{E}}, \\ q_2 := (-Q_{\mathrm{U}} + Q_{\mathrm{F}})/A_{\mathrm{E}} & \text{for } z_{\mathrm{F}} \leq z < z_{\mathrm{E}}, \\ q_1 = q_{\mathrm{U}} := -Q_{\mathrm{U}}/A_{\mathrm{U}} & \text{for } z < z_{\mathrm{F}}. \end{cases} \tag{5.17}$$

In the underflow and effluent zones all phases are assumed to have the same velocity, i.e., they follow the bulk flow. Then the total convective fluxes for ϕ and φ are given by

$$J(\phi,z,t) = \begin{cases} j_{\mathrm{E}}(\phi,t) := q_{\mathrm{E}}(t)\phi & \text{for } z \geq z_{\mathrm{E}}, \\ j_2(\phi,t) := q_2(t)\phi + j_{\mathrm{b}}(\phi) & \text{for } z_{\mathrm{F}} \leq z < z_{\mathrm{E}}, \\ j_1(\phi,t) := q_1(t)\phi + j_{\mathrm{b}}(\phi) & \text{for } z_{\mathrm{U}} \leq z < z_{\mathrm{F}}, \\ j_{\mathrm{U}}(\phi,t) := q_1(t)\phi & \text{for } z < z_{\mathrm{U}}, \end{cases}$$

$$F(\varphi,\phi,z,t) = \begin{cases} f_{\mathrm{E}}(\varphi,\phi,t) := -(1-\phi)q_{\mathrm{E}}(t)\varphi & \text{for } z \geq z_{\mathrm{E}}, \\ f_2(\varphi,\phi,t) & \text{for } z_{\mathrm{F}} \leq z < z_{\mathrm{E}}, \\ f_1(\varphi,\phi,t) & \text{for } z_{\mathrm{U}} \leq z < z_{\mathrm{F}}, \\ f_{\mathrm{U}}(\varphi,\phi,t) := -(1-\phi)q_1(t)\varphi & \text{for } z < z_{\mathrm{U}} \end{cases}$$

with the zone-settling flux functions (positive in the direction of sedimentation (decreasing z))

$$\begin{aligned} f_k(\varphi,\phi,t) &:= (1-\phi)f_{\mathrm{b}}(\varphi) + \big(j_{\mathrm{b}}(\phi) - (1-\phi)q_k(t)\big)\varphi \\ &= (1-\phi)f_{\mathrm{b}}(\varphi) + \big(j_k(\phi,t) - q_k(t)\big)\varphi, \quad k = 1,2. \end{aligned}$$

With the capillarity function $D(\phi)$, the batch flux $j_{\mathrm{b}}(\phi)$ is extended to $j_{\mathrm{b}}(\phi) - \partial_z D(\phi)$; cf. (5.15). Hence, the total flux of the aggregates for any $z \in \mathbb{R}$ is

$$\Phi(\phi, \partial_z\phi, z, t) := J(\phi,z,t) - \gamma(z)\partial_z D(\phi),$$

where the characteristic function is

$$\gamma(z) := \begin{cases} 1 & \text{for } z \in [z_{\mathrm{U}}, z_{\mathrm{E}}), \\ 0 & \text{for } z \notin [z_{\mathrm{U}}, z_{\mathrm{E}}), \end{cases}$$

and the total flux of the solids in the z-direction is (F and $\tilde{F}$ are positive in the downwards direction of sedimentation, which is opposite to the z-direction)

$$\Psi(\psi, \partial_z\psi, \phi, z, t) := -\tilde{F}(\psi, \phi, z, t) + \gamma(z)\frac{\psi}{1-\phi}\partial_z D(\phi), \tag{5.18}$$

where

$$\tilde{F}(\psi, \phi, z, t) := \begin{cases} F\left(\dfrac{\psi}{1-\phi}, \phi, z, t\right) & \text{if } 0 \le \phi < 1, \\ 0 & \text{if } \phi = 1. \end{cases}$$

The conservation law applied on the two phases with the total fluxes Φ and Ψ yields the governing system of equations (5.2) in the case capillarity are included. That system defines solutions on the real line and next we define the outlet concentrations of the flotation column.

5.3.4 Outlet concentrations

Given the PDE solutions $\phi = \phi(z,t)$ and $\varphi = \varphi(z,t)$ of (5.2), we define the boundary concentrations at each in- or outlet by $\phi_{\mathrm{U}}^{\pm} = \phi_{\mathrm{U}}^{\pm}(t) := \phi(z_{\mathrm{U}}^{\pm}, t)$, etc. Conservation of mass across $z = z_{\mathrm{U}}$ yields

$$j_1(\phi_{\mathrm{U}}^{+}, t) - \partial_z D(\phi)|_{z=z_{\mathrm{U}}^{+}} = j_{\mathrm{U}}(\phi_{\mathrm{U}}^{-}, t), \tag{5.19}$$

$$f_1(\varphi_{\mathrm{U}}^{+}, t) - \varphi_{\mathrm{U}}^{+}\,\partial_z D(\phi)|_{z=z_{\mathrm{U}}^{+}} = f_{\mathrm{U}}(\varphi_{\mathrm{U}}^{-}, t). \tag{5.20}$$

The underflow concentrations of the flotation column are defined by $\phi_{\mathrm{U}}(t) := \phi_{\mathrm{U}}^{-}(t)$ and $\varphi_{\mathrm{U}}(t) := \varphi_{\mathrm{U}}^{-}(t)$. These concentrations can in fact be obtained from the solution inside the column ($z_{\mathrm{U}} < z < z_{\mathrm{E}}$) from (5.19) and (5.20) together with a uniqueness condition; see [45].

For the effluent level $z = z_{\mathrm{E}}$, the analogous situation holds:

$$j_2(\phi_{\mathrm{E}}^{-}, t) - \partial_z D(\phi)|_{z=z_{\mathrm{E}}^{-}} = j_{\mathrm{E}}(\phi_{\mathrm{E}}^{+}, t), \tag{5.21}$$

$$f_2(\varphi_{\mathrm{E}}^{-}, \phi_{\mathrm{E}}^{-}, t) - \varphi_{\mathrm{E}}^{-}\,\partial_z D(\phi)|_{z=z_{\mathrm{E}}^{-}} = f_{\mathrm{E}}(\varphi_{\mathrm{E}}^{+}, \phi_{\mathrm{E}}^{+}, t), \tag{5.22}$$

In the one-dimensional PDE model (5.2) without boundary conditions, the solution $\phi = \phi(z,t)$ (analogously for φ) in the interval $z > z_{\mathrm{E}}$ is governed by the linear transport PDE $\partial_t\phi + (Q_{\mathrm{E}}/A_{\mathrm{E}})\partial_z\phi = 0$ and the boundary value $\phi_{\mathrm{E}}^{+}(t)$. The effluent outlet concentrations are defined by $\phi_{\mathrm{E}} := \phi_{\mathrm{E}}^{+}$ and $\varphi_{\mathrm{E}} := \varphi_{\mathrm{E}}^{+}$. In the concluding section, we discuss how bursting bubbles at the top can be incorporated in the model.

5.4 Steady-state analysis

5.4.1 Definition of a desired steady state

In the case of no capillarity, Bürger et al. in [18] provided detailed constructions of all steady states, and Bürger et al. [20, 28] sorted out the most interesting steady states for the applications and how to control these by letting the volumetric flows satisfy certain nonlinear inequalities, which can be visualized in so-called operating charts. We assume that Q_{F}, ϕ_{F}, andψ_{F} are given variables and that Q_{U} and Q_{W} are control variables. The purpose here is to provide an improved model of the froth region and we therefore focus on the steady states when a layer of froth in zone 2 is possible. We consider only solutions where the froth layer does not fill the entire zone 2, so that there is at least a small region above the feed inlet with aggregate volume fraction below the critical one. As mentioned before, it is assumed that the wash water is sprinkled at the top of the column, which is commonly done and gives fewer steady states to analyse. A *desired steady state* is defined to be a stationary solution that has

$$\begin{aligned} &\text{no aggregates below the feed level} && \Rightarrow \quad \phi_{\mathrm{U}} = 0, \\ &\text{no solids above the feed level} && \Rightarrow \quad \varphi_{\mathrm{E}} = 0, \\ &\text{a froth layer that does not fill the entire zone 2} && \Rightarrow \quad \phi(z_{\mathrm{F}}^{+}) < \phi_{\mathrm{c}}. \end{aligned} \tag{5.23}$$

The reversed implications do not hold in the two first statements for the following reasons. Since the bulk flow in zone 1 is directed downwards, there exist steady-state solutions with a standing layer of aggregates below the feed level. Analogously, if the bulk flow in zone 2 is directed upwards, there may be a layer of standing solids when their settling velocity is balanced by the upward bulk velocity; see [18].

5.4.2 Properties of the batch-flux density functions

With $\tilde{v}$ given by (5.12), the continuous batch-drift flux function is

$$j_{\mathrm{b}}(\phi) := \phi\tilde{v}(\phi) = \begin{cases} j_{\mathrm{bl}}(\phi) := \phi v_{\mathrm{term}}(1-\phi)^{n_{\mathrm{b}}} & \text{for } 0 \le \phi \le \phi_{\mathrm{c}}, \\ j_{\mathrm{bh}}(\phi) := \phi v_{\mathrm{term}} \dfrac{(1-\phi)^{2n_{\mathrm{S}}+1}}{(1-\phi_{\mathrm{c}})^{2n_{\mathrm{S}}+1-n_{\mathrm{b}}}} & \text{for } \phi_{\mathrm{c}} < \phi \le 1, \end{cases}$$

where we have introduced the low j_{bl} and high j_{bh} parts of it. Any function $u \mapsto u(1-u)^n$ has a unique inflection point at $u_{\mathrm{infl}} = 2/(n+1)$. Figure 5.3 shows the inflection points

$$\phi_{\mathrm{infl,l}}(n_{\mathrm{b}}) = \frac{2}{n_{\mathrm{b}}+1}, \qquad \phi_{\mathrm{infl,h}}(n_{\mathrm{S}}) = \frac{2}{2n_{\mathrm{S}}+1+1} = \frac{1}{n_{\mathrm{S}}+1}$$

of j_{bl} and j_{bh}, as functions of the exponents n and n_{S}, respectively. With the values $\phi_{\mathrm{c}} = 0.74$ and $n_{\mathrm{S}} = 0.46$ suggested in the literature (see Section 5.2), and the interval $2 \le n_{\mathrm{b}} \le 3.2$, there

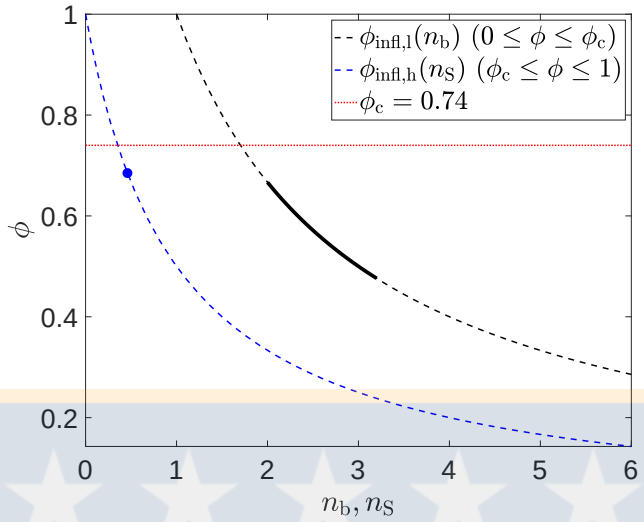

Figure 5.3: Evolution of the inflection points of j_{bl} and j_{bh}. The literature values $2 \le n_\mathrm{b} \le 3.2$ give an interval (solid black) of possible $\phi_{\mathrm{infl,l}}$ that lie entirely below $\phi_\mathrm{c} = 0.74$ (red line). With $n_\mathrm{S} = 0.46$, the inflection point (blue dot) $\phi_{\mathrm{infl,h}} = 1/(n_\mathrm{S}+1) \approx 0.685 < \phi_\mathrm{c}$; hence, j_{bh} is strictly convex for $\phi \ge \phi_\mathrm{c}$.

is only one inflection point of j_b in $0 \le \phi \le 1$ and this lies below ϕ_c; see Figure 5.4, which also shows that there may be a jump in the derivative of j_b at $\phi = \phi_\mathrm{c}$. Since

$$j_\mathrm{b}'(\phi) = \begin{cases} v_{\mathrm{term}}(1-\phi)^{n_\mathrm{b}-1}(1-(1+n_\mathrm{b})\phi) & \text{for } 0 < \phi < \phi_\mathrm{c}, \\ v_{\mathrm{term}}\dfrac{(1-\phi)^{2n_\mathrm{S}}(1-(2+2n_\mathrm{S})\phi)}{(1-\phi_\mathrm{c})^{2n_\mathrm{S}+1-n_\mathrm{b}}} & \text{for } \phi_\mathrm{c} < \phi < 1, \end{cases}$$

we get that

$$j_\mathrm{b}'(\phi_\mathrm{c}^-) \le j_\mathrm{b}'(\phi_\mathrm{c}^+) \quad \Leftrightarrow \quad n_\mathrm{b} \ge 1 + 2n_\mathrm{S} \approx 1.92. \tag{5.24}$$

When this is satisfied, the exponent in the compatibility condition (5.10) is nonnegative and the entire j_b has only one inflection point $\phi_{\mathrm{infl}} = \phi_{\mathrm{infl,l}} \in (0, \phi_\mathrm{c})$.

5.4.3 Properties of the zone flux functions

The zone flux functions j_k, $f_k(\cdot, \phi)$, $k = 1, 2$, have an additional linear term due to the bulk velocity of the zone. Let $j(\phi) = j_\mathrm{b}(\phi) + q\phi$ denote a general zone flux function, where we drop the t-variable when considering steady states. We will sometimes write out the dependence on q; $j(\phi; q)$. The inflection point ϕ_{infl} of j is independent of q, however, the local maximum $\phi^\mathrm{M} = \phi^\mathrm{M}(q) < \phi_\mathrm{c}$ depends on q. To provide an explicit definition, we first define

$$q_{\mathrm{neg}} := -j_\mathrm{b}'(0), \qquad \bar{\bar{q}} := -j_\mathrm{b}'(\phi_{\mathrm{infl}}).$$

For $q \le q_{\mathrm{neg}}$, $j(\cdot, q)$ is decreasing and for $q \ge \bar{\bar{q}}$, $j(\cdot, q)$ is increasing. For intermediate values of q, the local maximum exists and satisfies $0 = j'(\phi^\mathrm{M}) = j_\mathrm{b}'(\phi^\mathrm{M}) + q$. Since the restriction

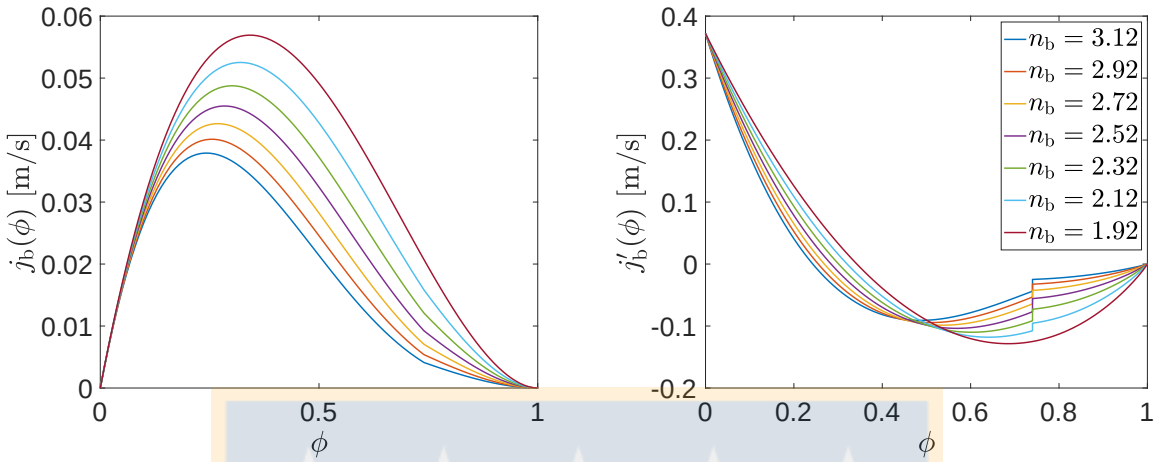

Figure 5.4: Plots of $j_b(\phi)$ (left) and $j_b'(\phi)$ (right) for $n_S = 0.46$, $v_{term} = 0.3718$ and various values of n_b that satisfy (5.24).

$(j_b|_{(0,\phi_{infl})})'$ is a strictly decreasing function, we can define

$$\phi^M = \phi^M(q) := \begin{cases} 0 & \text{if } q \le q_{neg}, \\ ((j_b|_{(0,\phi_{infl})})')^{-1}(-q) & \text{if } q_{neg} < q < \bar{\bar{q}}, \\ \phi_{infl} & \text{if } q \ge \bar{\bar{q}}. \end{cases}$$

For $q_{neg} < q < 0$, there is a zero of $j(\cdot; q)$ which we denote by $\phi_Z = \phi_Z(q) \in (0, 1)$. For a specific zone flux functions j_k, we use the notation $\phi_k^M = \phi^M(q_k)$ and $\phi_{kZ} = \phi_M(q_k)$.

In a similar way, one can define the local minimum point, greater than the inflection point, for $0 \le q < \bar{\bar{q}}$. We denote it by $\phi_{kM} = \phi_M(q_k)$. For $q \ge \bar{\bar{q}}$, we define $\phi_{kM}(q) := \phi_{infl}$. Furthermore, for a given ϕ_{kM}, we define ϕ_{km} as the unique value that satisfies

$$j_k(\phi_{km}; q) = j_k(\phi_{kM}; q), \qquad 0 \le \phi_{km} \le \phi_{infl}. \tag{5.25}$$

Analogous definitions can be made for the flux functions $f_k(\cdot, \phi, t)$, $k = 1, 2$.

5.4.4 Construction of steady states

We seek piecewise smooth and piecewise monotone steady-state solutions $\phi = \phi(z)$ of (5.2). Such solutions may contain jump discontinuities within or between the zones. In the case $D \equiv 0$, Bürger et al. [18] outlined the details on how to construct unique steady-state solutions and we will not go through the entire machinery here. The basic idea is to glue together solutions within each zone in a unique way so that the conservation of mass holds across the zone borders. Two such so-called Rankine-Hugoniot conditions (jump conditions) are (5.21) and (5.22). Since each such equation has two unknowns; for example, ϕ_E^- and ϕ_E^+ in (5.21), another so-called entropy condition in the theory of degenerate parabolic PDEs with spatially discontinuous coefficients

is needed to establish a unique pair of boundary values [45]. Furthermore, as the values ϕ_{E}^{-} and ϕ_{E}^{+} are obtained, these are substituted into (5.22) and a similar procedure yields φ_{E}^{-} and φ_{E}^{+}.

The new ingredient due to the drainage is the term $\partial_z D(\phi)|_{z=z_{\mathrm{E}}^{-}}$ in (5.21) and (5.22). The property (5.4) implies the following (see [45, 52] for further details). A discontinuity of the solution $\phi(\cdot,t)$, within or between zones, is possible only between two values in the interval $0 \le \phi \le \phi_{\mathrm{c}}$. Furthermore, since we are seeking piecewise smooth and piecewise monotone steady-state solutions, the fact $d(\phi) > 0$ implies that if one of the values of the discontinuity is ϕ_{c}, this must be the larger value and located on the right; i.e., the left value of the jump $\phi^{-} < \phi_{\mathrm{c}}$. Furthermore, $j_2(\phi) \ge j_2(\phi_{\mathrm{c}})$ for $\phi^{-} \le \phi \le \phi_{\mathrm{c}}$, and in a right neighbourhood of the jump, $\phi'(z) \ge 0$.

With these facts in mind, we now construct steady-state solutions. Let $H(z)$ denote the Heaviside function and assume that all volumetric flows and feed volume fractions are time independent. A stationary solution $\phi = \phi(z)$ of (5.2) satisfies, in the weak sense,

$$\frac{\mathrm{d}}{\mathrm{d}z}\left(A(z)\left(J(\phi,z) - \gamma(z)\frac{\mathrm{d}D(\phi)}{\mathrm{d}z}\right) - Q_{\mathrm{F}}\phi_{\mathrm{F}}H(z-z_{\mathrm{F}})\right) = 0, \quad z \in \mathbb{R}.$$

Integrating this identity with respect to z yields

$$A(z)\big(J(\phi,z) - \gamma(z)d(\phi)\phi'(z)\big) - Q_{\mathrm{F}}\phi_{\mathrm{F}}H(z-z_{\mathrm{F}}) = \mathcal{M}, \quad z \in \mathbb{R}, \tag{5.26}$$

where the constant mass flux $\mathcal{M}$ can be determined by setting z to a value either less than z_{U} or greater than z_{E}; then one gets

$$\begin{aligned} \mathcal{M} &= A_{\mathrm{U}} j_{\mathrm{U}}(\phi_{\mathrm{U}}) = -Q_{\mathrm{U}}\phi_{\mathrm{U}}, \\ \mathcal{M} &= A_{\mathrm{E}} j_{\mathrm{E}}(\phi_{\mathrm{E}}) - Q_{\mathrm{F}}\phi_{\mathrm{F}} =: \mathcal{M}_{\mathrm{E}} - Q_{\mathrm{F}}\phi_{\mathrm{F}}, \end{aligned}$$

where the effluent constant mass flux of aggregates $\mathcal{M}_{\mathrm{E}} := A_{\mathrm{E}} j_{\mathrm{E}}(\phi_{\mathrm{E}}) = Q_{\mathrm{E}}\phi_{\mathrm{E}}$ is also the constant mass flux above the feed inlet. For a desired steady state satisfying (5.23), we have $\phi_{\mathrm{U}} = 0$; hence, $\mathcal{M} = 0$ and the feed mass flux equals the effluent:

$$\phi_{\mathrm{U}} = 0 \quad \Leftrightarrow \quad Q_{\mathrm{F}}\phi_{\mathrm{F}} = \mathcal{M}_{\mathrm{E}}.$$

It is convenient to define the feed mass flux per area unit by

$$s_{\mathrm{F}} := \frac{Q_{\mathrm{F}}\phi_{\mathrm{F}}}{A_{\mathrm{E}}}. \tag{5.27}$$

With z in zone 2, (5.26) gives $\mathcal{M} = A_{\mathrm{E}}(j_2(\phi) - D(\phi)') - Q_{\mathrm{F}}\phi_{\mathrm{F}}$, which with $\mathcal{M} = 0$ and (5.27) implies that the solution ϕ in zone 2 satisfies

$$\begin{aligned} j_2(\phi) - d(\phi)\phi'(z) &= s_{\mathrm{F}}, \quad z_{\mathrm{F}} < z < z_{\mathrm{E}}, \\ s_{\mathrm{F}} &= q_{\mathrm{E}}\phi_{\mathrm{E}}. \end{aligned} \tag{5.28}$$

The boundary condition in (5.28) also implies that ϕ_{E} can be expressed in terms of given and control variables (recall that $Q_{\mathrm{E}} > 0$):

$$\phi_{\mathrm{E}} = \frac{A_{\mathrm{E}} s_{\mathrm{F}}}{Q_{\mathrm{E}}} = \frac{Q_{\mathrm{F}} \phi_{\mathrm{F}}}{Q_{\mathrm{W}} + Q_{\mathrm{F}} - Q_{\mathrm{U}}}. \tag{5.29}$$

Since we require that there be no aggregates in zone 1, the steady-state solution there is zero. For any jump across $z = z_{\mathrm{F}}$ from this zero volume fraction to any larger value $\bar{\phi}_2$, from which there should be a discontinuity in zone 2 at $z = z_{\mathrm{fr}}$, the bottom of the froth layer, the uniqueness condition [45] implies that $\bar{\phi}_2$ has to lie on an increasing part of $j_2(\cdot; q_2)$. This corresponds to cases (a) and (c) in [18, Section 3.2]. The latter case can only occur under special circumstances with a large $\bar{\phi}_2 > \phi_{2\mathrm{M}}$ (see definition in Section 5.4.3). Any small disturbance in a volumetric flow will make the case impossible and we therefore ignore that case. Consequently, we consider only $\bar{\phi}_2 \in [0, \phi_2^{\mathrm{M}}]$. Then $\bar{\phi}_2$ is the smallest positive solution of the jump condition equation at the feed level, namely

$$s_{\mathrm{F}} = j_2(\phi; q_2), \tag{FJC}$$

under the conditions [18]

$$s_{\mathrm{F}} \le j_2\big(\phi_2^{\mathrm{M}}; q_2\big), \tag{FIa}$$
$$\bar{\phi}_2 \le \phi_{1\mathrm{Z}}, \tag{FIb}$$

where ϕ_2^{M} and $\phi_{1\mathrm{Z}}$ are defined in Section 5.4.3. By the properties of j_2, we have $\phi_2^{\mathrm{M}} \le \phi_{\mathrm{infl}} < \phi_{\mathrm{c}}$. Therefore, $\bar{\phi}_2 < \phi_2^{\mathrm{M}} < \phi_{\mathrm{c}}$. Then $d(\bar{\phi}_2) = 0$, and the equation in (5.28) reduces to (FJC). Again with reference to [45] and without going into details, we claim that the solution in zone 2 is

$$\phi_2(z) = \begin{cases} \bar{\phi}_2, & z_{\mathrm{F}} < z < z_{\mathrm{E}}, \qquad \text{if } \phi_{\mathrm{E}} \le \phi_{\mathrm{c}}, \\ \begin{cases} \bar{\phi}_2, & z_{\mathrm{F}} < z < z_{\mathrm{fr}}, \\ \phi_{2\mathrm{par}}(z), & z_{\mathrm{fr}} < z \le z_{\mathrm{E}}, \end{cases} & \text{if } \phi_{\mathrm{E}} > \phi_{\mathrm{c}} \text{ and } z_{\mathrm{fr}} > z_{\mathrm{F}}, \end{cases} \tag{5.30}$$

where $\phi_{2\mathrm{par}}(z)$ is the strictly increasing solution of the ordinary differential equation (see (5.28)):

$$\begin{aligned} \phi'(z) &= \frac{j_2(\phi; q_2) - s_{\mathrm{F}}}{d(\phi)}, \\ \phi(z_{\mathrm{fr}}) &= \phi_{\mathrm{c}}, \quad \phi(z_{\mathrm{E}}) = \phi_{\mathrm{E}}, \end{aligned} \tag{5.31}$$

and where z_{fr} is the unknown location of the pulp-froth interface $\phi = \phi_{\mathrm{c}}$, which depends on s_{F} and ϕ_{E}.

See Figure 5.5 for illustrations of some steady-state solutions in zone 2. In (5.30) lies the fact that if $\phi_{\mathrm{E}} > \phi_{\mathrm{c}}$, then there is no discontinuity at $z = z_{\mathrm{E}}$, so that $\phi_{2\mathrm{par}}(z_{\mathrm{E}}^-) = \phi_{\mathrm{E}}^- = \phi_{\mathrm{E}}^+ = \phi_{\mathrm{E}}$. The boundary value problem (5.31) defines a function Z_{fr} via

$$z_{\mathrm{fr}} = Z_{\mathrm{fr}}(\phi_{\mathrm{F}}, Q_{\mathrm{F}}, Q_{\mathrm{U}}, Q_{\mathrm{W}}).$$

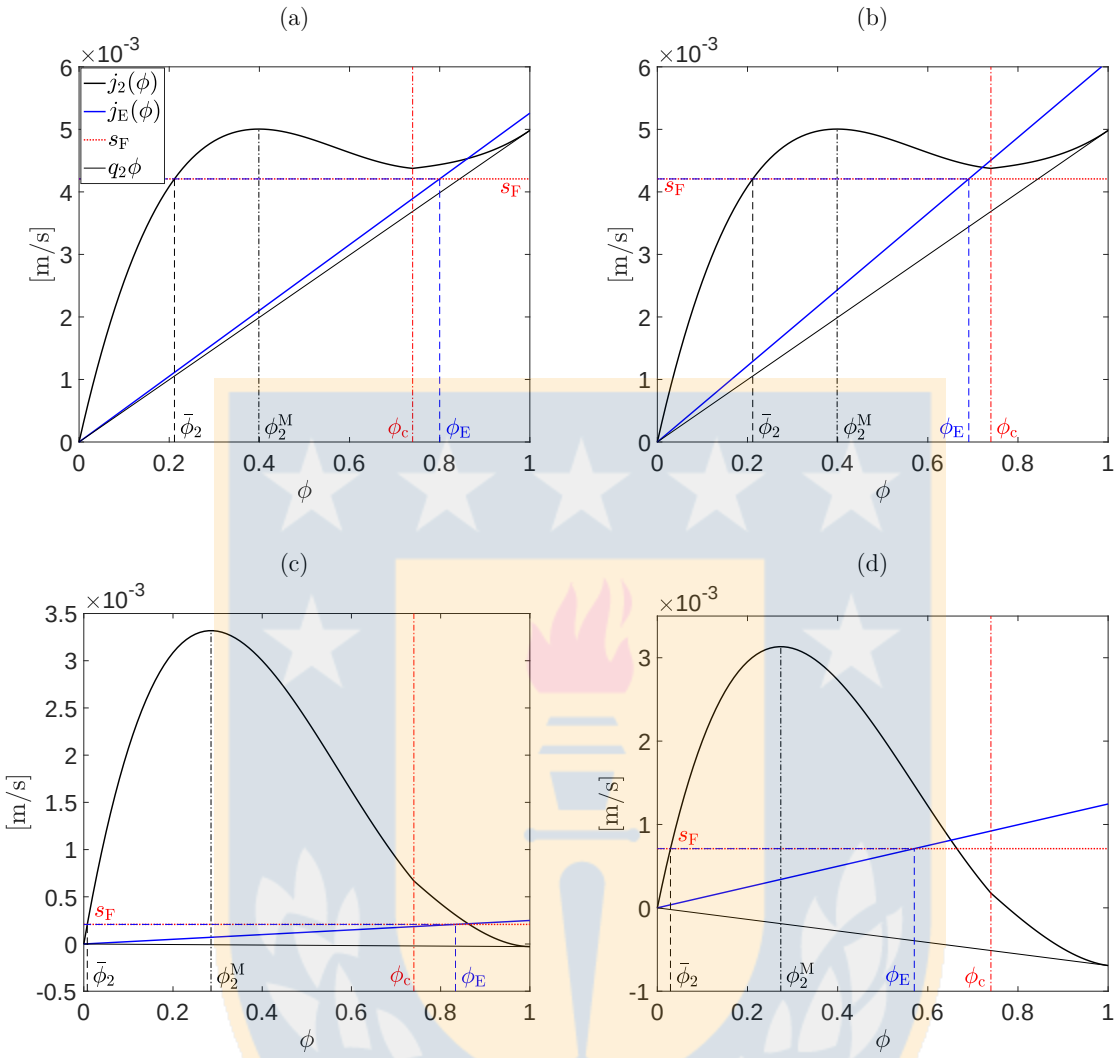

Figure 5.5: Possible steady-state values for zone 2 with (a, b) $q_2 > 0$ and (c, d) $q_2 < 0$. The case $\phi_E > \phi_c$ is shown in (a) and (c), where there is a continuously increasing solution $\phi_{par}(z) \in (\phi_c, \phi_E)$, while $\phi_E \leq \phi_c$ in (b) and (d), where the solution in zone 2 is the constant $\bar{\phi}_2$. For all the cases, we have $\phi_c = 0.74$, $n_b = 2.5$ and $n_S = 0.46$. For (a) and (b), $Q_2 := q_2 A_E = 3.6 \times 10^{-5} \mathrm{m}^3/\mathrm{s}$, $s_F = 4.21 \times 10^{-3}\,\mathrm{m/s}$ and (a) $Q_W = 2 \times 10^{-6}\,\mathrm{m}^3/\mathrm{s}$, (b) $Q_W = 8 \times 10^{-6}\,\mathrm{m}^3/\mathrm{s}$. For (c) we let $Q_2 = -2 \times 10^{-6}\,\mathrm{m}^3/\mathrm{s}$, $Q_W = 2 \times 10^{-6}\,\mathrm{m}^3/\mathrm{s}$ and $s_F = 2.07 \times 10^{-4}\,\mathrm{m/s}$, while for (d) we used $Q_2 = -5 \times 10^{-6}\,\mathrm{m}^3/\mathrm{s}$, $Q_W = 10^{-5} \mathrm{m}^3/\mathrm{s}$ and $s_F = 7.1 \times 10^{-4}\,\mathrm{m/s}$.

In light of (5.29) and (5.30), necessary conditions for a steady-state solution with a froth region are the inequalities

$$\phi_c < \phi_E \leq 1 \quad \Leftrightarrow \quad Q_F \left(1 - \frac{\phi_F}{\phi_c}\right) < Q_U - Q_W \leq Q_F(1 - \phi_F), \tag{Froth1}$$

$$z_F < Z_{fr}(\phi_F, Q_F, Q_U, Q_W) \tag{Froth2}$$

that should be satisfied for a steady-state solution with a froth-pulp interface in zone 2. The

requirement that $\phi_{2\mathrm{par}}(z)$ is strictly increasing from ϕ_{c} to ϕ_{E} means that the left inequality of (Froth1) is equivalent to $Z_{\mathrm{fr}}(\phi_{\mathrm{F}}, Q_{\mathrm{F}}, Q_{\mathrm{U}}, Q_{\mathrm{W}}) < z_{\mathrm{E}}$; hence, the latter inequality need not be invoked.

That $\phi_{2\mathrm{par}}(z)$ is strictly increasing, required by the entropy condition in [45], means that the right-hand side of (5.31) is positive in the interval $[\phi_{\mathrm{c}}, \phi_{\mathrm{E}})$. Furthermore, a discontinuity at $z = z_{\mathrm{fr}}$ from $\bar{\phi}_2$ up to ϕ_{c} can only occur (according to the entropy condition) if the graph of $j_2(\cdot; q_2)$ lies above s_{F} in the interval $(\bar{\phi}_2, \phi_{\mathrm{c}})$. These conditions imply (FIa), which we can abandon. The properties of $j_2(\cdot, ; q_2)$ (see Section 5.4.3) imply that we can write these necessary conditions for a solution with a froth region:

$$s_{\mathrm{F}} < j_2(\phi; q_2) \quad \text{for all } \phi \in (\phi_2^{\mathrm{M}}, \phi_{\mathrm{E}}) \quad \Leftrightarrow \quad s_{\mathrm{F}} \begin{cases} < j_2(\phi_{2\mathrm{M}}; q_2) & \text{if } \phi_{2\mathrm{M}} < \phi_{\mathrm{E}}, \\ \leq j_2(\phi_{\mathrm{E}}; q_2) & \text{if } \phi_{2\mathrm{M}} \geq \phi_{\mathrm{E}}, \end{cases} \tag{Froth3}$$

where equality holds if and only if $\phi_{2\mathrm{M}} = \phi_{\mathrm{E}}$.

5.4.5 Desired steady states and operating charts

From the derivation above concerning the aggregates and from the treatment in [18] concerning the solids, we here summarize the *desired steady states* that satisfy (5.23):

$$\phi_{\mathrm{SS}}(z) = \begin{cases} 0 & \text{for } z_{\mathrm{U}} < z < z_{\mathrm{F}}, \\ \bar{\phi}_2 & \text{for } z_{\mathrm{F}} < z < z_{\mathrm{fr}}, \\ \phi_{2\mathrm{par}}(z) & \text{for } z_{\mathrm{fr}} < z < z_{\mathrm{E}}, \\ \phi_{\mathrm{E}} & \text{for } z > z_{\mathrm{E}}, \end{cases} \tag{5.32}$$

$$\varphi_{\mathrm{SS}}(z) = \begin{cases} 0 & \text{for } z > z_{\mathrm{F}}, \\ \varphi_1 \in [0, \varphi_{1\mathrm{m}}] & \text{for } z_{\mathrm{U}} < z < z_{\mathrm{F}}, \\ \varphi_{\mathrm{U}} = \varphi_1 + A_{\mathrm{U}} f_{\mathrm{b}}(\varphi_1)/Q_{\mathrm{U}} & \text{for } z < z_{\mathrm{U}}. \end{cases} \tag{5.33}$$

Here, $\phi_{2\mathrm{par}}(z)$ is the solution of the ODE problem (5.31), ϕ_{E} is given by (5.29), $\varphi_{1\mathrm{m}}$ is given by (5.25) and $\varphi_1 > 0$ satisfies the jump condition at the feed level $z = z_{\mathrm{F}}$ (φ_1 is unique if condition (FIas) below holds; see [18])

$$Q_{\mathrm{F}} \psi_{\mathrm{F}} = A_{\mathrm{U}} f_1(\varphi_1, 0; q_1). \tag{FJCs}$$

In Figure 5.6, we have represented some examples of desired steady states with different values of z_{fr} obtained by fixing the values of the parameters ϕ_{F}, ψ_{F}, Q_{F} and Q_{W} and choosing different values for Q_{U}. As it can be seen, the location of z_{fr} is very sensitive to the choice of Q_{U}. For instance, it changes from $z_{\mathrm{fr}} = 0.8027\,\mathrm{m}$ in (c) to $z_{\mathrm{fr}} = 0.7081\,\mathrm{m}$ in (d) with a small variation in Q_{U} of $-1.6 \times 10^{-8}\,\mathrm{m}^3/\mathrm{s}$. We now collect the conditions for obtaining a desired steady state in terms of the input and control variables.

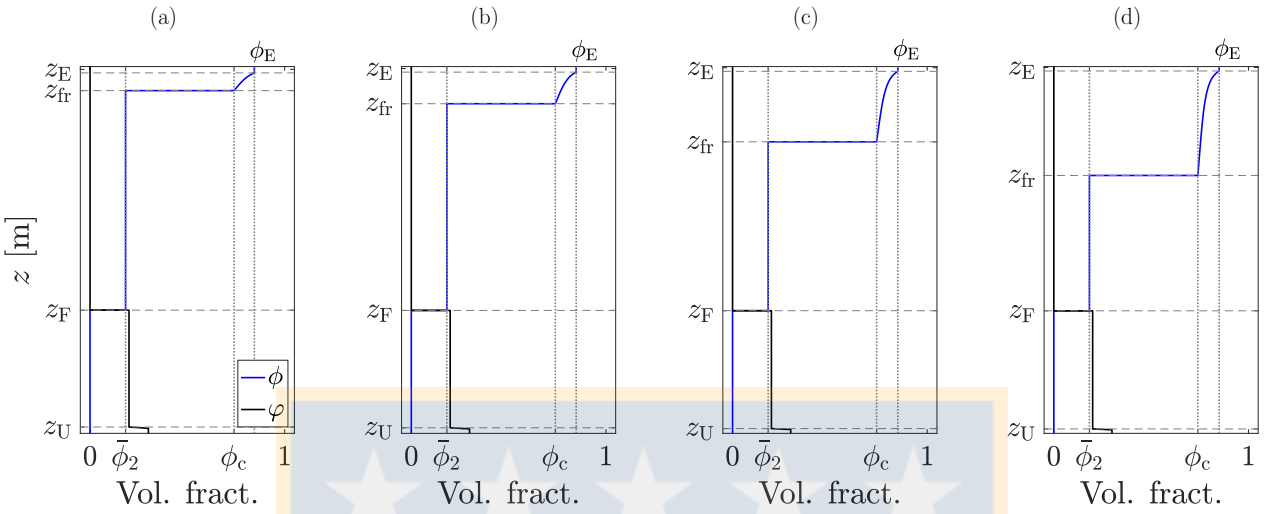

Figure 5.6: Examples of desired steady states given by (5.32) and (5.33). We use fixed values of $\phi_F = 0.3$, $\psi_F = 0.2$, $Q_F = 8.9927 \times 10^{-5}\,\mathrm{m}^3/\mathrm{s}$ and $Q_W = 2 \times 10^{-6}\,\mathrm{m}^3/\mathrm{s}$ and vary Q_U, choosing: (a) $Q_U = 5.9972 \times 10^{-5}\,\mathrm{m}^3/\mathrm{s}$, (b) $Q_U = 6.0083 \times 10^{-5}\,\mathrm{m}^3/\mathrm{s}$, (c) $Q_U = 6.0155 \times 10^{-5}\,\mathrm{m}^3/\mathrm{s}$ and (d) $Q_U = 6.0171 \times 10^{-5}\,\mathrm{m}^3/\mathrm{s}$. Once the values of ϕ_F, Q_U, Q_F and Q_W are chosen, the values of the effluent concentration ϕ_E are given by (5.29) and used as input in the ODE (5.31) to calculate the value of z_{fr}. In particular, we get (a) $\phi_E = 0.8443$, (b) $\phi_E = 0.8472$, (c) $\phi_E = 0.8491$ and (d) $\phi_E = 0.8495$. The values of ϕ_F, ψ_F, Q_U, Q_F and Q_W chosen here are used in Example 1 in Section 5.6 to recover these profiles using the numerical method proposed in Section 5.5.

Theorem 5.1. *The desired steady-state solution (5.32) and (5.33) of the PDE system (5.2) is possible only if the following inequalities are satisfied:*

$$\bar{\phi}_2 \le \phi_Z(-Q_U/A_U), \tag{FIb}$$

$$A_U f_1\big(\varphi_M(-Q_U/A_U), 0; -Q_U/A_U\big) \ge Q_F \psi_F. \tag{FIas}$$

$$Q_F\left(1 - \frac{\phi_F}{\phi_c}\right) < Q_U - Q_W \le Q_F(1-\phi_F), \tag{Froth1}$$

$$z_F < Z_{fr}(\phi_F, Q_F, Q_U, Q_W), \tag{Froth2}$$

$$s_F \begin{cases} < j_2(\phi_{2M}; q_2) & \text{if } \phi_{2M} < \phi_E, \\ \le j_2(\phi_E; q_2) & \text{if } \phi_{2M} \ge \phi_E, \end{cases} \tag{Froth3}$$

where we recall the definitions of q_2 (5.17) and ϕ_E (5.29):

$$q_2 = \frac{-Q_U + Q_F}{A_E}, \qquad \phi_E = \frac{Q_F \phi_F}{Q_W + Q_F - Q_U}.$$

Inequalities (FIb) and (FIas) can also be found in [18]. We visualize them together with (Froth1), (Froth2) and (Froth3) in the (Q_U, Q_F)-plane for fixed values of Q_W, ϕ_F, ψ_F and z_F; see Figure 5.7 for the choices $Q_W = 2 \times 10^{-6}\,\mathrm{m}^3/\mathrm{s}$, $\phi_F = 0.3$, $\psi_F = 0.2$, and $z_F = 0.33\,\mathrm{m}$. All

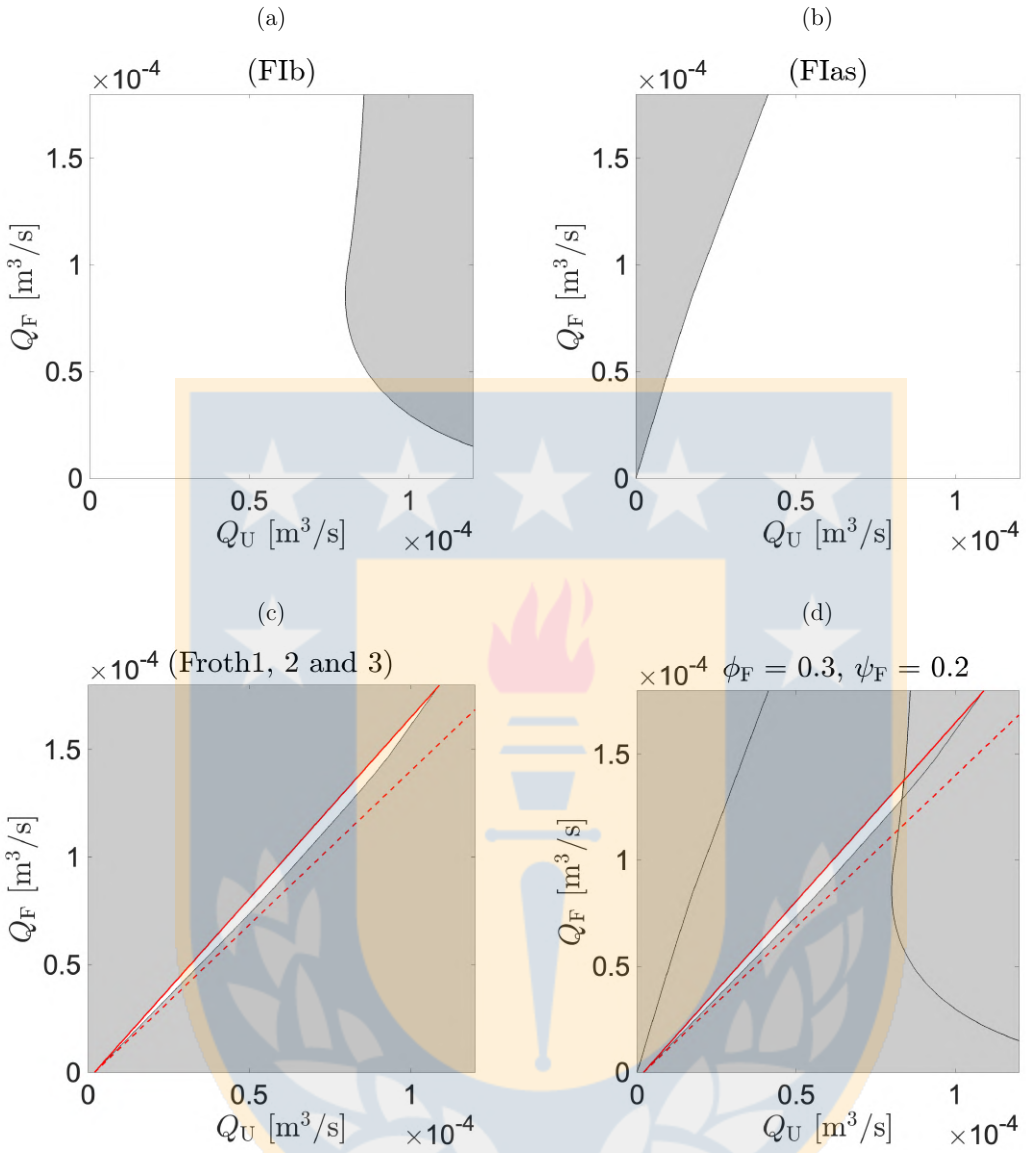

Figure 5.7: (a–c) Visualization of the conditions of Theorem 5.1 for $Q_W = 2 \times 10^{-6}\,\mathrm{m}^3/\mathrm{s}$, $\phi_F = 0.3$ and $\psi_F = 0.2$. (d) Operating chart showing the intersection of all the conditions, which are true in the white region.

the conditions are shown together in Figure 5.7 (d), which we call an *operating chart*. For any chosen point (Q_U, Q_F) in the white region, where all conditions in Theorem 5.1 are satisfied, a desired steady-state solution given by (5.32) and (5.33) can be reached.

The two inequalities in (Froth1) give rise to a wedge-shaped region with vertex at $(Q_U, Q_F) = (Q_W, 0)$; see Figure 5.7 (c). Thus, each wedge displayed in Figure 5.8 corresponds to a fixed value of Q_W, which can be read off at its vertex on the Q_U-axis. The strict inequality of (Froth1) corresponds to the lower dashed line of a wedge, and its slope is positive or negative depending on whether ϕ_F is greater or less than ϕ_c. The difference in slope of the two lines is $\phi_F(1/\phi_c - 1)$,

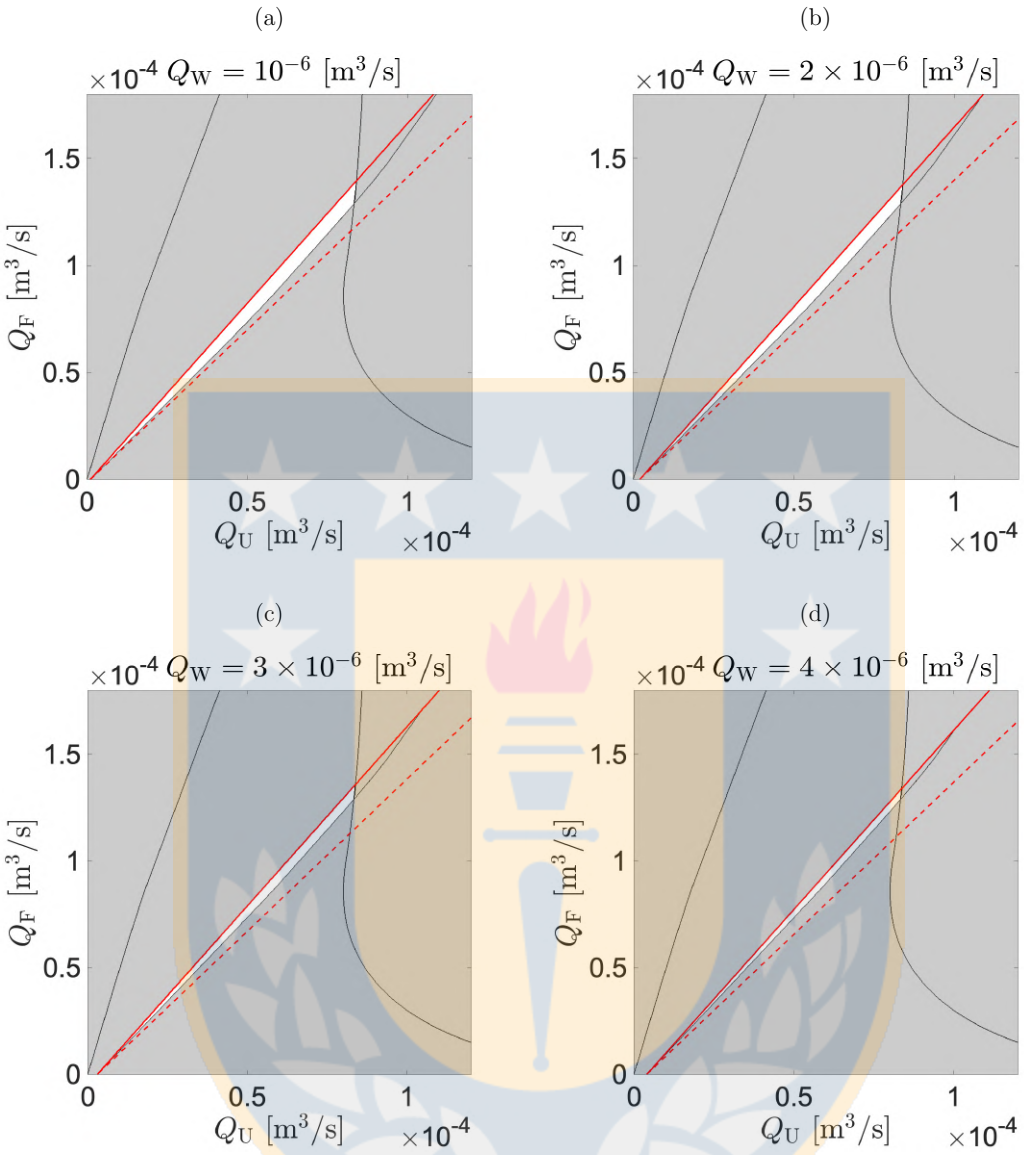

Figure 5.8: Dependence of the operating chart on the wash water flow Q_W for $\phi_F = 0.3$ and $\psi_F = 0.2$.

so the angle of the wedge increases with ϕ_F and decreases with ϕ_c. The lower part of the wedge is, however, cut off by conditions (Froth2) and (Froth3); see Figure 5.7 (c). Figure 5.8 shows also that the white region of the operating chart thins and will eventually disappear as Q_W increases.

Inequality (Froth2) is more involved than the others. For every given set of input and control values, one has to integrate the ODE of (5.31) backwards from $z = z_E$ for given ϕ_E towards lower z-values until ϕ_c is reached; the corresponding location defines $z = z_{fr}$. In Figure 5.9, the surface $z = Z_{fr}(\phi_F, Q_F, Q_U, Q_W)$ has been computed for two different values of ϕ_F and fixed values of Q_W and ψ_F. The same red and black curves as in Figures 5.7 and 5.8 of conditions

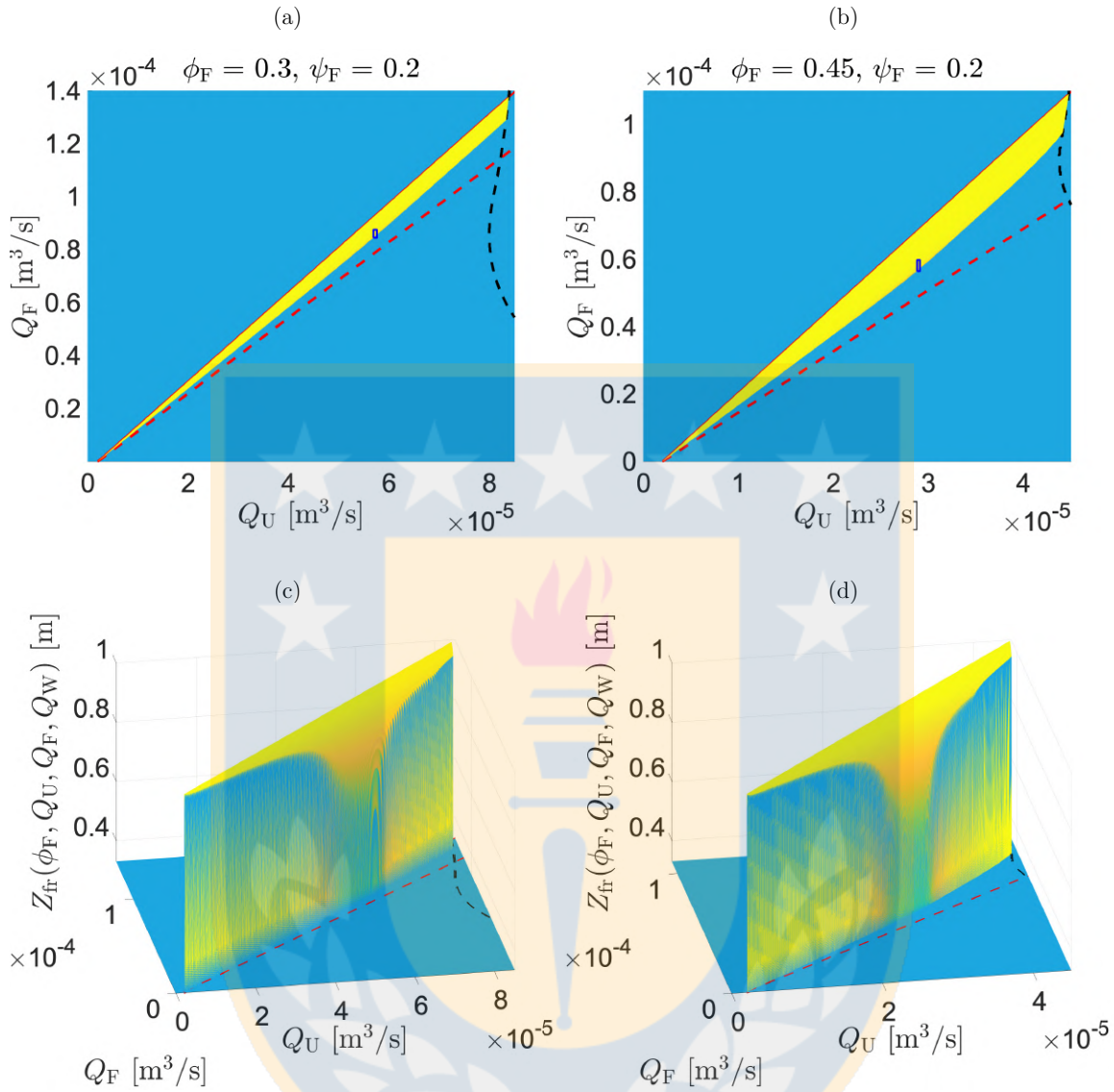

Figure 5.9: Operating charts for $Q_W = 2 \times 10^{-6}\,\mathrm{m}^3/\mathrm{s}$ and $\psi_F = 0.2$ with (a, c) $\phi_F = 0.3$ and (b, d) $\phi_F = 0.45$, showing the graphs of $(Q_F, Q_U) \mapsto Z_{fr}(\phi_F, Q_F, Q_U, Q_W)$ obtained by (5.31). The small rectangles in (a, b) are enlarged in Figure 5.10.

(Froth1) and (FIb), respectively, limit the white region in the operating charts. The study of the surface $Z_{fr}(\phi_F, Q_F, Q_U, Q_W)$ is crucial for the choice of values of Q_F, Q_U and Q_W for which we obtain a desired steady state with a froth region in $z = z_{fr}$, with z_{fr} a given value, as we will see in the numerical results in Section 5.6.

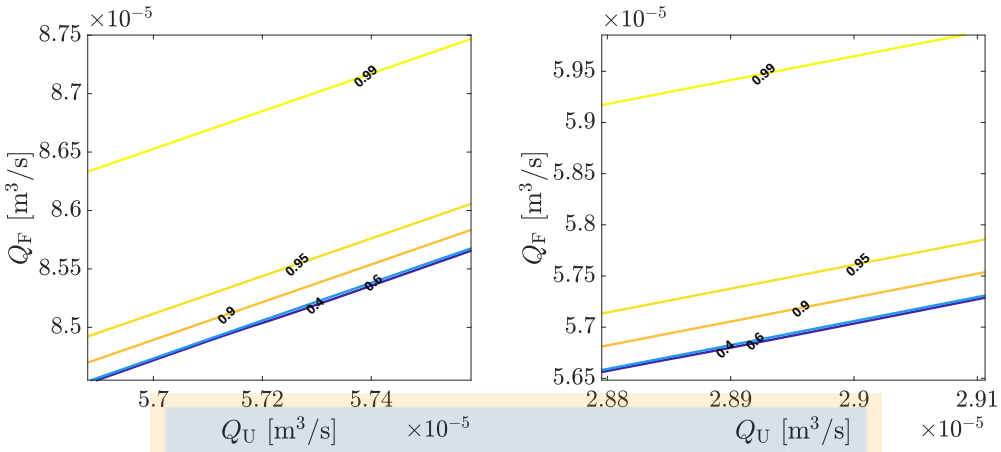

Figure 5.10: Enlarged views of the small rectangles marked in Figure 5.9 (a) and (b), respectively, showing contours of the function $(Q_F, Q_U) \mapsto Z_{fr}(\phi_F, Q_F, Q_U, Q_W)$.

5.5 Numerical method

5.5.1 Discretization and CFL condition

We define a computational domain of N cells by covering the vessel with $N-2$ cells and placing one cell each below and above for the calculation of the outlet volume fractions, see Figure 5.11, we repeat this figure from **Chapter 3** for the case $K = 1$ (Figure 3.3). Given the column height H, we define $\Delta z := H/(N-2)$ and the cell boundaries $z_i := i\Delta z$, $i = 0, 1, \ldots, N$. Furthermore, we define the cell intervals $I_{i-1/2} := [z_{i-1}, z_i)$ and $I_i := [z_{i-1/2}, z_{i+1/2})$. We place the column between $z_U := \Delta z = z_1$ and $z_E := z_U + H = (N-1)\Delta z = z_{N-1}$. The injection point z_F is assumed to belong to one cell $I_{i-1/2}$ and we define the dimensionless function

$$\delta_{F,i-1/2} := \int_{I_{i-1/2}} \delta_{z_F}(z)\,\mathrm{d}z := \begin{cases} 1 & \text{if } z_F \in I_{i-1/2}, \\ 0 & \text{otherwise.} \end{cases}$$

The cross-sectional area $A = A(z)$ is allowed to have a finite number of discontinuities and it is discretized by

$$A_i := \frac{1}{\Delta z}\int_{I_i} A(z)\,\mathrm{d}z, \qquad A_{i+1/2} := \frac{1}{\Delta z}\int_{I_{i+1/2}} A(z)\,\mathrm{d}z.$$

We simulate N_T time steps up to the final time $T := N_T\Delta t$, with the fixed time step Δt satisfying the Courant-Friedrichs-Lewy (CFL) condition

$$\Delta t\left(\frac{2\|Q\|_{\infty,T}}{A_{\min}} + M_1\|\tilde{v}'\|_\infty + \max\{\beta_1, \beta_2\}\right) \le \Delta z, \tag{CFL}$$

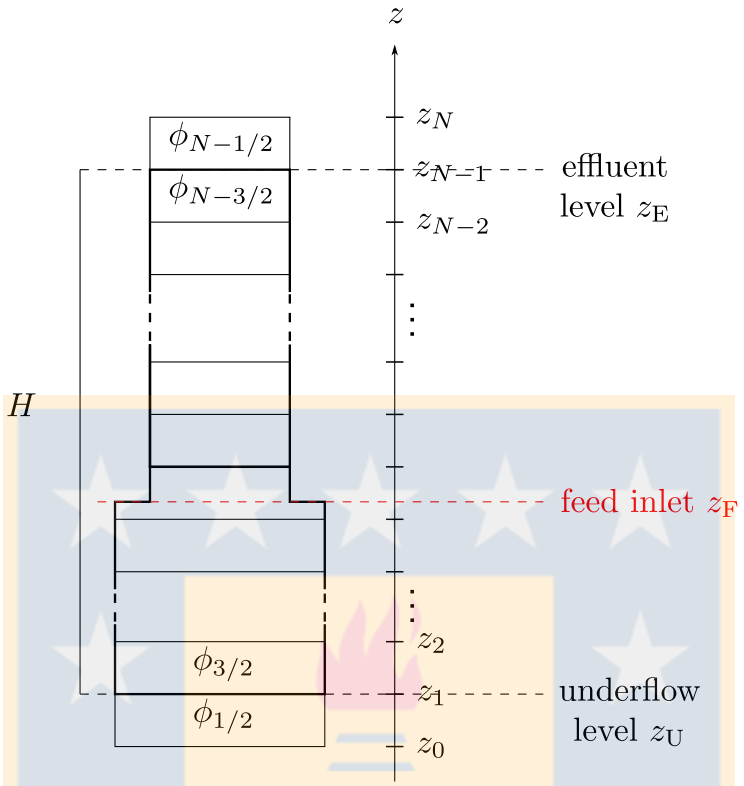

Figure 5.11: Grid covering the flotation column for the discretization of ϕ and ψ. The outlets z_U and z_E are each fixed on the boundaries between two cells and the feed inlet z_F is then located in a cell.

where

$$\beta_1 := M_1\|\tilde{v}\|_\infty + M_2\frac{\|d\|_\infty}{\Delta z}, \qquad \beta_2 := M_1\max\{v_{hs}(0), \|v'_{hs}\|_\infty\} + M_2(1-\phi_c)\frac{\|d\|_\infty}{\Delta z},$$

$$M_1 := \max_{i=1,2,\dots,N}\left\{\frac{A_{i-1}}{A_{i-1/2}}, \frac{A_i}{A_{i-1/2}}\right\}, \quad M_2 := \max_{i=1,2,\dots,N}\left\{\frac{A_{i-1}+A_i}{A_{i-1/2}}\right\},$$

$$A_{\min} := \min_{k=0,\frac{1}{2},1,\frac{3}{2},\dots,N} A_k, \qquad \|Q\|_{\infty,T} := \max_{0\le t\le T}(Q_F(t)+Q_W(t)), \qquad \|d\|_\infty := \max_{0\le\phi\le1}|d(\phi)|.$$

Finally, we set $t^n := n\Delta t$ for $n = 0, 1, \dots, N_T$.

The time-dependent feed functions are discretized as

$$Q_F^n := \frac{1}{\Delta t}\int_{t^n}^{t^{n+1}} Q_F(t)\,\mathrm{d}t, \qquad \phi_F^n := \frac{1}{\Delta t}\int_{t^n}^{t^{n+1}} \phi_F(t)\,\mathrm{d}t,$$

and the same is made for ψ_F.

5.5.2 Update of ϕ

The first equation of (5.2) depends only on ϕ and is discretized by a simple scheme on the cells $I_{i-1/2}$. The initial data are discretized by

$$\phi^0_{i-1/2} := \frac{1}{A_{i-1/2}\Delta z}\int_{I_{i-1/2}} \phi(z,0)A(z)\,\mathrm{d}z.$$

To advance from t^n to t^{n+1}, we assume that $\phi^n_{i-1/2}$, $i = 1,\dots,N$, are given. With the notation

$$a^+ := \max\{a,0\}, \quad a^- := \min\{a,0\}, \quad \gamma_i := \gamma(z_i), \quad \text{and} \quad q_i^{n+} := q(z_i,t^n)^+,$$

we define the numerical total flux at $z = z_i$ at time $t = t^n$ by

$$\Phi^n_i := \begin{cases} \phi^n_{1/2}q_0^{n-} & \text{for } i = 0,\\ \phi^n_{i-1/2}q_i^{n+} + \phi^n_{i+1/2}q_i^{n-} + \gamma_i\phi^n_{i-1/2}\tilde v(\phi^n_{i+1/2}) - \gamma_i\dfrac{D(\phi^n_{i+1/2}) - D(\phi^n_{i-1/2})}{\Delta z} & \text{for } i = 1,\dots,N-1,\\ \phi^n_{N-1/2}q_N^{n+} & \text{for } i = N, \end{cases} \tag{5.34}$$

where $\tilde v(\phi)$ is defined by (5.12). Since the bulk fluxes above and below the tank are directed away from it, the following terms that appear in (5.34) are zero:

$$\phi^n_{-1/2}q_0^{n+} = 0 \quad \text{and} \quad \phi^n_{N+1/2}q_N^{n-} = 0 \quad \text{for any values of } \phi^n_{-1/2} \text{ and } \phi^n_{N+1/2}.$$

To simplify the presentation, we use the middle line of (5.34) as the definition of Φ^n_i, $i = 0,\dots,N$, together with $\phi^n_{-1/2} := 0$ and $\phi^n_{N+1/2} := 0$. With the notation $\lambda := \Delta t/\Delta z$ and with $Q_i^{n+} := A_i q_i^{n+}$ etc., the conservation law on the interval $I_{i-1/2}$ implies the update formula

$$\begin{aligned} \phi^{n+1}_{i-1/2} &= \phi^n_{i-1/2} + \frac{\lambda}{A_{i-1/2}}\big(A_{i-1}\Phi^n_{i-1} - A_i\Phi^n_i + Q^n_{\mathrm F}\phi^n_{\mathrm F}\delta_{\mathrm F,i-1/2}\big)\\ &= \phi^n_{i-1/2} + \frac{\lambda}{A_{i-1/2}}\bigg(\phi^n_{i-3/2}Q^{n+}_{i-1} + \phi^n_{i-1/2}Q^{n-}_{i-1} + (A\gamma)_{i-1}\phi^n_{i-3/2}\tilde v(\phi^n_{i-1/2})\\ &\quad - \frac{(A\gamma)_{i-1}}{\Delta z}(D(\phi^n_{i-1/2}) - D(\phi^n_{i-3/2})) - \phi^n_{i-1/2}Q_i^{n+} - \phi^n_{i+1/2}Q_i^{n-} - (A\gamma)_i\phi^n_{i-1/2}\tilde v(\phi^n_{i+1/2})\\ &\quad + \frac{(A\gamma)_i}{\Delta z}(D(\phi^n_{i+1/2}) - D(\phi^n_{i-1/2})) + Q^n_{\mathrm F}\phi^n_{\mathrm F}\delta_{\mathrm F,i-1/2}\bigg), \quad i = 1,\dots,N. \end{aligned} \tag{5.35}$$

Theorem 5.2. *If the CFL condition (CFL) is satisfied and the initial data satisfy* $0 \le \phi(z,0) \le 1$, *then the update formula for* ϕ, *(5.35), is monotone and produces approximate solutions that satisfy*

$$0 \le \phi^n_{i-1/2} \le 1 \quad \textit{for } i = 1,\dots,N \textit{ and } n = 1,\dots,N_T. \tag{5.36}$$

The outline of the proof is presented below.

Proof. Details for the case $D \equiv 0$ are provided by [21]. Assume that $\phi^n_{i-1/2}$ and $\tilde\phi^n_{i-1/2}$, $i \in \mathbb{Z}$, $n = 0, 1, 2, \dots$ are two numerical solutions produced by the numerical scheme (5.35). Then monotonicity means that if $\phi^n_{i-1/2} \le \tilde\phi^n_{i-1/2}$ for all i, then $\phi^{n+1}_{i-1/2} \le \tilde\phi^{n+1}_{i-1/2}$ for all i, for all $n = 0, 1, 2, \dots$. For the case of a three-point scheme such as (5.35) this property can be verified by showing that $\partial\phi^{n+1}_{i-1/2}/\partial\phi^n_{k-1/2} \ge 0$ for all i and $k = i-1, i, i+1$. In fact, we have

$$
\begin{aligned}
\frac{\partial\phi^{n+1}_{i-1/2}}{\partial\phi^n_{i-3/2}} &= \frac{\lambda}{A_{i-1/2}}\left(Q^{n+}_{i-1} + (A\gamma)_{i-1}\big(\tilde v(\phi^n_{i-1/2}) + d(\phi^n_{i-3/2})/\Delta z\big)\right) \ge 0,\\
\frac{\partial\phi^{n+1}_{i-1/2}}{\partial\phi^n_{i+1/2}} &= \frac{\lambda}{A_{i-1/2}}\left(-Q^{n-}_{i} + (A\gamma)_{i}\big(-\phi^n_{i-1/2}\tilde v'(\phi^n_{i+1/2}) + d(\phi^n_{i+1/2})/\Delta z\big)\right) \ge 0,\\
\frac{\partial\phi^{n+1}_{i-1/2}}{\partial\phi^n_{i-1/2}} &= 1 + \frac{\lambda}{A_{i-1/2}}\Big(Q^{n-}_{i-1} + (A\gamma)_{i-1}\phi^n_{i-3/2}\tilde v'(\phi^n_{i-1/2}) - Q^{n+}_{i} - (A\gamma)_i\tilde v(\phi^n_{i+1/2})\\
&\qquad - \big((A\gamma)_{i-1} + (A\gamma)_i\big)d(\phi_{i-1/2})/\Delta z)\Big)\\
&\ge 1 - \lambda\left(\frac{2\|Q\|_{\infty,T}}{A_{\min}} + M_1\big(\|\tilde v'\|_\infty + \|\tilde v\|_\infty\big) + M_2\frac{\|d\|_\infty}{\Delta z}\right) \ge 0,
\end{aligned}
$$

where we have used the CFL condition (CFL). The rest of the proof, the boundedness $0 \le \phi^n_{i-1/2} \le 1$, follows by standard arguments, namely one verifies that if $\phi^n_{i-1/2} = 0$ for all i, then $\phi^{n+1}_{i-1/2} = 0$ for all i and likewise that if $\phi^n_{i-1/2} = 1$ for all i, then $\phi^{n+1}_{i-1/2} = 1$ for all i. Thus, appealing to the monotonicity of the scheme, one deduces that if $0 \le \phi^n_{i-1/2} \le 1$ for all i, then $0 \le \phi^{n+1}_{i-1/2} \le 1$ for all i, which proves (5.36). □

5.5.3 Update of ψ

We discretize the initial data by

$$
\psi^0_{i-1/2} := \frac{1}{A_{i-1/2}\Delta z}\int_{I_{i-1/2}} \psi(z,0)A(z)\,\mathrm{d}z.
$$

A consistent numerical flux corresponding to (5.18) is, for $i = 0, \dots, N$,

$$
\begin{aligned}
\Psi^n_i &:= \psi^n_{i-1/2}q^{n+}_i + \psi^n_{i+1/2}q^{n-}_i\\
&\quad - \gamma_i\left(G^n_i\big(\psi^n_{i-1/2}, \psi^n_{i+1/2}\big) + \frac{\psi^n_{i+1/2}}{1-\phi^n_{i+1/2}}\left(\phi^n_{i-1/2}\tilde v(\phi^n_{i+1/2}) - \frac{\Delta D^{n-}_i}{\Delta z}\right) - \frac{\psi^n_{i-1/2}}{1-\phi^n_{i-1/2}}\frac{\Delta D^{n+}_i}{\Delta z}\right),
\end{aligned}
$$

where $\Delta D^n_i := D(\phi^n_{i+1/2}) - D(\phi^n_{i-1/2})$, $\Delta D^{n-}_i := (\Delta D^n_i)^-$, and we set

$$
\psi^n_{-1/2} := 0 \quad \text{and} \quad \psi^n_{N+1/2} := 0
$$

with the same motivation as for ϕ above (these values are irrelevant). Here $G^n_i(\psi^n_{i-1/2}, \psi^n_{i+1/2})$ is the Engquist-Osher numerical flux [51] associated with the function

$$
f^n_{\mathrm{b},i}(\psi) := \psi\tilde v_{\mathrm{hs}}\left(\frac{\psi}{\psi^n_{\max,i}}\right), \qquad \tilde v_{\mathrm{hs}}(u) := \begin{cases} v_{\mathrm{hs}}(u) & \text{for } u < 1,\\ 0 & \text{for } u \ge 1, \end{cases} \tag{5.37}
$$

where we recall that $v_{\rm hs}$ is given by (5.16), and we define

$$\psi^n_{\max,i} := \min\{1-\phi^n_{i-1/2}, 1-\phi^n_{i+1/2}\} = 1-\max\{\phi^n_{i-1/2},\phi^n_{i+1/2}\}. \tag{5.38}$$

If $\hat\psi^n_i$ is the maximum point of $f^n_{{\rm b},i}$, then the Engquist-Osher numerical flux is given by

$$\begin{aligned}
&G^n_i\big(\psi^n_{i-1/2},\psi^n_{i+1/2}\big)\\
&=\begin{cases}
f^n_{{\rm b},i}(\psi^n_{i+1/2}) & \text{if } \psi^n_{i-1/2},\psi^n_{i+1/2}\le\hat\psi^n_i,\\
f^n_{{\rm b},i}(\hat\psi^n_i) & \text{if } \psi^n_{i-1/2}\le\hat\psi^n_i<\psi^n_{i+1/2},\\
-f^n_{{\rm b},i}(\hat\psi^n_i)+f^n_{{\rm b},i}(\psi^n_{i-1/2})+f^n_{{\rm b},i}(\psi^n_{i+1/2}) & \text{if } \psi^n_{i+1/2}\le\hat\psi^n_i<\psi^n_{i-1/2},\\
f^n_{{\rm b},i}(\psi^n_{i-1/2}) & \text{if } \hat\psi^n_i<\psi^n_{i-1/2},\psi^n_{i+1/2}.
\end{cases}
\end{aligned}$$

The marching formula is (for $i=1,\dots,N$)

$$\begin{aligned}
&\psi^{n+1}_{i-1/2}\\
&=\psi^n_{i-1/2}+\frac{\lambda}{A_{i-1/2}}\big(A_{i-1}\Psi^n_{i-1}-A_i\Psi^n_i+Q^n_{\rm F}\psi^n_{\rm F}\delta_{{\rm F},i-1/2}\big)\\
&=\psi^n_{i-1/2}+\frac{\lambda}{A_{i-1/2}}\Big\{\psi^n_{i-3/2}Q^{n+}_{i-1}+\psi^n_{i-1/2}Q^{n-}_{i-1}-\psi^n_{i-1/2}Q^{n+}_i-\psi^n_{i+1/2}Q^{n-}_i+Q^n_{\rm F}\psi^n_{\rm F}\delta_{{\rm F},i-1/2}\\
&\quad-(A\gamma)_{i-1}\bigg(G^n_{i-1}\big(\psi^n_{i-3/2},\psi^n_{i-1/2}\big)+\frac{\psi^n_{i-1/2}}{1-\phi^n_{i-1/2}}\bigg(\phi^n_{i-3/2}\tilde v(\phi^n_{i-1/2})-\frac{\Delta D^{n-}_{i-1}}{\Delta z}\bigg)-\frac{\psi^n_{i-3/2}}{1-\phi^n_{i-3/2}}\frac{\Delta D^{n+}_{i-1}}{\Delta z}\bigg)\\
&\quad+(A\gamma)_i\bigg(G^n_i\big(\psi^n_{i-1/2},\psi^n_{i+1/2}\big)+\frac{\psi^n_{i+1/2}}{1-\phi^n_{i+1/2}}\bigg(\phi^n_{i-1/2}\tilde v(\phi^n_{i+1/2})-\frac{\Delta D^{n-}_i}{\Delta z}\bigg)-\frac{\psi^n_{i-1/2}}{1-\phi^n_{i-1/2}}\frac{\Delta D^{n+}_i}{\Delta z}\bigg)\Big\}.
\end{aligned} \tag{5.39}$$

Theorem 5.3. *Assume that the assumptions of Theorem 5.2 are in effect. If the initial data satisfy $0\le\psi(z,0)\le 1-\phi(z,0)$ and the feed volume fraction $\psi_{\rm F}(t)\le 1-\phi_{\rm F}(t)$, then the update formula (5.39) is monotone and together with (5.35) it produces approximate solutions that satisfy*

$$0\le\psi^n_{i-1/2}\le 1-\phi^n_{i-1/2}\quad \textit{for all } i \textit{ and } n.$$

The outline of the proof is presented below.

Proof. The proof is similar to that of Theorem 5.2. We note that (5.39) is again a three-point scheme, and show that $\partial\psi^{n+1}_{i-1/2}/\partial\psi^n_{k-1/2}\ge 0$ for all $i=1,\dots,N$ and $k=i-1,i,i+1$. The contributions of the terms that contain D to $\partial\psi^n_{i-1/2}/\partial\psi^n_{i-3/2}$ and $\partial\psi^n_{i-1/2}/\partial\psi^n_{i-3/2}$ are

$$\frac{\lambda(A\gamma)_{i-1}}{A_{i-1/2}(1-\phi^n_{i-3/2})}\frac{\Delta D^{n+}_{i-1}}{\Delta z}\ge 0\quad\text{and}\quad -\frac{\lambda(A\gamma)_i}{A_{i+1/2}(1-\phi^n_{i+1/2})}\frac{D^{n-}_{i-1}}{\Delta z}\ge 0,$$

respectively. Now we utilize the estimations similar to those in the previous proof (see [21]) and add the terms with D to obtain

$$\frac{\partial\mathcal{K}^n_{i-1/2}}{\partial\psi^n_{i-1/2}}\ge 1-\lambda\bigg(\frac{2\|Q\|_{\infty,T}}{A_{\min}}+M_1\big(\max\{v_{\rm hs}(0),\|v'_{\rm hs}\|_\infty\}+\|\tilde v'\|_\infty\big)$$

$$+\frac{1}{A_{i-1/2}(1-\phi^n_{i-1/2})}\left((A\gamma)_{i-1}\frac{\Delta D^{n-}_{i-1}}{\Delta z}-(A\gamma)_i\frac{\Delta D^{n+}_i}{\Delta z}\right)\Bigg).$$

It is easy to estimate the integrated terms

$$\Delta D^n_i = D(\phi^n_{i+1/2})-D(\phi^n_{i-1/2})\le \|d\|_\infty(1-\phi_c).$$

Hence, we obtain with (CFL)

$$\frac{\partial \mathcal{K}^n_{i-1/2}}{\partial \psi^n_{i-1/2}}\ge 1-\lambda\left(\frac{2\|Q\|_{\infty,T}}{A_{\min}}+M_1\big(\max\{v_{\rm hs}(0),\|v'_{\rm hs}\|_\infty\}+\|\tilde v'\|_\infty\big)+M_2(1-\phi_c)\frac{\|d\|_\infty}{\Delta z}\right)\ge 0.$$

The inequalities proven imply that $\psi^{n+1}_{i-1/2}$ is a non-decreasing of each of $\psi^n_{k-1/2}$ for $k=i-1,i,i+1$, and therefore the scheme is monotone. Writing the scheme as

$$\psi^{n+1}_{i-1/}=\mathcal{K}_{i-1/2}\big(\psi^n_{i-3/2},\psi^n_{i-1/2},\psi^n_{i+1/2}\big),$$

assuming that $0\le\psi^n_{i-1/2}\le 1-\phi^n_{i-1/2}$ for all i and using that (5.37) and (5.38) ensure that $G^n_i(1-\phi^n_{i-1/2},1-\phi^n_{i+1/2})=0$ (see [21]), we get

$$\begin{aligned}
0\le{}&\frac{\lambda}{A_{i-1/2}}Q^n_{\rm F}\psi^n_{\rm F}\delta_{{\rm F},i-1/2}=\mathcal{K}_{i-1/2}(0,0,0)\le\psi^{n+1}_{i-1/2}\\
&=\mathcal{K}_{i-1/2}(\psi^n_{i-3/2},\psi^n_{i-1/2},\psi^n_{i+1/2})\le\mathcal{K}_{i-1/2}(1-\phi^n_{i-3/2},1-\phi^n_{i-1/2},1-\phi^n_{i+1/2})\\
&=1-\phi^n_{i-1/2}+\frac{\lambda}{A_{i-1/2}}\Bigg((1-\phi^n_{i-3/2})Q^{n+}_{i-1}+(1-\phi^n_{i-1/2})Q^{n-}_{i-1}\\
&\quad-(A\gamma)_{i-1}\left(\phi^n_{i-3/2}\tilde v(\phi^n_{i-1/2})-\frac{\Delta D^{n-}_{i-1}}{\Delta z}-\frac{\Delta D^{n+}_{i-1}}{\Delta z}\right)-(1-\phi^n_{i-1/2})Q^{n+}_i-(1-\phi^n_{i+1/2})Q^{n-}_i\\
&\quad+(A\gamma)_i\left(\phi^n_{i-1/2}\tilde v(\phi^n_{i+1/2})-\frac{\Delta D^{n-}_i}{\Delta z}-\frac{\Delta D^{n+}_i}{\Delta z}\right)+Q^n_{\rm F}\psi^n_{\rm F}\delta_{{\rm F},i-1/2}\Bigg).
\end{aligned}$$

Now we use that $\Delta D^{n-}_i+\Delta D^{n+}_i=\Delta D^n_i=D(\phi_{i+1/2})-D(\phi_{i-1/2})$, that $\psi^n_{{\rm F},k}\le 1-\phi^n_{{\rm F},k}$ and the update formula for ϕ (5.35) to obtain

$$\begin{aligned}
\psi^{n+1}_{i-1/2}&\le 1-\phi^{n+1}_{i-1/2}+\frac{\lambda}{A_{i-1/2}}\big(Q^{n+}_{i-1}+Q^{n-}_{i-1}-Q^{n+}_i-Q^{n-}_i+Q^n_{\rm F}\delta_{{\rm F},i-1/2}\big)\\
&=1-\phi^{n+1}_{i-1/2}+\frac{\lambda}{A_{i-1/2}}\big(Q^n_{i-1}-Q^n_i+Q^n_{\rm F}\delta_{{\rm F},i-1/2}\big)=1-\phi^{n+1}_{i-1/2},
\end{aligned}$$

since the latter parenthesis is zero irrespective of whether there is a source in the cell; $Q^n_{i-1}-Q^n_i+Q^n_{\rm F}=0$, or not; $Q^n_{i-1}-Q^n_i=0$. Details for the case $D\equiv 0$ are provided by [21]. □

5.6 Numerical simulations

We simulate the flotation process in the column in Figure 5.1 with the specific measures $A_{\rm E}=7.225\times10^{-3}\,{\rm m}^2\le A_{\rm U}=8.365\times10^{-3}\,{\rm m}^2$, $z_{\rm U}=0\,{\rm m}$, $z_{\rm F}=0.33\,{\rm m}$, $z_{\rm E}=1\,{\rm m}$ and

$H = 1\,\mathrm{m}$. For all the examples, we use the parameters given in [15, Table 1] to define v_{drain} and d_{cap} in (5.12)–(5.14): $\rho_{\mathrm{f}} = 10^3\,\mathrm{kg/m^3}$, $\mu = 10^{-3}\,\mathrm{Pa\,s}$, $r_{\mathrm{b}} = 4.13 \times 10^{-4}\,\mathrm{m}$, $C_{\mathrm{PB}} = 50$, $\gamma_{\mathrm{w}} = 3.5 \times 10^{-2}\,\mathrm{N/m}$, $g = 9.81\,\mathrm{m/s^2}$, and by [107], $n_{\mathrm{S}} = 0.46$ and $m = 1.28$, from which we obtain $d_{\mathrm{cap}} = 3.1045 \times 10^{-3}\,\mathrm{m}$. For the velocity functions $\tilde{v}$ and v_{hs}, given by (5.12) and (5.16), respectively, we use $n_{\mathrm{b}} = 2.5$, $v_{\mathrm{term}} = 2.7 \times 10^{-2}\,\mathrm{m/s}$, $n_{\mathrm{RZ}} = 1.5$ and $v_\infty = 5.0 \times 10^{-3}\,\mathrm{m/s}$. The critical volume fraction is $\phi_{\mathrm{c}} = 0.74$ according to [89, Eq. (21)].

5.6.1 Example 5.1

We show steady-state solutions for fixed $Q_{\mathrm{F}} = 8.9927 \times 10^{-5}\,\mathrm{m^3/s}$ and $Q_{\mathrm{W}} = 2.0 \times 10^{-6}\,\mathrm{m^3/s}$ for various values of Q_{U}; see Figure 5.12(a). For these values and with the feed volume fractions $\phi_{\mathrm{F}} = 0.3$ and $\psi_{\mathrm{F}} = 0.2$, we solve the ODE (5.31) to obtain 'exact' solutions (i.e., the ODE is solved numerically), and the value of z_{fr} for each point; see the solid lines in Figure 5.12(c) and (d). The dots in the same plots show the numerical solutions, which are obtained by simulating a long time from any initial data. All solutions have the same volume fraction ϕ_{E} at the top, since this is given by the explicit formula (5.29). Figure 5.12(b) shows the steady state for the solids with particles only below the feed level.

A clear difference between the two types of solution of ϕ can be seen near the discontinuity. This is an inaccuracy of the numerical solution, which seems to converge to the exact one as $N \to \infty$; see Figure 5.13, which shows the steady-state solution for the solid point in Figure 5.12(a) for various values of N.

5.6.2 Example 5.2

We start from a tank filled with only water at time $t = 0\,\mathrm{s}$, i.e., $\phi(z, 0) = \psi(z, 0) = 0$ for all z, when we start pumping aggregates, solids, fluid and wash water with $\phi_{\mathrm{F}} = 0.3$ and $\psi_{\mathrm{F}} = 0.2$. In the white region of the operating chart in Figure 5.14, we choose the point (diamond symbol) $(Q_{\mathrm{U}}, Q_{\mathrm{F}}) = (5.85, 8.846) \times 10^{-5}\,\mathrm{m^3/s}$. The wash water volumetric flow is $Q_{\mathrm{W}} = 2.0 \times 10^{-6}\,\mathrm{m^3/s}$. Then $Q_{\mathrm{E}} = 1.4496 \times 10^{-4}\,\mathrm{m^3/s}$ and one obtains a desired steady state with a thin layer of froth at the top and solids only below the feed level after about 500 s; see Figures 5.15 (a) and 5.16 (a).

Once the system is in steady state at $t = 500\,\mathrm{s}$, we perform two different changes corresponding to the points marked with a square (left) and a circle (right) in the operating chart in Figure 5.14 with the corresponding responses seen in Figures 5.15 and 5.16, respectively. The jump from the middle point (diamond) to the left point (square) means a jump from $Q_{\mathrm{U}} = 5.85 \times 10^{-5}\,\mathrm{m^3/s}$ to the smaller value $5.0 \times 10^{-5}\,\mathrm{m^3/s}$ and produces the solution in Figure 5.15. After $t = 1000\,\mathrm{s}$, there is no froth in zone 2 and the solids volume fraction is slightly higher in the new steady state.

If the jump from the middle point (diamond) instead goes to the right point (circle), i.e., the new value at $t = 500\,\mathrm{s}$ is the larger $Q_{\mathrm{U}} = 6.3 \times 10^{-5}\,\mathrm{m^3/s}$, Figure 5.16 shows the reaction of the

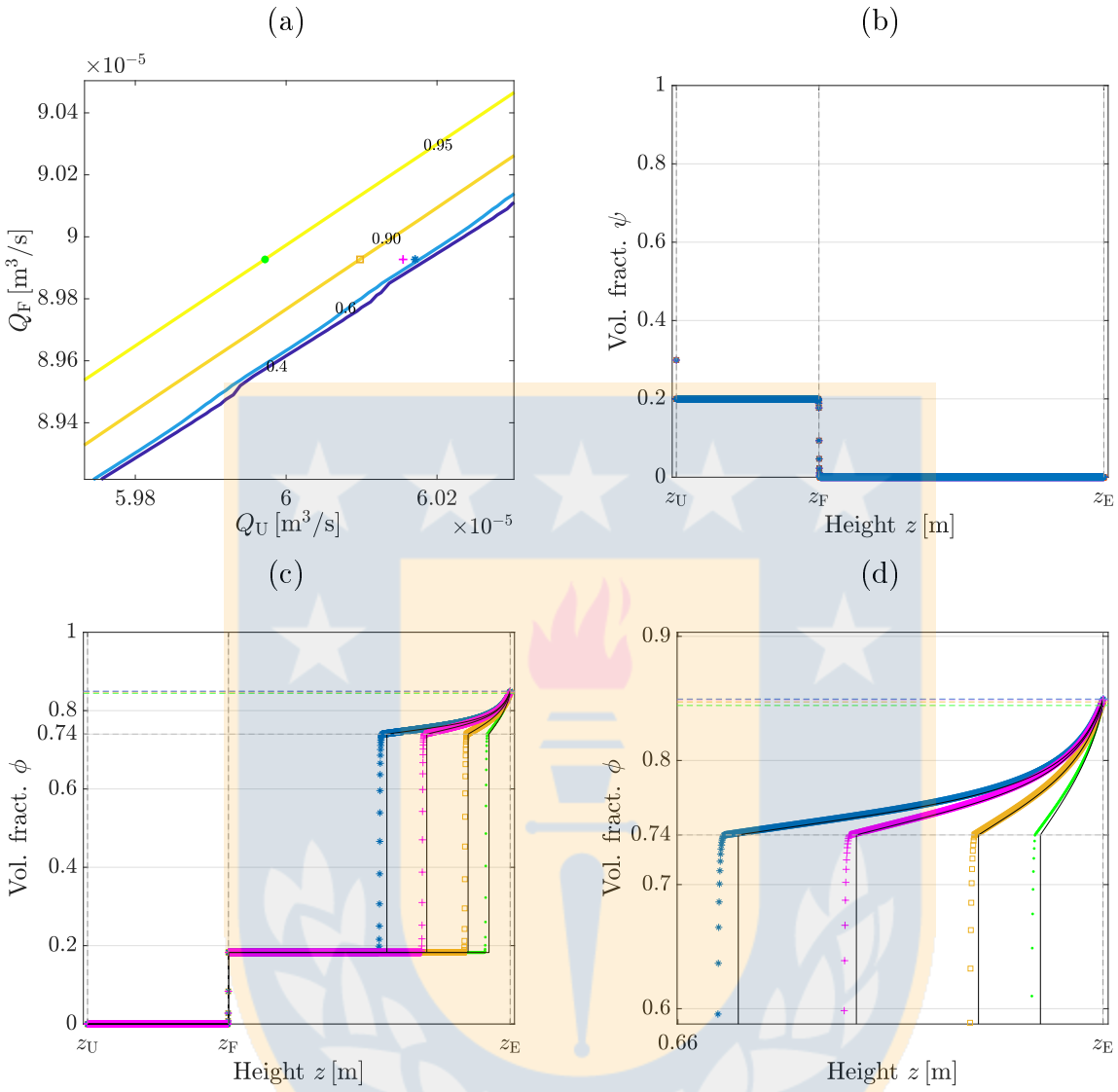

Figure 5.12: Example 5.1: (a) Contour lines of $(Q_F, Q_U) \mapsto Z_{fr}(\phi_F, Q_F, Q_U, Q_W)$ for $Q_W = 2 \times 10^{-6}\,\mathrm{m}^3/\mathrm{s}$, $\psi_F = 0.2$ and $\phi_F = 0.3$. (b) Approximate volume fraction of solids ψ computed with $N = 3200$. (c) Approximate solution (dots) versus exact solution (solid lines) of volume fraction of aggregates ϕ corresponding to the four point in plot (a) computed with $N = 3200$. (d) Enlarged view of (c).

system until $t = 2000\,\mathrm{s}$. The aggregates fill the entire column while the solids volume fraction has a lower value in the new steady state. We have demonstrated that operating points outside the white region lead to non-desired steady states.

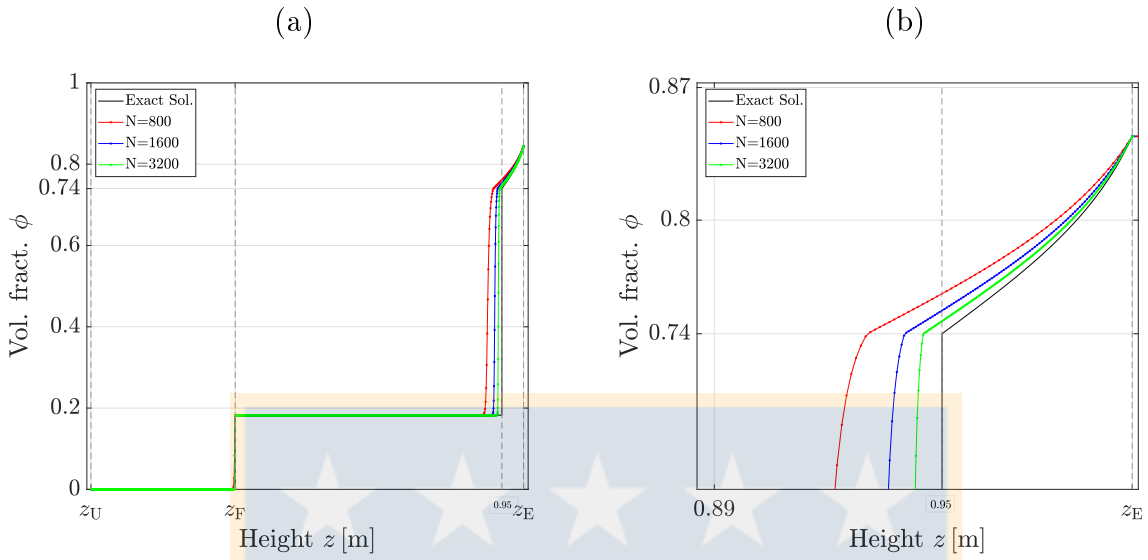

Figure 5.13: Example 5.1: (a) Approximate solution for the point represented by a dot in Figure 5.12(a) with various values of N. (b) Enlarged view of (a).

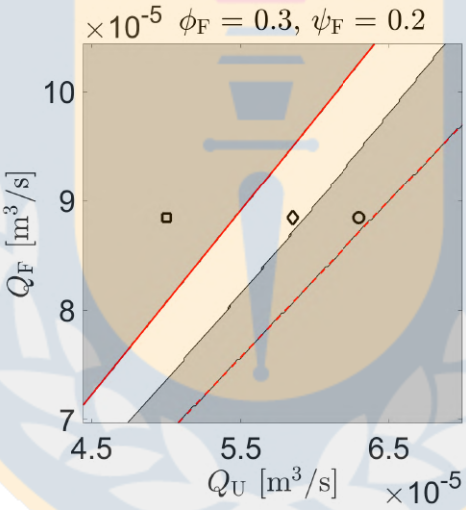

Figure 5.14: Example 5.2: An operating charts for $\phi_F = 0.3$ and $\psi_F = 0.2$. The point $(Q_U, Q_F) = (5.85, 8.846) \times 10^{-5}\,\mathrm{m}^3/\mathrm{s}$ marked with a diamond in the white region results in a desired steady state with a froth layer at the top of the column. The points marked with a square $(Q_U, Q_F) = (5.0, 8.846) \times 10^{-5}\,\mathrm{m}^3/\mathrm{s}$ and a circle $(Q_U, Q_F) = (6.3, 8.84) \times 10^{-5}\,\mathrm{m}^3/\mathrm{s}$ result in no froth (Figure 5.15) or a tank full of froth (Figure 5.16), respectively. (The plot is a zoom of Figure 5.8 (b) and the black curves are smoother than they here appear due to numerical resolution.)

5.6.3 Example 5.3

Again, the tank is filled with only water at time $t = 0\,\mathrm{s}$ when we start feeding it with $\phi_F = 0.3$ and $\psi_F = 0.2$. The wash water flow is $Q_W = 4.0 \times 10^{-6}\,\mathrm{m}^3/\mathrm{s}$ and hence the effluent volumetric

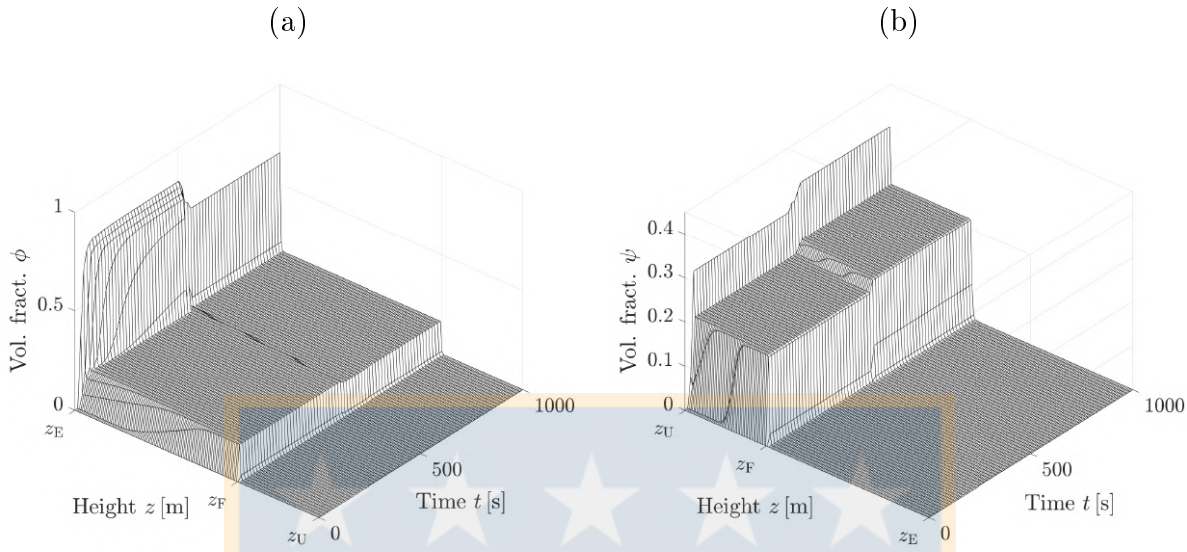

Figure 5.15: Example 5.2: Simulation with $N = 1600$ of the volume fractions of (a) aggregates ϕ and (b) solids ψ from a tank filled of only water. The initial operating point $(Q_U, Q_F) = (5.85, 8.846) \times 10^{-5}\,m^3/s$ (diamond in Figure 5.14) is at $t = 500\,s$ changed to $(5.0, 8.846) \times 10^{-5}\,m^3/s$ (square in Figure 5.14).

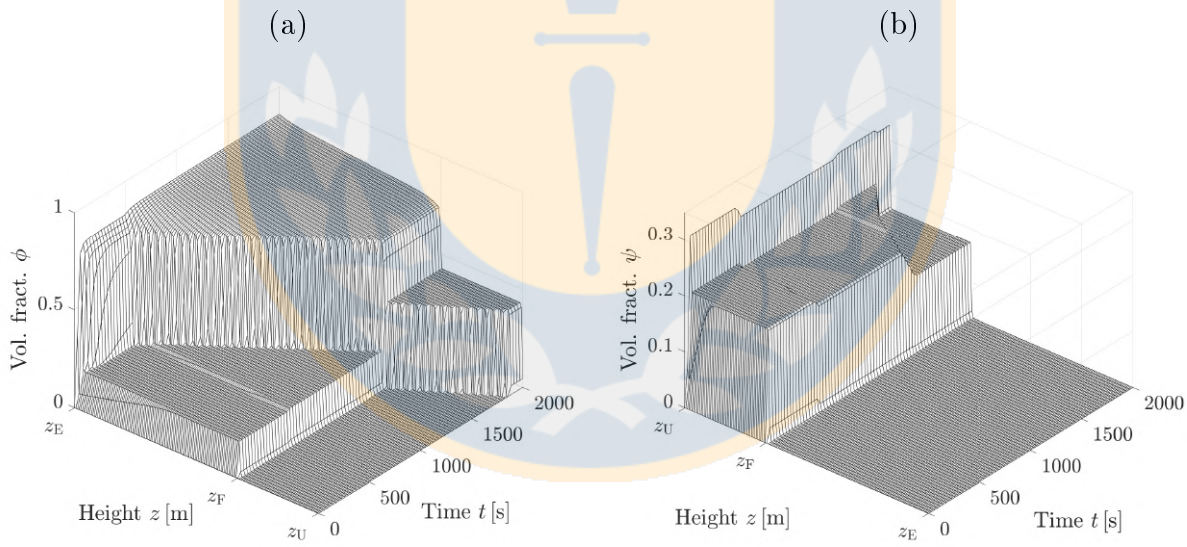

Figure 5.16: Example 5.2: Simulation with $N = 1600$ of the volume fractions of (a) aggregates ϕ and (b) solids ψ from a tank filled of only water. The initial operating point $(Q_U, Q_F) = (5.85, 8.846) \times 10^{-5}\,m^3/s$ (diamond in Figure 5.14) is at $t = 500\,s$ changed to $(6.3, 8.846) \times 10^{-5}\,m^3/s$ (circle in Figure 5.14).

flow is $Q_E = 1.75 \times 10^{-5}\,m^3/s$. From the corresponding operating chart in Figure 5.17 (a), we choose the point of volumetric flows $(Q_U, Q_F) = (3.15, 4.5) \times 10^{-5}\,m^3/s$ lying in the white

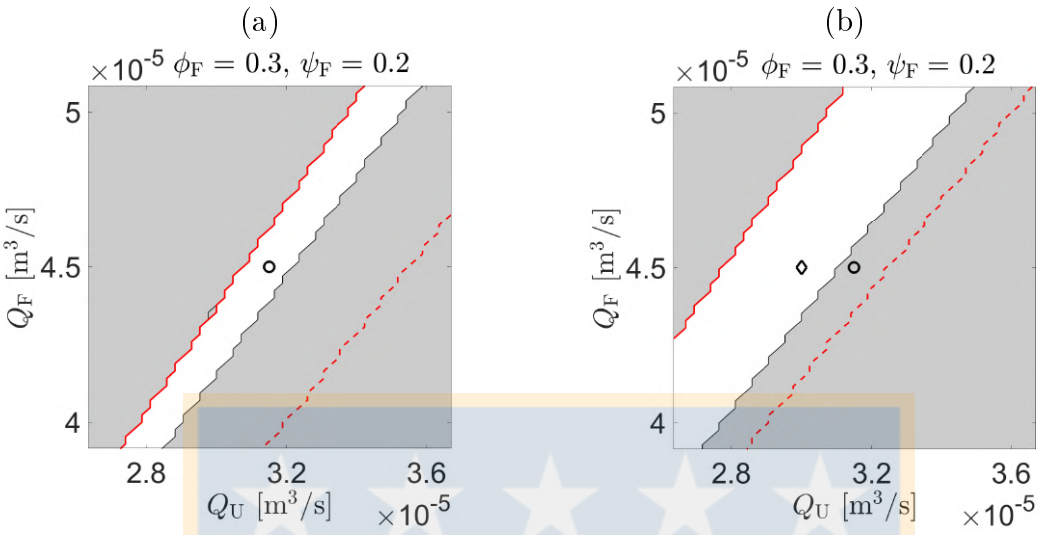

Figure 5.17: Example 5.3. Operating charts for $\phi_F = 0.3$ and $\psi_F = 0.2$ with (a) $Q_W = 3.15 \times 10^{-5}\,\mathrm{m}^3/\mathrm{s}$, (b) $Q_W = 3.0 \times 10^{-5}\,\mathrm{m}^3/\mathrm{s}$. The initial point $(Q_U, Q_F) = (3.15, 4.5) \times 10^{-5}\,\mathrm{m}^3/\mathrm{s}$ is marked with a circle and the one after the control action $(Q_U, Q_F) = (3.0, 4.5) \times 10^{-5}\,\mathrm{m}^3/\mathrm{s}$ with a diamod. (The curves are smoother than they appear here due to numerical resolution.)

region. Then a desired steady state builds up quickly and at $t = 250\,\mathrm{s}$ there is a thin froth layer at the top of in zone 2 and with solids only in zone 1; see Figure 5.18.

Once the system is in steady state, we change at $t = 300\,\mathrm{s}$ the volumetric flow of the wash water from $Q_W = 4.0 \times 10^{-6}\,\mathrm{m}^3/\mathrm{s}$ to $1.0 \times 10^{-6}\,\mathrm{m}^3/\mathrm{s}$ and simulate the reaction of the system. In the corresponding operating chart for this new set of variables, the point $(Q_U, Q_F) = (3.15, 4.5) \times 10^{-5}\,\mathrm{m}^3/\mathrm{s}$ is no longer in the white region; see Figure 5.17 (b, circle point), and no desired steady state is feasible. As it can be seen in Figure 5.18 (a), with less flow of wash water flushing the aggregates out at the top, the froth layer increases downwards. At time $t = 1000\,\mathrm{s}$, we make a control action and change the volumetric flow from $Q_U = 3.15 \times 10^{-5}\,\mathrm{m}^3/\mathrm{s}$ to $3.0 \times 10^{-5}\,\mathrm{m}^3/\mathrm{s}$ so that the new point lies inside the white region of the corresponding operating chart in Figure 5.17 (b, diamond point). Figures 5.18 (a) and (c) show that a second desired steady state is reached after $t = 1500\,\mathrm{s}$. Figures 5.18 (b) and (d) show that the solids settle in any case.

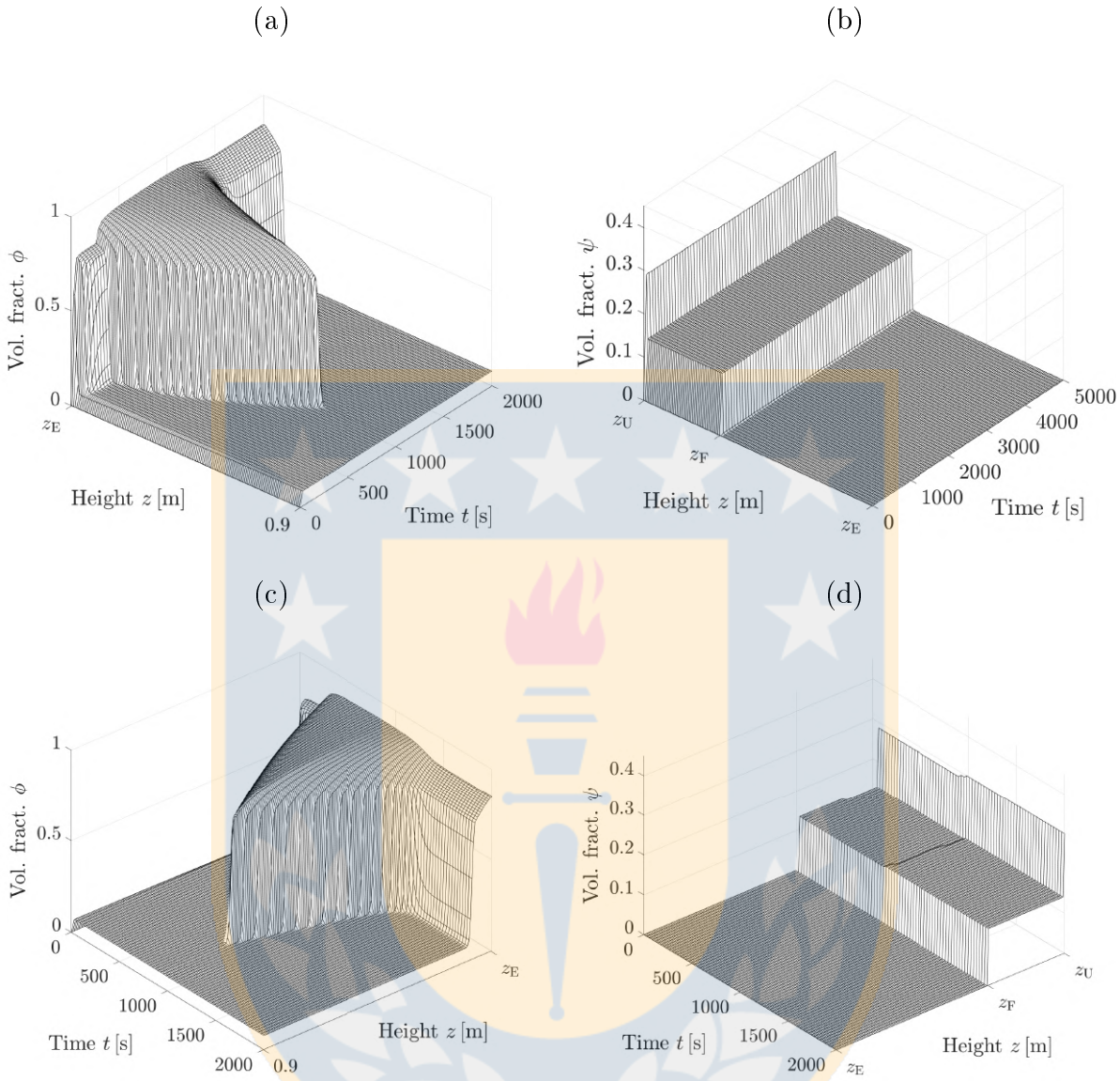

Figure 5.18: Example 5.3: Time evolution of the volume fraction (a, c) of aggregates ϕ and (b,d) solids ψ computed with $N = 1600$ and seen from two different angles. A step change down in Q_{W} occurs at $t = 300\,\mathrm{s}$ and a control action by decreasing Q_{U} is made at $t = 1000\,\mathrm{s}$.

Conclusions and future works

Conclusions

Here we present a summary with the main contributions and conclusions of the thesis.

- In **Chapter 1** we described a flotation column model that is consistent with the established drift- and solids-flux theories, which have been proposed separately for the bubble-liquid subsystem of a flotation column and for the settling of particles. The mathematical and numerical analysis provides a framework that complements the flux constructions done in some recent papers [38, 54, 106, 111] and leads to a simple but formally complete model of steady states and transient operation of the flotation column. The novelty of the approach (for the application to flotation) consists in the implementation of recently developed knowledge on the determination and well-posedness of solutions to conservation laws with discontinuous flux. While some of the mathematical details and a complete classification of steady states have been studied in [18], the benefits of the approach should become clear through the consistency between the operating charts and the response of the system to changes in the feed inputs and control actions. That said, we emphasize that the steady states and the nonlinear conditions behind the operating charts in Section 1.3 are valid to *any* pair of functions j_{b} and f_{b} that satisfy the assumptions in Section 1.2.4. Of course, the operating charts, and in particular the existence, size, and shape of the region of feasibility of the different steady states (the "white regions" of the fifth plot of Figure 1.2, the third plot of Figure 1.3, and the plots of Figure 1.5) depend on the particular choices of j_{b} and f_{b}. In the same spirit we mention that the flotation column has been subdivided into three zones of equal height (zones 1, 2 and 3) for illustrative purposes only; the model allows any sizes of the zones and any variation with height of the cross-sectional area.

  We recall that the present model is a quasilinear first-order system of conservation laws, whose solutions, that is the profiles of ϕ and φ (or ψ) in general has discontinuous, both stationary ones at the boundaries between zones and possibly moving ones within zones. The latter property is easily visible in the sharp discontinuities that travel at non-constant speed; see Figures 1.6 to 1.12.

Another simplification within the present approach that could give rise to further refinement of the model concerns the assumption of a uniform bubble size, and hence unique terminal settling velocity $v_{\mathrm{term,a}}$ of an aggregate. We have adapted this assumption from works focussing on drift flux theory e.g., [38, 54, 105], but it is also present, for instance, in [84, 91]. That said, we are well aware that within the bubbly region, bubble diameters are in fact distributed (a problem that was addressed early, see e.g. [47]). Within the froth region, the bubble diameter, which strongly influences the factor $v_{\mathrm{term,a}}$, is assumed constant here but in reality is difficult to predict since it depends on a combination of some inherent stability of the films between the bubbles and the liquid content (via the capillary pressure that this exerts). This stability is crucially important to the performance of the froth, but modelling it for transient simulations in a transient sense seems to be a challenge.

- In **Chapter 2** we have applied the three-phase flow model described in **Chapter 1** with specific constitutive relationships for the drift flux $j_{\mathrm{b}}(\phi)$ and settled flux $f_{\mathrm{b}(\varphi)}$. A concrete outcome is that the DAF thickening process with additional sedimentation of particles can be simulated dynamically and its stationary operation controlled via an operating chart that visualizes a region of admissible values of the volumetric control flows of the feed and of the underflow. Depending on the distribution of aggregates and solids in the tank at a certain time point, one may have to perform several control actions where the last of them is to choose $(Q_{\mathrm{U}}, Q_{\mathrm{F}})$ in the admissible region. On the other hand, if $(Q_{\mathrm{U}}, Q_{\mathrm{F}})$ lies *outside* the admissible region, a desired steady state cannot be attained. The model and the operating chart become particularly important if the density of the particles is only slightly larger than that of water, which we have demonstrated in Section 2.4.4.

- **Chapter 3** is mainly for the detailed presentation of the new numerical method for a triangular system of two PDEs, whose flux functions have several spatial discontinuities due to in- and outflows of a one-dimensional tank with possibly varying cross-sectional area as described in **Chapter 1**. The triangular structure is utilized in the following way in the numerical scheme. The numerical update formula corresponding to the first scalar equation contains, for the nonlinear term, a numerical flux where the the volume fraction in the left cell is multiplied with the velocity computed in the right cell; see [23]. The update formula for the second equation uses Engquist-Osher numerical flux for the term modelling the nonlinear relative flux of the secondary phase, chosen in a particular way since this flux also depends on the primary phase volume fraction. The other terms of the second update formula are also chosen in such a way that the entire scheme is proved to be monotone under a the CFL condition (3.18). We prove that the numerically obtained volume fractions satisfy the invariant-region property that they stay between zero and one, as it is physically expected. The numerical scheme is applied to simulate the hydrodynamic movement of simultaneously rising aggregates (air bubbles with attached hydrophobic particles) and settling hydrophilic particles in the fluid under in- and outflows

of a flotation column. As a demonstration of the capabilities of the numerical method, three different settings are simulated.

In [18], the authors proposed a staggered scheme to compute numerical solutions for a flotation column, following the approach of Karlsen et al. [64,67]. Although the staggered scheme worked for a single inlet for a mixture of aggregates and solids, we have, in the case of several feed inlets, found it difficult to get consistent numerical solutions with respect to different mesh sizes.

- **Chapter 4** contains a convergence analysis for the approximate numerical solutions under certain simplifying assumptions. We proved that if cross-sectional area is constant, then the scheme for the primary phase, in the sense of Definition 4.2.1, converges to an entropy solution. Assuming in addtion that there are no flux discontinities we used compensated compactness to prove that the numerical solution of the secondary phase converges to a weak solution. It remains to prove uniqueness.

- The one-dimensional model of a flotation column described in **Chapters 1–3**, is a triangular hyperbolic 2×2 system of nonlinear PDEs of the first order. In **Chapter 5**, we propose an extended model where the drainage of liquid in the froth layer due to capillarity is included. The traditional derivation of the drainage PDE, valid only within the froth, is combined with further experimental findings from the literature to end up in a constitutive relationship between the relative velocity of aggregates to fluid (or suspension of hydrophilic solids), which in the governing equations yields a second-order-derivative degenerate nonlinear term.

  An analysis of the possible steady states with a froth layer at the top of the column (desired steady states) leads to several inequalities involving the feed input variables and other control volumetric flows; see Theorem 5.1. Those inequalities are visualized in operating charts; see Figure 5.8, in which the white region shows the necessary location of an operating point $(Q_{\mathrm{U}}, Q_{\mathrm{F}})$ for having a desired steady state after a time of transient behaviour.

  With parameters extracted from the literature, the white region of an operating chart is quite small, meaning that the existence of a froth layer is very sensitive to small changes in any of the control variables Q_{U} and Q_{W}. Different operating points $(Q_{\mathrm{U}}, Q_{\mathrm{F}})$ in the white region give rise to different thicknesses of the froth layer. Unfortunately, our model anticipates a very sensitive dependence of the pulp-froth interface location z_{fr} on the operating point; see Figure 5.9, where the yellow surface shows that the most common values of z_{fr} is close to one, meaning a thin froth layer. The surfaces seen in plots (c) and (d) indicate a very large gradient from z_{fr} just below one down to $z_{\mathrm{fr}} = 0.33 = z_{\mathrm{F}}$. (Even finer resolutions indicate that the graph is continuous.) The numerical scheme suggested resolves discontinuities well and numerical results (e.g., those of Figure 5.16) show that the volume fractions, and their sum, stay between zero and one, as is proven in Theorems 5.2 and 5.3.

Overall, the steady-state analysis, boundedness properties of the numerical solutions, and simulation results indicate that the model is useful for the simulation of flotation columns and could be used, for example, to simulate the effect of various alternative control actions. In light of this practical interest it would be desirable to obtain a well-posedness (existence and uniqueness) result for the underlying model. The first equation of (5.2) (the one for ϕ) as a scalar strongly degenerate parabolic equation with discontinuous flux that is independent of ψ can be handled by known arguments (cf., e.g., [26, 68, 69]). The corresponding model for $D \equiv 0$ (without capillarity) is a triangular system of conservation laws for which convergence results of monotone schemes to a weak solution are available, at least for the case of fluxes without spatial discontinuity [34, 67]. It is not clear at the moment whether the corresponding arguments, based on the compensated compactness method, can also be applied to the system (5.2). Therefore, well-posedness of the model is at the moment left as an open problem.

Future Work

- In most applications, the adhesion of hydrophobic particles to bubbles takes place in collection region. This is a region of countercurrent flow: bubbles move upward and solid particles settle [9,115] while the attachment of hydrophobic particles to bubbles occurs. In future work, we will extend the model described in **Chapter 1** into one that accounts for the aggregation process. This requires including reaction terms. In addition, a separate PDE needs to be introduced for a third field variable, for instance the number of solid particles attached to a single bubble at each spatial position and time. The resulting 3×3 convection-reaction system is likely to form a model that could be used for design and control simulations (so-called model-predictive control; see [10, 78, 80].

- As pointed out by [85], one important phenomenon that takes place on the surface of froth is the bursting of bubbles, with the consequence that the average liquid content of the froth that reaches the overflow lip cannot be lower than that of the froth flowing out of the cell. The model of a flotation column with drainage can certainly be extended to include this phenomenon. For instance, one could incorporate the possibility of bursting bubbles at the top by assuming that the flotation column is constructed in a way such that a portion α of the froth overflows with unbursting aggregates, whereas for the portion $1-\alpha$, the aggregates burst. The latter means that the gas 'disappears' (i.e., is released into the surrounding air), whereas the suspension and the hydrophobic particles attached to the bursting bubbles follow the effluent stream. There is practical interest in quantifying this effect [85]. Hence, the effluent volume fraction of aggregates would then be $\phi_{\mathrm{E}} := \alpha\phi_{\mathrm{E}}^{+}$, and the solids $\varphi_{\mathrm{E}} := \varphi_{\mathrm{E}}^{+}$. Under the present assumptions, the factor α does not influence the solution inside the column. It could however depend on the wash water flow, and this could be an extension of the model.

- Another application with potential modelling advantages is counter-current"washing" of solids, a process of solvent extraction in hydrometallurgy by coupling a series of clarifier-thickeners [108]. The process is also known as *leaching* [97, Ch. 10]. Contrary to biological applications, it seems that to model such applications, one has to include the effect of mass transfer into the governing equations. In particular, counter current decantation (CCD) thickener circuits are used to recover soluble metal as pregnant liquor solution from ore leach residue. The basis of CCD operation is to concentrate suspended solids thereby minimizing liquor content in underflow slurry that flow in one direction. Then the underflow slurry liquor is diluted with wash liquor that flows in the opposite direction and the suspended solids are concentrated again and again. The amount of liquor in the thickener underflow contributes to determining the number of CCD stages required to recover the desired amount of soluble metal. Furthermore, similar results could be achieved at a lower wash quantity, reducing the size of downstream equipment. High density thickeners (HDT) are designed to use gravity and compression, and minimize the amount of liquor in the underflow thus minimizing the number of CCD stages. It would be of interest to develop a networked model of several of these units (along with a corrsponding numerical scheme, etc.), possibly extended to reactive settling, to arrive at a mathematical model of CCD.

Conclusiones y Trabajos Futuros

Conclusiones

A continuación, se presenta un resumen con los principales aportes y conclusiones generadas en esta tesis.

- En el **Capítulo 1** describimos un modelo de columna de flotación que es consistente con las teorías establecidas de flujo de sólidos y de deriva, que se han propuesto por separado para el sub-sistema burbuja-líquido de una columna de flotación y para la sedimentación de partículas. El análisis matemático y numérico proporciona un marco que complementa las construcciones de flujo realizadas en algunos trabajos recientes [38, 54, 106, 111] y conduce a un modelo simple pero formalmente completo de los estados estacionarios y el funcionamiento transitorio de la columna de flotación. La novedad del enfoque (para la aplicación a la flotación) consiste en la implementación de los conocimientos recientemente desarrollados sobre la determinación y el buen planteamiento de las soluciones de las leyes de conservación con flujo discontinuo. Aunque algunos de los detalles matemáticos y una clasificación completa de los estados estacionarios han sido estudiados en [18], los beneficios del enfoque deberían quedar claros a través de la consistencia entre los gráficos de operación y la respuesta del sistema a los cambios en las entradas de alimentación y las acciones de control. Dicho esto, hacemos hincapié en que los estados estacionarios y las condiciones no lineales detrás de los gráficos de operación en la Sección refsec:ss son válidos para *cualquier* par de funciones j_b y f_b que satisfacen los supuestos de la Sección 1.2.4. Por supuesto, los gráficos de operación, y en particular la existencia, el tamaño y la forma de la región de viabilidad de los diferentes estados estacionarios (las "regiones blancas" de la quinta gráfica de la Figura 1.2, la tercera gráfica de la Figura 1.3, y las gráficas de la Figura 1.5) dependen de las elecciones particulares de j_b y f_b. Con el mismo espíritu, mencionamos que la columna de flotación se ha dividida en tres zonas de igual altura (zonas 1, 2 y 3) sólo con fines ilustrativo; el modelo permite cualquier tamaño de las zonas y cualquier variación con la altura del área de la sección transversal.

  Recordemos que el presente modelo es un sistema cuasi-lineal de leyes de conservación de primer orden, cuyas soluciones, es decir los perfiles de ϕ y φ (o ψ) en general tienen discontinuidad, tanto estacionaria en los límites entre zonas como posiblemente en movimiento

dentro de las zonas. Esta última propiedad es fácilmente visible en las discontinuidades agudas que se desplazan a velocidad no constante; véanse las Figuras 1.6 a 1.12.

Otra simplificación dentro del presente enfoque que podría dar lugar a un mayor refinamiento del modelo se refiere a la suposición de un tamaño de burbuja uniforme y, por lo tanto, una velocidad de asentamiento terminal única $v_{\mathrm{term,a}}$ de un agregado. Hemos adaptado esta suposición de trabajos que se centran en la teoría del flujo de deriva, por ejemplo, [38,54,105], pero también está presente, por ejemplo, en [84,91]. Dicho esto, somos muy conscientes de que dentro de la región burbujeante, los diámetros de las burbujas están, de hecho, distribuidos (un problema que se abordó antes, véase, por ejemplo, [47]). Dentro de la región de la espuma, el diámetro de la burbuja, que influye fuertemente en el factor $v_{\mathrm{term,a}}$, se asume constante aquí pero en realidad es difícil de predecir ya que depende de una combinación de cierta estabilidad inherente de las películas entre las burbujas y el contenido líquido (a través de la presión capilar que esto ejerce). Esta estabilidad es de vital importancia para el rendimiento de la espuma, pero modelarla para simulaciones transitorias en un sentido pasajero parece ser un desafío.

- En el **Capítulo 2** hemos aplicado el modelo de flujo trifásico descrito en el **Capítulo 1** con relaciones constitutivas específicas para el flujo de deriva $j_{\mathrm{b}}(\phi)$ y el flujo de sólidos $f_{\mathrm{b}(\varphi)}$. Un resultado concreto es que el proceso de espesamiento por flotación de aire disuelto (DAF por sus siglas en inglés, *Dissolved Air Flotation*) con sedimentación adicional de partículas puede simularse dinámicamente y su operación estacionaria controlarse a través de un gráfico operativo que visualiza una región de valores admisibles de los flujos de control volumétrico de alimentación y del flujo inferior. Dependiendo de la distribución de agregados y sólidos en el tanque en un momento determinado, es posible que deba realizar varias acciones de control donde la última de ellas es elegir $(Q_{\mathrm{U}}, Q_{\mathrm{F}})$ en la región admisible. Por otro lado, si $(Q_{\mathrm{U}}, Q_{\mathrm{F}})$ se encuentra *fuera* de la región admisible, no se puede alcanzar el estado estacionario deseado. El modelo y el gráfico de operaciones se vuelven particularmente importantes si la densidad de las partículas es solo un poco más grande que la del agua, lo cual demostramos en la Sección 2.4.4.

- El **Capítulo 3** es principalmente para la presentación detallada del nuevo método numérico para un sistema triangular de dos EDPs, cuyas funciones de flujo tienen varias discontinuidades espaciales debido a flujos de entrada y salida de un tanque unidimensional con área de sección transversal posiblemente variable como se describe en el **Capítulo 1**. La estructura triangular se utiliza de la siguiente manera en el esquema numérico. La fórmula de actualización numérica correspondiente a la primera ecuación escalar contiene, para el término no lineal, un flujo numérico donde la fracción de volumen en la celda de la izquierda se multiplica por la velocidad calculada en la celda de la derecha; ver [23]. La fórmula de actualización de la segunda ecuación utiliza el flujo numérico de Engquist-Osher para el término que modela el flujo relativo no lineal de la fase secundaria, elegido de manera particular ya que este flujo también depende de la fracción de

volumen de la fase primaria. Los otros términos de la segunda fórmula de actualización también se eligen de tal manera que se demuestra que todo el esquema es monótono bajo la condición CFL (3.18). Probamos que las fracciones volumétricas obtenidas numéricamente satisfacen la propiedad de región invariante, es decir, que se mantienen entre cero y uno, como se espera físicamente. El esquema numérico se aplica para simular el movimiento hidrodinámico de agregados que ascienden simultáneamente (burbujas de aire con partículas hidrofóbicas adheridas) y partículas hidrofílicas que sedimentan en el fluido bajo los flujos de entrada y salida de una columna de flotación. Como demostración de las capacidades del método numérico, se simulan tres configuraciones diferentes.

En [18], los autores propusieron un esquema escalonado para calcular soluciones numéricas para una columna de flotación, siguiendo el enfoque de Karlsen et al. [64, 67]. Aunque el esquema escalonado funcionó para una sola entrada para una mezcla de agregados y sólidos, en el caso de varias entradas de alimentación, nos resultó difícil obtener soluciones numéricas consistentes con respecto a diferentes tamaños de malla.

- El **Capítulo 4** contiene un análisis de convergencia para las soluciones numéricas aproximadas bajo ciertas suposiciones simplificadas. Probamos que si el área de la sección transversal es constante, entonces el esquema para la fase primaria, en el sentido de la Definición 4.2.1, converge a una solución de entropía. Suponiendo además que no hay discontinuidades de flujo, usamos compacidad compensada para probar que la solución numérica de la fase secundaria converge a una solución débil. Queda por probar la unicidad.

- El modelo unidimensional de una columna de flotación descrito en los **Capítulos 1–3**, es un sistema triangular hiperbólico 2×2 de EDPs no lineales de primer orden. En el **Capítulo 5**, proponemos un modelo extendido donde se incluye el drenaje de líquido en la capa de espuma debido a la capilaridad. La derivación tradicional de la EDP de drenaje, válida solo dentro de la espuma, se combina con otros hallazgos experimentales de la literatura para terminar en una relación constitutiva entre la velocidad relativa de los agregados al fluido (o suspensión de sólidos hidrofílicos), que en las ecuaciones gobernantes lleva a un termino de derivadas de segundo orden degenerado y no-lineal.

  Un análisis de los posibles estados estacionarios con una capa de espuma en la parte superior de la columna (estados estacionarios deseados) conduce a varias desigualdades que involucran las variables de entrada de alimentación y otros flujos volumétricos de control; ver Teorema 5.1. Esas desigualdades se visualizan en gráficos de operación; consulte la Figura 5.8, en la que la región blanca muestra la ubicación necesaria de un punto de operación $(Q_{\mathrm{U}}, Q_{\mathrm{F}})$ para tener un estado estacionario deseado después de un tiempo de comportamiento transitorio.

  Con parámetros extraídos de la literatura, la región blanca de un gráfico operativo es bastante pequeña, lo que significa que la existencia de una capa de espuma es muy sensible a pequeños cambios en cualquiera de las variables de control Q_{U} y Q_{W}. Diferentes puntos

de operación (Q_U, Q_F) en la región blanca dan lugar a diferentes espesores de la capa de espuma. Desafortunadamente, nuestro modelo anticipa una dependencia muy sensible de la ubicación de la interfaz pulpa-espuma z_{fr} en el punto de operación; vea la Figura 5.9, donde la superficie amarilla muestra que los valores más comunes de z_{fr} están cerca de uno, lo que significa una capa delgada de espuma. Las superficies que se ven en los gráficos (c) y (d) indican un gradiente muy grande desde z_{fr} justo debajo de uno hasta $z_{fr} = 0.33 = z_F$. (Resoluciones aún más finas indican que el gráfico es continuo). El esquema numérico sugerido resuelve bien las discontinuidades y los resultados numéricos (por ejemplo, los de la Figura 5.16) muestran que las fracciones de volumen, y su suma, se mantienen entre cero y uno, como se demuestra en los Teoremas 5.2 y 5.3.

En general, el análisis de estados estacionarios, las propiedades de acotación de las soluciones numéricas y los resultados de la simulación indican que el modelo es útil para la simulación de columnas de flotación y podría usarse, por ejemplo, para simular el efecto de varias acciones de control alternativas. A la luz de este interés práctico, sería deseable obtener un resultado de buen planteamiento (existencia y unicidad) para el modelo subyacente. La primera ecuación de 5.2 (para ϕ) como una ecuación parabólica escalar fuertemente degenerada con flujo discontinuo que es independiente de ψ puede manejarse mediante argumentos conocidos (por ejemplo, [26, 68, 69]). El modelo correspondiente para $D \equiv 0$ (sin capilaridad) es un sistema triangular de leyes de conservación para el cual se dispone de resultados de convergencia de esquemas monótonos a una solución débil, al menos para el caso de flujos sin discontinuidad espacial [34,67]. No está claro por el momento si los argumentos correspondientes, basados en el método de compacidad compensada , también se pueden aplicar al sistema 5.2. Por lo tanto, el buen planteamiento del modelo se deja por el momento como un problema abierto.

Trabajo Futuro

- En la mayoría de las aplicaciones, la adhesión de partículas hidrofóbicas a las burbujas tiene lugar en la región de recolección. Esta es una zona de flujo a contracorriente: las burbujas se mueven hacia arriba y las partículas sólidas se asientan [9, 115] mientras se produce la unión de partículas hidrofóbicas a las burbujas. En trabajos futuros, extenderemos el modelo descrito en los **Capítulos 1–3** a uno que tenga en cuenta el proceso de agregación. Esto requiere incluir términos de reacción. Además, se debe introducir una EDP separada para una tercera variable de campo, por ejemplo, el número de partículas sólidas unidas a una sola burbuja en cada posición espacial y tiempo. Es probable que el sistema de convección-reacción de 3×3 resultante forme un modelo que podría usarse para simulaciones de diseño y control (el llamado control-predictivo del modelo; consulte [10, 78, 80]).

- Como se señala en [85], un fenómeno importante que tiene lugar en la superficie de la espuma es el estallido de burbujas, con la consecuencia de que el contenido medio de líquido de la espuma que llega al borde de desbordamiento no puede ser inferior al del espuma que sale de la celda. El modelo de una columna de flotación con drenaje ciertamente puede extenderse para incluir este fenómeno. Por ejemplo, se podría incorporar la posibilidad de rompimiento de burbujas en la parte superior asumiendo que la columna de flotación está construida de tal manera que una porción α de la espuma se desborda con agregados que no revientan, mientras que para la porción $1-\alpha$, los agregados estallaron. Esto último significa que el gas "desaparece" (es decir, se libera en el aire circundante), mientras que la suspensión y las partículas hidrofóbicas adheridas a las burbujas que revientan siguen la corriente del efluente. Existe un interés práctico en cuantificar este efecto [85]. Por lo tanto, la fracción de volumen de los agregados en el efluente sería $\phi_{\mathrm{E}} := \alpha\phi_{\mathrm{E}}^{+}$, y los sólidos $\varphi_{\mathrm{E}} := \varphi_{\mathrm{E}}^{+}$. Bajo las presentes suposiciones, el factor α no influye en la solución dentro de la columna. Sin embargo, podría depender del flujo de agua de lavado, y esto podría ser una extensión del modelo.

- Otra aplicación con posibles ventajas de modelado es el “lavado” de sólidos a contracorriente, un proceso de extracción por solvente en hidrometalurgia mediante el acoplamiento de una serie de clarificadores-espesadores [108]. El proceso también se conoce como *lixiviación* [97, Ch. 10]. Al contrario de las aplicaciones biológicas, parece que para modelar tales procesos, uno tiene que incluir el efecto de la transferencia de masa en las ecuaciones gobernantes. En particular, los circuitos espesadores de decantación en contracorriente (CCD por sus siglas en inglés, *counter current decantation*) se utilizan para recuperar metal soluble como solución de licor cargado de residuos de lixiviación de minerales. La base de la operación CCD es concentrar los sólidos en suspensión, minimizando así el contenido de licor en el lodo de desbordamiento inferior que fluye en una dirección. Luego, el licor de suspensión de flujo inferior se diluye con licor de lavado que fluye en la dirección opuesta y los sólidos en suspensión se concentran una y otra vez. La cantidad de licor en el flujo inferior del espesador contribuye a determinar el número de etapas CCD requeridas para recuperar la cantidad deseada de metal soluble. Además, se podrían lograr resultados similares con una menor cantidad de lavado, reduciendo el tamaño del equipo corriente abajo. Los espesadores de alta densidad están diseñados para utilizar la gravedad y la compresión, y minimizar la cantidad de licor en el flujo inferior, lo que minimiza el número de etapas CCD. Sería interesante desarrollar un modelo en red de varias de estas unidades (junto con un esquema numérico correspondiente, etc.), posiblemente extendido a la decantación reactiva, para llegar a un modelo matemático de CCD.

References

[1] B. Andreianov, C. Donadello, S. S. Ghoshal, and U. Razafison, *On the attainable set for a class of triangular systems of conservation laws*, J. Evol. Equ., 15 (2015), pp. 503–532.

[2] B. Andreianov and D. Mitrović, *Entropy conditions for scalar conservation laws with discontinuous flux revisited*, in Ann. Inst H. Poincaré Anal. Non linéaire, vol. 32, 2015, pp. 1307–1335.

[3] S. Ata, *Phenomena in the froth phase of flotation — a review*, Int. J. Miner. Process., 102-103 (2012), pp. 1–12.

[4] M. Azhin, K. Popli, A. Afacan, Q. Liu, and V. Prasad, *A dynamic framework for a three phase hybrid flotation column*, Miner. Eng., 170 (2021), p. 107028.

[5] M. Azhin, K. Popli, and V. Prasad, *Modelling and boundary optimal control design of hybrid column flotation*, Can. J. Chem. Eng., 99 (2021), pp. S369–S388.

[6] O. A. Bascur, *A unified solid/liquid separation framework*, Fluid/Particle Sep. J., 4 (1991), pp. 117–122.

[7] O. A. Bascur, *A flotation model framework for dynamic performance monitoring*, in International Mineral Processing Seminar, PROCEMIN, R. Kuyvenhoven, ed., 2011, pp. 328–339.

[8] S. Beheir and M. Aziz, *Removal of zn (ii) from dilute aqueous solutions and radioactive process wastewater by foam separation*, J. Radioanal. Nucl. Chem., 209 (1996), pp. 75–89.

[9] L. Bergh and J. Yianatos, *Flotation column automation: state of the art*, Control Eng. Pract., 11 (2003), pp. 67–72.

[10] L. Bergh and J. Yianatos, *The long way toward multivariate predictive control of flotation processes*, J. Process. Control, 21 (2011), pp. 226–234.

[11] S. Boscarino, R. Bürger, P. Mulet, G. Russo, and L. M. Villada, *Linearly implicit IMEX Runge–Kutta methods for a class of degenerate convection-diffusion problems*, SIAM J. Sci. Comput., 37 (2015), pp. B305–B331.

[12] J. Bratby and W. Ambrose, *Design and control of flotation thickeners*, Water Sci. Tech., 31 (1995), pp. 247–261.

[13] C. E. Brennen, *Fundamentals of Multiphase Flow*, Cambridge University Press, 2005.

[14] A. Bressan, G. Guerra, and W. Shen, *Vanishing viscosity solutions for conservation laws with regulated flux*, J. Differ. Equ., 266 (2019), pp. 312–351.

[15] P. R. Brito-Parada, S. J. Neethling, and J. J. Cilliers, *The advantages of using mesh adaptivity when modelling the drainage of liquid in froths*, Miner. Eng., 33 (2012), pp. 80–86.

[16] R. Bürger, S. Diehl, S. Farås, I. Nopens, and E. Torfs, *A consistent modelling methodology for secondary settling tanks: A reliable numerical method*, Water Sci. Tech., 68 (2013), pp. 192–208.

[17] R. Bürger, S. Diehl, and M. C. Martí, *A conservation law with multiply discontinuous flux modelling a flotation column*, Networks Heterog. Media, 13 (2018), pp. 339–371.

[18] R. Bürger, S. Diehl, and M. C. Martí, *A system of conservation laws with discontinuous flux modelling flotation with sedimentation*, IMA J. Appl. Math., 84 (2019), pp. 930–973.

[19] R. Bürger, S. Diehl, M. C. Martí, and Y. Vásquez, *A degenerating convection-diffusion system modelling froth flotation with drainage*. Preprint 2022–06, Centro de Investigación en Ingeniería Mathemática (CI^2MA), Universidad de Concepción, Chile.

[20] R. Bürger, S. Diehl, M. C. Martí, and Y. Vásquez, *Flotation with sedimentation: Steady states and numerical simulation of transient operation*, Miner. Eng., 157 (2020), p. 106419.

[21] R. Bürger, S. Diehl, M. C. Martí, and Y. Vásquez, *A difference scheme for a triangular system of conservation laws with discontinuous flux modeling three-phase flows*. In preparation, 2022.

[22] R. Bürger, S. Diehl, and C. Mejías, *A difference scheme for a degenerating convection-diffusion-reaction system modelling continuous sedimentation*, ESAIM: Math. Modelling Num. Anal., 52 (2018), pp. 365–392.

[23] R. Bürger, A. García, K. H. Karlsen, and J. D. Towers, *A family of numerical schemes for kinematic flows with discontinuous flux*, J. Eng. Math., 60 (2008), pp. 387–425.

[24] R. Bürger, K. H. Karlsen, N. H. Risebro, and J. D. Towers, *Well-posedness in BV_t and convergence of a difference scheme for continuous sedimentation in ideal clarifier-thickener units*, Numer. Math., 97 (2004), pp. 25–65.

[25] R. Bürger, K. H. Karlsen, H. Torres, and J. D. Towers, *Second-order schemes for conservation laws with discontinuous flux modelling clarifier–thickener units*, Numer. Math., 116 (2010), pp. 579–617.

[26] R. Bürger, K. H. Karlsen, and J. D. Towers, *A model of continuous sedimentation of flocculated suspensions in clarifier-thickener units*, SIAM J. Appl. Math., 65 (2005), pp. 882–940.

[27] R. Bürger, K. H. Karlsen, and J. D. Towers, *An Engquist-Osher-type scheme for conservation laws with discontinuous flux adapted to flux connections*, SIAM J. Num. Anal., 47 (2009), pp. 1684–1712.

[28] R. Bürger, s. Diehl, M. C. Martí, and Y. Vásquez, *Simulation and control od dissolved air flotation and column froth flotation with simultaneous sedimentation*, Water Sci. Tech., 81 (2020), pp. 1723–1732.

[29] R. Bürger, W. L. Wendland, and F. Concha, *Model equations for gravitational sedimentation-consolidation processes*, Z. Angew. Math. Mech., 80 (2000), pp. 79–92.

[30] M. C. Bustos, F. Concha, R. Bürger, and E. M. Tory, *Sedimentation and Thickening: Phenomenological Foundation and Mathematical Theory*, Kluwer Academic Publishers, Dordrecht, The Netherlands, 1999.

[31] R. Butler, R. Finger, J. Pitts, and B. Strutynski, *Advantages of cothickening primary and secondary sludges in dissolved air flotation thickeners*, Water Environ. Res., 69 (1997), pp. 311–316.

[32] S. Chavadej, W. Phoochinda, U. Yanatatsaneejit, and J. Scamehorn, *Clean-up of oily wastewater by froth flotation: effect of microemulsion formation iii: use of anionic/nonionic surfactant mixtures and effect of relative volumes of dissimilar phases*, Sep. Sci. Tech., 39 (2004), pp. 3097–3112.

[33] T. Chung and D. Kim, *Significance of pressure and recirculation in sludge thickening by dissolved air flotation*, Water Sci. Tech., 36 (1997), pp. 223–230.

[34] G. M. Coclite, S. Mishra, and N. H. Risebro, *Convergence of an Engquist-Osher scheme for a multi-dimensional triangular system of conservation laws*, Math. Comp., 79 (2010), pp. 71–94.

[35] M. Crandall and L. Tartar, *Some relations between nonexpansive and order preserving mappings*, Proc. Amer. Math. Soc., 78 (1980), pp. 385–390.

[36] E. B. Cruz, *A comprehensive dynamic model of the column flotation unit operation*, PhD thesis, Virginia Tech, Blacksburg, Virginia, 1997.

[37] V. Danilov and D. Mitrovic, *Delta shock wave formation in the case of triangular hyperbolic system of conservation laws*, J. Differ. Equ., 245 (2008), pp. 3704–3734.

[38] J. E. Dickinson and K. P. Galvin, *Fluidized bed desliming in fine particle flotation – part I*, Chem. Eng. Sci., 108 (2014), pp. 283–298.

[39] S. Diehl, *A conservation law with point source and discontinuous flux function modelling continuous sedimentation*, SIAM J. Appl. Math., 56 (1996), pp. 388–419.

[40] S. Diehl, *Dynamic and steady-state behavior of continuous sedimentation*, SIAM J. Appl. Math., 57 (1997), pp. 991–1018.

[41] S. Diehl, *Operating charts for continuous sedimentation I: Control of steady states*, J. Eng. Math., 41 (2001), pp. 117–144.

[42] S. Diehl, *Operating charts for continuous sedimentation II: Step responses*, J. Eng. Math., 53 (2005), pp. 139–185.

[43] S. Diehl, *A regulator for continuous sedimentation in ideal clarifier-thickener units*, J. Eng. Math., 60 (2008), pp. 265–291.

[44] S. Diehl, *The solids-flux theory – confirmation and extension by using partial differential equations*, Water Res., 42 (2008), pp. 4976–4988.

[45] S. Diehl, *A uniqueness condition for nonlinear convection-diffusion equations with discontinuous coefficients*, J. Hyperbolic Differential Equations, 6 (2009), pp. 127–159.

[46] S. Diehl, G. Sparr, and G. Olsson, *Analytical and numerical description of the settling process in the activated sludge operation*, in Instrumentation, Control and Automation of Water and Wastewater Treatment and Transport Systems, R. Briggs, ed., IAWPRC, Pergamon Press, 1990, pp. 471–478.

[47] G. Dobby, J. Yianatos, and J. Finch, *Estimation of bubble diameter in flotation columns from drift flux analysis*, Canad. Metall. Quart., 27 (1988), pp. 85–90.

[48] R. Droste and R. Gehr, *Theory and practice of water and wastewater treatment*, John Wiley & Sons, 2018.

[49] G. A. Ekama, J. L. Barnard, F. W. Günthert, P. Krebs, J. A. McCorquodale, D. S. Parker, and E. J. Wahlberg, *Secondary Settling Tanks: Theory, Modelling, Design and Operation*, IAWQ scientific and technical report no. 6. International Association on Water Quality, England, 1997.

[50] G. A. Ekama and P. Marais, *Assessing the applicability of the 1D flux theory to full-scale secondary settling tank design with a 2D hydrodynamic model*, Water Res., 38 (2004), pp. 495–506.

[51] B. Engquist and S. Osher, *One-sided difference approximations for nonlinear conservation laws*, Math. Comp., 36 (1981), pp. 321–351.

[52] S. Evje and K. H. Karlsen, *Monotone difference approximations of BV solutions to degenerate convection-diffusion equations*, SIAM J. Numer. Anal., 37 (2000), pp. 1838–1860.

[53] J. A. Finch and G. S. Dobby, *Column Flotation*, Pergamon Press, London, 1990.

[54] K. P. Galvin and J. E. Dickinson, *Fluidized bed desliming in fine particle flotation – part II: Flotation of a model feed*, Chem. Eng. Sci., 108 (2014), pp. 299–309.

[55] K. P. Galvin, N. G. Harvey, and J. E. Dickinson, *Fluidized bed desliming in fine particle flotation – part III flotation of difficult to clean coal*, Minerals Eng., 66–68 (2014), pp. 94–101.

[56] S. K. Godunov, *A finite difference method for the numerical computations of discontinuous solutions of the equations of fluid dynamics*, Mat. Sb., 47 (1959), pp. 271–306. (In Russian).

[57] I. I. Goldfarb, K. B. Kann, and I. R. Shreiber, *Liquid flow in foams*, Fluid Dynamics, 23 (1988), pp. 244–249.

[58] J. Haarhoff and E. Bezuidenhout, *Full-scale evaluation of activated sludge thickening by dissolved air flotation*, WATER SA, 25 (1999), pp. 153–166.

[59] B. Haffner, Y. Khidas, and O. Pitois, *The drainage of foamy granular suspensions*, J. Colloid Interface Sci., 458 (2015), pp. 200–208.

[60] H. Holden and N. H. Risebro, *Front Tracking for Hyperbolic Conservation Laws*, Second Edition, Springer Verlag, Berlin, 2015.

[61] K. Howe, D. Hand, J. Crittenden, R. Trussell, and G. Tchobanoglous, *Principles of water treatment*, John Wiley & Sons, 2012.

[62] P. Ireland and G. Jameson, *Liquid transport in a multi-layer froth*, J. Colloid Interf. Sci., 314 (2007), pp. 207–213.

[63] E. L. Isaacson and J. B. Temple, *Analysis of a singular hyperbolic system of conservation laws*, J. Differential Equations, 65 (1986), pp. 250–268.

[64] K. Karlsen, S. Mishra, and N. Risebro, *Semi-godunov schemes for general triangular systems of conservation laws*, J. Eng. Math., 60 (2008), pp. 337–349.

[65] K. Karlsen and N. Risebro, *Convergence of finite difference schemes for viscous and inviscid conservation laws with rough coefficients*, ESAIM: Math. Model. Numer. Anal., 35 (2001), pp. 239–269.

[66] K. Karlsen and D. Towers, *Convergence of a godunov scheme for conservation laws with a discontinuous flux lacking the crossing condition*, J. of Hyperbolic Differ. Equ., 14 (2017), pp. 671–701.

[67] K. H. Karlsen, S. Mishra, and N. H. Risebro, *Convergence of finite volume schemes for triangular systems of conservation laws*, Numer. Math., 111 (2008), pp. 559–589.

[68] K. H. Karlsen, N. H. Risebro, and J. D. Towers, *Upwind difference approximations for degenerate parabolic convection-diffusion equations with a discontinuous coefficient*, IMA J. Numer. Anal., 22 (2002), pp. 623–664.

[69] K. H. Karlsen, N. H. Risebro, and J. D. Towers, *L^1 stability for entropy solutions of nonlinear degenerate parabolic convection-diffusion equations with discontinuous coefficients*, Trans. Royal Norwegian Society Sci. Letters (Skr. K. Nor. Vidensk. Selsk.), 3 (2003), pp. 1–49.

[70] K. H. Karlsen and J. D. Towers, *Convergence of a Godunov scheme for conservation laws with a discontinuous flux lacking the crossing condition*, J. Hyperbolic Differential Equations, 14 (2017), pp. 671–701.

[71] S. A. Koehler, S. Hilgenfeldt, and H. A. Stone, *A generalized view of foam drainage: experiment and theory*, Langmuir, 16 (2000), pp. 6327–6341.

[72] S. KRuzkov, *First order quasi-linear equations with several independent variables*, Math. USSR Sb., 10 (1970), pp. 217–243.

[73] G. J. Kynch, *A theory of sedimentation*, Trans. Faraday Soc., 48 (1952), pp. 166–176.

[74] E. J. La Motta, J. A. McCorquodale, and J. A. Rojas, *Using the kinetics of biological flocculation and the limiting flux theory for the preliminary design of activated sludge systems. I: Model development*, J. Environ. Eng., 133 (2007), pp. 104–110.

[75] D. Langberg and G. Jameson, *The coexistence of the froth and liquid phases in a flotation column*, Chem. Eng. Sci., 47 (1992), pp. 4345–4355.

[76] R. A. Leonard and R. Lemlich, *Laminar longitudinal flow between close-packed cylinders*, Chem. Eng. Sci., 20 (1965), pp. 790–791.

[77] R. J. LeVeque, *Numerical Methods for Conservation Laws*, Birkhäuser Verlag, 1992.

[78] L.G.Bergh and J. Yianatos, *Dynamic simulation of operating variables in flotation columns*, Min. Eng., 8 (1995), pp. 603–613.

[79] S. Lin and C. Lo, *Treatment of textile wastewater by foam flotation*, Environ. Tech., 17 (1996), pp. 841–849.

[80] M. Maldonado, A. Desbiens, and R. D. Villar, *Potential use of model predictive control for optimizing the column flotation process*, Int. J. Mineral Process., 93 (2009), pp. 26–33.

[81] L. Metcalf and H. Eddy, *Wastewater Engineering: Treatment and Resource Recovery*, vol. 5th edn., McGraw-Hill, New York, 2014.

[82] D. Mitrovic, *New entropy conditions for scalar conservation laws with discontinuous flux*, Discrete Contin. Dyn. Syst., 30 (2011), pp. 1191–1210.

[83] D. Mitrovic, V. Bojkovic, and V. Danilov, *Linearization of the riemann problem for a triangular system of conservation laws and delta shock wave formation process*, Math. Meth. Appl. Sci., 33 (2010), pp. 904–921.

[84] G. Narsimhan, *Analysis of creaming and formation of foam layer in aerated liquid*, J. Colloid Interface Sci., 345 (2010), pp. 566–572.

[85] S. J. Neethling and P. R. Brito-Parada, *Predicting flotation behaviour – the interaction between froth stability and performance*, Miner. Eng., 120 (2018), pp. 60–65.

[86] S. J. Neethling and J. J. Cilliers, *Simulation of the effect of froth washing on flotation performance*, Chem. Eng. Sci., 56 (2001), pp. 6303–6311.

[87] S. J. Neethling and J. J. Cilliers, *The entrainment of gangue into a flotation froth*, Int. J. Mineral Process, 64 (2002), pp. 123–134.

[88] S. J. Neethling and J. J. Cilliers, *Solids motion in flowing froths*, Chem. Eng. Sci., 57 (2002), pp. 607–615.

[89] S. J. Neethling and J. J. Cilliers, *Modelling flotation froths*, Int. J. Miner. Proc., 72 (2003), pp. 267–287.

[90] S. J. Neethling, H. T. Lee, and J. J. Cilliers, *A foam drainage equation generalized for all liquid contents*, J. Physics: Condensed Matter, 14 (2002), pp. 331–342.

[91] R. Pal and J. Masliyah, *Flow characterization of a flotation column*, Can. J. Chem. Eng., 67 (1989), pp. 916–923.

[92] E. Y. Panov, *Existence and strong pre-compactness properties for entropy solutions of a first-order quasilinear equation with discontinuous flux*, Arch. Rational Mech. Anal., 195 (2010), pp. 643–673.

[93] W. Peng, G. Han, Y. Cao, K. Sun, and S. Song, *Efficiently removing pb (ii) from wastewater by graphene oxide using foam flotation*, Colloids Surf., 556 (2018), pp. 266–272.

[94] S. Qian, Z. Wu, H. Zheng, and Y. Geng, *Study on riboflavin recovery from wastewater by a batch foam separation process*, Sep. Sci. Tech., 44 (2009), pp. 2681–2694.

[95] P. Quintanilla, S. J. Neethling, and P. R. Brito-Parada, *Modelling for froth flotation control: A review*, Minerals Eng., 162 (2021), p. 106718.

[96] M. Reali, L. J. Patrizzi, and J. S. Cordeiro, *Comparison of thickening of sludges produced in two water treatment plants by using daf and gravity*, Minerva, 2 (2019), pp. 195–201.

[97] J. F. Richardson, J. H. Harker, and J. R. Backhurst, *Chemical Engineering, Particle Technology and Separation Processes*, vol. 2, Butterworth-Heinemann, fifth ed., 2002.

[98] J. F. Richardson and W. N. Zaki, *Sedimentation and fluidization: part I.*, Trans. Inst. Chem. Engineers (London), 32 (1954), pp. 35–53.

[99] K. Rietema, *Science and technology of dispersed two-phase systems—I and II*, Chem. Eng. Sci., 37 (1982), pp. 1125–1150.

[100] J. Rubio, M. L. Souza, and R. W. Smith, *Overview of flotation as a wastewater treatment technique*, Minerals Eng., 15 (2002), pp. 139–155.

[101] C. Sarrico, *A distributional product approach to δ-shock wave solutions for a generalized pressureless gas dynamics system*, Int. J. Math., 25 (2014), p. 1450007.

[102] J. Saththasivam, K. Loganathan, and S. Sarp, *An overview of oil–water separation using gas flotation systems*, Chemosphere, 144 (2016), pp. 671–680.

[103] W. Shen, *On the cauchy problems for polymer flooding with gravitation*, J. Differ. Equ., 261 (2016), pp. 627–653.

[104] P. Stevenson, *Dimensional analysis of foam drainage*, Chem. Eng. Sci., 61 (2006), pp. 4503–4510.

[105] P. Stevenson, S. Ata, and G. M. Evans, *Convective–dispersive gangue transport in flotation froth*, Chem. Eng. Sci., 62 (2007), pp. 5736–5744.

[106] P. Stevenson, P. S. Fennell, and K. P. Galvin, *On the drift-flux analysis of flotation and foam fractionation processes*, Can. J. Chem. Eng., 86 (2008), pp. 635–642.

[107] P. Stevenson and C. Stevanov, *Effect of rheology and interfacial rigidity on liquid recovery from rising froth*, Ind. Eng. Chem. Res., 43 (2004), pp. 6187–6194.

[108] L. Svarovsky, *Countercurrent washing of solids*, in Solid-Liquid Separation, L. Svarovsky, ed., Butterworth-Heinemann, Oxford, fourth edition ed., 2001, ch. 15, pp. 442–475.

[109] Y. Tian, M. Azhin, X. Luan, F. Liu, and S. Dubljevic, *Three-phases dynamic modelling of column flotation process*, IFAC-PapersOnLine, 51 (2018), pp. 99–104.

[110] Y. Tian, X. Luan, F. Liu, and S. Dubljevic, *Model predictive control of mineral column flotation process*, Mathematics, 6 (2018), p. 100.

[111] J. Vandenberghe, J. Choung, Z. Xu, and J. Masliyah, *Drift flux modelling for a two-phase system in a flotation column*, Can. J. Chem. Eng., 83 (2005), pp. 169–176.

[112] G. Verbist, D. Weaire, and A. M. Kraynik, *The foam drainage equation*, J. Physics: Condensed Matter, 8 (1996), pp. 3715–3731.

[113] G. B. Wallis, *One-Dimensional Two-Phase Flow*, McGraw-Hill, New York, 1969. 281 pp.

[114] L. K. Wang, N. K. Shammas, W. A. Selke, and D. B. Aulenbach, *Flotation thickening*, in Biosolids Treatment Processes. Handbook of Environmental Engineering, vol 6., H. Y. Wang L. K., Shammas N. K., ed., Humana Press,Totowa, New Jersey, 2007, pp. 71–100.

[115] J. Yianatos, R. Bucarey, J. Larenas, F. Henríquez, and L. Torres, *Collection zone kinetic model for industrial flotation columns*, Minerals Eng., 18 (2005), pp. 1373–1377.